**ANUL LIV** **2010**

# S T U D I A

# UNIVERSITATIS BABEŞ-BOLYAI

# CHEMIA

## SPECIAL ISSUE

**Desktop Editing Office:** 51ST B.P. Hasdeu Street, Cluj-Napoca, Romania, Phone + 40 264-405352

## CUPRINS – CONTENT – SOMMAIRE – INHALT

Studia Universitatis Babes-Bolyai Chemia has been selected for coverage in Thomson Reuters products and custom information services. Beginning with V. 53 (1) 2008, this publication is indexed and abstracted in the following:

- Science Citation Index Expanded (also known as SciSearch®)
- Chemistry Citation Index®
- Journal Citation Reports/Science Edition

STUDIA UBB CHEMIA, LV, Sp.Iss., 2010

# HETEROLOGOUS EXPRESSION OF GRANZYME H IN *ESCHERICHIA COLI*

**BÁLINT EMESE-ÉVA[a], MIKLÓSSY ILDIKÓ[b], ÁBRAHÁM BEÁTA[b], SZILÁGYI LÁSZLÓ[b,c], LÁNYI SZABOLCS[b]**

**ABSTRACT.** Granzyme H belongs to the family of serine proteases, which plays an important role in fighting infections as part of the natural immune system. This enzyme is produced by natural killer cells and the T lymphocytes, inducing apoptosis in target cells. The precise role of the enzyme is not yet clarified; its crystal structure is unknown. The sequence encoding Granzyme H was cloned from human lymphocytes for heterologous expression. The assembled pET17cGraH expression vector contains the sequence encoding granzyme H under the control of a strong inducible promoter. Protein production was carried out in *E. coli Bl21(DE3)plysS* cultures.

***Keywords:*** *apoptosis, Granzyme H, heterologous expression, serine proteases*

## INTRODUCTION

The human Granzyme family is constituted of five members: Granzyme A, B, K, M, and H are present in placental mammals, being crucial components of the immune response by elimination of host cells infected by intracellular pathogens.

Granyzmes are released by cytotoxic T lymphocytes and by resting natural killer cells. The enzymes secreted by these two cell-types are granule associated enzymes, so called “granzymes” [1]. These cytotoxic granules contain a protein named perforin, which forms pores on the surface of cell membranes, and also contain serin proteases responsible for the breakdown of proteins.

Granzyme B and H are evolutionary strongly related, showing a 71% structural homology in their amino acid composition, also being located on the same chromosome. Sedelies et al found that Granzyme H is frequently more abundant than Granzyme B in NK cells, fact that proves a

[a] *“Politehnica” University of Bucharest, Faculty of Applied Chemistry and Materials Science, Splaiul Independenței No. 313, RO-060042, Bucharest, Romania, iovu@tsocm.pub.ro*
[b] *Sapientia University, Faculty of Sciences, Libertății Square, No. 1, RO-530100, Miercurea Ciuc, Romania, mtt@sapientia.siculorum.ro*
[c] *“Eötvös Lóránd”University, Department of Biochemistry, Pázmány Street, No. 17/c, 1117, Budapest, Hungary, szilagyl@elte.hu*

role for Granzyme H in complementing the pro-apoptotic function of Granzyme B in human NK cells [2]. Despite the high-leveled similarity in amino acid composition, a study demonstrated that Granzyme H is capable of inducing cell death in a caspase-independent manor [3].

Granzyme H is a specific human enzyme, a chimotripsin-like serine protease which's coding sequence is located on chromosome 14. According to Andrade et al., Granzyme H was reported to proteolitically inactivate adenoviral proteins necessary for replication [4].

The aim of this study is to express the recombinant Granzyme H in a prokaryotic system in order to study the expression conditions and quantity of the produced protein for further applications: determination of enzymatic properties and crystallization.

## RESULTS AND DISCUSSION

As resulted from **Figure 1.**, we obtained a significant amount of insoluble protein with a molecular weight of 33kDa, corresponding to the molecular weight of Granzyme H. It can be observed that 4 h of induction does not increase significantly the amount of the expressed protein in comparison with 1.5 h induction. This means that the induction time should not exceed 2 h, but variation of temperature may help to produce soluble proteins.

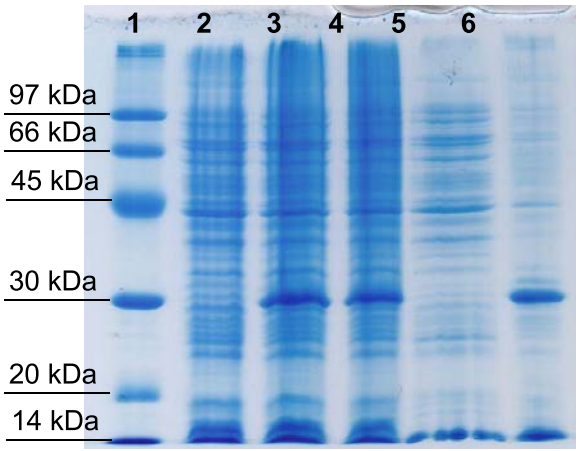


**Figure 1.** Expression of Granzyme H.

Lane 1: Molecular weight marker (Amersham); lane 2: Cell pellet before induction; lane 3: cell pellet after 1.5 h of induction; lane 4: cell pellet after 4 h of induction; lane 5: soluble proteins after sonication; lane 6: insoluble proteins (inclusion bodies) after sonication.

## CONCLUSIONS

Following the transformation of E. coli Bl21(DE3)plysS host strain with pET17c-GraH vector we succeeded in the expression of Granzyme H.

The expressed protein can be found in significant quantity, but in insoluble form. Several conditions need to be improved, for example by lowering the expression temperature at 20 $^{o}$C, which may increase the produced soluble protein level [5].

An advantage of the insoluble protein production is the formation of relatively pure inclusion body aggregates, from which Granzyme H can be easily purified.

## EXPERIMENTAL SECTION

### *Plasmids and bacterial strains*

The cloning and expression of the recombinant Granzyme H was carried out in the pET system from Novagen, a system which is operating under control of the bacteriophage T7 promoter.

The coding sequence of the Granzyme H was cloned from human lymphocytes and subcloned in a pET17c vector, resulting in the pET17c-GraH vector. *E. coli Bl21(DE3)plysS* (Stratagene) strain was used (genotype: $F^{-}$, *ompT,* $hsdS_B$ ($r_B^{-}$, $m_B^{-}$), *gal dcm, λ(DE3), pLysS,* $Cm^r$), as a high-stringency protease deficient expression host.

### *Protein expression*

Electrocompetent BL21(DE3)pLysS cells were obtained following a protocoll described in the operator's manual (Xcell GenePulser, BioRad). Pulsing was carried out conform the manufacturer's manual. After electroporation, cell suspension supplemented with SOC media (2% bactotryptone, 0.5% yeast extract, 0.05% NaCl, 0.01 M $MgCl_2$, 0.01 M $MgSO_4$, 0.02 M glucose, pH7, reagents from Merck) was incubated 3 h at 37 $^{0}$C, and plated on LB agar containing 100 μg/ml Ampicillin. The plates were incubated overnight at 37 $^{0}$C

A single colony was inoculated in 2 ml LB broth with100 μg/ml Ampicillin and incubated overnight at 37 °C at 250 rpm. To prevent leaky protein expression, 1 % glucose was added to the overnight culture. Glucose was removed by centrifugation. After centrifugation cells were diluted to a final volume of 200 ml. They were incubated with shaking (250 rpm) at 37 °C, until they reached the OD600 to 0.4-0.6 value, indicating the logarithmic growth phase.

At this point, an end-concentration of 0.5 mM IPTG (isopropyl-thio-galactopyranoside, Sigma) was added to the culture, allowing the T7 RNA polymerase expression and target gene-expression. The culture was further incubated for 4 h in the same conditions. 1 ml samples were taken before

the induction and during the expression period, each hour. Samples for electrophoresis were centrifuged and stored at -20°C.

Cell disruption was conducted by resuspension in 20 ml of distilled water supplemented with 0.25 g/ml lysozyme and freezing at -80 °C for 2 h. To completely disassociate the cellular components, cell suspensions were melted and sonicated (sonicator Dr.Hierschler) 5 cycles of 10 sec at 70% amplitude, with 10sec pause between the cycles. This procedure was accomplished on ice to prevent excess heat formation and denaturation of the protein.

Insoluble proteins accumulated in inclusion bodies were obtained by centrifugation for 15 min at 4°C, 14000 rpm.

Sample preparation for electrophoresis was conducted according to Laemmli [4], and the produced proteins separated on a 15% SDS-PAGE were visualized by Coomassie staining.

**ACKNOWLEDGMENTS**

The work has been funded by the Sectorial Operational Programme Human Resources Development 2007-2013 of the Romanian Ministry of Labour, Family and Social Protection through the Financial Agreement POSDRU/88/ 1.5/S/60203.

## REFERENCES

1. D. Masson, P.J. Peters, H.J. Geuze, J. Borst, J. Tschopp, *FEBS Letters*, **1986**, *208*, 84.
2. K.A. Sedelies, T.J. Sayers, K.M. Edwards, W. Chen, D.G. Pellicci, D.I. Godfrey, J.A. Trapani, *The Journal of Biological Chemistry*, **2004**, *279*, 25.
3. H. Johnson, L. Scorrano, S.J. Korsmeyer, T.J. Ley, *Blood,* **2003**, *101*, 3093-3101
4. F. Andrade, E. Fellows, D.E. Jenne, A. Rosen, CSH. Young, *EMBO Journal*, **2007**, *26*, 2148.
5. I. Miklóssy, L. Szilágyi, B. Ábrahám, Sz. Szilveszter, Sz. Lányi, *Studia UBB Chemia*, **2009**, *2*, 11.
6. U.K. Laemmli, *Nature*, **1970**, 680.

STUDIA UBB CHEMIA, LV, Sp.Iss., 2010

# HETEROLOGOUS EXPRESSION OF *BACILLUS LICHENIFORMIS* α-AMYLASE IN *PICHIA PASTORIS*

**BODOR ZSOLT[a], ORBÁN KÁLMÁN-CSONGOR[a], MIKLÓSSY ILDIKÓ[b], JUHÁSZ KATALIN[b], ÁBRAHÁM BEÁTA[a], LÁNYI SZABOLCS[b]**

**ABSTRACT.** The *Pichia pastoris* expression system has the potential for a very high production level of foreign proteins. The α-amylase enzyme (1,4-α-D-glucan-glucanohydrolase) catalyze the endohydrolysis of 1,4-α-D-glucosidic linkages of starch and related poly- and oligosaccharides producing maltose and larger oligosaccharides. *Bacillus licheniformis* α-amylase (BLA) is a highly thermostable enzyme which is widely used in biotechnological processes. In this study, the gene encoding the α-amylase from *Bacillus licheniformis* was amplified by PCR and cloned into *P. pastoris* X33 host strain using the vector pPICZαA allowing methanol induced expression and secretion of the protein, using the methanol-controlled alcohol oxidase *(AOX1)* expression system promoter. The ultimate goal of our research is the development of a new technology for amylolytic enzyme production, applicable in fermentation processes of starch-containing materials, technology which can be applied in case of different industrial enzymes as well.

***Keywords:*** *Bacillus licheniformis, α-amylase, heterologous expression, Pichia pastoris, AOX1 promoter*

## INTRODUCTION

The methylotrophic yeast *Pichia pastoris* has been developed as a commercial expression system for recombinant proteins [1,2]. The tightly controlled and methanol inducible *AOX1* gene [3], encoding the enzyme responsible for a vast majority of the alcohol oxidase activity in the cell has proven to be a valuable tool in the expression of recombinant proteins in this host organism [4]. Vectors are designed for carrying the *AOX1* promoter region, selectable marker which endows antibiotic resistance and the α-mating factor from *Saccharomyces cerevisiae* which enables signaling of extracellular secretion of the cloned protein [5].

[a] *Politehnica University of Bucharest, Faculty of Applied Chemistry and Material Science, Splaiul Independenței Nr. 313, sector 6, RO-060042, Romania, e-mail: decanat@sim.pub.ro*

[b] *Sapientia University, Cluj-Napoca, Faculty of Sciences, Piața Libertății, Nr. 1, RO-530140, Miercurea-Ciuc, Romania, e-mail: bodorzsolt@sapientia.siculorum.ro*

Recombinant protein production in the yeast strain has several advantages like very high levels of secretion, posttranslational modifications glycosylation, methylation, a promoter derived from the alcohol oxidase I gene *(AOX1)* of *P. pastoris* that is uniquely suited for the controlled expression of foreign genes that integrate into the *Pichia* genome [6] and the ability to engineer secreted proteins that can be purified from growth medium without harvesting the yeast cells themselves [7]. The used expression vectors have an expression cassette, promoter region, multiple cloning site (for foreign coding sequence), alcohol oxidase open reading frame, α-mating factor and selectable markers [6-8].

Because of its remarkably high thermal resistance *Bacillus licheniformis* α-amylase has become the most widely used in starch liquefaction processes [9]. α-Amylase's official name is 1,4-α-D-Glucan glucanohydrolase; EC 3.2.1.1 [9-11], acts upon large polymers of starch by randomly cleaving α-1,4-glucosidic linkages, to give diverse products including dextrins and progressively smaller polymers composed of glucose units [12-14]. α-Amylases have potential application in wide number of industrial processes such as food, fermentation, textile to paper industries [12,14-17]. However, the cost of producing this enzyme is high [18] due to the extreme living conditions of the *Bacillus* species (high temperature, pH, complex medium) [19].

One possibility to resolve these problems is the heterologous expression of the thermostable enzyme. The expressed α-amylase used in starch industry must be active and stable at low pH and high temperature.

Expression of a foreign gene in *P. pastoris* requires three basic steps: (a) the insertion of the gene into an expression vector; (b) integration of the expression vector into the *P. pastoris* genome; and (c) selection of potentially expressing strains for the foreign gene [7]. In this article, we report a simple, efficient, economical and industrially applicable and reproducible method for heterologous expression. The α-amylase encoding gene was isolated from the thermophilic bacteria *B. licheniformis* and after transformation into *Escherichia coli* the amylase coding gene was cloned and expressed in *P. pastoris*. The expressed proteins can be concentrated and purified by subjecting the supernatant to ultrafiltration, precipitation, and/or adsorption/elution chromatography [9].

## RESULTS AND DISCUSSION

The SamyL gene of *B. licheniformis* was amplified with forward and reverse primers that introduced *Eco*RI and *Xba*I sites respectively.

The small fragment containing the coding sequence for the α-amylase was obtained essentially as described in Experimental section. **Figure 1** shows the PCR products where the reaction was carried out in seven samples and the molecular weight is 1500 bp.

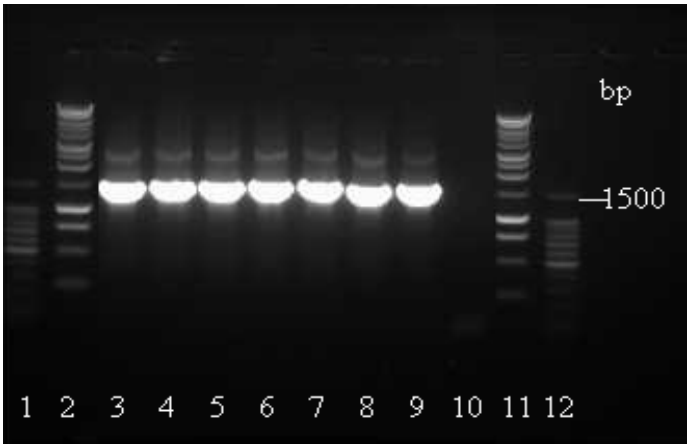


**Figure 1.** Image of the electrophoresis gel illustrating the PCR reaction results Lanes 1,12: 100 bp DNA ladders; lanes 2,11: 1 kb DNA ladders; lanes 3-9: PCR reaction products; lane10: negative control

### *Construction of the pPICZαA-SamyL vector*

Construction of the recombinant pPICZαA-SamyL vector was performed as described in Experimental section; the total ligation reaction and the control reaction being transformed into chemically competent *Escherichia coli* TOP10F' cells provided in the Invitrogen EasySelect Pichia Expression Kit. 100 µL of each of the heat shocked cell suspensions were placed on solid low salt LB medium with 25 µg/mL Zeocin. On figure 2 the result of the ligation are shown.

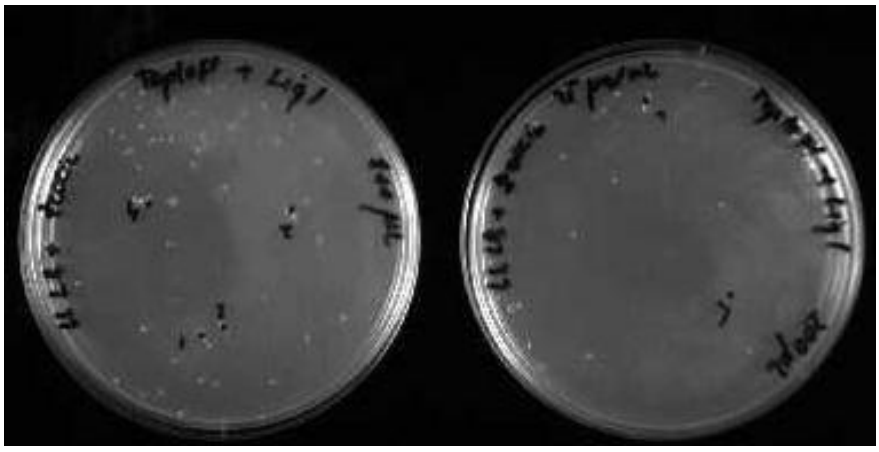

**Figure 2.** Results of ligation

Minipreps were prepared from 6 colonies on plate as described in Experimental section, and analyzed for the presence of the insert by double digestion with *Xba*I and *Eco*RI, respectively in order to check for the correct

conformation of the obtained recombinant plasmid and for the presence of the insert. Minipreps were obtained in 50 µL of TE buffer, from which 4 µL were loaded on an 1% TAE agarose gel and separated by electrophoresis at 7 V/cm$^2$ voltage. The **figure 3** (system GelDoc, BioRad) illustrates the fragments that were used to construct the vector and the results from the digestion reactions.

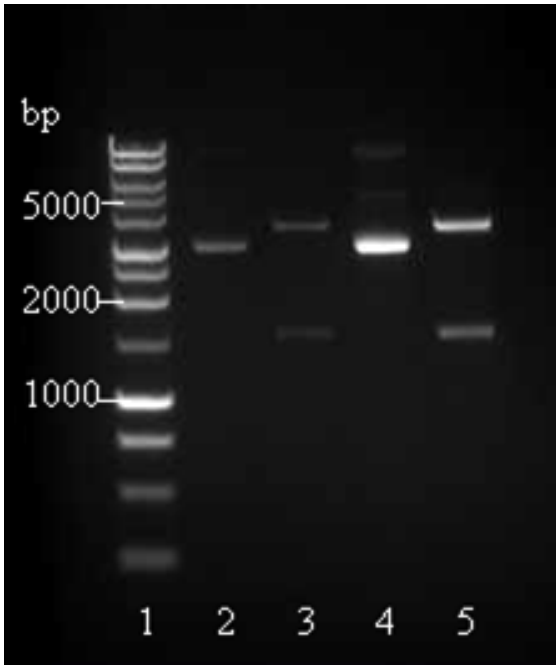


**Figure 3.** Illustration and verification of the obtained pPICZαA-SamyL expression vector

Lane 1: 1 kb DNA ladder (Promega);
lanes 2,4: undigested pPICZαA-SamyL;
lanes 3,4: digested with *Xba*I and *Eco*RI

We can observe that the coding sequence of the α-amylase is integrated into the vector and the double digested fragment size is 1500 bp.

## *Expression of α-amylase in Pichia pastoris*

The obtained pPICZαA-SamyL vector was linearized with the restriction endonuclease *Sac*I, which cleaves the *AOX1* site. Digestion reaction with *Sac*I was performed as described in Experimental section and verified on a 1% agarose gel by electrophoresis. The **figure 4** presents the linearized pPICZαA-SamyL vector.

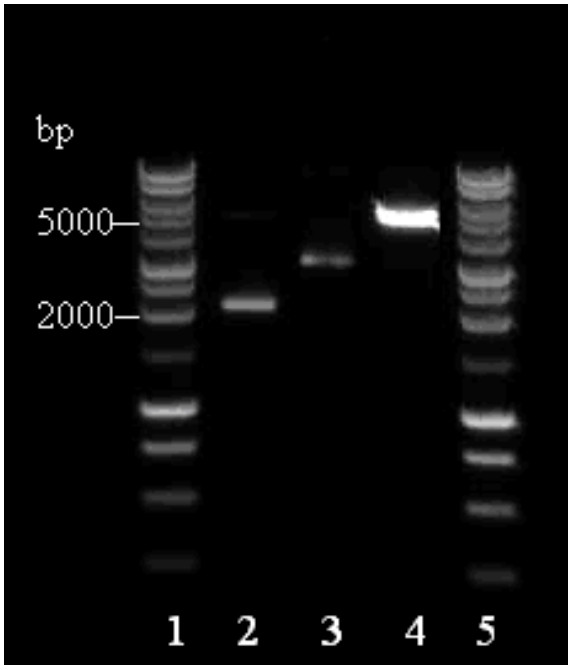


**Figure 4.** Image of the electrophoresis gel illustrating linearization of the pPICZαA-SamyL vector with *Sac*I

Lanes 1,5: 1 kb DNA ladders (Fermentas);
lane 2: pPICZαB 50 ng;
lane 3: pPICZαA-SamyL;
lane 4: pPICZαA-SamyL *Sac*I digest

Transformation of the *Sac*I digested plasmid pPICZα-SamyL into electrocompetent host cells of *P. pastoris* resulted in over one hundred colonies on YPD (Zeocin 100 μg/mL). Ten of these colonies were randomly chosen for screening by PCR.

Total genomic DNA was isolated in order to screen by PCR reaction for those transformants, which have successfully integrated the α-amylase coding sequence into their genome. The PCR reaction was set up including the recombinant pPICZαA-SamyL vector as a template for the positive control reaction. On **figure 5** is presented the electrophoresis gel with the PCR reaction products.

As shown on figure 5, two (colonies nr. 6,7) of the ten transformed colonies resulted the expected PCR products, representing the integrated coding sequence of the amylase. In consequence, production cultures were prepared starting from colony nr. 6 in order to achieve extracellular expression of the target protein.

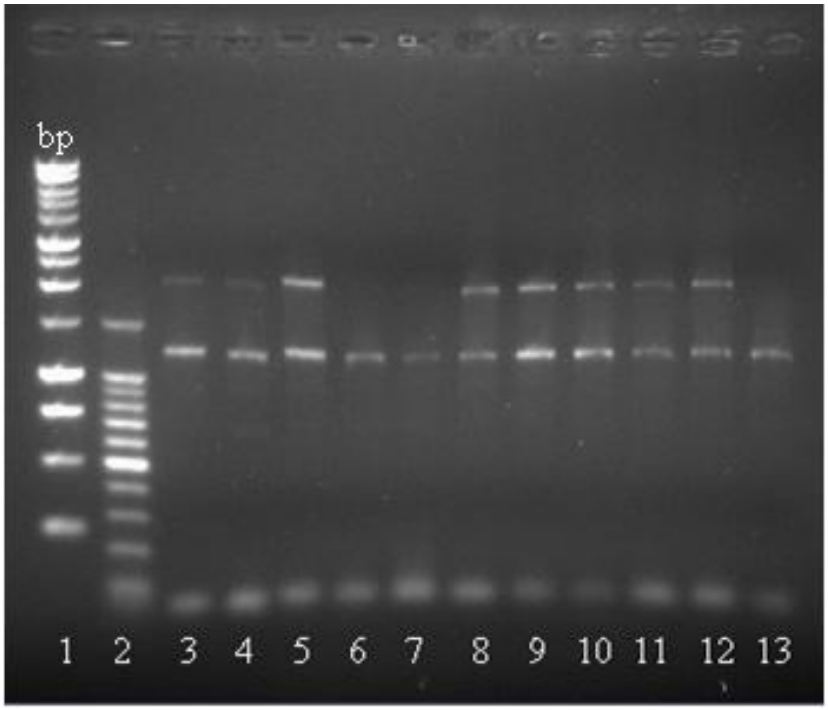


**Figure 5.** Illustration of the PCR screening results for genomic integration of the target sequence

Lane 1: 1 kb DNA ladder (Promega);
lane 2: 100 bp DNA ladder (Promega);
lanes 3-12: PCR products of genomic DNA from 10 transformed colonies;
lane 13: positive control

Expression was carried out as described in Experimental section, in a final volume of 100 mL in BMMY inducer medium. As temperature has a major effect on induction of the *AOX1* promoter, the cultures were grown at 30ºC; continuous induction was achieved by supplementing the growth medium with 0.5% of methanol every 24 hours. Presence of the protein of interest in the culture supernatant was verified by SDS-PAGE; 1 mL of the culture have been sampled before induction and every 24 hours from the induced culture, samples from the supernatant containing secreted proteins were analyzed on 12.5% acrylamide gels after TCA precipitation, adding equal volume of SDS-sample buffer to the samples. According to the data obtained with the ProtParam Tool (Expasy Proteomics Server), the molecular weight of the expressed amylase is in the range of 58 kDa. In figure nr. 6, results obtained after electrophoretic separation of the extracellularry-produced proteins are presented.

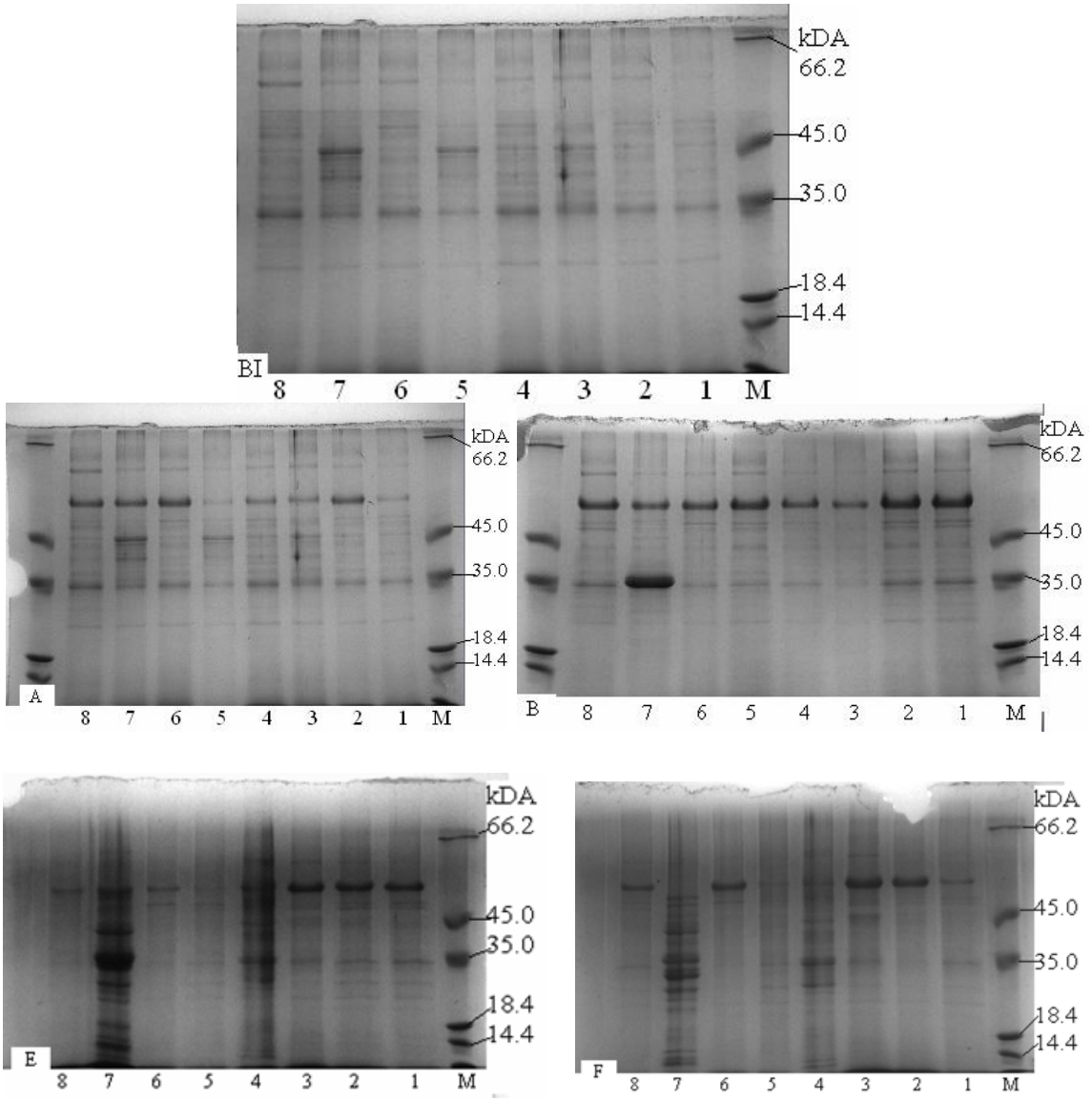


**Figure 6.** Illustration of the obtained proteins from culture supernatants of *Pichia* X33 transformants Part BI: before induction; Part A: secreted proteins of X33/6 after 1 day of induction; lane M: molecular weight marker; lanes 1-8: different colonies secreted proteins; Part B: secreted proteins of X33/6 after 2 days of induction; Part E: secreted proteins of X33/6 after 5 days of induction; Part F: secreted proteins of X33/6 after 6 days of induction

Analyzing the obtained proteins we can observe that after adding 0.5% methanol the expression has started. The amount of the expressed amylase was decreasing after the 5'th and 6'th days, but we can observe that in case of the 2,3,6 and 8 colonies the protein quantity remain constant.

## CONCLUSIONS

In the present study we demonstrate a practical procedure for high-level production of full-length recombinant proteins from *Pichia pastoris*. The α-amylase coding gene of *Bacillus licheniformis* was cloned and expressed successfully in *P. pastoris* by using the pPICZαA vector. The α-amylase genes encoding the plasmids were integrated into the yeast genome as a result of genetic recombination and were replicated autonomously.

The *Pichia* expression system was considered to provide high-level extracellular expression of a heterologous protein offering simple purification possibilities. The data presented in the Results chapter show that construction of the recombinant pPICZαA-SamyL vector was completed successfully. The restriction analysis of the isolated vector gave results that confirm the calculated lengths of the restriction fragments. All digestion reactions yielded fragments with the expected length, the restrictase *Sac*I was chosen to linearize the vector.

Our expression experiments revealed that single transformant colony showed large variations in expression levels after few days. Transformation of electrocompetent *Pichia* X33 cells was completed successfully; expression of the α-amylase protein proved to be successful in *Pichia* X33 strain.

Future application of this enzyme could be considered as a saccharifying enzyme in the starch syrup production [1,6]. Further study will be required to determine the structure, the activity and optimum pH range of the expressed amylase.

## EXPERIMENTAL SECTION

Plasmids are the most frequently used cloning and expression vectors, due to their reliability. In the past three decades there have been a number of straightforward methods described for cloning into plasmid vectors.

The *Bacillus licheniformis* amylase gene was a generous gift from University of Szeged. *P. pastoris* X33 and pPICZαA purchased from Invitrogen were used as host and vector for heterologous expression of the amylase. Chemically competent *E. coli* TOP10F' was used for plasmid construction. The easiest and most successful cloning strategy is based on use of two different restrictases on both the carrier and the passenger DNA molecule, which create noncomplementary protruding termini, making the further ligation reaction more effective.

### *Construction of the pPICZαA-SamyL vector*

Amplification of the SamyL gene was performed using (Palm Cycler, Corbett Research) thermocycler with the oligonucleotids (primers)

SamyI_R1 R, (5' CCC T_CT AGA GAT CTT TGA ACA TAA ATT GAA ACC 3') and SamyI_F2 F, 5' GC G_AAT TCA ACA TCA AAA AGT TTG CAA AAC AAG C 3' designed to incorporate *Xba*I and *Eco*RI restriction sites to the PCR product. The PCR reaction was realised in a total volume of 50 µL (0.1 µg template, 0.2 mM dNTP mix, 2.5 mM $MgCl_2$, 0.5 µM oligonucleotides, 5U/µL aTaq polimerase, Promega).

For the construction of the pPICZαA-SamyL vector, the restriction endonucleases *Eco*RI and *Xba*I were used; in the first step the α-amylase vector, containing the target gene was digested with the two enzymes, resulting in the small fragment. 10 µg of plasmid DNA was digested with 10 U of *Xba*I (Fermentas) in 100 µL of 1x Red buffer (Fermentas), at 37°C for 4 hours, and verified by an 1% agarose gel electrophoresis; the digest was precipitated with ethanol, redissolved in 50 µL 1xY Tango buffer (Fermentas) and further digested with 10 U of *Xba*I for 4 hours at 37°C, and 2 µL were analysed by 1% agarose gel electrophoresis in TAE (Tris-acetate-EDTA) buffer with ethidium-bromide staining and visualized by GelDoc System from BioRad.

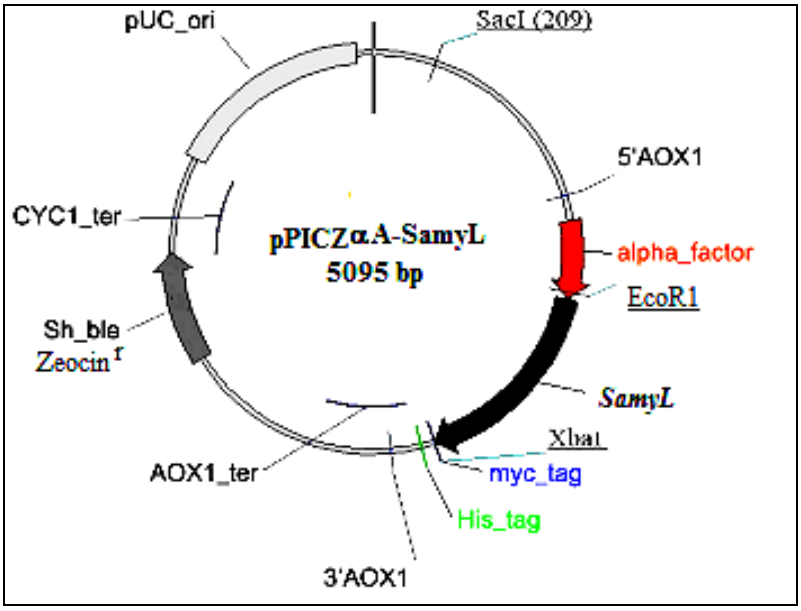


**Figure 7.** Map of pPICZαA-SamyL

The figure 7 summarizes the features of the vector. The vector map was designed with the VNTI software on the basis of data provided by Invitrogen in the users manual EasySelect *Pichia* Expression Kit.

The total amount of the digestion mixture was separated on a preparative 1% agarose gel and the 1500 bp small fragment containing the coding sequence was excised and isolated by the MiniElute Gel Extraction Kit (Qiagen) according to the instructions of the manufacturer. The isolated fragment

was obtained in 50 µL of TE buffer (Tris-EDTA, Fluka). For the preparation of the large fragment, 100 µg of pPICZαA (Invitrogen) plasmid DNA were digested with 10 U of *Eco*RI (Fermentas) and *Xba*I (Fermentas) in 1x Y Tango Buffer (Fermentas) for 4 hours at 37°C; the large fragment was obtained as described above in 30 µL of TE buffer. The purity of both isolates (large and small fragment) was verified by gel electrophoresis. The ligation reaction consists in formation of new phospohodiesther bonds between the 5' termini and 3' hydroxyl groups of the double stranded DNA molecules, which is carried out by the enzyme ligase, among which the T4 phage ligase is considered highly effective, thus frequently used in molecular biology studies. The ligation reaction was set up in a total volume of 20 µL, containing 14 µL of small fragment, 2 µL of pPICZαA large fragment and 1 µL T4 ligase (Invitrogen) in 2 µL 10x Ligation Buffer (Invitrogen) at 25°C for 1 hour, together with one control ligation without the small fragment. The ligation and control mixtures were transformed into 100 µL of chemically competent *E. coli* Top10F' cells (Invitrogen) and plated on low salt LB medium (Bactotryptone 1%, Yeast extract 0.5%, NaCl 0.5%, pH 7, Fluka) with 25 µg/mL Zeocin (Invitrogen). To isolate the recombinant plasmid, 6 transformed colonies were picked up with sterile toothpicks and grown overnight (12 hours) in 5 mL of low salt LB with Zeocin (25 µg/mL), at 37°C and 150 rpm. Cells were harvested by centrifugation at 5000 rpm for 2', plasmid DNA was isolated and purified by the Plasmid Miniprep Kit (Qiuagen), according to the instructions of the manufacturer. The plasmid preparates were obtained in 50 µL of TE buffer and verified by agarose gel electrophoresis. Insertion of the fragment of interest and the correct assembling of the recombinant plasmid were checked by double digestion with *Xba*I and *Eco*RI for the presence of the insert, and loaded for verification on a 1% agarose gel together with the obtained minipreps for separation by electrophoresis.

### *Extracellular expression in Pichia pastoris*

For high-level extracellular secretion of the α-amylase, *Pichia pastoris* strain X33 with *his4* genotype, $His^+$, $Mut^+$ phenotype was used (Invitrogen). As *Pichia* strains express only a low number of native proteins and also at low levels extacellularry, obtention of the target protein in a secreted form assures simple and effective isolation and purification of the product. Transformation into *Pichia* strains requires linearization of the recombinant vector, as it integrates the coding sequence of interest via homologous recombination between the transforming DNA and regions of homology within the genome. Linearization of the recombinant pPICZαA-SamyL vector was carried out by digestion with the restriction endonuclease *Sac*I*,* which has a unique restriction site at the *AOX1* locus of the vector, thus permits efficient integration into

the *Pichia* genome. The digestion reaction was set up as follows: 40 µL of isolated plasmid preparate was digested with 5 µL of 15 U of *Sac*I (Sigma) in 6 µL of 10x *Sac*I Buffer (Sigma) in a total volume of 61 µL for 2 hours at 37ºC, and checked by agarose gel electrophoresis. The resulted linearized plasmid DNA was further used for transformation of the chosen *Pichia* strain X33. Electroporation of the *Pichia* strain was carried out using a BioRad GenePulser eletroporation apparatus, electrocompetent *Pichia* X33 cells being obtained by a modified protocol published in the *Pichia* EasySelect Expression Kit from Invitrogen.

Preparation of electrocompetent cells was carried out by diluting a fresh overnight culture of X33 cells to $OD_{600}$ = 0.1 in a total volume of 100 mL of YPD media, incubating overnight again at 30°C, until an $OD_{600}$ of 1.5. Cells were harvested by centrifugation at 1500xg for 5 minutes at +4°C, then resuspended in 100 mL of ice-cold sterile water. Cells were centrifuged again as in the previous step and the pellet resuspended in 25 mL of sterile water; followed by centrifugation as above and resuspension in 4 mL of ice-cold 1 M sorbitol (Sigma). After a final centrifugation at 1500xg for 5 minutes at +4°C, the cell pellet was resuspended in 200 µL of 1 M sorbitol, and aliquots of 80 µL were used for transformation by electroporation. For every transformation 80 µL of electrocompetent *Pichia* cells were used by adding 10 µL (~5 µg) of linearized pPICZαA-SamyL recombinant vector into chilled 2 cm electroporation cuvettes (BioRad) with linearized plasmids using a Bio-Rad GenePulser, at C = 25 µF; PC = and kept on ice for 5 minutes. The cells were transformed 200 Ω, V = 2.0 kV with a time constant of 5.2 ms.

They were allowed to recover in 1 mL of ice-cold 1 M sorbitol, the cell suspension was transferred into a sterile tube and incubated at 30°C for 1,5 hours without shaking.

Transformants were selected on YPD agar (1% yeast extract, 2% peptone, 2% glucose, 2% agar-agar, reagents from Merck) agarized plates containing 100 µg/mL Zeocin. Control transformation reactions were also set up, containing no plasmid DNA; incubation at 30°C was prolonged until colonies were visible (on average 3-4 days).

PCR analysis of *Pichia* integrants was performed in order to scan for transformed colonies, which have integrated the amylase coding sequence into their genome. The 5' *AOX1* primer 5'- respectively the 3' *AOX1* primer were used. Genomic DNA was isolated from 10 transformed X33 colonies by the Wizard Genomic DNA Purification Kit (Promega), according to the instructions of the manufacturer; purified genomic DNA was obtained in a volume of 50 µL. The PCR reaction was set up as follows: 5 µL 10x Taq buffer, 5 µL 25 mM $MgCl_2$, 1 µL 25 mM dNTP, 1 µL of 5', respectively 3' *AOX1* primer (10 pmol/µL), 5 U Taq Polymerase and 1 µg of template genomic DNA for a reaction volume of 50 µL. For amplification controls 100 ng of recombinant

plasmid pPICZαA-SamyL (positive control). The PCR reaction was performed in Corbett Research Thermal Cycler, with the following program: 1 cycle of heat soak at 94°C 2 min, 25 cycles of denaturation at 94°C 1 min, annealing at 55°C for 1 min, extension at 72°C for 1 min and 1 cycle of final extension at 72°C for 7 min. PCR products were loaded onto an 1% TAE agarose gel for electrophoresis.

Controlled expression of the recombinant protein was achieved by use of the methanol-inducible promoter *AOX1,* which is known to yield highest expression levels upon induction with 0.1-5% methanol. To ensure derepression, the recombinant colonies were firstly grown on complex media supplemented with glycerol.

Small-scale expression experiments of the recombinant *Pichia* strains were carried out in glass reaction tubes. The inoculums was prepared by transfer of a single recombinant colony to 10 mL BMGY (Buffered Glycerol-Complex Medium: 1% yeast extract, 2% peptone, 100 mM potassium phosphate, 1.34% Yeast Nitrogen Base, 4 x $10^{-5}$% biotin, 1% glycerol, all reagents from Merck); to ensure good aeration, baffled flasks were used in which the culture volume did not exceed 20% of the flask volume. Cultures were grown at 30°C with shaking at 150 rpm (CERTOMAT BS-T, SARTORIUS) until $OD_{600}$ reached 3-4 (16-20 hours), corresponding to log-phase growth.

Cells were harvested by centrifugation at 3000xg for 5', and the supernatant was treated with trichloracetic acid (TCA) to extract total protein. The expression experiments was prepared by cell resuspension in 100 mL inducer medium BMMY (Buffered Methanol-Complex Medium: 1% yeast extract, 2% peptone, 100 mM potassium phosphate, 1.34% Yeast Nitrogen Base, 4 x $10^{-5}$% biotin, 0.5% glycerol, all reagents from Merck) to an $OD_{600}$ of 1 to induce expression. *Pichia* cultures were further incubated at 30°C with shaking at 150 rpm and grown in shake flasks with baffles for expression of the α-amylase up to 6 days. To maintain induction, the media was supplemented every 24 hours with 0.5% methanol; 1 mL samples for further analysis by SDS-PAGE were taken before induction and every 24 hours post-induction, centrifuged at maximum speed in a micro centrifuge (Hettich), and both the pellets and the separated supernatant were stored at -80°C until assaying. After 6 days of expression, culture supernatants were separated by centrifugation and stored at -80°C until purification procedures.

### *SDS-PAGE*

Denaturation of the proteins and a linear structure, as well as negative surface charge is assured by the β-mercaptoethanol and SDS loading buffer contained in the loading buffer, as well as by keeping the samples for 10' at 95°C.

Separation of the proteins was carried out in 12.5% polyacrylamide running gel (acrylamide-bis-methylene-acrylamide monomer (Sigma Aldrich), SDS 10%, ammonium persulphate, TEMED), in a 2 phase-2 electrolyte system (electrophoresis apparatus – BioRad Tetra cell). 15 µL of each sample was run at one time, together with a molecular weight marker (Promega), with the parameters of the electromagnetic field of 30 mA constant amperage and 150 W power.

Comassie Blue G250 (Sigma Aldrich) dyeing was used for visualization of the electrophoretic bands, destaining with 50% ethanol and 10% acetic acid solution.

**ACKNOWLEDGMENTS**

The authors are very grateful to Professor László Szilágyi for his generous assistance.

## REFERENCES

1. B. Karakaş, M. Inan, M. Certel, *Journal of Molecular Catalysis B: Enzymatic*, **2010**, *64,* 129.
2. D.B. Choi, E.Y. *Park, Process Biochemistry*, **2006**, *41*, 390.
3. L. Lange, M. Skjøt, *Journal of Biotechnology*, **2008**, *133*, 424.
4. M. Mack, M. Wannemacher, B. Hobl, P. Pietschmann, B. Hock, *Protein Expression and Purification*, **2009**, *66*, 165.
5. R. Daly, M.T.W. Hearn, *Journal of Molecular Recognition*, **2005**, *18*, 119.
6. W. Claremont, W. Beaverton, *Molecular Biotechnology*, **2000**, *16*, 23.
7. P. Li, A. Anumanthan, X.-G. Gao, K. Ilangovan, V.V. Suzara, N. Düzgüneş, V. Renugopalakrishnan, *Appl Biochem Biotechnol*, **2007**, *142*, 105.
8. J.L. Cereghino, J.M. Cregg, *FEMS Microbiology*, **2000**, *24*, 45.
9. M.H. Ashraf, “Studies on the Biosynthesis of Alpha Amylase by a Mutant Strain of *Bacillus*, Species”, ***, Pakistan, **2004**, chapters 2,3.
10. M. Hashemi, S.H. Razavi, S.A. Shojaosadati, S.M. Mousavi, K. Khajeh, M. Safari, *Journal of Bioscience and Bioengineering*, **2010**, Vol. 110, No. *3*, 333.
11. N. Declerck, M. Machius, P. Joyet, G. Wiegand, R. Huber, C. Gaillardin, *Biologia, Bratislava*, *57/Suppl.,* **2002**, *11*, 203.
12. R. Gupta, P. Gigras, H. Mohapatra, V.K. Goswami, B. Chauhan, *Process Biochemistry*, **2003**, *38*, 1599.

13. G. Dong, C. Vieille, A. Savchenko, J.G. Zeikus, *Applied and Environmental Microbiology*, **1997**, Vol. 63, No. *9*, 3569.
14. M. Asgher, M.J. Asad, S.U. Rahman, R.L. Legge, *Journal of Food Engineering*, **2007**, *79*, 950.
15. R.H. Sajedi, H.N.-Manesch, K. Khajeh, R. Ahmadvand, B. Ranjbar, A. Asoodeh, F. Moradian, *Enzyme and Microbial Technology*, **2005**, *36*, 666.
16. M.J.E.C. van der Maarel, B. van der Veen, J.C.M. Uitdehaag, H. Leemhuis, L. Dijkhuizen, *Journal of Biotechnology*, **2002**, *94*, 137.
17. D. Gangadharan, K.M. Nampoothiri, S. Sivaramakrishnan, A. Pandey, *Food Research International*, **2009**, *42*, 436.
18. S.B. Oyeleke, A.A. Oduwole, *African Journal of Microbiology Research*, **2009**, Vol. *3 (4)*, 143.
19. A. Kumari, T. Rosenkranz, A.M. Kayastha, J. Fitter, *Biophysical Chemistry*, **2010**, *161*, 54.

STUDIA UBB CHEMIA, LV, Sp.Iss., 2010

# SELECTION OF LACTIC ACID BACTERIA ISOLATED FROM TRADITIONALLY MANUFACTURED CHEESE VARIETIES

**BOTH EMESE[a], GYÖRGY ÉVA[b], ÁBRAHÁM BEÁTA[b], MIKLÓSSY ILDIKÓ[b], LÁNYI SZABOLCS[b]**

**ABSTRACT.** In this report lactic acid bacteria, isolated from traditionally manufactured cheeses were selected by their resistance to gastric acidity and bile salts, adhesion to epithelial cells and inhibition of pathogen growth. 39 bacterial strains were isolated on selective media. Four bacterial strains were selected by their increased capacity to tolerate gastric acid and bile salts, each strains showing good adhesion capacity to IEC-6 intestinal epithelium cells. Some of selected strains inhibit growth of pathogenic bacteria by their metabolites.

***Keywords:*** *probiotics, isolation, tolerance, epithelial cells, adhesion*

## INTRODUCTION

Lactic acid bacteria and other probiotic microorganisms have many documented health effects [1]. Lactic acid bacteria (LAB) are present in the intestine of most animals, the beneficial effects of these microorganisms on human and animal health, including the effect on the immune system, has been extensively reported. LAB are present in many functional foods and are frequently used as probiotics to improve their biological effects on the host. The activation of immune response by LAB requires many complex interactions among the different constituents of the intestinal ecosystem (microbiota, epithelial cells and immune cells). They are acid-tolerant, strictly fermentative, gram-positive microorganisms, which produce lactic acid as main product. They are anaerobe and aerotolerant, as well. The most frequently cited definition is Fuller's [2], who defined probiotics as "a live microbial feed supplement, which beneficially affects the host animal by improving its intestinal microbial balance" [3].

[a] *"Politehnica" University of Bucharest, Faculty of Applied Chemistry and Material Science, Bucharest, Roumania, bothemese@sapientia.siculorum.ro*

[b] *Sapientia University, Cluj Napoca, Faculty of Sciences, Piața Libertății nr.1., RO- Miercurea Ciuc, Roumania, gyorgyeva@sapientia.siculorum.ro*

One of the most important criteria for probiotic bacteria is that the strains belonging to bacterial species that are present in the intestinal microbiota could have a better chance of survival [4]. Many mechanisms have been described by which probiotics could enhance intestinal health, such as competition for nutrients, inhibition of the epithelial and mucosal adherence of pathogens, inhibition of epithelial invasion by pathogens, the production of antimicrobial substances (lactic/acetic acid, hydrogen peroxide, bacteriocins) and the stimulation of mucosal immunity [5].

The prevention of pathogen colonization of the gut by probiotic bacteria is demonstrated in many recent researches. Probiotics influences both intestinal epithelial cells and immune cells of the gut, but these effects are still being unraveled. Probiotics, through their effects on the host's immune system, might ameliorate diseases triggered by disordered immune responses [6].

Our aim is to isolate lactic acid bacteria from cheese and to select them basing on their essential probiotic properties. These strains are nowadays frequently utilized in probiotic products and their surviving rate in digestive track is important to colonize the intestine and to exert their beneficial properties on the host. These properties are the following: tolerance to gastric acidity and bile salts, adhesion to epithelial cells and inhibiting pathogen bacterial growth.

## RESULTS AND DISCUSSIONS

### Isolation of lactic acid bacteria

LAB were isolated from traditionally manufactured cheese by appropriate dilutions with saline, plated on MRS (de Man Rogosa Sharpe) [7] agar. Cheese varieties were collected from sheepfolds (Harghita county, Roumania), from traditional manufacturers. Cheese varieties raw material was sheep milk, products were fresh-made (ripened 24 h).

Thirty-nine well-isolated colonies were picked up and transferred to MRS agar in test tubes and reinoculated to obtain pure cultures. Then they were stored in MRS agar at 4$^{o}$C.

The isolated strains were tested for their biochemical and morphological properties. The strains were Gram-stained and examined microscopically for cellular morphology and Gram-stain phenotype, tested for catalase and oxidase-activity, lactose digestion, oxygen utilization and colony morphology. All of the examined strains were gram-positive (14 cocci and 25 rods), catalase-negative, oxidase-negative (37 of 39 strains). 30 of 39 strains ferment lactose to acids. Most of them are anaerobes (23 strains), aerobe-facultative anaerobes (5 strains), anaerobe-facultative aerobes (9 strains) and microaerofiles (2 strains). To describe the colony morphology, the following aspects must be taken into account: diameter, form, margin, elevation, color, surface and

density. The diameter of colonies varies between 0.1-6.0 mm, their form is round, and their margin is regulated in 29 cases, dentated at 4 strain-colonies and irregular in the case of 6 strains. The color of colonies are white at 30 strains, cream-colored at 8 strains and cream-colored with yellow center in the case of one strain colony. The surface in both cases was bright, the density of colonies varied from translucent to opaque (17 translucent, 5 opaque and 17 translucent, but opaque at center).

The selected strains were identified genetically by 16S ribosomal DNA sequencing, strain Szj102.1., SRj104.2.: *Lactobacillus brevis,* strain SRj102.2.2.*: Serratia quinivorans*, SGt102.2.2: *Enterococcus faecium.*

## Tolerance to simulated gastric and intestinal juice

Basing on the results obtained in the determination of tolerance to simulated gastric juice, which contains hydrochloric acid (pH=2), it can be observed that 26 bacterial strains have high sensitivity to hydrochloric acid (i.e. there are no viable cells after 90 minutes of incubation), at 4 strains high tolerance to acidic conditions can be established, (the viability rate of these strains is higher than 40%), 7 strains show viability between 10-30%, and two of the isolated strains have viability under 10% compared to the initial colony forming unit (CFU) numbers (Figure 1.).

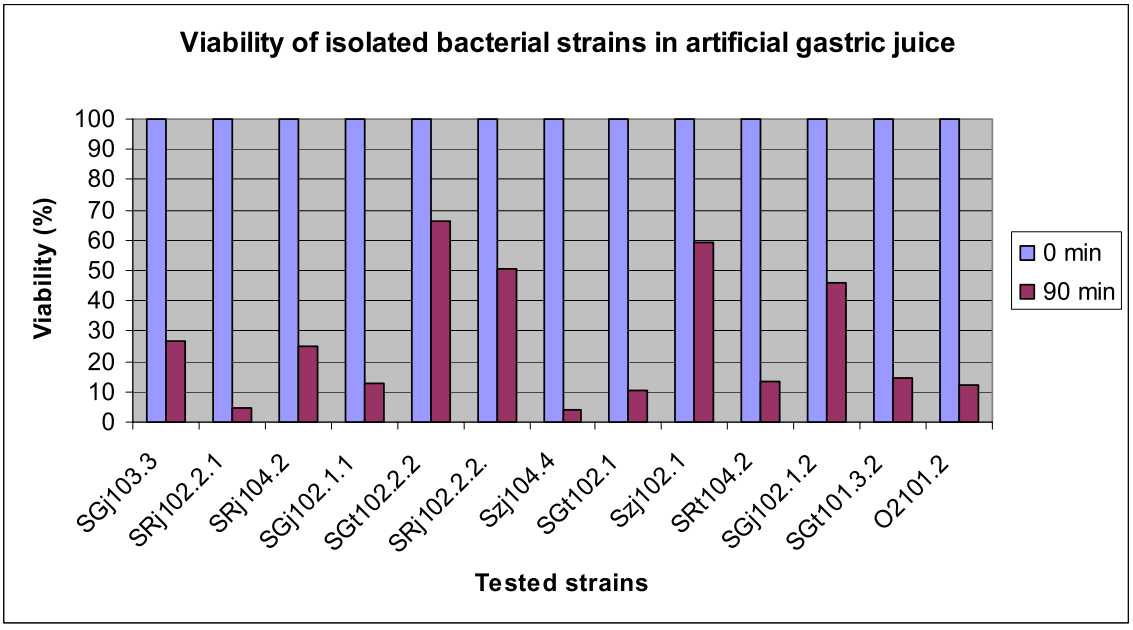


**Figure 1.** Viability rate of tested bacterial strains incubated in artificial gastric juice.

Simulated intestinal juice has a drastic effect on lactic acid bacteria; in the case of 7 strains there can not be observed viable cells after 180 minutes of incubation. 4 bacterial strains show better tolerance to bile salts, their viability rate is positive (Figure 2).

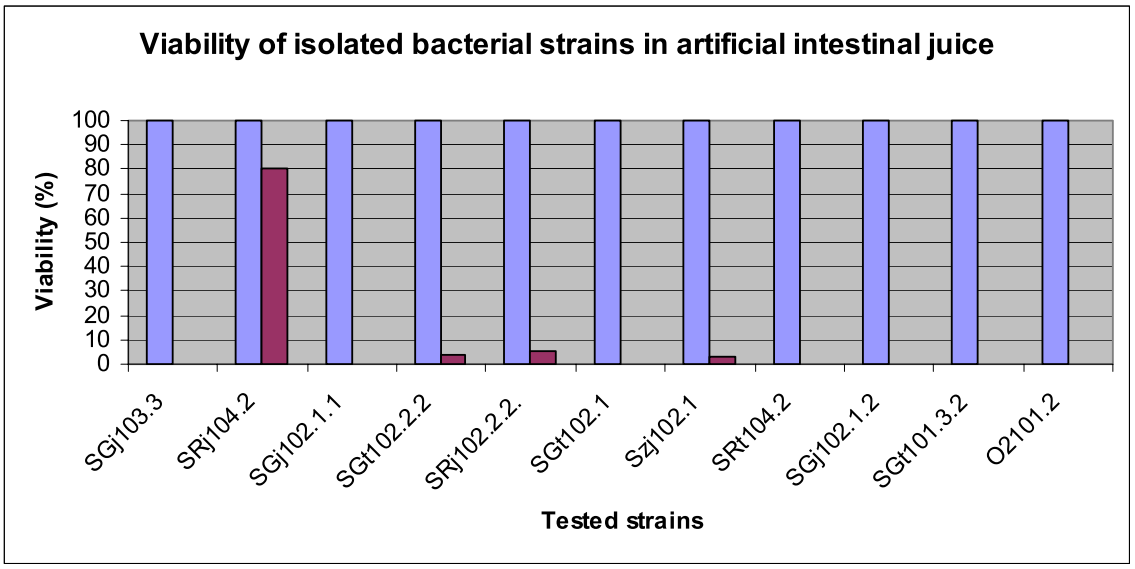


**Figure 2.** Viability rate of tested bacterial strains incubated in artificial intestinal juice.

## *In vitro* adhesion study

The adhesion ability was determined after gram-staining. The results show that the adherence of the examined probiotic strains is good to IEC-6 epithelial cells in *in vitro* conditions. The adhesion ability results are expressed in the following form: number of adhered bacterial cells/100 epithelial cell.

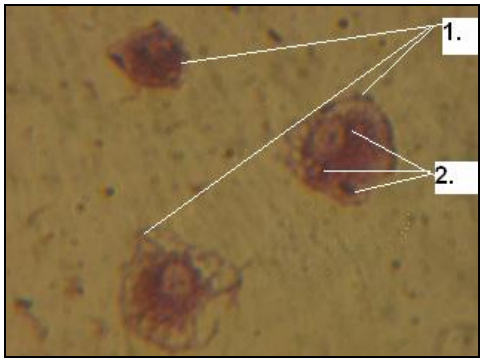


**Figure 3.** Bacterial cells (2) adhered on the surface of intestinal epithelial cells (1), after gram-staining.

Taking into account previous examinations, using known probiotic strains [8] and observing on microscope the adhesion-capacity of 20 randomly selected epithelial cells, we drew the conclusion that their ability proved to be good, from which it follows that the adhesion capacity of the analyzed strains is: SGt 102.2.2.: 240 bacterial cells adhered/100 epithelial cells, Szj102.1.: 180 bacterial cells adhered /100 epithelial cells, SRj104.2.: 133 bacterial cells adhered/100 epithelial cells, SRj 102.2.2.: 233 bacterial cells adhered /100 epithelial cells.

## Antibiosis tests

The Petri-dishes containing the nutritive media with pathogen bacteria and the supernatants of lactic acid bacterial strains were incubated for 48 hours. After the incubation the inhibition zone diameter can be analized. In the case of *Salmonella enteritidis* an inhibition of growth can be observed around the following supernatants: SRj102.2.2, Szj102.1 and SGt102.2.2 (see Figure 4.). The diameters of the inhibition zones are listed in Table 1. There is no discernible inhibition on growth in the case of the following bacteria: *Staphylococcus aureus* 5973, *Bacilus cereus* 2, *Escherichia coli* ATCC 13706 and *Listeria monocytogenes.*

**Figure 4.** Inhibition of *Salmonella enteritidis* by lactic acid bacterial supernatants (1- SRj104.2., 2- SGt102.2.2., 3- SRj102.2.2., 4- Szj102.1.).

**Table 1.** Inhibition zones of different lactic acid bacterial strains (n=6).

| Tested strain | Diameter (mm) of inhibition zone against *Salmonella enteritidis* |
|---|---|
| *Lactobacillus brevis* Szj102.1. | 4.333 ± 0.471405 |
| *Serratia quinivorans* SRj102.2.2. | 3.333 ± 0.471405 |
| *Enterococcus faecium* SGt102.2.2. | 4.166 ± 0.235702 |
| *Lactobacillus brevis* SRj104.2. | 0 |

## CONCLUSIONS

39 bacterial isolates were characterized from a biochemical and morphological point of view. The isolates were selected basing on their tolerance to gastric acid an bile salts, as well as on their adhesion to epithelial cells and inhibition of pathogen growth. There are strains with increased gastric acid- and bile salt-tolerance and their adhesion on the epithelial cell- surface is good, three of the strains have bacteriostatic effects on *Salmonella enteritidis.* Basing on the results obtained, after identifying the bacterial isolates and examining their effects on the immune system, we have the chance to find probiotic bacterial strains.

## EXPERIMENTAL SECTION

### Isolation of lactic acid bacteria

Lactic acid bacteria were isolated from cheeses on selective media (MRS agar), obtaining pure colonies. LAB were isolated from traditionally manufactured cheese by appropriate dilutions with saline, plated on MRS agar and incubated aerobically or anaerobically at 37$^{o}$C for 2-3 days. Thirty-nine well-isolated colonies were picked up and transferred to MRS agar in test tubes and reinoculated to obtain pure cultures. Then they were stored in MRS agar at 4$^{o}$C.

The isolated strains were tested for their biochemical and morphological properties. The strains were gram-stained and examined microscopically for cellular morphology and Gram-stain phenotype, tested for catalase and oxidase-activity, lactose digestion, oxygen utilization and colony morphology.

### Tolerance to simulated gastric and intestinal juice

The bacterial cultures obtained on MRS agar media after an incubation time of 48 hours at 37$^{o}$C are suspended in sterile 0.5 w/v% sodium chloride solution ($10^5$CFU= colony forming units/ml). The tolerance test is carried out as described elsewhere [8].

### *In vitro* adhesion study

IEC-6 cells were grown in Minimal Essential Medium (MEM) Earle's Base, supplemented with 5% (v/v) foetal bovine serum (FBS), 0.1 IU/ml insulin and gentamicin, ampicillin and kanamycin. Incubation was at 37$^{o}$C in the presence of 5% $CO_2$. The medium was changed every second day. Adhesion assays were performed with cells at late post-confluence (15 days in culture). IEC-6 cells were seeded at $10^5$ cells per well in 12-well microtiter

plates to obtain confluence. The incubation was at 37°C in the presence of 5% $CO_2$. Before the adherence assay, IEC-6 cells were washed twice with sterile phosphate-buffered saline solution. Adhesion study is described elsewhere [8].

## Antibiosis tests

Lactic acid bacterial strains were cultivated in MRS-broth for 10 days at 37°C. Their supernatans were used for this study. Pathogen bacterial strains: *Salmonella enteritidis*, *Staphylococcus aureus* 5973, *Bacilus cereus* 2, *Escherichia coli* ATCC 13706 and *Listeria monocytogenes* were cultivated for 24 hours and suspended in agar media. Then a drop of 0.1 ml of the broth culture of the isolated strains was placed in the wells cut, and incubated at 37°C for 48 hours and observed for inhibition zones.

**ACKNOWLEDGMENTS**

The work has been funded by the Sectoral Operational Programme Human Resources Development 2007-2013 of the Romanian Ministry of Labour, Family and Social Protection through the Financial Agreement POSDRU/6/1.5/S/16.

## REFERENCES

1. A. Ouwehand, E.M. Tuomola, S. Tolkko, S. Salminen, *International Journal of Food Microbiology*, **2001**, *64,* 119-126.
2. Y.W. Park: “Bioactive Components in Milk and Dairy Products”, Wiley-Blackwell, **2009**, chapter 12.
3. T. Vasiljevic, N.P. Shah, *International Dairy Journal*, **2008**, *18*, 714-728.
4. L. Morelli, *International Dairy Journal*, **2002**, *17*, 1278-1283.
5. A.L. Servin, M.H. Coconnier, *Best Practice & Research Clinical Gastroenterology*, **2003**, *17*, 741-754.
6. K. Shida, M. Nanno, *Trends in Immunology,* **2008**, *29*, 565-573.
7. J.C. de Man, M. Rogosa, M.E. Sharpe, *J. Appl. Bacteriol.*, **1960**, *23,* 130-135.
8. E. Both, Cs.Z. Kibédi Szabó, É. György, É. Tamás, I. Miklóssy, B. Ábrahám, Sz. Lányi*, Studia UBB Chemia,* **2009**, *Special Issue 2*, 27-34.

STUDIA UBB CHEMIA, LV, Sp.Iss., 2010

# ISOLATION AND IDENTIFICATION OF PROBIOTIC LACTIC ACID BACTERIA AND EXAMINATION OF THEIR TOLERANCE AGAINST STRESS FACTORS

**FÜSTÖS ZOLTÁN [a,b], BELÁK ÁGNES[b], MARIANA FERDEŞ[a], MARÁZ ANNA[b]**

**ABSTRACT.** Probiotics are living microorganisms which have beneficial effect on the metabolism of the host organism when they pass into the large intestine. The number of living cells declines dramatically when they are going through the gastro-intestinal system, thus consumption of probiotic products with higher cell concentrations is recommended. Potential probiotic lactic acid bacterial strains were isolated from different yoghurts and food supplements and identified by traditional microbiological and molecular biological methods. According to the results the isolated strains belonged to Lactobacillus acidophilus, L. casei, L. rhamnosus, L. helveticus and L. delbrueckii subsp. bulgaricus. The tolerance of L. acidophilus, L. casei and L. rhamnosus against lactic acid, sodium chloride and sucrose was investigated by determination of the growing ability of the strains in a culture media containing different concentrations of these compounds. Among the tested strains L. rhamnosus had similar growth rate as L. casei in lactic acid and media sucrose containing, while it showed a better tolerance for sodium chloride. L. acidophilus strain proved to be more sensitive for lactic acid and sucrose as the above mentioned strains.

***Keywords:*** *probiotics, isolation, identification, stress tolerance*

## INTRODUCTION

The concept of probiotics is not new and probiotic products have been consumed by humans in the form of fermented foods for thousands of years. Health benefits of probiotics have also been long known because Hippocrates and other scientists in the early ages reported that fermented milk could cure some disorders of the digestive system. Even Biblical scriptures mentioned the use of probiotics when treating body ailments. It was in 1907 when Elie Metchnikoff first proposed the concept of probiotics as it is known today. He observed that consuming large amounts of fermented milk products

[a] *University Politehnica of Bucharest, Faculty of Applied Chemistry and Material Science, Str. Polizu, Nr.1-7, RO-011061 Bucharest, Romania, fustoszoli@yahoo.com*
[b] *Corvinus University of Budapest, Faculty of Food Science, Department of Microbiology and Biotechnology, Somlói út 14-16., H-1118 Budapest, Hungary, anna.maraz@uni-corvinus.hu*

containing lactobacilli prolonged the life of humans and he gave the first scientific explanation for the beneficial effects of lactic acid bacteria being present in fermented milk. Today it is accepted that the daily intake of these probiotics contributes to improving and maintaining a well balanced intestinal biota and prevents gastrointestinal disorders (Ranadheera et al., 2010). According to the definition of the World Health Organization probiotics are living microorganisms which - when administered in adequate amounts - provide a health benefit to the host. Beneficial effects are manifested by, for example, the inhibition of pathogenic bacteria, the synthesis of vitamin B and bacteriocins in the colon, by lowering of ammonia level of the blood, the absorption of cholesterol, and the inhibition of tumour formation (Capela et al., 2005; Kos et al., 2007).

An important question to be answered is how much the "adequate amounts" of probiotics are. The level of viable microorganisms in probiotic foods has to be at least $10^7$ cfu/g to provide better efficacy in regulating beneficial effects (Ranadheera et al., 2010). In most cases the number of viable microorganisms in probiotic products decreases dramatically during the storage process because of the physico-chemical properties (such as low pH, buffering capacity, etc.) of food carriers used for probiotic delivery. These physical and chemical characteristics present significant stress factors that influence the survival of probiotic microorganisms (Gupta and Abu-Ghannam, 2012, Ranadheera et al., 2010).

The increasing application of probiotic cultures in food products underlines the need for an exact identification of these beneficial microorganisms and distinguishing them from the original microbial population of the digestive system. Moreover, certain probiotic activities are not only species- but also strain-specific; therefore, the identification of probiotic bacteria is indispensable at least at species level. Current techniques used for the identification and typing of microorganisms comprise multiple DNA-based methods such as pulsed-field gel electrophoresis (PFGE), randomly amplified polymorphic DNA (RAPD) analysis, ribotyping and species-specific PCR (Kos et al., 2007).

The majority of known probiotic bacteria belong to *Lactobacillus* (e.g. *L. bulgaricus, L. acidophilus, L. casei, L. helveticus, L. lactis, L. salivarius, L. plantarum*) or *Bifidobacterium* spp., but certain strains of *Bacillus, Streptococcus*, *Pediococcus* and *Enterococcus* spp. also proved to have probiotic effects (Musikasang et al., 2009).

The main purpose of our research was to isolate and identify potential probiotic lactic acid bacteria and determine their susceptibility against the stress factors typical for the different food environments. The isolation, identification and examination of the growth of probiotic lactic acid bacteria are significant milestones of the main objectives, involved in the title of this paper as well.

## RESULTS AND DISCUSSIONS

### Isolation of probiotic bacteria

Samples were taken from three commercially fermented dairy products (yoghurts) and two food supplements (a synbiotic product for teenagers and adults, and a probiotic infant formula). From the samples which were inoculated and cultivated on deMan-Rogosa Sharpe (MRS) agar plates supplemented with the antifungal antibiotic Nystatin, altogether twenty-six colonies were isolated that had differences in colony morphology (Table 1.). From the probiotic yoghurts type 1 and type 2, four and two bacteria were isolated, respectively. Two strains were isolated from normal yoghurts, while the majority of the isolates originated from synbiotic capsules (12 strains) and probiotic infant formula (6 strains). Based on microscopic cell morphology examination four strains (marked with asterix in Tabel 1.) showed typical *Bifidobacterium* properties, thus they were not used for further investigations.

**Table 1.** The sources and codes of isolated strains

| Nr. | Products used for sampling | Code of isolates |
|---|---|---|
| 1 | Probiotic yoghurt, type 1 | VA1 |
| 2 | Probiotic yoghurt, type 1 | VA2 |
| 3 | Probiotic yoghurt, type 1 | VA3 |
| 4 | Probiotic yoghurt, type 1 | VA4 |
| 5 | Normal yoghurt | EMJ1 |
| 6 | Normal yoghurt | EMJ2 |
| 7 | Probiotic yoghurt, type 2 | BJP1 |
| 8 | Probiotic yoghurt, type 2 | BJP2 |
| 9 | Synbiotic capsule | PB1 |
| 10 | Synbiotic capsule | PB2 |
| 11 | Synbiotic capsule | PB3 |
| 12 | Synbiotic capsule | PB4 |
| 13 | Synbiotic capsule | PB5 |
| 14 | Synbiotic capsule | PB6 |
| 15 | Synbiotic capsule | PB7 |
| 16 | Synbiotic capsule | PB8 |
| 17 | Synbiotic capsule | PB9 |
| 18 | Synbiotic capsule | PB10 |
| 19 | Synbiotic capsule | PB11 |
| 20 | Synbiotic capsule | PB12 |
| 21 | Probiotic infant formula | BPK1* |
| 22 | Probiotic infant formula | BPK2* |
| 23 | Probiotic infant formula | BPK3* |
| 24 | Probiotic infant formula | BPK4* |
| 25 | Probiotic infant formula | BPK5 |
| 26 | Probiotic infant formula | BPK6 |

*- strains proved as bifidobacteria

## Gram staining and catalase test

All the examined isolates (22) stained positively with Gram staining procedure and gave negative catalase reaction, which are the typical characteristics of lactic acid bacteria (Salminen et al., 2004).

## Differentiation of the isolates on mMRS-BPB chromogenic medium

Since anaerobic conditions were used during the isolation of bacteria the *Bifidobacterium* species - if present in the products - could also form colonies on MRS agar. As species of *Bifidobacterum* are also Gram-positive and catalase-negative bacteria, they could not be distinguished from *Lactobacillus* species using Gram staining and catalase test. However, by the application of the modified deMan-Rogosa Sharpe agar supplemented with bromophenol blue (mMRS-BPB) as culturing medium under anaerobic conditions, the differentiation of these two genera was feasible (Lee and Lee, 2008). Moreover, this medium enabled the differentiation of the most important *Lactobacillus* species based on the marked differences in colony morphology. Figure 1. shows the differences between colony morphology of *Lactobacillus rhamnosus* PB10 and *Bifidobacterium animalis* subsp. *lactis* BPK6 strains.

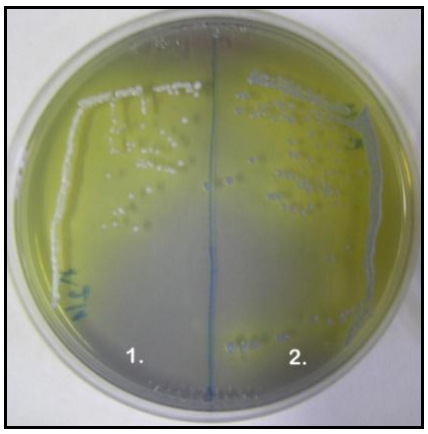


**Figure 1.** Colonies of *Lactobacillus rhamnosus* PB10 (1.) and *Bifidobacterium animalis* subsp. *lactis* BPK6 (2.) on mMRS-BPB agar grown under anaerobic conditions for 48 hours

## Identification and typing of bacterial isolates by molecular biological methods

After differentiating the isolates on mMRS-BPB agar the selected isolates were cultivated in MRS broth and the cellular DNA was extracted by the method described by Hoffman and Winston (1987).

The isolates were genotyped by using the Randomly Amplified Polymorphic DNA (RAPD-PCR) method with the application of the M13 primer (Rossetti and Giraffa, 2005). The PCR products were separated by agarose gel electrophoresis and visualized by ethidium-bromide staining. Figure 2. shows an example for RAPD patterns (fingerprints) of the bacterium isolates. Based on the comparison of these fingerprints with each other and with that of the reference strains (BC2 - *Lactobacillus acidophilus* N2, BC3 - *Lactobacillus delbrueckii* subsp. *bulgaricus* B397, BC4 – *Lactobacillus rhamnosus* VT1, BE – *Lactobacillus sakei* DSM 20017) the clonal identity of the isolates was determined.

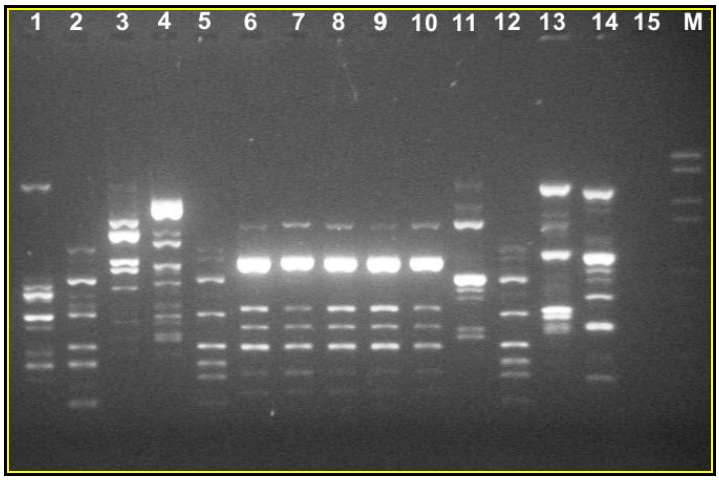


**Figure 2.** Example of RAPD-PCR patterns on agarose gel. 1- BC2; 2- BC3; 3- BC4; 4- BE; 5- PB1; 6- PB2; 7- PB3; 8- PB4; 9- PB5; 10- PB6; 11- PB7; 12- PB8; 13- BPK5; 14- BPK5; 15- control; M-molecular weight marker

It was found that the bacterium isolates belonged to eight different clusters (Table 2). Moreover, an evaluation of the results made it possible to separate the isolates originated from the same products into different groups (for instance: VA2, VA4 - from probiotic yoghurt type 1; PB3, PB8, PB10 - from symbiotic capsule; BPK6, BPK5 - from infant formula; and EMJ1 - from a normal yoghurt).

Single representative isolates were selected from each cluster, with the exception of cluster 1 where two isolates were elected from. In the latter case, slight differences in the RAPD patterns of the VA2 and BJP2 isolates were recognised.

Identification of the isolates at species level was done by sequence analysis. 16S rDNA sequences flanked by the 27f-519r primer pair (Thanantong et al., 2006) were amplified by a PCR reaction. The amplification resulted in PCR products of approximately the same size; however, in case of BPK5 isolate the amplicon proved to be smaller in size (Figure 3.).

**Table 2.** Eight different similarity clusters of the RAPD-PCR analysis

| | Clusters | | | | | | | |
|---|---|---|---|---|---|---|---|---|
| | **1** | **2** | **3** | **4** | **5** | **6** | **7** | **8** |
| **Code of the Isolates** | VA1<br>VA2<br>VA3<br>BJP1<br>BJP2 | VA4 | PB2<br>PB3<br>PB4<br>PB5<br>PB6<br>PB 9 | PB1<br>PB 8<br>PB 11<br>PB12 | PB7<br>PB10 | BPK 6 | PBK 5 | EMJ1<br>EMJ2 |

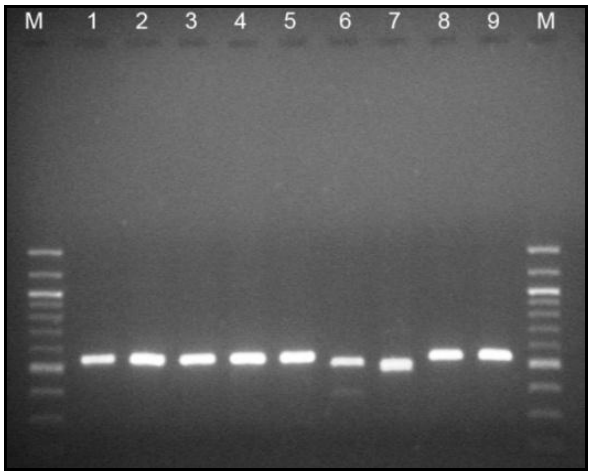


**Figure 3.** Agarose gel electrophoresis of the 16S rDNA-specific PCR products. M- molecular weight marker; 1- VA2; 2- VA4; 3- PB3; 4- PB8; 5- PB10; 6- BPK6; 7- BPK5; 8- BJP2; 9- EMJ1

**Table 3.** List of species identified by DNA sequencing

| **Strains** | **Results of identification** | **Similarity index** | **RAPD cluster** |
|---|---|---|---|
| BJP2 | *Lactobacillus acidophilus* | 100% | 1 |
| VA2 | *Lactobacillus acidophilus* | 100% | 1 |
| VA4 | *Lactobacillus casei* | 99% | 2 |
| PB3 | *Lactobacillus helveticus* | 99% | 3 |
| PB8 | *Lactobacillus casei* | 99% | 4 |
| PB10 | *Lactobacillus rhamnosus* | 99% | 5 |
| BPK6 | *Bifidobacterium animalis* subsp. *lactis* | 99% | 6 |
| BPK5 | Could not be evaluated | - | 7 |
| EMJ1 | *Lactobacillus delbrueckii* subsp. *bulgaricus* | 99% | 8 |

The PCR products obtained were sequenced and the sequences were aligned to the 16S rDNA bacterial sequences found in the GeneBank. The species identity of our isolates is indicated in Table 3.

Based on the results of RAPD analysis done by the application of M13 primer and 16S rDNA sequencing it can be concluded that the same strains of *Lactobacillus acidophilus* could be isolated from probiotic yoghurt type 1 and type 2 that are products of different companies.

## Examination of growing ability of the strains under different stress conditions

Determination of cell concentrations was performed by measuring the optical density (OD) at 600 nm in different time points. Growth curves are illustrated on Figures 4-12.

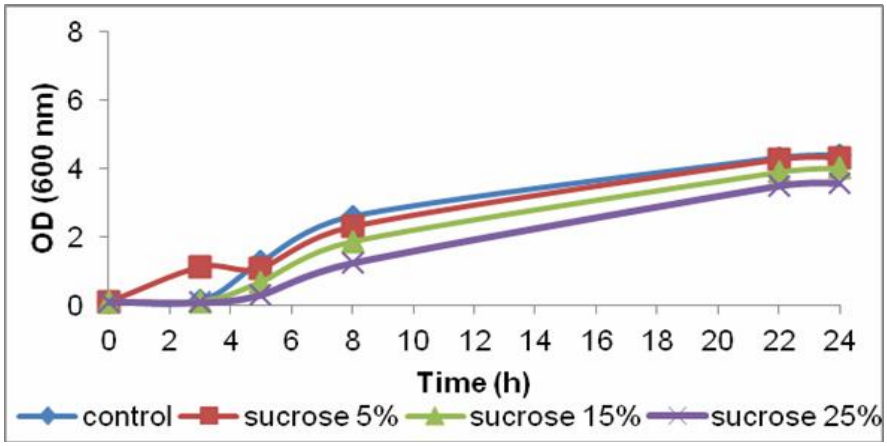


**Figure 4.** The growth curves of *L. acidophilus* VA2 in different sucrose concentrations (pH 5.7)

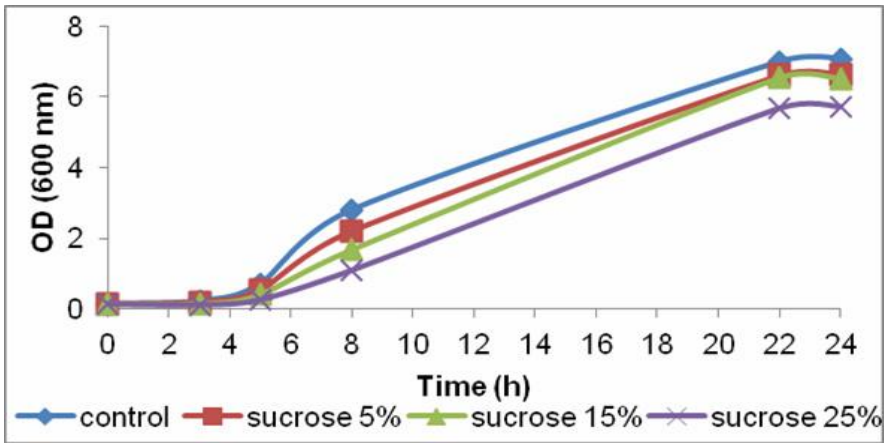


**Figure 5.** The growth curves of *L. rhamnosus* PB10 in different sucrose concentrations (pH 5.7)

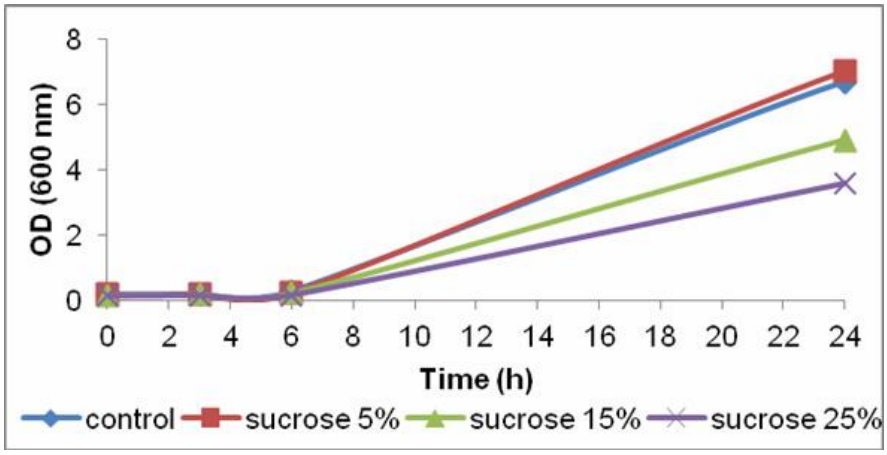


**Figure 6.** The growth curves of *L. casei* PB8 in different sucrose concentrations (pH 5.7)

Comparing the results of growing ability under different sucrose concentrations – as shown in Figures 4-6 – it can be assessed as a general rule that the higher amount of sucrose in the culture media presents an important stress factor. Moreover, there is an observable difference between the three strains belonging to different species, namely that *L. casei* and *L. rhamnosus* had approximately the same growth kinetic, but *L. acidophilus* showed a declining growth rate.

The sodium chloride tolerance (Figures 7-9) of these three strains showed that the greatest growth ability could be detected in the case of *L. rhamnosus*, followed by the *L. acidophilus* strain. Interestingly, *L. casei* showed the highest sensitivity against this stress factor.

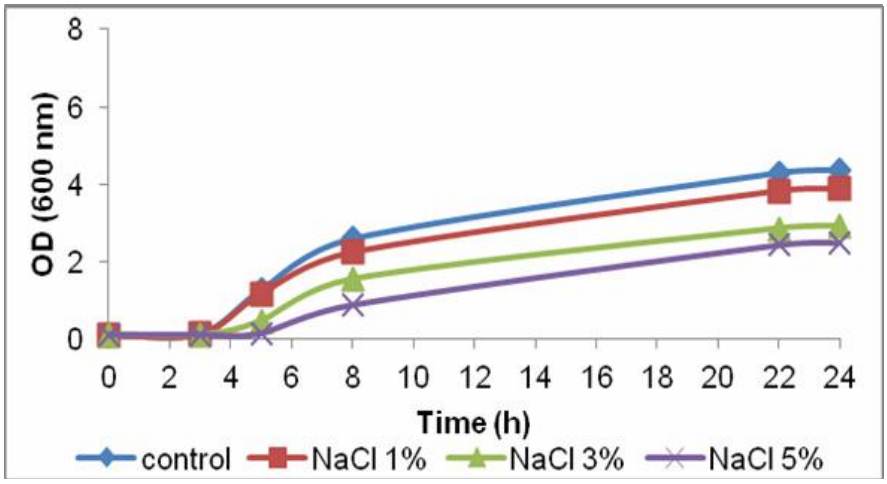


**Figure 7.** The growth curves of *L. acidophilus* VA2 in different NaCl concentrations (pH 5.7)

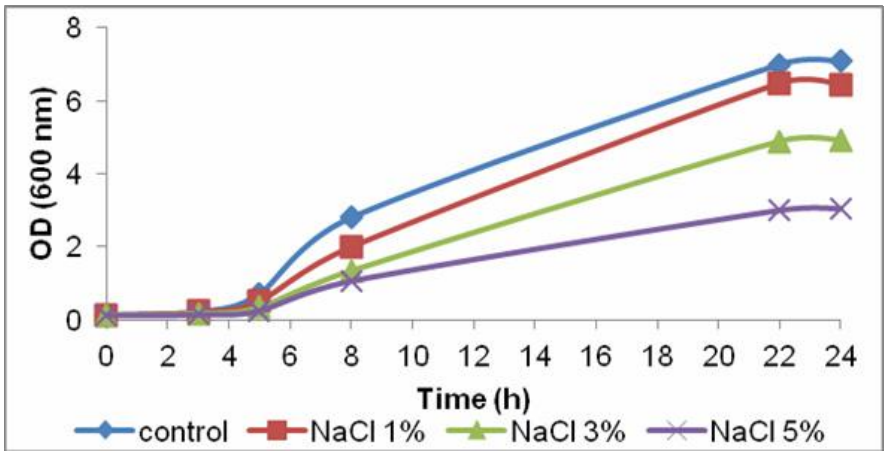


**Figure 8.** The growth curves of *L. rhamnosus* PB10 in different NaCl concentrations (pH 5.7)

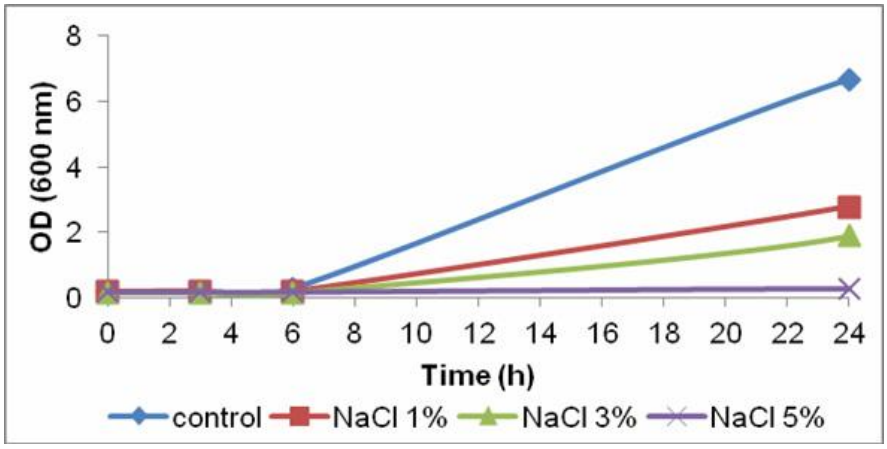


**Figure 9.** The growth curves of *L. casei* PB8 in different NaCl concentrations (pH 5.7)

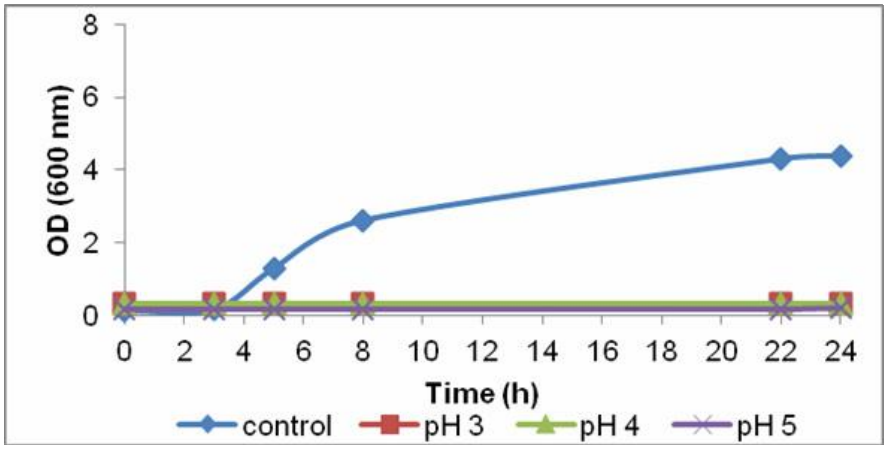


**Figure 10.** The growth curves of *L. acidophilus* VA2 at different pH values. pH of the control was 5.7

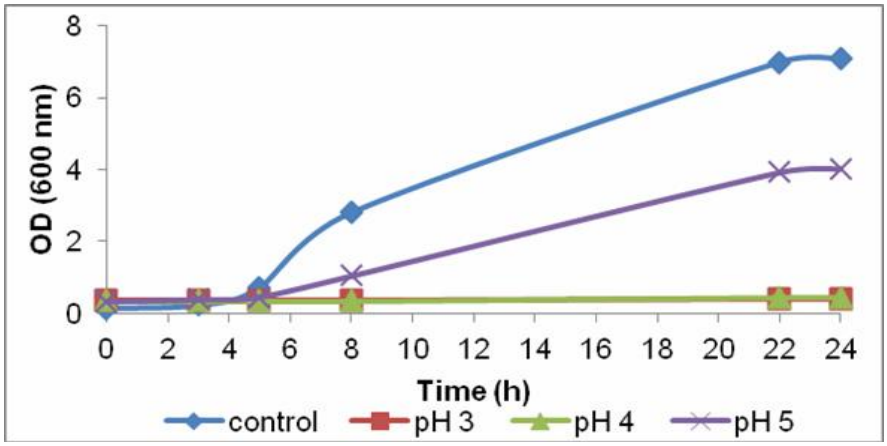


**Figure 11.** The growth curves of *L. rhamnosus* PB10 at different pH values. pH of the control was 5.7

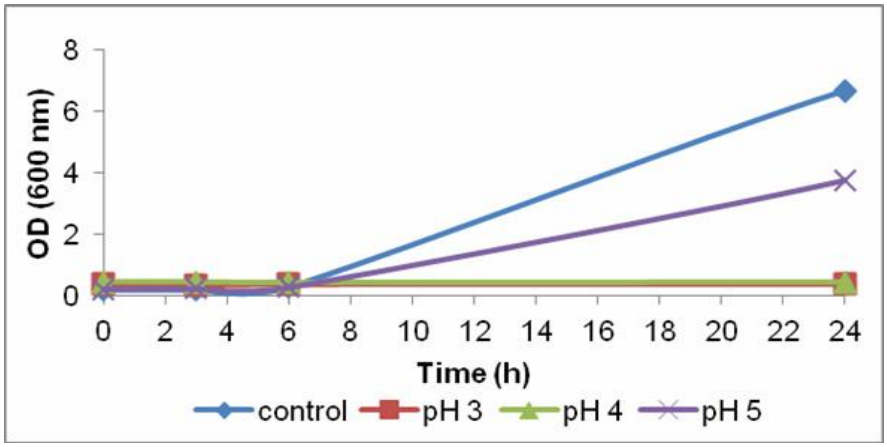


**Figure 12.** The growth curves of *L. casei* PB8 at different pH values. pH of the control was 5.7

According to the results illustrated on Figures 9-12 lactic acid which was used for the regulation of pH had the most significant growth inhibitory effect among the three investigated stress factors. The growth of the strains could be observed only above pH 4, and there was a similar growth tendency observed in the case of *L. casei* and *L. rhamnosus*. However, the weak acid tolerance of *L. acidophilus* was surprising, because this species is known as having a good acid tolerance.

## CONCLUSIONS

Potential probiotic lactic acid bacteria were isolated and discriminated from the bifidiobacteria and each other by using the chromogenic MRS medium mMRS-BPB. Based on the RAPD-PCR typing followed by molecular

identification of the isolates five *Lactobacillus* and one *Bifidiobacterium* species were identified. Three of them (*Lactobacillus acidophilus* VA2, *L. casei* PB8 and *L. rhamnosus* PB10) were selected and their growing abilities were investigated in culture media containing different concentrations of lactic acid, sodium chloride and sucrose. Comparing the sensitivity of the three strains against these stressing factors we can conclude that the *L. rhamnosus* had a similar growth rate as *L. casei* in media containing lactic acid or sucrose, while it showed better tolerance for sodium chloride than the other two species. *L. acidophilus* proved to be sensitive to sucrose and lactic acid but it had a better tolerance against sodium chloride, than *L. casei*. As the final conclusion it can be said that *L. rhamnosus* had the best tolerance against the investigated stress conditions, which suggests the future use of this species for microencapsulation or as a probiotic supplement in various food products.

## EXPERIMENTAL SECTION

### Isolation of probiotic bacteria

An initial suspension of the collected samples (yoghurts and food supplements) was made in salt-peptone solution (0.85% NaCl and 0.1% Bacto-peptone). After this step ten-fold dilution series were prepared from which 0.1 ml quantities were spread on MRS agar (Merck 1.10661.0500) containing 0.01% Nystatin. After incubation for 48 hours at 37°C under anaerobic conditions (in anaerobic jar containing anaerobic sachet - Anaerocult A, Merck 1.13829.0001) pure cultures of the isolated colonies having different morphological properties were made using MRS agar plates.

### Gram staining and catalase test

From the pure cultures of the isolates cultivated in MRS broth, Gram staining and catalase test were performed as it is described in the Bacteriological Analytical Manual (BAM, 1998). The catalase test was done by dropping 3% $H_2O_2$ solution to the bacterial colonies grown on agar plates, and gas formation was checked in each case.

### Differentiation on mMRS-BPB agar

The modified deMan-Rogosa Sharpe agar containing bromophenol blue (Lee and Lee, 2008) was prepared in the following way: required quantity of deMan-Rogosa Sharpe agar granule and L-cysteine-HCl (final conc. 0.05%) were dissolved in 1000 ml of distilled water and bromophenol blue (BPB) was added to the final concentration of 0.002%. The pH was adjusted to 6.5 ± 0.2 and then it was autoclaved. The isolates were grown on this agar under anaerobic conditions for two days at 37°C.

## RAPD-PCR analysis

The selected isolates were cultivated in MRS broth for 24 hours at 37°C under aerobic conditions. The DNA was extracted from 1 ml cultures as it is described by Hoffman and Winston (1987).

Genomic DNA from each isolate was used as a template for PCR fingerprinting (RAPD-PCR) using the M13 minisatellite primer (Rossetti and Giraffa, 2005, Albesharat et al., 2011). Amplification reactions were performed according to the optimised protocol: denaturation at 95°C for 5 min was followed by 35 cycles of 95°C for 30 sec (denaturing), 40°C for 30 sec (annealing) and 72°C for 1.5 min (extension). Final extension was carried out at 72°C for 5 min. Reactions were carried out in 25 µl final volume. The reaction mixture contained 10x DNA polymerase puffer, 2.5 µmol of M13 primer, 2 µl of extracted DNA, 1.25 mmol $MgCl_2$, 0.3 U of *Taq* polymerase (DyNAzyme™ II, Finnzymes) and 0.3 mmol of dNTP. PCR amplified DNAs were separated by gel electrophoresis (1.2 V $cm^{-1}$) using 1.5% (w/v) agarose gel and visualised by staining with ethidium bromide. DNA molecular size marker MW VI. (Boehringer Mannheim, Germany) was used to estimate the size of the amplicons.

## Molecular identification of bacterium isolates

Specific PCR targeting the 16S rDNA (Pang et al., 2011) was used for the amplification of an approximately 500 bp long sequence by the 27f and 519r primers (Thanantong et al., 2006). The reaction was carried out according to the following protocol: initial denaturation for 5 minutes at 95°C was followed by 35 cycles of 95°C for 30 sec (denaturing), 55°C for 1 min (annealing) and 72°C for 1 min (extension). Final extension was carried out at 72°C for 3 min. Reactions were carried out in a final volume of 25 µl. The reaction mixture contained 10x DNA polymerase puffer, 2.5 µl of 27f and 519r primers (2 pmol/µl for each), 1 µl of template DNA, 1 mmol $MgCl_2$, 0.3 U of *Taq* polymerase (DyNAzyme™II, Finnzymes) and 0.375 mmol of dNTP. PCR amplicons were visualised by ethidium bromide staining after agarose gel electrophoresis (1.2 V $cm^{-1}$) in 1% (w/v) agarose gel.

Sequencing of the PCR amplified region (500 bp) of the 16S rDNA was applied to identify the isolates at species level. DNA sequencing was carried out by the BayGen Institute, Szeged, Hungary. Identification of the isolates was performed by comparing the obtained nucleotide sequences with that of known bacteria deposited in the GeneBank using the BLAST program (http://blast.ncbi.nlm.nih.gov/Blast.cgi).

## Determination of the growth curves

Three strains belonging to *Lactobacillus acidophilus* VA2, *L. casei* PB8 and *L. rhamnosus* PB10 were selected for further investigations. These strains were cultivated under aerobic conditions at 37°C for 24 hours in MRS

broth. From these cultures 1 ml was inoculated into MRS broth as a control having initial pH 5.7 and in MRS broth with pH 3.0, 4.0, 5.0 adjusted by lactic acid as well as different concentrations of NaCl (1%, 3% and 5%) or sucrose (5%, 15% and 25%). During the incubation of the strains the optical density (OD) was measured at 600 nm (Rao et al, 2004, Ayad et al., 2006).

**ACKNOWLEDGMENTS**

The authors are grateful to the Hungarian Ministry of Education & Culture and the Balassi Institution for providing a fellowship for Zoltán Füstös at Corvinus University of Budapest.

## REFERENCES

1. R.D.C.S. Ranadheera, S.K. Baines, M.C. Adams, *Food Research International*, **2010**, *43,* 1-7.
2. B. Kos, J. Šušković, J. Beganović, K. Gjuračić, J. Frece, C. Iannaccone, F. Canganella, *World Journal of Microbiology and Biotechnology*, **2008**, *24*, 699–700.
3. P. Capela, T.K.C. Hay, N.P. Shah, *Food Research International*, **2006**, *39*, 203.
4. S. Gupta, N. Abu-Ghannam, *Critical Reviews in Food Science and Nutrition*, **2012**, *52*, 183-199.
5. H. Muskiasang, A. Tani, A. H-kittikun, S. Maneerat, *World Journal of Microbiology and Biotechnology,* **2009**, *25*, 1337.
6. S. Salminen, A. von Wright, A. Ouwehand, "Lactic Acid bacteria", Marcel Dekker, Inc., New York, 2004, chapter 1.
7. H.M. Lee, Y. Lee, *Letters in Applied Microbiology*, **2008**, *46*, 676–681.
8. C. Hoffman, F. Winston, *Gene*, **1987**, *57*, 267-272.
9. L. Rossetti, G. Giraffa, *Journal of Microbiological Methods*, **2005**, *63*, 135-144.
10. N. Thanantong, S. Edwards, O.A.E. Sparagano, *Annals of the New York Academy of Sciences*, **2006**, *1081*, 276-279.
11. "Bacteriological Analytical Manual" R32: Gram Stain, FDA, 8th Edition, Revision A, **1998**, chapter 2.
12. R. Albesharat, M.A. Ehrmann, M. Koraklib, S. Yazajic, R.F. Vogela, *Systematic and Applied Microbiology*, **2011**, *34*, 148-155.
13. H. Pang, M. Zhang, G. Qin, Z. Tan, Z. Li, Y. Wang, Y. Cai, *Animal Science Journal*, **2011**, *82*, 642–653.
14. M.S. Rao, J. Pintado, W.F. Stevens, J.P. Guyot, *Bioresource Technology*, **2004**, *94*, 332.
15. E.H.E. Ayad, N. Omran, M. El-Soda, *Lait*, **2006**, *86*, 319.

STUDIA UBB CHEMIA, LV, Sp.Iss., 2010

# PREPARATION AND MODELLING OF THE STRUCTURE OF TRANSFERRIN-$Fe^{3+}$-AZIRIDINE-CARBOXYLATE COMPLEX

**GÁLICZA JUDIT[a], ORBÁN CSONGOR KÁLMÁN[a], KILÁR FERENC[b,c], MIKLÓSSY ILDIKÓ[a,d], ÁBRAHÁM BEÁTA[a,d], LÁNYI SZABOLCS[a,d]**

**ABSTRACT.** The absorption of the iron ions by the cells is realised through a transport protein, the transferrin, via receptor mediated endocytosis. The presence of a synergistic anion (which *in vivo* is the bicarbonate) is crucial for stabilizing the iron-binding site of human serum-transferrin. This efficient cellular uptake pathway has been exploited for the site-specific delivery of anticancer drugs. We substituted bicarbonate with another synergistic anion, the aziridine carboxylate, which possesses cytotoxic effect against the cancer cells. Using in silico methods we determined, that this substitution has no significant change in the polypeptide folding or domain orientation in the structure of human serum transferrin.

***Keywords:*** *human serum transferrin, iron uptake, synergistic anion, in silico method*

## INTRODUCTION

Human serum transferrin is a glycoprotein, member of the transferrins family, which are an important class of iron-binding proteins that are widely distributed in the physiological fluid of vertebrates. The primary role of serum transferrin is therefore to bind, transport and release of the iron to supply the growing cells. The most important role of the iron is in the newly synthesised hemoglobin synthesis in new blood cells [1]. Serum transferrin is mainly synthesized by hepatocytes in liver in a concentration of 2.5 mg/ml, but only 30% is saturated with iron in the plasma [2].

The human serum transferrin contains 678 amino acid residues and, including the two asparagine-linked glycans, has an overall molecular weight of ~79,550 kDa. This protein is divided into two evolutionary related lobes, in

[a] *POLITEHNICA University of Bucharest, Applied Chemistry and Material Science, Bucharest, 010737, Romania*
[b] *University of Pécs, Medical School, Institute of Bioanalysis, Pécs, 7624, Hungary*
[c] *University of Pécs, Department of Analytical and Environmental Chemistry, Pécs, 7624, Hungary*
[d] *SAPIENTIA University, Faculty of Technological and Social Sciences, Technical Science Department, Miercurea Ciuc, 530104, Romania*

which 40% of the residues are identical. The N-lobe consist from amino acid residues ranging from1 to 336 and C-lobe consist from residues ranging from 337 to 678 [3], being linked by a short spacer sequence (figure 1).

**Figure 1.** The X-ray cristal structure of N-termianl lobe of human serum transferrin [Protein Data Bank-1A8E (http://www.rcsb.org/pdb/)]

Each lobe contains two domains comprising a series of α-helices, which overlay a central β-sheet backbone, forming a deep, hydrophilic metal ion-binding site (Figure 2). The binding site in both N- and C-terminal lobes has four conserved amino acids including two tyrosine, one aspartic acid and one histidine (N-terminal lobe – Asp-63, Tyr-95, Tyr-188 and His-249) [4]. Iron is bound in a distorted octahedral coordination involving four amino acid ligands and two oxygen atoms donated by a carbonate molecule to stabilize the iron atom [5]. The synergistic relationship of metal and anion refers to the fact that neither binds tightly in the absence of the other.

When iron is released, the two domains of each lobe, termed the NI- and NII domains and the CI- and CII-domains, rotate around a hinge to change the protein conformation from „closed" to "open". While the iron ligands play a primary role in iron binding, other residues (including Gly-65, Glu-83, Tyr-85, Arg-124, Lys-206, Ser-248 and Lys-296 in the transferrin N-lobe) make up a second shell network that also contributes to the stabilization of the iron binding site [4, 6].

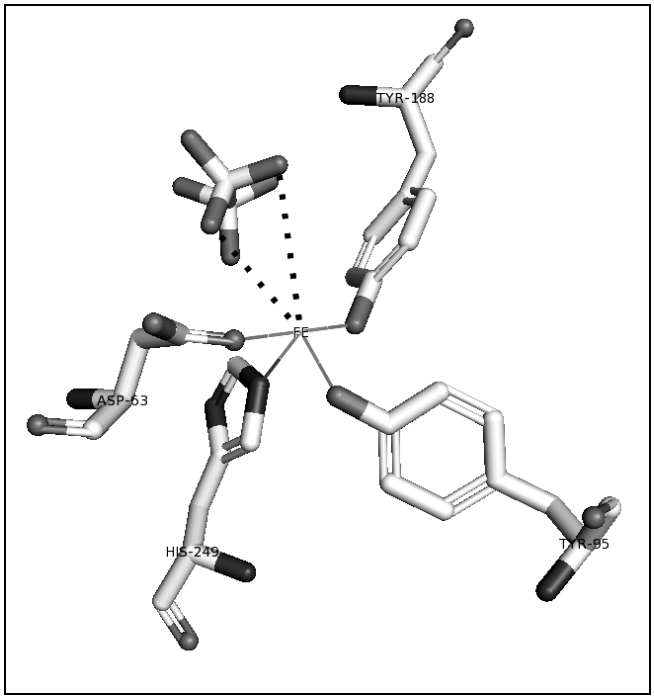


**Figure 2.** The iron binding site of N-lobe of human serum transferrin

The absorption of transferrin-coupled iron ions by the cells is through the transferrin-transferrin receptor system, via receptor mediated endocytosis. Transferrin has capability to bind *in vitro* several other metals (ex. $Ga^{3+}$ $In^{3+}$, $Bi^{3+}$, $Ti^{4+}$, $Ru^{3+}$) expect iron ions [7-13] or it have possibility to replace bicarbonate synergistic anions to another.

In the literature are described many transferrin complexes formatted with different type of anions: inorganic anions (sulphate, sulphite, nitrate, nitrite, phosphate, borate), aldehydes and ketones (dihydroxyacetone, glyceraldehyde), monocarboxylic acids (acetate, propionate) and several monocarboxylic acids with proximal aldehyde, ketone, alcohol- (glycolate, glioxylate), amino- (glycine, phenylalanine), or thiol functional groups (thioglycolate), dicarbxylic acids (oxalate, malonate) [2, 14-17].

Our aim is to replace the bicarbonate anion with aziridine-carboxylate at the iron binding of human apo-Tf.

Aziridine is a three-membered heterocycle with one amine group and two methylene groups. This functional group is content of a series natural and synthetic organic compound. The simple natural alkaloid, aziridine also called ethyleneimine was detected in various foodstuffs including baker's yeast (*Sacharomices cerevisiae*). Aziridine-2-carboxylic acid (Figure 3.), a metabolite, is isolated from scaly wood mushroom (*Agaricus silvaticus*) [18, 19].

In the literature there are described the crystal structures of the transferrin complexes formed with different anions, ex. oxalate or bicarbonate, but there is no information about binding geometry of aziridine-carboxylate to transferrin's binding site, this anion was newer complexed or conjugated with Tf. Therefore, we realized a molecular model using a docking program (AutoDock Vina) to predict the possibility of using aziridine-carboxylate as synergistic anion at iron binding of transferrin.

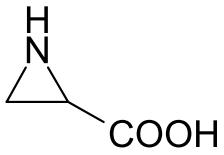


**Figure 3.** Chemical structure of aziridine-2-carboxilic acid

Based on these findings the Tf-Fe(III)-aziridine-carboxylate complex was prepared. The complexation reaction was analysed using high performance capillary electrophoresis techniques: capillary zone electrophoresis (CZE) and capillary isoelectric focusing (cIEF).

## RESULTS AND DISCUSSION

There are data in the literature regarding to the binding of oxalate and bicarbonate to the transferrin, however there is no information about the binding of aziridine-carboxilate to the protein. Therefore, in order to verify the ability of transferrin to bind the aziridine-carboxilate anion we used molecular docking technique. For this purpose we used AutoDock Vina. The results were visualised in PyMol.

In Figure 4 is presented the obtained bond lengths and binding geometry. The distances obtained from the model are compared with crystallographic data from the literature regarding the oxalate and bicarbonate anions binding to the transferrin and are presented in Table 1.

**Table 1.** Bond distances in metal and anion sites.

| Anion bond | Distance (Å) |
|---|---|
| Fe-carbonate1 O1 | 2.06 |
| Fe-carbonate1 O2 | 2.24 |
| Fe-carbonate2 O1 | 1.99 |
| Fe-carbonate2 O2 | 2.42 |
| Fe-oxalate O1 | 2.05 |
| Fe-oxalate O2 | 2.16 |
| Fe-aziridine-carboxylate O1 | 2.6 |
| Fe-aziridine-carboxylate O2 | 2.7 |

The crystallographic data and kinetic analysis show that the oxalate in the oxalate complex to the iron is bond more tightly than in the case of bicarbonate complex [16]. Our results show that the aziridine-carboxylate is the most loosely bound by transferrin from the anions. This result was however expected taking into account the slightly larger size of the anion. This loose bond can have the advantage of ease of release of the anion and the iron once reached inside the cell.

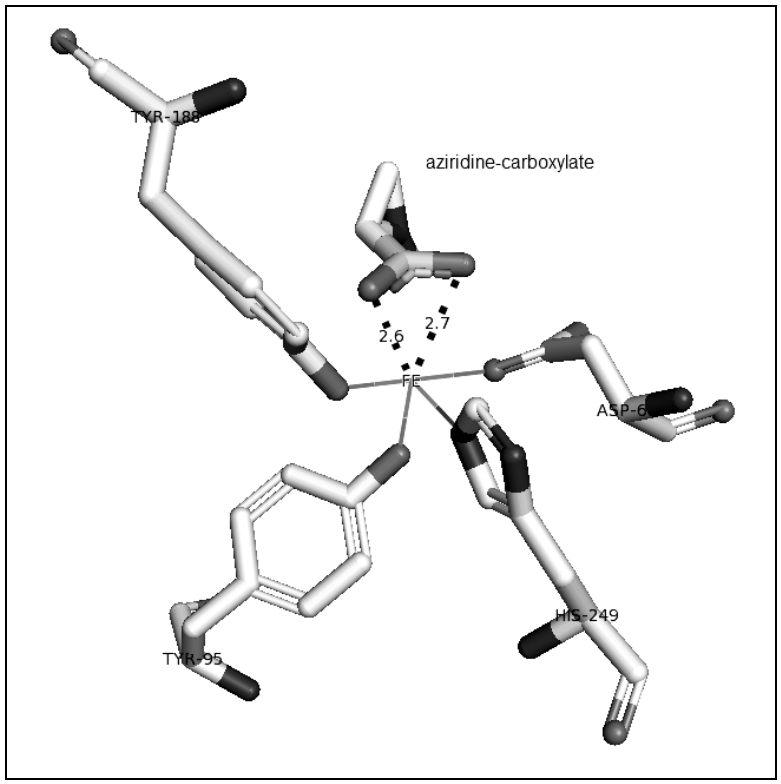


**Figure 4.** The geometry of the binding of the aziridine-carboxylate to the holo-transferrin's N-lobe (1A8E) trough iron (theoretical model).
The distances between the anion and the iron is expressed in Å. The model was realized with AutoDock Vina, and visualized by PyMol, represented as sticks.

In Figure 5-a, b are shown the 3D structure of the iron complexed aziridine-carboxylate human serum transferrin. Substitution of carbonate to another synergistic anion, such as aziridine-carboxylate produces no significant changes in polypeptide folding or domain orientation in human serum transferrin as revealed by our structure.

Based on these findings we propose that aziridine-carboxylate binds in a symmetrical bidentate fashion, in the same manner as the oxalate. The overall results of this molecular docking study and the data from the literature support the synthesis of transferrin-iron-aziridine-carboxylate complex.

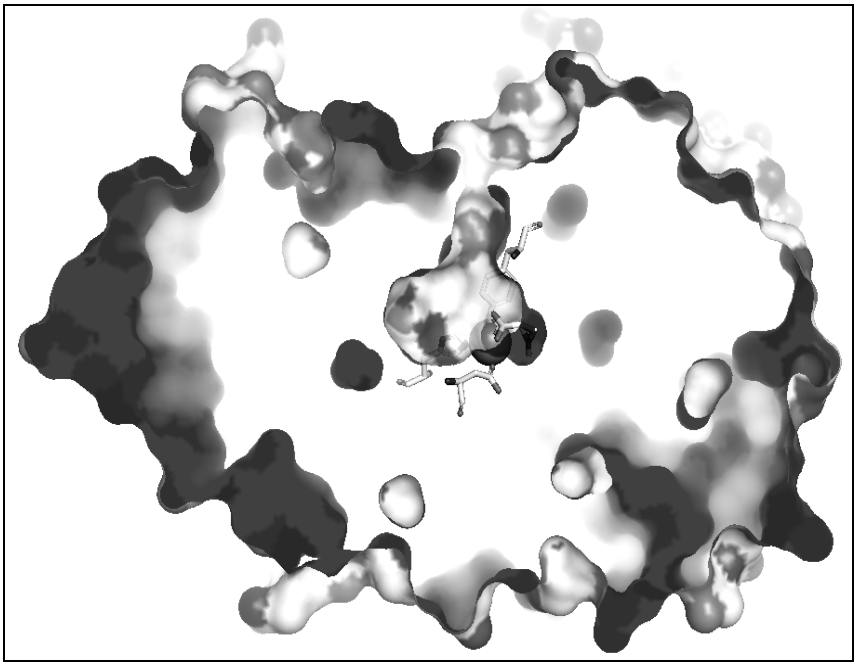

**A**

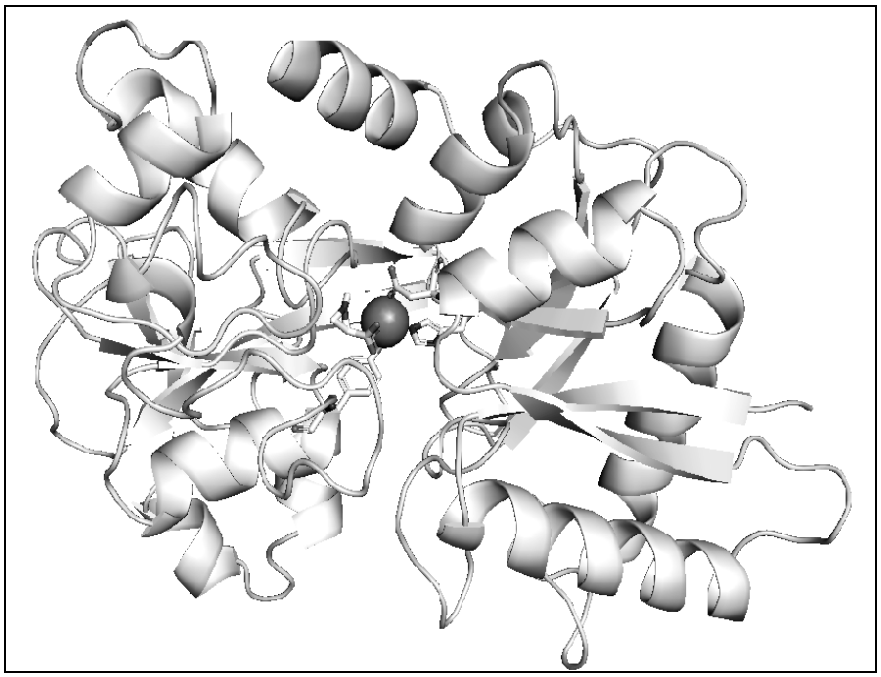

**B**

**Figure 5.** Theoretical model of the binding of aziridine-carboxylate to the active site of the N-lobe holo-transferrin (1A8E) trough iron.
**A**: surface representation of the N-lobe, the residues from the active site and the aziridine-carboxylate are represented as sticks, iron as ball.
**B:** ribbons representation of the N-lobe, residues from the active site and the aziridine-carboxylate represented as sticks, iron as ball.
Models realized with AutoDock Vina, and visualized by PyMol.

## CONCLUSIONS

During experiments we realized a molecular model using a docking program (AutoDock Vina) to predict the possibility of using aziridine-carboxylate as synergistic anion at iron binding of transferrin. The obtained data of binding geometry predict that aziridine-carboxylate has loosely, but realisable bound by transferrin. Based on these findings we prepared the transferrin complex using the aziridine-carboxylate as synergistic anions at human serum transferrin's iron binding. The complexation reaction and its analysis using CZE and cIEF techniques [17] demonstrate that the substitution of carbonate to another synergistic anion, such as aziridine-carboxylate produces no significant changes in polypeptide folding or domain orientation in human serum transferrin as revealed by our structure.

## EXPERIMENTAL SECTION

### Material and methods

Iron-saturated human serum transferrin, the ferric chloride ($FeCl_3$) powder, 2-[4-(2-hydroxyethyl)piperazin-1-yl]ethanesulfonic acid (HEPES), Li-aziridine-2-carboxylate was purchased from Sigma-Aldrich, and the iron-free transferrin from Behring Werke AG. The chelating agent, nitrilotriacetic acid (NTA) was a Fluka product. Other used chemical reagents, sodium chloride (NaCl), hydrochloric acid (HCl) were Reanal product.

### Complexation of transferrin with synergistic anions

The complexation reactions were realized conform to the protocol determined by Kilár et. al [18]. At the complexation reactions we used aziridine-carboxylate as synergistic anions.

Samples containing 15 mg/ml holo-Tf were prepared in a HEPES buffer (20 mM, pH=8.1) which including also 20 mM Li-aziridine-2-carboxylate. Solid $FeCl_3$ was dissolved in 6 M HCl and was added to NTA solution (100 mg/ml, prepared in 1 M NaOH) to achieve $Fe^{3+}$:NTA ratio 1:2. This iron-NTA solution was added to the samples containing the anion. To get the desired iron-saturation the ratio of apo-Tf:$Fe^{3+}$ was 1:2. All steps of Tf-$Fe^{3+}$-aziridine-carboxylate complex formation were realized under nitrogen atmosphere. After 30 minutes of incubation the iron-saturated Tf samples were dialysed in HEPES buffer (20 mM. pH 7.5) on 4°C for 16 h.

### Modelling of transferrin-Fe3+-anion ternary complexes

For modelling of transferrin-complexes we used the AutoDock Vina molecular docking program and PyMol v.1.3 for visualizing and construction of the ligand [19].

The human serum transferring (1A8E) macromolecule was prepared using AutoDockTools-1.5.2. An AutoDock-specific coordinate file (PDBQT) was created in which the partial charge of the iron was set to 3.00. A configuration file was written for the AutoDock Vina software, in which the search space was defined and the maximum number of binding nodes to generate was set to 50.

**ACKNOWLEDGMENTS**

The authors would like to thank to the Sectoral Operational Programme Human Resources Development 2007-2013 of the Romanian Ministry of Labour, Family and Social Protection through the Financial Agreement POSDRU/6/1.5/S/16., Science, Please! Research Team on Innovation (SROP-4.2.2/08/1/2008-0011) for financial and intellectual support.

## REFERENCES

1. Z.M. Qian, H.Y. Li, H.Z. Sun, K. Ho, *Pharmacological Reviews*, **2002**, *54*, 561.
2. A. Leibman, P. Aisen, Blood, **1979**, *53*, 1058.
3. R.T.A. Macgillivray, E. Mendez, S.K. Sinha, M.R. Sutton, J. Linebackzins, K. Brew, *Proceedings of the National Academy of Sciences of the United States of America-Biological Sciences*, **1982**, *79*, 2504.
4. P.T. Gomme, K.B. McCann, *Drug Discovery Today*, **2005**, *10*, 267.
5. T.E. Adams, A.B. Mason, Q.Y. He, P.J. Halbrooks, S.K. Briggs, V.C. Smith, R.T.A. MacGillivray, S.J. Everse, *Journal of Biological Chemistry*, **2003**, *278*, 6027.
6. D. Rinaldo, M.J. Field, *Biophysical Journal*, **2003,** *85*, 3485.
7. A. Berczi, M. Ruthner, V. Szuts, M. Fritzer, E. Schweinzer, H. Goldenberg, *European Journal of Biochemistry*,**1993**, *213*, 427.
8. H.Z. Sun, H.Y. Li, A.B. Mason, R.C. Woodworth, P.J. Sadler, *Journal of Biological Chemistry*, **2001**, *276*, 8829.
9. R. Hernandez, J. Lamboy, L.M. Gao, J. Matta, F.R. Roman, E. Melendez, *Journal of Biological Inorganic Chemistry*, **2008**, *13*, 685.
10. D. Griffith, S. Ceeco, E. Zangrando, A. Bergamo, G. Sava, C.J. Marmion, *Journal of Biological Inorganic Chemistry*, **2008**, *13*, 511.
11. M.X. Zhang, D.R. Gumerov, I.A. Kaltashov, A.B. Mason, *Journal of the American Society for Mass Spectrometry*, **2004**, *15*, 1658.
12. W.R. Harris, Y. Chen, K. Wein, *Inorganic Chemistry*, **1994**, *33*, 4991.
13. W.R. Drobyski, R. UlHaq, D. Majewski, C.R. Chitambar, *Blood*, **1996**, *88*, 3056.
14. D. Lubgan, Z. Jozwiak, G.G. Grabenbauer, L.V.R. Distel, Cellular & Molecular Biology Letters, **2009**, *14,* 113.
15. K. Barabas, J.A. Sizensky, W.P. Faulk, *Journal of Biological Chemistry*, **1992**, *267*, 9437.
16. P.J. Halbrooks, A.B. Mason, T.E. Adams, S.K. Briggs, S.J. Everse, *Journal of Molecular Biology*, **2004**, *339*, 217.
17. J. Gálicza, A. Vargová, C. K. Orbán, V. Sándor, B. Ábrahám, F. Kilár, S. Lányi, *Protein Journal*, **2011**, JOPC-D-11-00115.
18. F. Kilar, S. Hjerten, *Electrophoresis*, **1989**, *10*, 23.
19. O. Trott, A. J. Olson, J*ournal of Computational Chemistry*, **2010**, *31*, 455.

STUDIA UBB CHEMIA, LV, Sp.Iss., 2010

# STABILIZATION OF HEMICELLULASE ENZYMES WITH NANO-LAYER

**HEGEDÜS IMRE[a], NAGY ENDRE[a,*], KUKOLYA JÓZSEF[b], BARNA TERÉZ[c], FEKETE CSABA ATTILA[c]**

**ABSTRACT.** In order to increase their stability, the conjugation of hemicellulase enzyme molecules with a polymer nano-layer is reported. This enzyme nanobiocomposites as single enzyme nanoparticles (SENs) have a good stability under extreme conditions. Thus, after 6 hours at 80 $^{o}$C, SENs have 40% of its original activity but the natural enzymes lost their activity after a half an hour.

***Keywords:*** *single enzyme nanoparticles, enzyme stability, nano-bio-composites, hemicellulase enzymes*

## INTRODUCTION

An *extremophile* is an organism that thrives in and may even require physically or geochemically extreme conditions that are detrimental to most life on Earth. A *thermophile* is an organism — a type of extremophile — that thrives at relatively high temperatures, between 45 and 80 °C. Cellular components of thermophilic organisms, enzymes, proteins and nucleic acids, are also thermostable. Thermostable enzymes are highly specific hence they have considerable potential for many industrial application [1].

*Thermobifida* spp. are gram-positive, compost- and soil-inhabiting bacteria with broad degradative activity on plant cell wall constituents. *Thermobifida fusca*, the most extensively studied species of this genus, is the model organism of thermophilic, aerobic cellulolytic bacteria. *Thermobifida fusca* produces multiple extracellular enzymes including cellulases that are responsible for the decomposition of cellulose and lignocellulose residues, which make up the bulk of agricultural and urban wastes. While there are ample data on the cellulolytic system of *T. fusca,* the hemicellulolytic enzyme system of this species is still poorly characterized [1] (Figure 1).

[a] *Research Institute of Chemical and Process Engineering, FIT, University of Pannonia Egyetem u. 2., H-8200 Veszprém, Hungary, Tel.: +3688-624-040, Fax: +3688-624-038*

[b] *Szent István University, Faculty of Agriculture and Environmental Sciences, Páter K. u. 1. H-2100, Gödöllő, Hungary. *Corresponding author; e-mail: nagye@mik.vein.hu; web: www.richem.hu*

[c] *University of Debrecen, Faculty of Science and Technology, Research Institute of Genetics and Applied Microbiology, Egyetem tér 1. H-4032 Debrecen, Hungary*

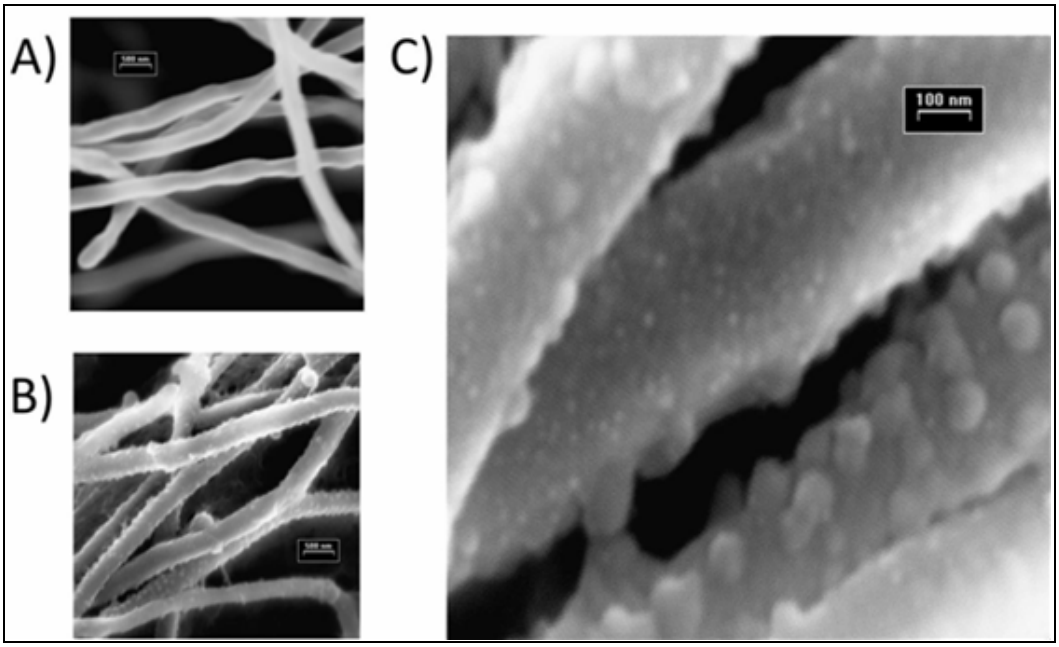


**Figure 1.** Hyphal surface of *Thermobifida fusca* TM51 A) Smooth surface of mycelium grown on glucose B) Cellulosome-like structures emerged upon induction by cellulose C) Cellulosome-like structures at higher magnification

Hemicelluloses act as linkers between lignin and cellulose. The high percentage of hemicellulose fraction in the cell wall of higher plants makes this material the second most abundant biopolymer in nature (Figure 2).

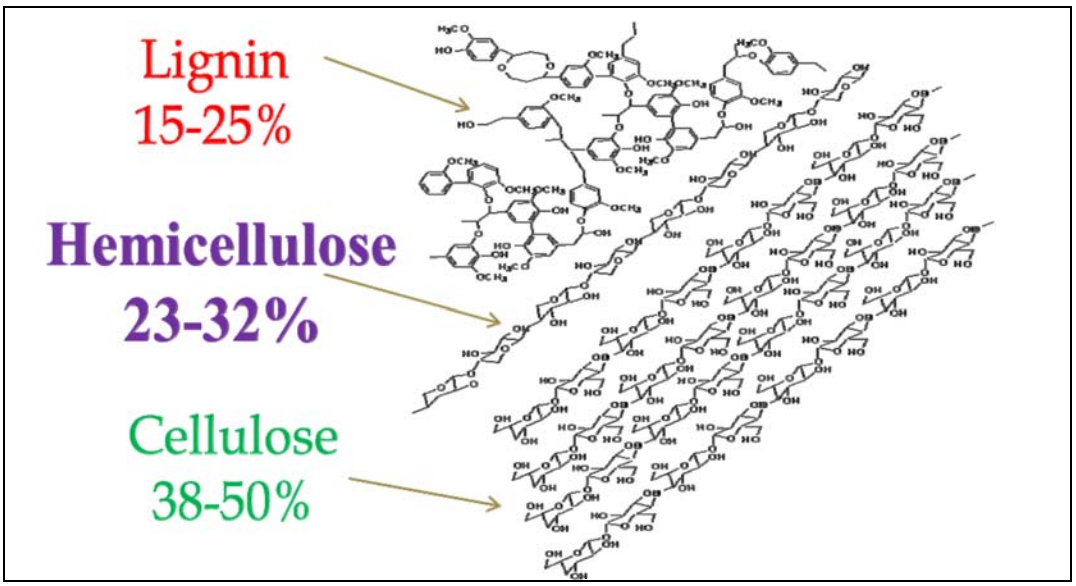


**Figure 2.** Major components in lignocellulosic biomass

Single enzyme nanoparticles (SENs) represent a new approach in industrial enzyme research [2, 3] (Figure 3). Classical techniques for improving the stability of enzymes are enzyme immobilization to the surface or inner cavity of the carrier, modification of the surface of the enzyme, protein engineering, reaction medium engineering and cross-linked enzyme crystals. The new approach in the industrial enzyme stabilization is the reducing the size of the enzyme carriers. Nano-carriers provide minimum diffusional limitation, maximum surface area per unit mass, and high enzyme loading. Nano-carriers are 1) a) metal [4], or b) magnetic nanoparticles [5], 2) Enzyme molecules could be encapsulated into a) hyperbranched polymers [6] b) dendrimers [7, 8]. 3) Single enzyme nanoparticles means single enzyme molecules encapsulated with a) polymer network (nanogel) [9] b) inorganic layer. The inorganic layer could be α) hollowed metal or silica nano-sphere [10, 11] β) mezoporous silica [12] or γ) magnetic nanolayer [13] (Figure 3).

The form of SEN means that each enzyme molecule is surrounded with a nanometer scale polymer matrix layer, resulting in stabilization of enzyme activity without any serious limitation for the substrate transfer from solution to the active site of the enzyme. The synthesis of SEN particles is needed more or less simple laboratorial technique.

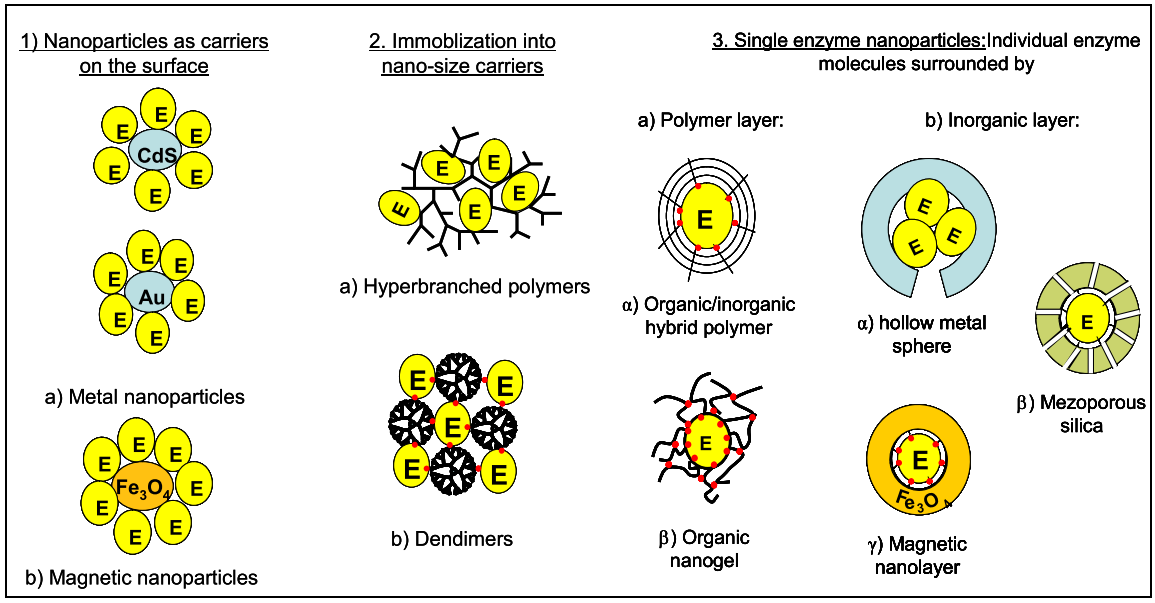


**Figure 3.** Nanotechnological methods for enzyme stabilization.

The utilization of single enzyme nanoparticles is possible industrial and scientific areas. This technique can be used for stabilization of enzymes in industrial enzyme research. Thus, using mesoporous silica gels single enzyme nanoparticles can fixed into the inner wall of the mezopores and it means that nanoreactors can be fabricated (Figure 4) [2].

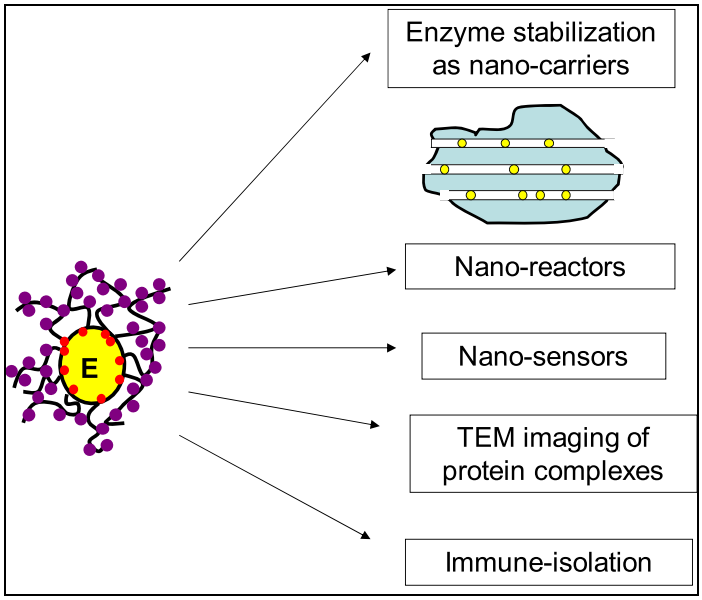


**Figure 4.** Utilization of single enzyme nanoparticles

The polymer layer of the single enzyme nanoparticles is electrodense so transmission electron microscopic detection of the three-dimensional structures of the enzyme complexes can be realized easily. Polymers composed with MAPS monomers have a good biocompatibility and no toxicity [14]. It means that the technique of the preparation of single enzyme nanoparticles can be used in biological areas.

Previously we have decided to apply this technique for industrial bioethanol synthesis able to comply with the requirements of green chemistry. We would like to investigate that how can the SEN-enzymes digest higher-size substrates. We investigated the chemical stability of different enzymes and enzyme complexes in the form of SEN.

## RESULTS AND DISCUSSION

The preparation process of single enzyme nanoparticles (SEN) has three steps (Figure 5). The detailed description of the procedure was described earlier [2, 3]. The first step is a modification of CK enzyme complex and its solubilization in a hydrophobic medium. The second step is the polymerization of the vinyl group in hexane, and the final (third) step is hydrolysis and condensation of the trimethoxysilyl functional group (TMS). Julaba F12 cryostate was used to keep the reaction mixture at 0 $^{o}$C. For the polymerization step, the enzyme should be dissolved in a hydrophobic medium (n-hexane).

The surfaces of the enzymes have hydrophobic and hydrophilic regions. If hydrophilic parts of the surface of the enzymes are covered by surfactant molecules, the enzyme lost its hydrophilic characteristic and became hydrophobic, so the enzyme can not solve in water but can solve in hydrophobic solvents, e.g. hexane. During the hydrophobic ion pairing ion-pairs are bounded between the ionic part of the surfactant and the ionic part on the surface of the enzyme.

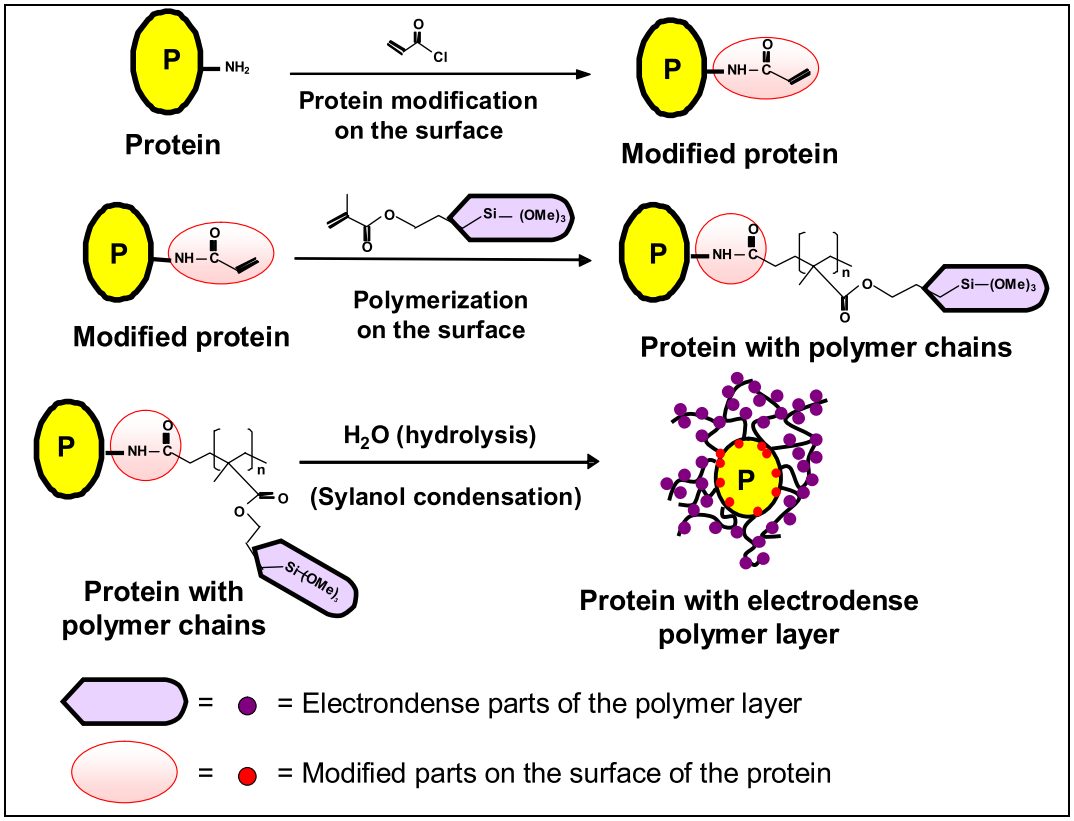


**Figure 5.** Thee-step method to synthesize single enzyme nanoparticles

Polymerization on the surface of the enzyme can only be achieved if there is direct contact between the enzyme surface and the hexane medium. For this reason, the specific solubilization method of hydrophobic ion pairing may be used (Figure 6). In this process, vinyl groups on the enzyme surface (synthesized in the first step) are well exposed to the organic solvent (and reagents).

We measured the activities of natural enzymes (enzymes without polymer layer) and compared the activities of the SEN-products. The concentrations of the resulting SEN-products were measured at the second step (in hexane media) by the absorbance at 280 nm. Relative activities was calculated, the activities of the SEN-enzymes were divided by the activities of the natural enzymes. The

activity of SEN-mannosidase is 47.8% of the natural mannosidase enzyme. The activity of SEN-xylosidase enzyme is 55.3% of the natural one and the activity of SEN-endomannanase is 63.0% of the natural endomannanase.

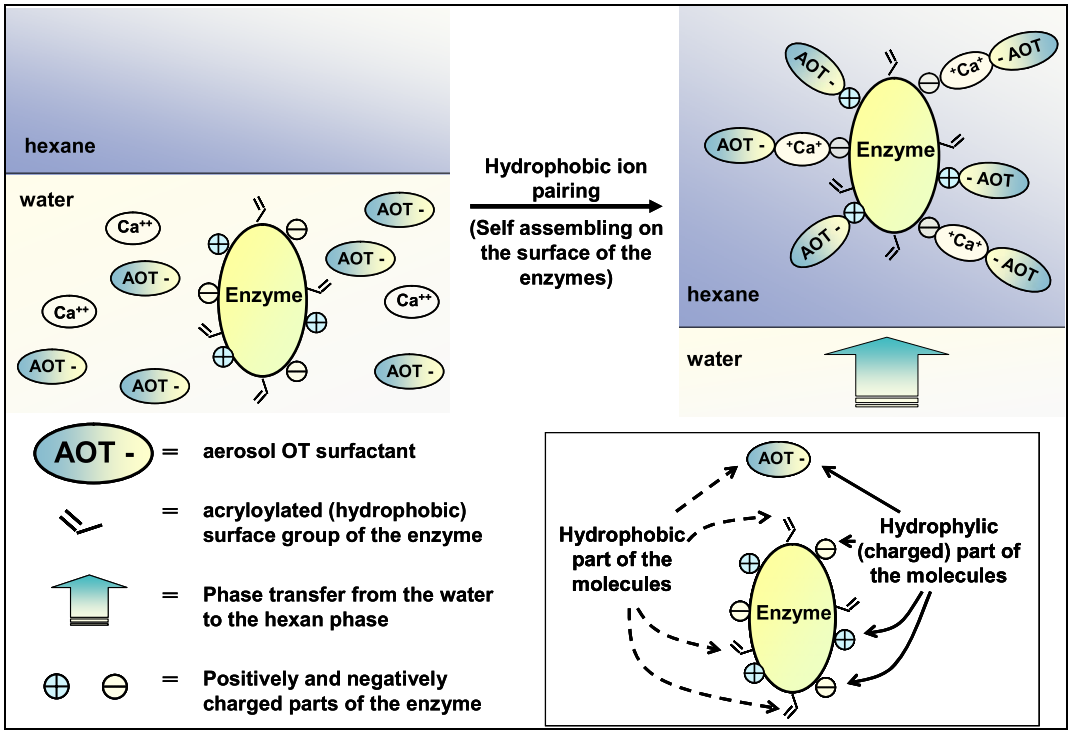


**Figure 6.** Mechanism of hydrophobic ion pairing

The size distribution of the endomannanase enzyme during the preparation was investigated (Figure 7). The peak of the size distribution of the natural endomannanase enzyme (EM/water) is about 6 nm, but the peak of the size distribution of the SEN-endomannanase (SEN-EM/water) is about 15 nm. SEN-mannosidase and SEN-xylosidase have higher peak of their size distribution (about 60 nm).

The results show that the range of the size of the enzyme nanoparticles on the hexane phase after the hydrophobic ion pairing process are between 2-10 nm (EM/hexane, see above, Figure 7). We measured three different enzymes (EM = endomannanase, MM = mutant mannosidase, MN = β-mannosidase, XI = β-xylosidase enzyme).

At +4 °C single enzyme nanoparticles from β-xylosidase enzymes have 40% of its original activity, while the natural β-xylosidase enzymes lost its activity after about 40 days (Figure 8). At 80 °C after 6 hours SENs of β-mannosidase enzymes have 40% of its original activity but the natural enzymes lost their activity after a half an hour (Figure 9).

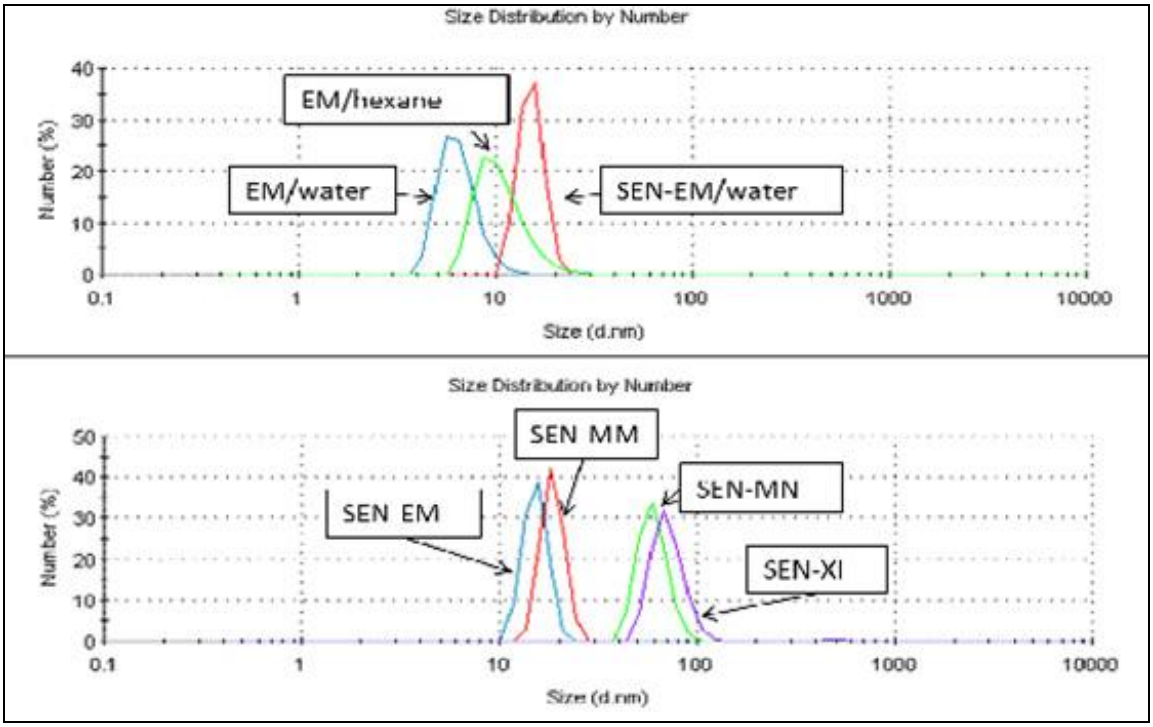


**Figure 7.** Size distribution of different type of single enzyme nanoparticles after the solvatation in hexane using hydrophobic ion pairing (EM = endomannanase, MM = mutant mannosidase, MN = β-mannosidase, XI = β-xylosidase enzyme)

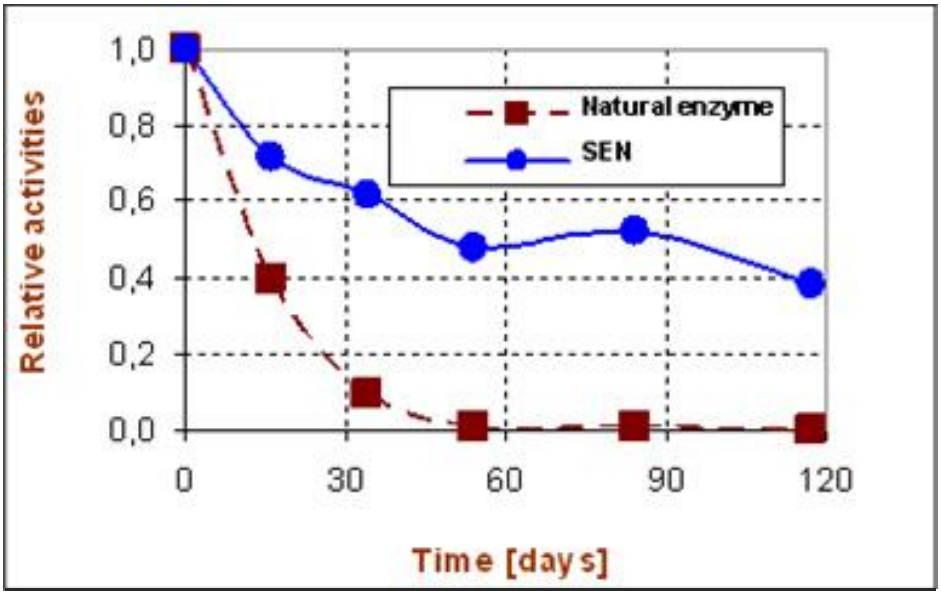


**Figure 8.** Stability of SEN β-xylosidase enzymes and control β-xylosidase enzymes at +4 °C

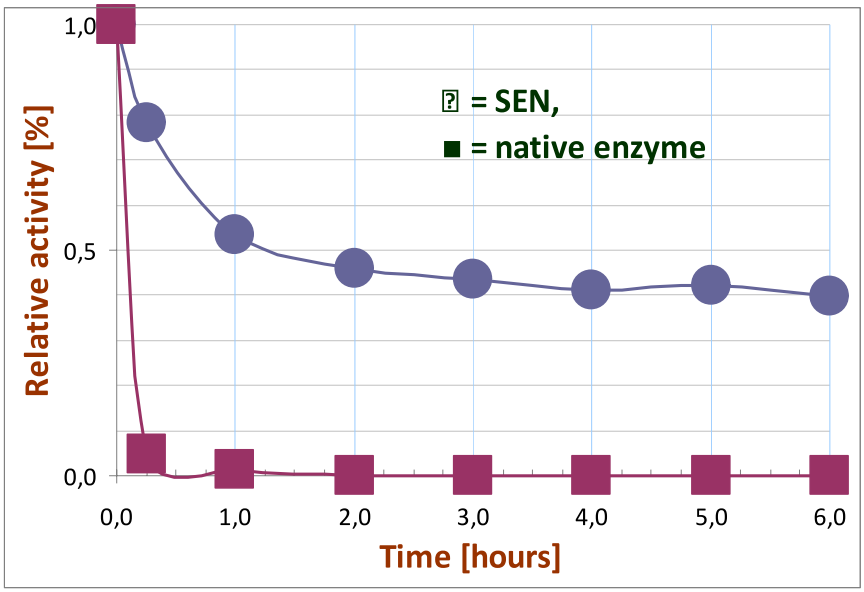


**Figure 9**. Stability of SEN β-mannosidase enzymes and natural β-mannosidase enzymes at 80 °C

## CONCLUSIONS

Single enzyme nanoparticles (SENs) were fabricated using thermostable hemicellulase enzyme molecules from Thermobifida fusca (β-D mannosidase, β-D-xylosidase, endomannanase and mutant β-D mannosidase enzymes). Each individual enzyme molecule were covered with a polymer nano-layer in order to increase their stability. the stabilization of thermophyl enzymes seemed successfully This enzyme nanobiocomposites have a good stability under extreme conditions. Even after 6 hours at 80 °C, SENs have 40% of its original activity but the natural enzymes lost their activity after a half an hour.

## EXPERIMENTAL SECTION

Enzymes: endomananase (EM), β-xylosidase (XI) and β-mannosidase (MN) from Thermobifida fusca and mutant β-mannosidase (MM). Enzymes were isolated from Thermobifida fusca species in Szent István University, Faculty of Agriculture and Environmental Sciences, Gödöllő and were purified in University of Debrecen, Faculty of Science and Technology, Research Institute of Genetics and Applied Microbiology, Debrecen.

Chemicals: acryloyl chloride, 1,3-bis[tris(hydroxymethyl)methylamino] propane or Bis-Tris propane (Sigma®), sodium bis(2-ethylhexyl) sulphosuccinate or aerosol OT (AOT) (Fluka®), disodium hydrogen phosphate, potassium dihydrogen phosphate, calcium chloride, 2-propanol, n-hexane (Spektrum-3d®, Scharlau®), methacryloxypropyltrimetoxysilane (MAPS), 2,2-azobis(2,4-dimethyl-valeronitrile) (Fluka®), 3,5-dinitro-salicylic acid (Sigma®).

Cryostate was used to keep the reaction mixture at 0 $^{o}$C during the first step of the preparation of SEN. A gas chromatographic syringe (volume 5 μl) was used for the addition of a few microlitres of acryloyl chloride to the enzyme solution. The polymerization step in the synthesis of single enzyme nanoparticles (SEN) was carried out in a double-walled stirring vessel. The solution was irradiated by a UV-lamp made by Vilber Lourmat®. Filtration of the surface-polymerized enzymes was carried out with a syringe filter (pore size 0.1 μm) made by Millipore®.

UV-spectra were recorded and enzyme activity measurements carried out by means of a Biochrom 4060 spectrophotometer made by Pharmacia®. A New Brunswick Scientific G24 incubator shaker was used for the stability measurements. For the detection of the size distribution of the enzyme nanoparticles Malvern Zeta-sizer® was used.

## ABBREVATIONS

| | |
|---|---|
| AOT: | sodium bis(2-ethylhexyl) sulfosuccinate (aerosol OT) |
| EM | endomannanase |
| MM | mutant mannosidase |
| SEN: | single enzyme nanoparticle |
| MAPS: | methacryloxypropyltrimethoxysilane |
| MN | β-mannosidase |
| TEM: | transmission electron microscope |
| XI | β-xylosidase |

## ACKNOWLEDGMENTS

This work was supported by the National Office for Research and Technology (NKTH TECH_08_A3/2-2008-0385).

## REFERENCES

1. J. Kukolya, I. Nagy, M. Láday, O. Oravecz, K. Máraligeti, L. Hornok, *Int. J. Evol. Microbiol.*, **2002**, *52*, 1193-1199.
2. J. Kim, J.W. Grate, P. Wang, *Chemical Engineering Science*, **2006**, *61* (3), 1017-1026.
3. I. Hegedűs, E. Nagy, *Chemical Engineering Science*, **2009**, *64*,1053-1060.
4. R. Hong, T. Emrick, V.M. Rotello, *Journal of American Chemical Society*, **2004**, *126* (42), 13572-13572.
5. J. Hong, D. Xu, P. Gong, H. Ma, L. Dong, S. Yao, *Journal of Chromatography B*, **2007**, *850*, 1-2, 499-506.

6. Y. Ge, Y. Ming, D. Lu, M. Zhang, Z. Liu, *Biochemical Engineering Journal*, **2007**, *36*, 93-99.

7. Y-L. Zeng, H-W. Huang, J-H. Jiang, M-N. Tian, Ch-X. Li, G-L. Shen, R-Q. Yu, *Analytica Chimica Acta*, **2007**, *604*,170-176.

8. K. Yao, Y. Zhu, X. Yang, C. Li, *Materials Science and Engineering: C* , **2008**, *28* (8), 1236-1241.

9. Y. Ming, Y Ge, Z. Liu, P. K. Ouyang, *Journal of American Chemical Society*, **2006**, *128*, 11008-11009.

10. R. Kumar, A.N. Maitra, P.K. Patanjali, P. Sharma, *Biomaterials*, **2005**, *26*, 6743–6753.

11. R.S. Kumar, S. Das, A. Maitra, *Journal of Colloid and Interface Science*, **2005**, *284*, 358–361.

12. R.R. Naik, M.M. Tomczak, H.R. Luckarift, J.C. Spain, M.O. Stonea, *Chemical Communications,* **2004**, 1684–1685.

13. Z. Yang, S. Shihui, Z. Chunjing, *Biochemical and Biophysical Research Communications*, **2008**, *367*, 169-175.

14. A. Mori, C. Ohtsuki, T. Miyazaki, A. Sugino, M. Tanihara, K. Kuramoto, A. Osaka, *Journal of Materials Science: Materials in Medicine* **2005**, *16* 713–718.

STUDIA UBB CHEMIA, LV, Sp.Iss., 2010

# PROBLEMS OCCURRING DURING THE PROCESSING OF MICROALGAE PROPAGATED FOR OIL PRODUCTION

**HODAI ZOLTÁN[a,*], HORVÁTH GÉZA[a], HANÁK LÁSZLÓ[a], BOCSI RÓBERT[a]**

**ABSTRACT.** At the University of Pannonia we study algae cultures used to clean industrial wastewater and to absorb industrial carbon dioxide. Amongst others, in the focus of our work are processing and separating operations. We aim to separate the algae from the nutrient solution the simplest and most economic way. Furthermore, we try to define the useful components of algae and their optimal extraction, based on the optimization of techniques of extraction and other economic and environmental aspects.

***Keywords:*** *carbon dioxide absorption, microalgae, separation, flocculation, filtration*

## INTRODUCTION

Microalgae are regarded as one of Earth's most efficient organisms because of their productivity and generally high oil contents. As for their productivity, microalgae are capable of doubling their biomass in 24 hours [1, 2, 3, 4]. According to a literature survey, their oil content is 20 % on the average (certain algae species can reach 60-80 %) [1, 5, 6, 7]. Research in oil production from algae is mainly focused on microalgae. These are photosynthesizing organism the size of which does not exceed 0.5 mm. They are, with a good chance, a solution to the reduction of carbon dioxide and nitrous oxides, because they transfer them in a photosynthetic pathway [8]. The product of this process contains a significant amount of solar energy stored in chemical bonds, and as a result, "high volumes" of biodiesel can be retrieved from them [4, 9, 10, 11]. In addition to the above mentioned, microalgae are not only capable of cleaning exhaust gases, but they also utilize certain components of wastewaters, this way cleaning them. The contamination provides additional nutrients for the algae, starting their exponential growth.

Whatever the advantages, the biggest obstacles are the expenditures. The harvest, dehydration, drying and the extraction of the lipids and their conversion are the most critical steps in the production of alga-based fuels

[a] *University of Pannonia, Institute of Chemical and Process Engineering, H-8201 Veszprém, Egyetem u 10. Pf. 158.,** hodaizoltan@gmail.com

because of their high investment and operation costs. The biggest challenge for the technology is cost-reduction, which can mainly be achieved at the separation steps.

The harvest can be carried out with microfiltration, centrifugation, flocculation [12], with sonochemical techniques, or with any other techniques [13] they are under development. Presently, the combined separation technology appears to be economically feasible. The combination of flocculation and microfiltration results in a separation of appropriate speed, quality and cost. The aim of this paper is to present the tendency of certain special alga species towards flocculation with the use of different techniques and flocculants. The flocculation of the algae can be achieved by two means. Firstly, with the so-called autoflocculation technique, secondly, by chemical means, e.g. by the addition of aluminum sulfide, iron chloride, or iron(III) sulfate [14] to the solution, which results in the coagulation of the algae [15, 16]. Of the two methods, chemical flocculation is capable of increasing the alga concentration more efficiently. Thus the experiments described in the followings deal with chemical flocculation too, examining the effect of different flocculants and their combinations with respect to the alga solutions.

## RESULTS AND DISCUSSION

### Autoflocculation experiments

The simplest way to achieve the phenomenon of autoflocculation is by the cessation of the carbon dioxide feed. When ceasing the carbon dioxide feed, the slow sedimentation of the algae commences. The roles and the effect on sedimentation of in-sprayed oxygen, irradiated light and temperature are not yet clear. The examination of the phenomenon is the subject of present laboratory measurements.

### Cessation of the carbon dioxide feed

The experiment was carried out by taking samples of 500 $cm^3$ from the propagation reactor, from different alga species and at different states of propagation (Figure 1). The average rate of sedimentation was $3 \times 10^{-9}$ m/s in the case of algae taken at the propagation phase, which is an unacceptably low value. The average sedimentation rate of the algae after the propagation phase was somewhat higher, $6 \times 10^{-9}$ m/s, but this is still unacceptably low for us. Although the effect of the other parameters is still under investigation, this method does not seem feasible at present.

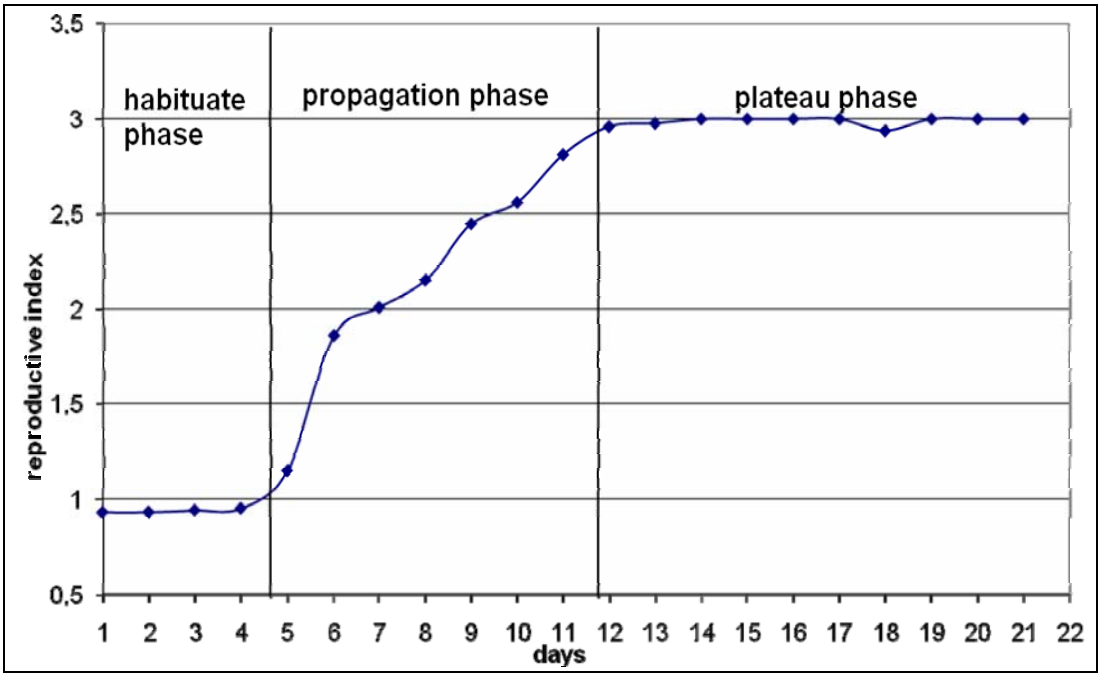


**Figure 1.** The reproduction of the microalgae

## Flow choke with carbon dioxide

This is a novel approach to autoflocculation, which has been developed at the Institute of Chemical and Process Engineering of the University of Pannonia. The technology is an extension of the phenomenon of autoflocculation. The rates of sedimentation somewhat rise (Table 1), and a more complete sedimentation can be observed than in the former experiment (Figure 2).

**Table 1.** Comparison of autoflocculation experiments

| | **Autoflocculation method used** | |
|---|---|---|
| **Sedimentation of algae in the propagation phase** | **Cessation of the $CO_2$ feed** | **Flow choke with $CO_2$** |
| **mean sedimentation rate [m/s]** | $3\times10^{-9}$ | $7\times10^{-9}$ |
| **Sedimentation of algae after the propagation phase** | **Cessation of the $CO_2$ feed** | **Flow choke with $CO_2$** |
| **mean sedimentation rate [m/s]** | $6\times10^{-9}$ | $9\times10^{-9}$ |

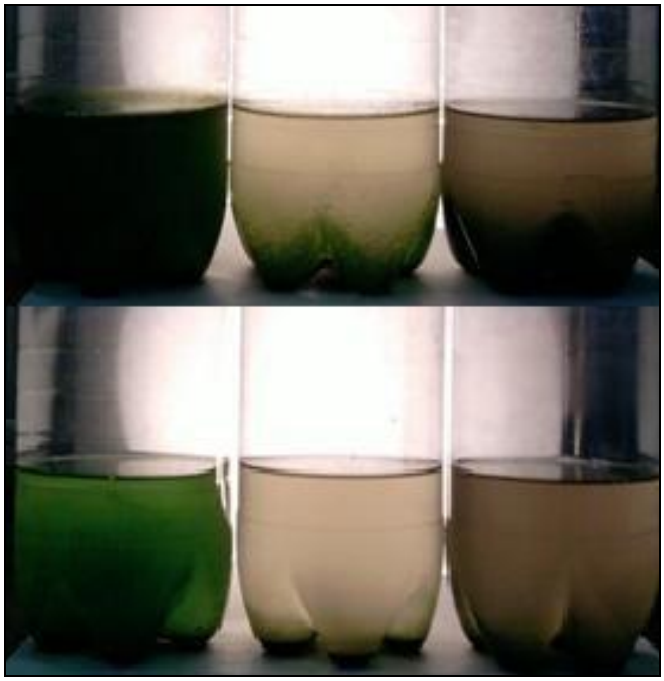

**Figure 2.** Top part: the result of the cessation of the carbon dioxide feed; Bottom part: the result of flow choke with carbon dioxide

## The analytics of the chemical flocculation experiments

### *The use of the Particle Charge Detector (PCD)*

The colloidically solved particles and algae in the aqueous solution carry electric charge if they have dissociative functional groups on their surfaces. If the counter-ions are separated from the particles, a flow potential can be measured (mV). In order to determine the quantity of charge polyelectric titration was carried out, in which the flow potential = 0 mV was used to indicate the end-point. To the sample was added a polyelectrolite of opposing charge (poly-diallyl-dimethyl-ammonium-chloride; Poly-DADMAC) as a titrating agent the charge quantity of which is known. The effect of the flocculants was followed by PCD measurements and defined with the clarification experiments. It is important to note that the potential is hard to reproduce because it is also dependent on different external factors (temperature, molar weight, particle size, etc.). These also make the interpretation of the results difficult. (Because of the great amount of experimental datas and the complex correlation between them, correlation analysis needed to achieve better understanding.)

Experiences gained with the measurements: 1. the shape of the titration curve is dependent on the alga species, 2. the specific quantity of charge is a function of the propagation phase, 3. the specific quantity of charge decreases with the increase of pH, 4. the specific quantity of charge somewhat decreases over time.

## Clarification experiments

### *Sedimentation with basification*

The addition of NaOH to the mixture is advantageous in the later steps because it decreases the specific quantity of charge. Thus the first experiments meant increasing the pH to 10-11. As for the freshly harvested algae that were still in the propagation phase, excellent flocculation and appropriate rate of sedimentation ($6 \times 10^{-3}$ m/s) was observed. In the case of plateau phase algae mixture the procedure was uneffective, so to increase the rate of sedimentation, we needed an additional additive which accelerates the sedimentation of the flakes.

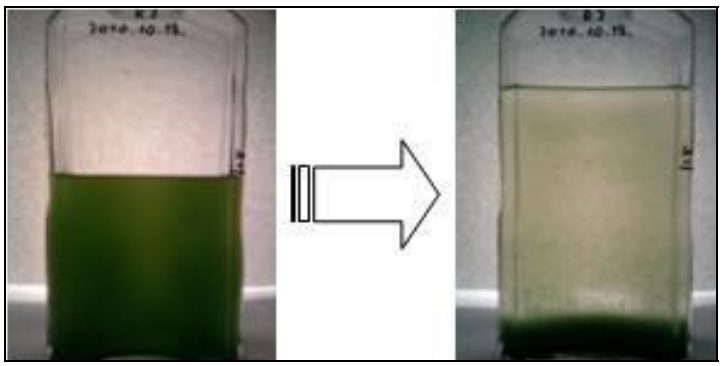

**Figure 3.** Sedimentation achieved with NaOH
(freshly harvested algae, from propagation phase)

### *Sedimentation with basification and the addition of additives*

Iron(III) sulfate was added (3 – 6 $cm^3$ $Fe_2(SO_4)_3$ / 1 l algae solution) to the basified solution and it was found that this enhances the process of flocculation; and after quick sedimentation ($1{,}4 \times 10^{-2}$ m/s) a thick layer of algae remained on the bottom of the mixture. Although the sedimentation is excellent, further experiments should be carried out because the additional iron makes the subsequent analytics and signal processing difficult.

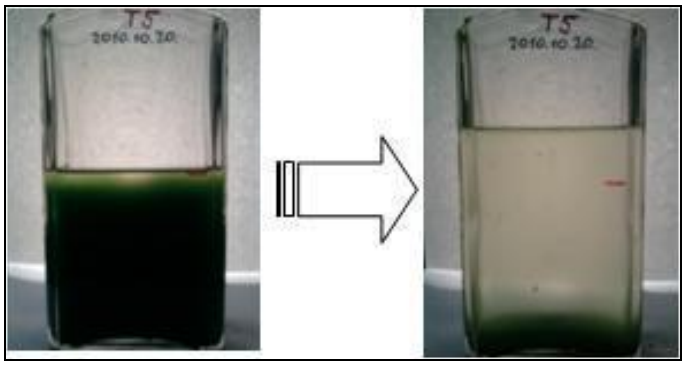

**Figure 4.** Sedimentation achieved with NaOH + $Fe_2(SO_4)_3$

### *Addition of NaOH and cationic flocculant*

The $Fe_2(SO_4)_3$ was replaced with a cationic flocculant, polyDADMAC, which was used for the analytical measurements ($C_{P\text{-}DADMAC}$=2,4 g/l: 60 – 100 $cm^3$ Poly-DADMAC / 1 l algae solution). In the near future we plan to utilize cationic starch derivatives both for cost efficiency and for environmental protection reasons. The results were acceptable in most of the experiments, but the rate of sedimentation is significantly lower (7,6 × $10^{-3}$ m/s) than in the former experiment. An increase in the rate is necessary.

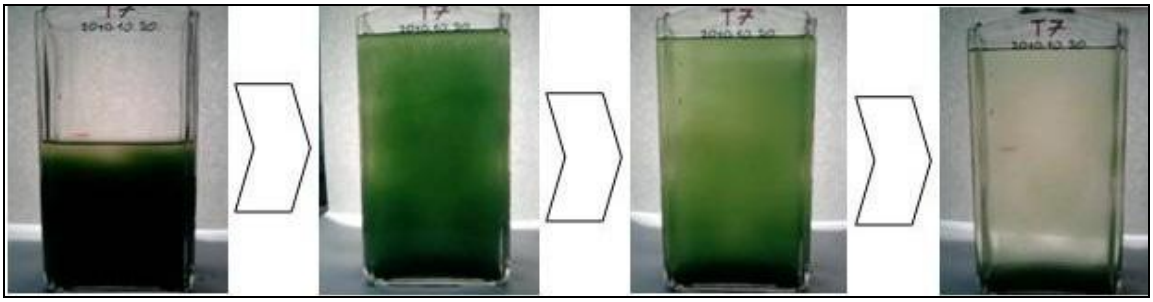

**Figure 5.** Sedimentation achieved with NaOH + cationic flocculant

### *Addition of NaOH, cationic flocculant and $Fe_2(SO_4)_3$*

The former experiment can be accelerated by adding less flocculant and substantially less $Fe_2(SO_4)_3$ to the basified solution then earlier. (39 – 65 $cm^3$ Poly-DADMAC/ 1 l algae solution and 1,2 – 2,4 $cm^3$ $Fe_2(SO_4)_3$ / 1 l algae solution) The result was spectacular with excellent flocculation and appropriate rate of sedimentation (2,2 × $10^{-2}$ m/s).

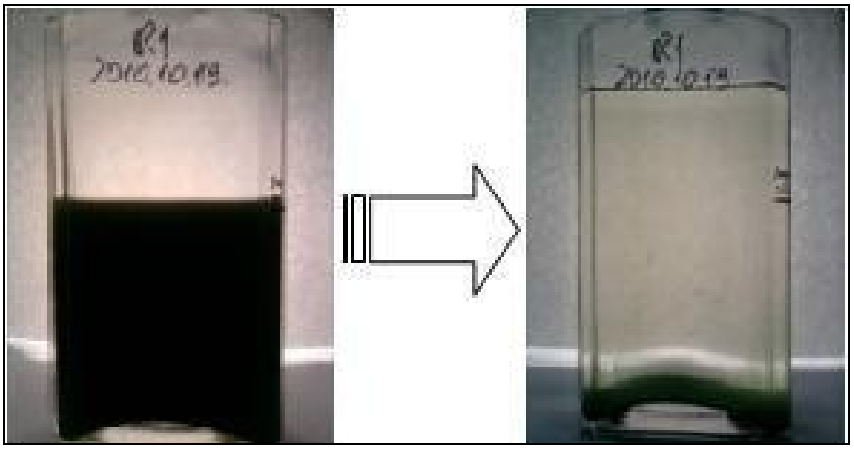

**Figure 6.** Sedimentation achieved with NaOH + cationic flocculant + $Fe_2(SO_4)_3$

## RESULTS

The autoflocculation experiments show satisfactory results, but because of the low settling speed we have not adapted the procedure in practice. The examined phenomenon – called $CO_2$ choke – we will study further, and want to develop a usable procedure in practice. The need of chemical substances have been optimized (the composition of the flocculation agent is the variable of the separation method). ((Use NaOH 10 -11 pH + 39 – 65 $cm^3$ Poly-DADMAC + 1,2 – 2,4 $cm^3$ $Fe_2(SO_4)_3$) / 1 l algae solution.) Table 2 shows the summarized and averarged results of our investigation.

**Table 2.** Results of the flocculation experiments

| Life cycle | Time between harvest and preparation [h] | Sedimentate procedure | Mean sedimentation rate [m/s] |
|---|---|---|---|
| propagation phase | *independent* | Cessation of the carbon dioxide feed | $3*10^{-9}$ |
| propagation phase | *independent* | $CO_2$ choke | $7*10^{-9}$ |
| plateau phase | *independent* | Cessation of the carbon dioxide feed | $6*10^{-9}$ |
| plateau phase | *independent* | $CO_2$ choke | $9*10^{-9}$ |
| propagation phase | 0-12 | NaOH | $6*10^{-3}$ |
| plateau phase | 0-36 | NaOH | 0 |
| propagation/plateau phase | 0-36 | NaOH + Iron(III) sulfate | $1,4*10^{-2}$ |
| propagation/plateau phase | 0-36 | NaOH + cationic flocculant | $7,6*10^{-3}$ |
| propagation/plateau phase | 0-36 | NaOH + cationic flocculant + Iron(III) sulfate | $2,2*10^{-2}$ |

Figure 7 show the comparison of the experiments.

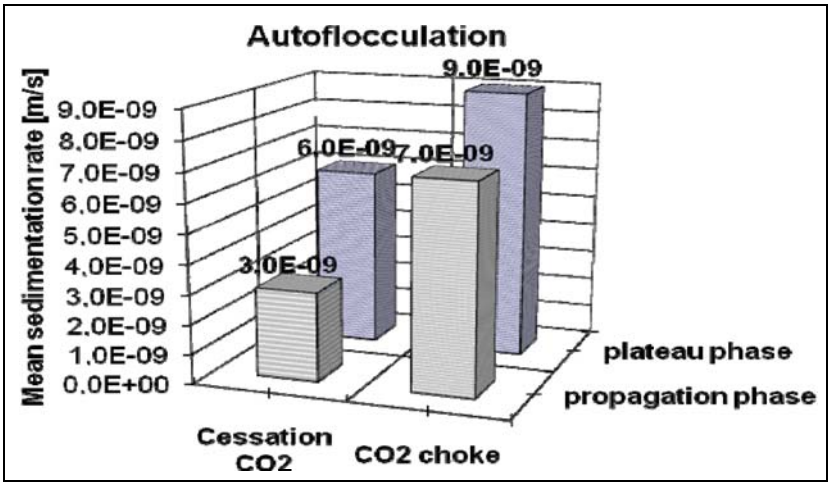


**Figure 7/a.** Results of the flocculation experiments

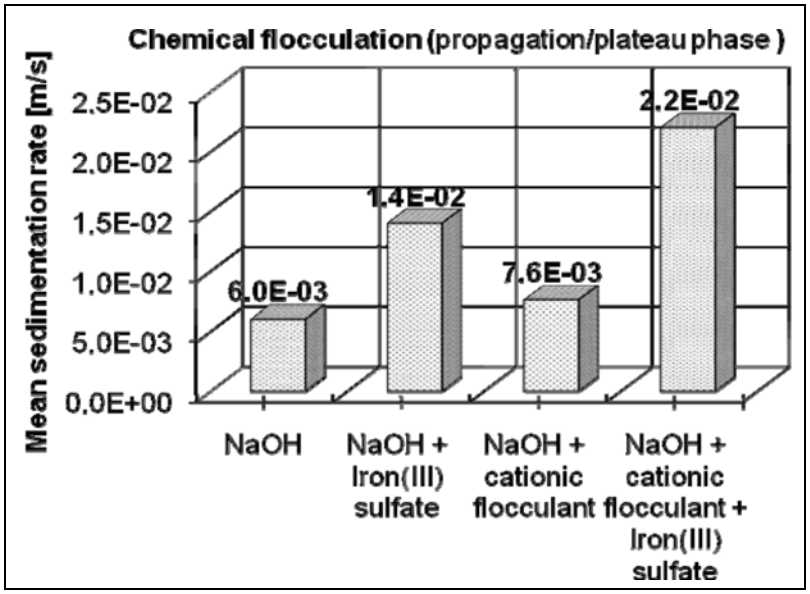


**Figure 7/b.** Results of the flocculation experiments

**ACKNOWLEDGEMENTS**

The authors express their gratitude to Chemical Engineering Institute Cooperative Research Centre of the University of Pannonia and the TÁMOP-4.2.1/ B-09/1/KONV-2010-0003 application for financial support of this research study.

## REFERENCES

1. E. Kojima, K. Zhang, *Journal of Bioscience and Bioengineering*, **1999**, *87*, 811.
2. M. Briggs, "Widescale Biodiesel Production from Algae", University of New Hampshire, Physics Department, August **2004**.
3. S.R. Chae, E.J. Hwang, H.S. Shin, *Bioresource Technology* **2006**, *97*, 322.
4. Y. Chisti, "Biodiesel from microalgae", Institute of Technology and Engineering, Massey University, New Zealand, February **2007**.
5. E.W. Becker, J. Baddiley, "Microalgae: Biotechnology and Microbiology", Cambridge Univ. Press, Cambridge, Inc., New York, **1994**, p. 178.
6. G.C. Dismukes, "Algal Photosynthesis", Princeton Univ. Press, Princeton, february **2008**.
7. D. Song, J. Fu, D. Shi, *Chinese Journal of Biotechnology*, March **2008**, *24*, 3.
8. Dr. T. Nakamura ; Dr. M. Olaizola; Dr. S.M. Masutani, "Recovery and Sequestration of CO2 from Stationary Combustion Systems by Photosynthesis of Microalgae" U.S. Department of Energy, Office of Fossil Energy National Energy Technology Laboratory, March **2006**.

9. J. Sheehan, T. Dunahay, J. Benemann, P. Roessler, “Biodiesel from Algae”, A Look Back at the U.S. Department of Energy’s Aquatic Species Program, NREL Report NREL/TP-580-24190, **1998**.
10. J. Burlew, “Algae Culture: From Laboratory to Pilot Plant”, Carnegie Institute, Washington DC, **1953**.
11. S.H. Choe, I.H. Jung, *Industrial and Engineering Chemistry*, **2002**, *8*, 297.
12. G.A. Shelef, A. Sukenik, M. Green, “Microalgae Harvesting and Processing: A Literature Review, Report”, Solar Energy Research Institute, Golden Colorado, SERI/STR-231-2396, **1984**.
13. E. Poelman, N. De Pauw, B. Jeurissen, “Potential of electrolytic flocculation for recovery of micro-algae”, *Resources Conservation and Recycling*, **1997**, *19*, 1.
14. de Godos I, *Bioresource technology*, **2010**, *10*, 16.
15. Ny. Uduman, Y. Qi, M. K. Danquah, A.F.A. Hoadley, *Chemical Engineering Journal*, **2010**, *162*, 935.
16. R.M. Knuckey, M.R. Brown, R. Robert, D.M.F. Frampton, *Aquacultural Engineering*, **2006**, *35*, 300.

STUDIA UBB CHEMIA, LV, Sp.Iss., 2010

# EXTRACTION AND IDENTIFICATION OF SECONDARY METABOLITES FROM SIBERIAN GROUNDSEL

**KAPÁS ÁRPÁD[1,2], ÁBRAHÁM BEÁTA[b], LÁNYI SZABOLCS[b], MARTA STROESCU[a], TĂNASE GH. DOBRE[a]**

**ABSTRACT.** Siberian groundsel (*Ligularia sibirica* (L.) Cass) contains many volatile compounds, pyrrolizidine alkaloids and eremophilane sesquiterpenes. This study focuses on the identification of some semi volatile and nonvolatile secondary metabolite components of from this plant, by using liquid and gas chromatography with mass spectrometry detection (LC-MS and GC-MS). From the root extracts has been identified one preudoguianolide compound by LC-MS method, in addition one guianolide and one germacrene sesquiterpene by GC-MS method. Leaf extracts analyses have been not resulted identification of any compounds.

***Keywords:*** *Ligularia sibirica, mass spectrometry, fragmentation mechanism, eremophilane sesquiterpenes, pyrrolizidine alkaloids*

## INTRODUCTION

Many plants produce valuable bioactive secondary metabolites for pharmaceutical industry, however studying the phytochemical composition and isolation of these compounds are important part of developing new medicines and therapies.

Genus *Ligularia* is widely spread in Europe and Asia, 20 to 40 species from the existing 211 species have been used in traditional folk medicine [1] being antipyretic, diuretic and choleretic agents for clearing heat and removing toxins from human body [2]. They have relieving phlegm and cough effect, invigorating circulation of blood and reducing pain [3, 4].

The most known chemical constituents from *Ligularia* species are eremophilane-type sesquiterpenes, with some cytotoxic and anti-tumor activities [3, 5-7].

The relict species of Siberian groundsel (*Ligularia sibirica* (*L.*) *Cass*) contain eremophilane sesquiterpenes and pyrrolizidine alkaloids, such as volatile compounds [8]. Isolated eremophilanes from this plant (fig. 1) [9,10] are not tested

[1] *Universitatea Politehnica din Bucureşti, Facultatea Ştiința şi Ingineria Materialelor, Str. Polizu, Nr. 1-7, RO-010737, Bucureşti, Romania, tghdobre@gmail.com*

[2] *Universitatea Sapientia, Cluj-Napoca, Facultatea Miercurea Ciuc, Departamentul Ştiințe Tehnice, Pța. Libertății, Nr. 1, RO-530104, Miercurea Ciuc, Romania, kapasarpad@sapientia.siculorum.ro*

from biological activity viewpoint, but tussilagine and iso-tussilagine pyrrolizidine alkaloids are possessing antimicrobial and immune system stimulator effect and are used in anti HIV-1 [11], HSV-1 and HSV-2 treatments [3, 12, 13].

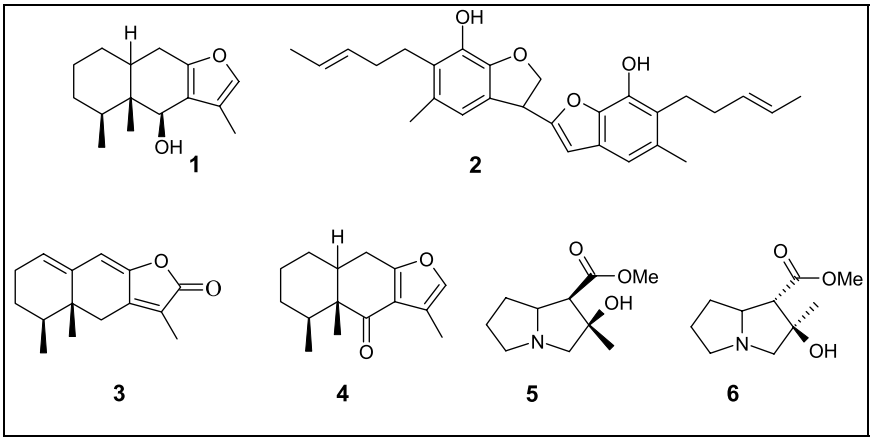


**Figure 1.** Identified compounds from *L. sibirica*; ligularol (1), ligularine A (2), ligularenolide (3), ligularone (4), tussilagine (5) and iso-tussilagine (6)

Chromatography - mainly the gas chromatography and high performance liquid chromatography - is mostly employed separation technique in analytical chemistry, particularly for the isolation of relatively small concentration of compounds and mainly quantitative estimation of compounds from different matrices, for example vegetal and mammalian tissue extracts [14].

Mass spectrometry (MS) coupled with GC and HPLC are powerful techniques for identifying molecular structures and quantitative measurement. Essentially, the mass spectrometry is an analytical method based on the separation of ionized molecules in inhomogeneous electric and magnetic fields and the separation is given by the mass/charge ratio differences of the ionized molecular fragments. After the separation of molecules on columns, the molecules are ionized and fragmented by different methods (fast atom bombardment (FAB), atmospheric pressure ionization and electrospray ionization (APCI and ESI), matrix assisted laser desorption/ionization (MALDI)), ions are formed in the source region and they are accelerated by an electric field in the mass analyzer [15, 16]. The quadrupole analyzer instrument executes the separation of the ions. It is constructed from four electrode rods, arranged opposite from each for other and opposite pair electrodes are connected electrically and a voltage, consisting of both radiofrequency and direct-current components that produce an oscillating electric field which functions as a band pass filter to transmit the specific mass/ charge ratio [15, 16]. In the mass spectrometer, molecular ions are energetically unstable, and some of them break up in smaller parts, named fragments. This process is named fragmentation mechanism that shows hard dependence from volatilization degree of molecules and from the applied ionization method [16].

In the case of GC-MS, the probe is almost totally volatilized and is more powerful ionized during electric impact ionization and that way the fragmentation process is more specific and more complete than in the case of LC-MS coupled by soft ionization modes, for examples ESI and APCI [15-17]. Consequently, identification of compounds is easier in case of GC-MS, having large a database. For or LC-MS (caused by incomplete fragmentation and large number of setting parameters) the identification is more difficult, because of lack of an extended database.

The aims of this study is developing an analytical method, like gas chromatography and liquid chromatography with mass spectrometry detection, for identification of compounds obtained from extracts of the studied plant species.

## RESULTS AND DISCUSSION

### Result of liquid chromatographic analysis of root and rhizome extract

The mass spectra of the identified compounds were obtained with LC-MS method (without using standard) by determination of their fragmentation mechanisms.

LC-MS analysis of extract resulted presumably identification of one pair of pseudoguaianolide lactone, named erigerolide or britanin, which are showing similar m/z 366 $[M]^{+,}$ 306 $[M\text{-}CH3COOH]^{+}$ and 246 $[M\text{-}2\times CH_3COOH]^{+}$ characteristic ions for GC-MS detection [18]. Two from the three identical fragments, m/z 367 $[M+H]^{+}$ (100) and m/z 307 have been observed in the peak at 18.4 min retention time (fig. 2). The fragmentation mechanisms of pseudoguianlolides, including erigerolide and britanin has been described by Tsai and his coworkers [19], when m/z 307 ion brake into m/z 109, 123 and 95 representative fragment ions (fig. 3 and 4).

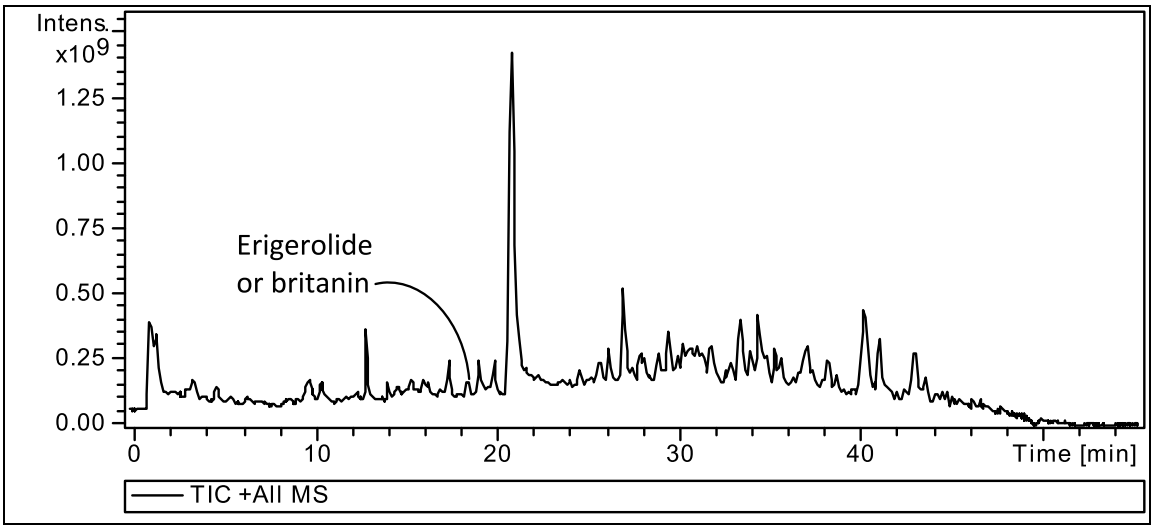


**Figure 2.** LC-MS chromatogram of root and rhizome extract

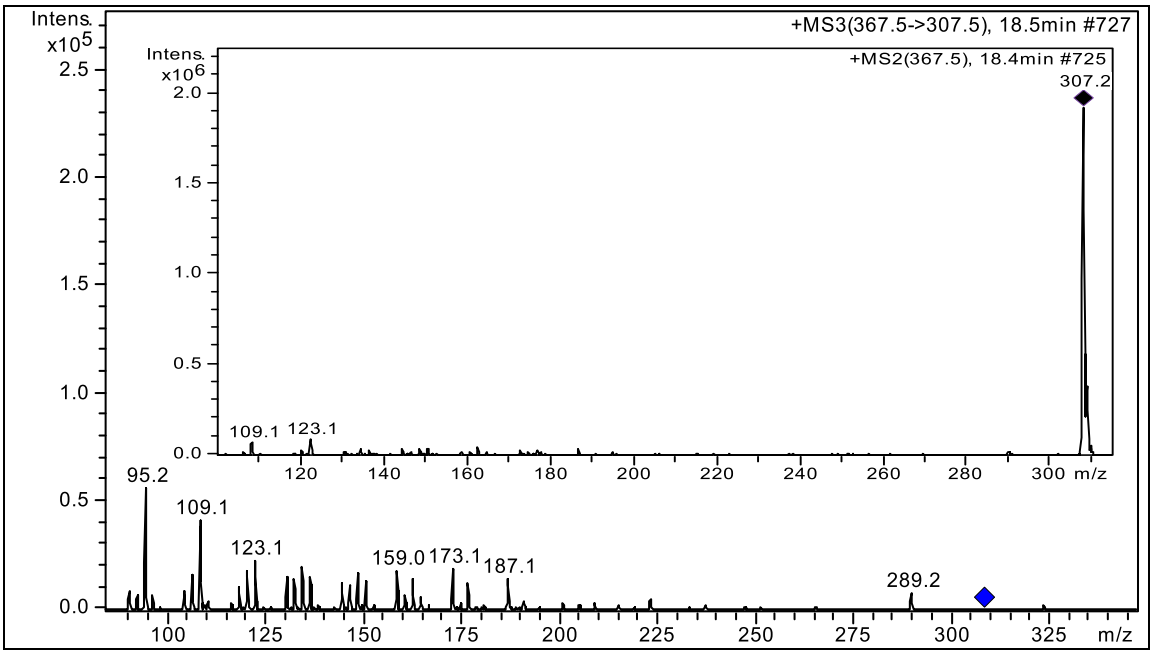


**Figure 3.** LC-MS$^2$, LC-MS$^3$ spectrum of erigerolide or britanin

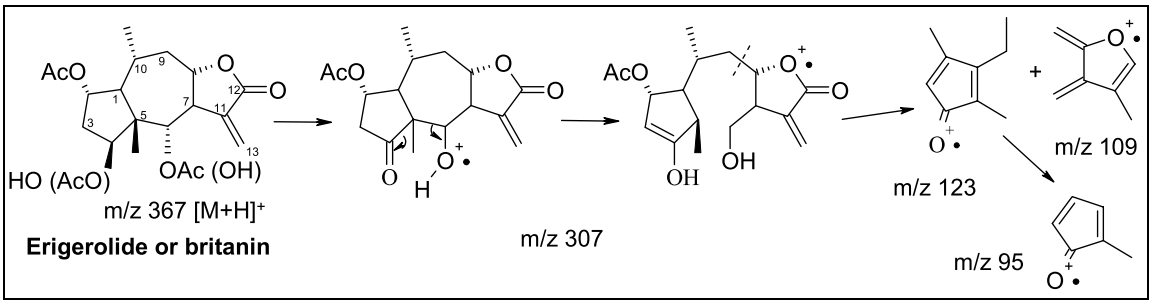


**Figure 4.** Presumed fragmentation mechanism of erigerolide or britanin

## Result of gas chromatographic analysis of root and rhizome extract

Gas chromatography analysis of root and rhizome extract resulted separation and identification of only one germacrene (fig. 5) and one guianolide sesquiterpene named achillin ($t_r$=11.43 and 13.52 in fig. 6). Other compounds are presumably not volatile or they van be decomposed easy in gas chromatograph injector. Both compounds have m/z 246 $[M]^+$ spectra.

From biological viewpoint, only achillin is known as anti-inflammatory, antifeedant and plant growth inhibitor substance [20, 21]. It has no anticancer activity to RKO and RKO-E6 colon cancer cell lines [22]. Bilogical activity of erigerolide, britanin and identified germacrene compound is not described in literature.

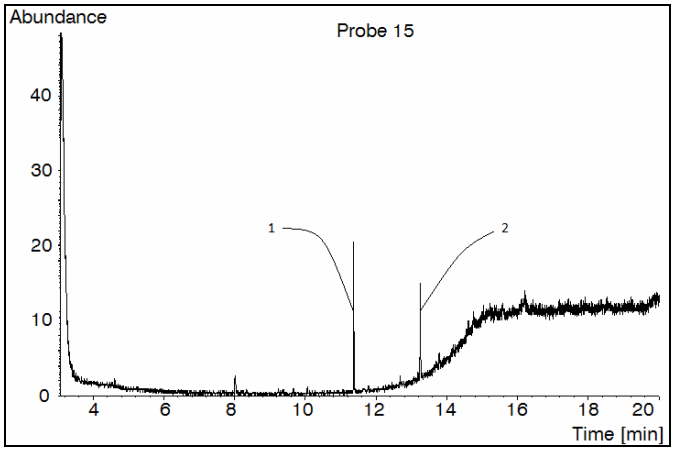


**Figure 4.** GC-MS chromatogram of extract of the root extracts; one germacrene (1) and achillin (2)

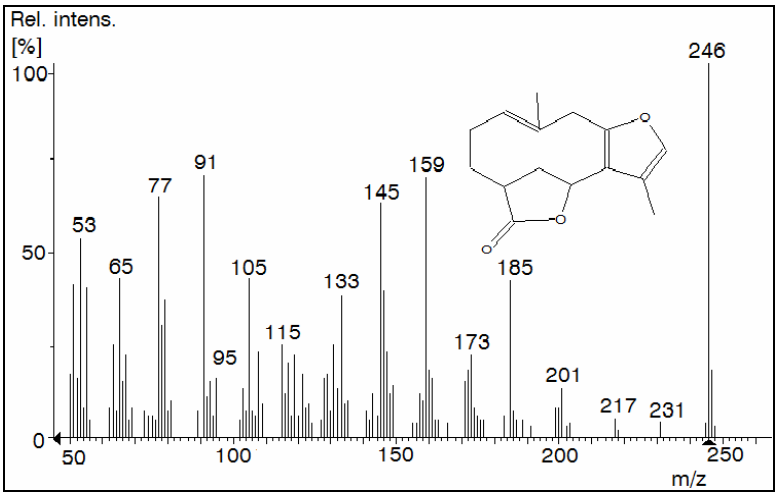


**Figure 5.** GC-MS spectra of germacrene

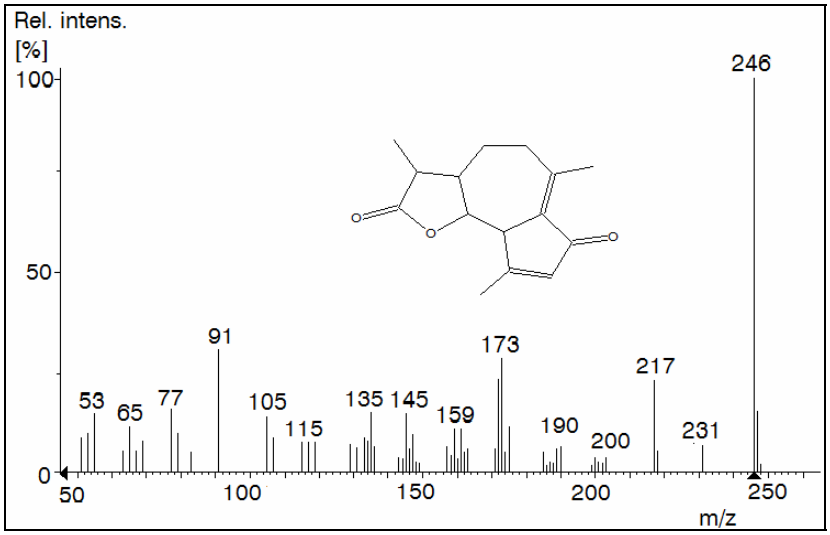


**Figure 6.** GC-MS spectra of achillin

## CONCLUSIONS

Nevertheless, compounds isolated by other authors were not identified in this study. Composition differences between the Romanian and Mongolian species could partly be due to habitats and partly due to genetic properties differences between the two plants. The less successful GC-MS and LC-MS analysis of extracts requires executing further research for extraction, separation, purification and structure elucidation of compounds.

## EXPERIMENTAL SECTION

### Materials and apparatus

The plant (*L. sibirica*) was collected in September of 2009 in Harghita marsh from Harghita County, Romania and stored in a cool and dry place. All the necessary chemicals (dichlormethane, ammonium hydroxide, anhydrous sodium-sulfate, acetonitrile, methanol and hydrochloric acid ) were obtained from Sigma Aldrich Co.

### Extraction procedure

Four grams of powdered rhizome and roots were suspended in 1 ml of ammonium-hydroxide solution (25% v/v concentration) and were extracted with 30 ml of dichloromethane at room temperature in ultrasonic bath at 10 minutes. The obtained extract was filtered through a layer of anhydrous sodium-sulfate and stored in dark at 4 °C temperature. Before analysis they were evaporated, resolved in acetonitril-methanol-acetic acid solution (75:25:1) or *n*-hexane and finally filtered with a syringe filter.

For the extraction of leaves we used the same extraction procedure as in the case roots and rhizomes The filtered extract was evaporated under reduced pressure at 40 °C and the residue was dissolved in 30 ml of 2% sulfuric acid. The acid soluble fraction was filtered and neutralized to pH 9-9.5 with ammonium-hydroxide solution, and then was extracted two times with amount of 30 ml of chloroform at room temperature. For LC-MS analysis the extract was evaporated and resolved in acetonitril-methanol-acetic acid mixture (75:25:1).

### Liquid chromatography with mass spectrometry detection

The LC separations were performed using Agilent 1100 HPLC system, column: Phenomenex Luna $C_{18}$ (2), (10 cm × 2.0 mm × 2.5 μm), the flow rate was 0.2 ml/min at 25 °C temperature. In all cases the injected volume was 4 μl of acetonitril extract. The mass spectrometry in every case was executed by using one Agilent LC MSD XCT Plus mass spectrometer with positive ionization

mode with 40 psi pressure nebulizer gas, 8 ml/min flow rate dry gas at 350 °C temperature. The eluent composition were 1% aqueous solution of acid acetic (A) and solution of acetonitril-1% and acetic acid (B). The gradient program was the following: from 0 to 55 min: 30 to 100 % B, from 55 to 65 min: 100% B eluent and finally 10 minutes postrun.

### Gas chromatography with mass spectrometry detection

GC-MS experiments were executed by Agilent 6890 N Network GC System, Agilent 5975 mass selector detector and Agilent 19091S-602b HP-1MS (25.0 m × 200 μm × 0.33 μm) column. The carrier was He gas at pressure 168.0 kPa and 1.5 ml/min flow rate. Temperature program was started from 150 °C at 0 min with 10 °C/min temperature gradient to 325 °C. 1 μl from the diluted (1:25) sample was injected at 250 °C injector temperature. Detection was performed in scan mode from m/z 50 to 600, at 70 eV. MS Quad and MS source temperatures were set at 150 and 230 °C respectively.

**ACKNOWLEDGEMENTS**

The work has been funded by the Sectoral Operational Programme Human Resources Development 2007-2013 of the Romanian Ministry of Labour, Family and Social Protection through the Financial Agreement POSDRU/6/1.5/S/16.

We would like to express our gratitude to those who helped us in laboratory work to complete this project, as follows: Ferenc Kilár, Attila Fellinger, Ágnes Dörnyei, Borbála Boros and Anita Bufa from the University of Pécs.

## REFERENCES

1. X.G. Zhao, Y.T. Wang, M. Zhang, L.S. Xu, G.J. Xu, G. Lin, Y.Y. Cui, L.A. Damani, *Zhong Cao Yao*, **1998**, *29*, 343.
2. C.M. Liu, D.Q. Fei, Q.H. Wu, K. Gao, *Journal of Natural Products*, **2006**, *69*, 695.
3. J.Q. Liu, M. Zhang, C.F. Zhang, H.Y. Qi, A. Bashall, S.W.A. Bligh, Z.T. Wang, *Phytochemistry*, **2008**, *69*, 2231.
4. K. Gao, W. Shu, W. Jian Jia, Z. Jian Jia, *Phytochemistry*, **2007**, *47*, 269.
5. K. Gao K., Y. Jia, *Journal of Lanzhou University*, **1997**, *33*, 77.
6. Y.F. Han, J. Pan, K. Gao, Z.J. Jia, *Chemical Pharmautical Bulletin*, **2005**, *53*, 1338.
7. D.Q. Fei, S.G. Li, C.M. Liu, G. Wu, K. Gao, *Journal of Natural Products*, **2007**, *70*, 241.
8. Á. Kapás, B. Ábrahám, C.D. András, S. Lányi, T.G. Dobre, *Studia UBB Chemia*, **2009**, *Ed. spec.*, 21.
9. H. Ishii, T. Tozyo, H. Minato, *Tetrahedron Letters*, **1965**, *21*, 2605.

10. C. Bicchi, P. Rubiolo, C. Frattini, P. Sandra, F. David, *Journal of Natural Products*, **1991**, *54*, 941.
11. S. Meryl, US Patent, 6355684, **2002**.
12. O. Rangel, J. Angel, US Patent, 7604823, **2006**.
13. H. Wiedenfeld, S. Narantuya, M. Duma, A. Monhbaatar, *Scientia Pharmaceutica*, **2003**, *71*, 129.
14. E. Heftmann, "Chromatography: Fundamentals and Techniques", Elsevier, B.V., Amsterdam, **2004**, chapter 2.
15. E. Hoffmann,V. Stroobant "Mass Spectrometry: Principles and Applications", Wiley Intersience, Inc., New Delhi, **2007**, chapter 6.
16. R.E. Ardrey, Liquid chromatography-mass spectrometry: an introduction. John Wiley and Sons Ltd., Chichester, **2003**, chapter 4 and 5.
17. M.C. McMaster, GC/MS: a practical user's guide, John Wiley and Sons, Inc., **2007**, Hoboken, New Jersey, chapter 4.
18. M.K. Makhmudov, B. Tashkhodzhaev, F.B. Zhonkhozhaeva, I.D. Sham'yanov, *Chemistry of Natural Compounds*, **1994**, *29*, 191.
19. L. Tsai, R.J. Highet, W. Herz, *Journal of Organic Chemistry*, **1969**, *34*, 945.
20. J.B. Harborne, H. Bexter, G.P. Moss, Phytochemical dictionary: A handbook of bioactive compounds from plants, Washington, Taylor and Francis, Inc., **1993**, chapter 5.
21. K. Zitterl-Eglseer, J. Jurenitsch, S. Korhammer, E. Haslinger, S. Sosa, R.D. Loggia, W. Kubelka, C. Franz, *Planta Medicina*, **1991**, *57*, 444.
22. J.E. Mullally, F.A. Fitzpatrick, *Molecular Pharmacology*, **2002**, *62*, 351.

STUDIA UBB CHEMIA, LV, Sp.Iss., 2010

# PURIFICATION AND CLEAVING OF THE HUMAN GITRL EXPRESSED AS FUSION PROTEIN

**KOVÁCS ERIKA[a], SZABÓ MÁRIA[a], GÁLICZA JUDIT[a], MIKLÓSSY ILDIKÓ[b], SZILÁGYI LÁSZLÓ[b,c], ÁBRAHÁM BEÁTA[b], LÁNYI SZABOLCS[b]**

**ABSTRACT.** The glucocorticoid-induced tumor necrosis factor (TNF) receptor (GITR) is a member of the TNF receptor superfamily. GITR is activated by its ligand, GITRL. GITRL is a type II transmembrane protein. Human tumor cells express high levels of the GITRL; the presence of it thus can be used as a potential tumor marker. In the present study, the constructed pETM52-hGITRL recombinant vector was transformed into the chemically competent *Escherichia coli* BL21 Star (DE3) strain. After induction with 0.5 mM isopropyl β-D-thiogalactoside (IPTG), the expression was maintained at 37$^{o}$C for an additional 4h. The protein was obtained in sufficient quantity for refolding studies, after which it was purified by affinity chromatography then cleaved from the fusion partner by tobacco etch virus (TEV) protease treatment.

**Keywords:** *GITR, human GITRL, tumor marker, affinity chromatography, TEV protease*

## INTRODUCTION

Tumor necrosis factor receptor superfamily member 18 (TNFRSF18) also known as glucocorticoid-induced tumor necrosis factor receptor (TNFR) family-related protein (GITR) in mouse or activation-inducible TNFR family receptor (AITR) in human is a type I transmembrane protein [1, 2]. The GITR was initially identified as a dexamethasone-inducible molecule on a murine T cell hybridoma [1]. Human GITR and its ligand, GITRL were identified independently by two groups in 1999 [2, 3]. In human tumor models triggering of GITR on NK cells by cell surface-expressed GITRL diminishes effector functions of NK cells [4, 5]. Neutralization of soluble GITRL present in tumor cell supernatants

[a] *Politehnica University, Faculty of Applied Chemistry and Material Science, Splaiul Independenței, Nr. 313, RO-060042 Bucharest, Romania, kovacserka@yahoo.com*
[b] *Sapientia University, Department of Technical and Natural Sciences, Piața Libertății, Nr. 1, RO-530104 Miercurea-Ciuc, Romania, lanyiszabolcs@spientia.siculorum.ro*
[c] *Eötvös Loránd University, Department of Biochemistry, Pázmány Péter Street 1/C, H-1117 Budapest, Hungary, szilagyl@elte.hu*

and patient sera using a GITR-Ig fusion protein restored NK cell reactivity [6], but in mouse tumor models injection of anti-GITR-mAb into tumors provoked potent tumor-specific immunity [7]. This finding suggests that GITR plays a different role in mice and in humans [8], as described more detailed previously [9].

Our aim is the construction of a bacterial expression system, which makes possible the heterologous expression of the human GITRL in soluble form [9]. In this study, we expressed the extracellular region of the human GITRL as a fusion protein, the fusion partner being the molecular chaperone protein DsbA. The solubilized protein was renatured and purified by affinity chromatography, followed by cleavage of the hGITRL from the fusion partner by TEV (tobacco etch virus) protease treatment.

## RESULTS AND DISCUSSION

### Expression of the human GITRL as a fusion protein

Expression of GITRL in bacterial system reported by previous studies [10, 11, 12] resulted in formation of insoluble inclusion bodies. In our construct, pETM52-hGITRL the putative chaperone action of the fusion partner DsbA might promote the correct folding of hGITRL.

The coding sequence of the hGITRL gene was isolated from human brain cDNA, as described before [9]. The isolated gene was cloned in the pETM52 expression vector. The multiple cloning site of pETM52 allows fusion of GITRL to the C terminus of a leaderless DsbA (disulfide-bond A oxidoreductase) protein sequence. DsbA protein is believed to promote formation the native structure of its fusion partners [13].

The recombinant plasmid was transformed into chemically competent *Escherichia coli* BL21 Star (DE3) cells. A starter culture from one single colony was grown overnight at 37$^{o}$C in Luria-Bertani (LB) medium containing 20 µg/ml kanamycine and 1% glucose. The starter culture was added to inoculate 250 ml of LB supplemented with 20 µg/ml kanamycine. The expression culture was grown at 37°C to an $OD_{600\ nm}$ of 0.8, then induced with 0.5 mM isopropyl-1-thio-β-D-galactopyranoside (IPTG). The induced culture was grown for an additional 4h.

The result of the fusion protein expression is presented in Figure 1. As identified by SDS-PAGE the expressed fusion protein consisted of about 60% of total bacterial protein. Contrary to our expectation, the majority of the fusion protein was found in inclusion bodies and a small fraction of the protein was found in soluble form. As this soluble protein precipitated after purification by affinity chromatography, refolding of the insoluble fraction of the protein was carried out in order to obtain hGITRL in sufficient quantity in native form for further studies.

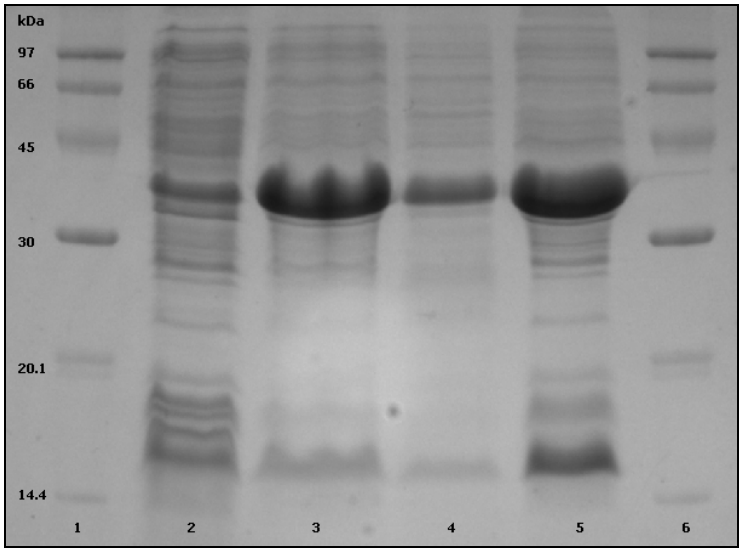


**Figure 1.** Illustration of hGITRL-DsbA expressed in *E. coli*. Lanes 1, 6. protein molecular weight marker, Amersham; Lane 2. proteins from the expression culture before induction; Lane 3. cellular proteins after 4 hours of expression; Lanes 4. soluble proteins; Lane 5. insoluble proteins;

Solubilization of inclusion bodies was performed by guanidine hydrochloride. The refolding of the solubilized inclusion body was achieved by rapid dilution in an oxidized and reduced glutathione system followed by dialysis in Tris-HCl buffer. Figure 2. shows that efficiency of the protein refolding from insoluble fractions was about 95%.

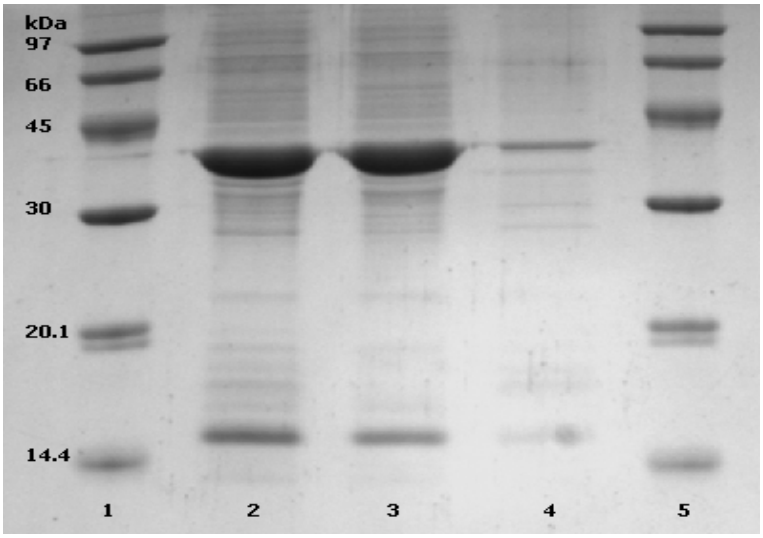


**Figure 2.** Renaturated hGITRL-DsbA analyzed by 16.5% SDS-PAGE. Lane 1. protein molecular weight marker, Amersham; Lane 2. total refolded protein after dialysis. Lane 3. soluble protein after dialysis. Lane 4. insoluble protein after dialysis.

## Purification of the hGITRL by affinity chromatography

The obtained fusion protein, containing a 6xHistidine tag between DsbA and the GITRL sequence, was purified on the principle of affinity chromatography as the $(His)_6$tag is forming a chelate complex with $Ni^{2+}$ ions. The fusion protein was eluted from the affinity matrix with 250 mM imidazole (Figure 3).

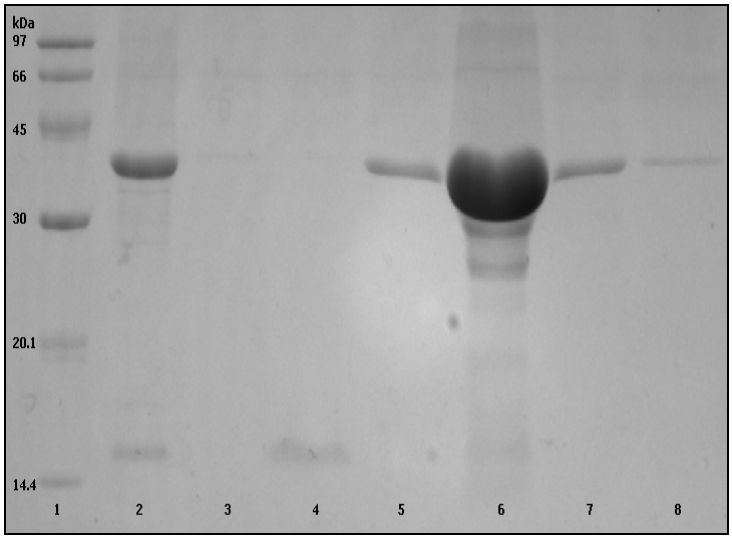


**Figure 3.** Purification of the obtained protein by affinity chromatography. Lane 1. protein molecular weight marker, Amersham; Lane 2. soluble proteins after renaturation; Lane 3. unbound proteins; Lane 4. protein fraction collected after washing; Lanes 5,6,7,8. elution fractions with 250 mM imidazole.

Absorption spectrum of the purified fusion protein was measured by Beckman DU-650 Spectrophotometer, the molar extinction coefficient of the fusion protein for calculations being determined by ProtPARAM TOOL based on the amino acid sequence. The yield of the purified hGITRL-DsbA was about 50-60 mg/liter culture.

## Cleaving of the human GITRL from DsbA by TEV protease

The fusion protein contains a TEV protease cleavage site between DsbA and hGITRL, so the fusion partner can be removed by TEV protease treatment. The purified fusion protein was dialyzed in Tris-HCl buffer, and then the protein of interest (hGITRL) was cleaved from DsbA by TEV protease treatment, as presented in Figure 4. During the TEV protease treatment of the fusion protein, probes were retained in different timepoints for electrophoresis. The quantity of the cleaved protein showed an increase in function of time of the TEV treatment.

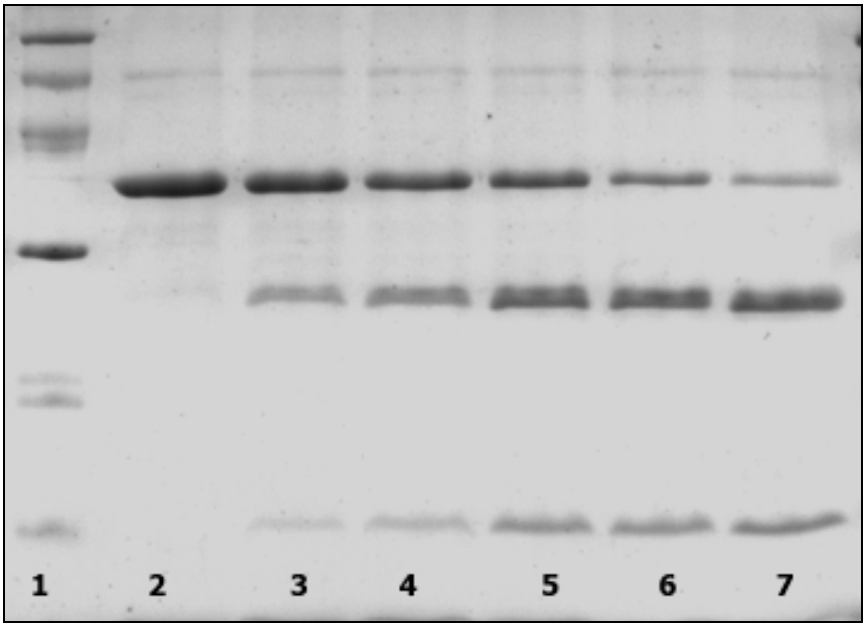


**Figure 4.** Results of the cleavage by TEV protease treatment of the fusion protein (hGITRL-DsbA). Lane 1. Low Protein Marker, Amershan; Lane 2. purified fusion protein; Lane 3. cleaved fusion protein by TEV protease after 1 hour; Lane 4. after 2 hours; Lane 5. after 4 hours; Lane 6. after 8 hours; Lane 7. after 24 hours.

## CONCLUSION

Production of the hGITRL-DsbA fusion protein in *Escherichia coli* was realized successfully. The pETM52 expression vector, containing the DsbA sequence as fusion partner for the protein of interest, was used for the first time to obtain hGITRL gene expression. Previous studies reported that expression of GITRL in *Escherichia coli* resulted in formation of insoluble inclusion bodies [10, 11, 12], but do not contain information about conditions and efficiency of protein refolding. In our study, although the protein was mainly produced as inclusion body, the efficiency of the refolding was about 95%, so we can state that an effective refolding method was elaborated. This unusually high yield is considered to be a result of the chaperon function of DsbA. The fusion protein was purified by affinity chromatography, after which the native state hGITRL was cleaved from the fusion partner from by TEV protease treatment.

Our aim for the future is to separate the cleaved fusion protein by gel filtration, testing the hGITRL activity and the association of recombinant GITRL with different human T cell lines or primary lymphocytes. The study of GITRL would also open alternative pathways for tumor detection and for monitoring of efficacy of various cancer therapies.

## EXPERIMENTAL SECTION

### Expression of the human GITRL as fusion protein

Isolation of total RNA from human brain and the synthesis of cDNA are described previously [14]. The gene of human GITRL (amino acids position 56-177) was isolated from human brain cDNA using forward primer, G1: 5'-CCATGGAGCCCTGTATGGCTAAGTTTGGACC-3' and reverse primer, GITRL: 5-GCGGATCCTACATGTGCTGAAGGGAATGAGG-3' [20]. This gene was inserted in pETM52 expression vector. The pETM52 plasmid was a generous gift of H.B. (EMBL Laboratories, Heidelberg). The construction of the pETM52 vector is described prevoiusly [10]. Construction of the recombinant vector was obtained following a modified protocol as described elsewhere [9]. 1 µl recombinant plasmid was transformed into 100 µl chemically competent *Escherichia coli* BL21 Star (DE3) cells. Protein expression was carried out based on a modified protocol as described before [15]. To produce hGITRL, 250 ml LB medium supplemented with 20 µg/ml kanamycine was inoculated with the starter culture (a single colony was grown overnight at 37°C in 10 ml LB medium containing 20 µg/ml kanamycine and 1% glucose) and was grown at 37°C until $OD_{600}$=0.8. Induction of transcription of the hGITRL gene was realized by IPTG (Sigma) in a final concentration of 0.5 mM and culture was maintained at 37°C in a shaking incubator at 250 rpm for an additional 4 h. After the derepression period cells were harvested by centrifugation (15 minutes at 5000 rpm, 4°C) and lyzed by sonication. The inclusion body was washed three times with 30 ml of 10 mM Na-phosphate buffer pH 7.0, 0.1 M NaCl and 0,1% β-mercaptoethanol.

The inclusion body was solubilized by 10 ml 6 M guanidine hydrochloride (Gu-HCl, Sigma) treatment, supplemented with 50 mM Tris-HCl buffer pH 8.8 and 1 mM dithiothreitol (DTT, Serva) and was reduced overnight at room temperature. The solubilized material was refolded by the fast dilution method in an oxidized/reduced glutathione (Sigma) system. 2 ml of the solubilized material was diluted into 60 ml ice-cold refolding buffer (0.8 M Gu-HCl, 0.1 M Tris-HCl pH 8.0, 5 mM $CaCl_2$, 0.5 mM EDTA, 5 mM reduced glutathione and 0.5 mM oxidized glutathione). The solution was stirred by magnetic stirring at 4°C for 8 h. The refolded protein was dialyzed in 50 mM NaCl and 10 mM Tris-HCl buffer pH 8.0.

### Purification of the obtained protein by affinity chromatography

Affinity purification of the His-tagged protein was carried out by adsorption on a Ni-charged polymer matrix (Porfinity IMAC Ni-charged Resin, BioRad). Soluble proteins resulted from 60 ml of diluted protein were adsorbed on 3 ml of Ni-NTA Sepharose resin, after washing of the resin with 20 ml Binding Buffer (50 mM sodium phosphate buffer pH 8.0 supplemented with 0.3 M NaCl) for

equilibration. After the adsorbtion of the soluble proteins the beads were washed again with Washing Buffer (50 mM sodium phosphate buffer supplemented with 0.5 M NaCl). Elution of the protein from the adsorber matrix was realized by four-step elution with a 250 mM concentration of elution agent imidazole (Sigma), which has increased binding affinity to the Ni-charged matrix with respect to the 6xHis-tagged proteins. The supernatant containing the purified protein was stored at 4°C; from each fraction electrophoresis probes of 20 µl were retained.

### Cleaving of human GITRL from DsbA by TEV protease

The eluted fraction was dialyzed in 20 mM Na-phosphate buffer, pH 8.0 supplemented with 100 mM NaCl. The dialysis buffer was changed two times, after which the protein solution was centrifuged. The cleavage with a tobacco etch virus (TEV protease recombinant, Invitrogen) protease was performed in 1mM DTT at room temperature.

**ACKNOWLEDGMENTS**

This study was supported by the Department of Technical Sciences, University of Sapientia and the Department of Biochemistry, Eötvös Loránd University.

The work has been funded by the Sectoral Operational Programme Human Resources Development 2007-2013 of the Romanian Ministry of Labour, Family and Social Protection through the Financial Agreement POSDRU/6/1.5/S/19 and the national grant of the 4th Programme Parteneriates in the Priority Fields nr. 42-147/2008.

## REFERENCES

1. G. Nocentini, L. Giunchi, S. Ronchetti, L.T. Krausz, A. Bartoli, R. Moraca, G. Migliorati, C. Riccardi, *Proceedings of the National Academy of Sciences of the United States of America,* **1997**, *94*, 6216.
2. B. Kwon, K.-Y. Yu, J. Ni, G.-L. Yu, I.-K. Jang, Y.-J. Kim, L. Xing, D. Liu, S.-X. Wang, B.S. Kwon, *The Journal of Biological Chemistry*, **1999**, *274*, 6056.
3. A.L. Gurney, S.A. Marsters, R.M. Huang, R.M. Pitti, D.T. Mark, D.T. Baldwin, A.M. Gray, A.D. Dowd, A.D. Brush, A.D. Heldens, A.D. Schow, A.D. Goddard, W.I. Wood, K.P. Baker, P.J. Godowski, A. Ashkenazi, *Current Biology*, **1999**, *9*, 215.
4. K.M. Baltz, M. Krusch, A. Bringmann, P. Brossart, F. Mayer, M. Kloss, T. Baessler, I. Kumbier, A. Peterfi, S. Kupka, S. Kroeber, D. Menzel, M.P. Radsak, H.G. Rammensee, H.R. Salih, *The Journal of the Federation of American Societies for Experimental Biology*, **2007**, *21*, 2442.

5. K.M. Baltz, M. Krusch, T. Baessler, B.J. Schmiedel, A. Bringmann, P. Brossart, H.R. Salih, *Blood*, **2008**, *112*, 3735.
6. B. Liu, Z. Li, S.P. Mahesh, S. Pantanelli, F.S. Hwang, W.O. Siu, R.B. Nussenblatt, *The Journal of Biological Chemistry*, **2008**, *283*, 8202.
7. K. Ko, S. Yamazaki, K. Nakamura, K. Hirota, T. Yamaguchi, J. Shimizu, T. Nomura, T. Chiba, S. Sakaguchi, *The Journal of Experimental Medicine*, **2005**, *202*, 885.
8. G. Nocentini, C. Riccardi, *European Journal of Immunology*, **2005**, *35*, 1016.
9. E. Kovács, M. Pálfi, I. Miklóssy, L. Szilágyi, B. Ábrahám, Sz. Lányi, *Studia UBB Chemia*, **2009**, Special Issue *2*, 83.
10. K. Chattopadhyay, U.A. Ramagopal, A. Mukhopadhaya, V.N. Malashkevich, T.P. DiLorenzo, M. Brenowitz, S.G. Nathenson, S.C. Almo, *Proceedings of the National Academy of Sciences of the United States of America*, **2007**, *104*, 19452.
11. Y. Jiao, F. Zheng, X. Li, B. Wang, S. Guo, *Chinese Journal of Biotechnology*, **2009**, *25*, 708.
12. D. Cui, S. Wang, Y. Chen, J. Tong, J. Ma, L. Tang, X. Yang, Y. Shi, J. Tian, L. Lu, H. Xu, *Cellular and Molecular Immunology*, **2010**, *7*, 316.
13. A. Dümmler, A.-M. Lawrence, A. de Marco, *Microbial Cell Factories*, **2005**, *4*, 1.
14. J. Tóth, E. Siklódi, P. Medveczky, K. Gallatz, P. Németh, L. Szilágyi, L. Gráf, M. Palkovits, *Neurochemical Research*, **2007**, *32*, 1423.
15. I. Miklóssy, L. Szilágyi, B. Ábrahám, Sz. Szilveszter, Sz. Lányi, *Studia UBB Chemia*, **2009**, Special Issue *2*, 11.

STUDIA UBB CHEMIA, LV, Sp.Iss., 2010

# PHOSPHORUS MOBILIZATION FROM DIFFERENT INORGANIC PHOSPHATES BY BACTERIA PROPOSED FOR BIOFERTILIZER

**LASLO ÉVA[a,*], GYÖRGY ÉVA[b], MARA GYÖNGYVÉR[b], SZENTES SAROLTA[a], ANDRÁS CSABA[b], LÁNYI SZABOLCS[b]**

**ABSTRACT.** Phosphorus is absorbed by the plants as orthophosphate anions ($HPO_4^{2-}$ and $H_2PO_4^-$). The concentration of soluble phosphate in soil is low and it must be supplemented from other sources. Some of the bacteria with phosphate solubilising capacity are able to transform the accumulated insoluble phosphates in the soil into soluble forms, making them available for plants.

Our aim was to assay phosphorus mobilization from different inorganic phosphates (calcium and iron phosphate, hydroxyapatite) by bacteria isolated from rhizospheric soil proposed for biofertilizer production.

***Keywords:*** *calcium phosphate, iron phosphate, hydroxyapatite, phosphorus solubilisation*

## INTRODUCTION

Plant growth promoting rhizobacteria use different mechanisms to improve the growth of plants. One of these plant growth promoting traits is mineral phosphate solubilisation. Due to this process, the bacteria increase the bioavailability of the phosphorus and improve soil fertility.

Phosphorus is the second most important plant growth limiting macronutrient. This element plays a central role in different metabolic pathways, photosynthesis, respiration, cell division, energy transport, as well as signal transduction. With these, it contributes to the development and growth of the plant biomass [2].

The insoluble mineral phosphate content of soils is high, while the soluble orthophosphate content, which is available both for bacterial and plant use, is relatively low [2]. Phosphorus used as fertiliser rapidly enters the immobilized complexes, reacts with metal ions such as $Fe^{2+}$, $Al^{3+}$ in acidic soils and $Ca^{2+}$ in alkaline soils. The insoluble forms are $CaHPO_4$, $Ca_3(PO_4)_2$,$FePO_4$ and $AlPO_4$ [3,4].

[a] *Universitatea POLITEHNICA din Bucureşti*, *Facultatea de Chimie Aplicată şi Ştiința Materialelor; Spl. Independenței, 313, Sector 6, RO-060042 Bucureşti; lasloeva@sapientia.siculorum.ro*

[b] *Universitatea SAPIENTIA Cluj-Napoca,, Facultatea de Ştiințe Sociale şi Tehnice; Piața Libertății nr. 1, RO-530104 Miercurea-Ciuc*

Phoshate-solubilising bacteria mobilize the insoluble mineral phosphate through two mechanisms: production of low molecular weight organic acids and $H^+$ extrusion [5]. In the first mechanism the transformation of the accumulated insoluble phosphates of soil into a soluble form is related to the direct oxidation pathway in the periplasmatic space of the bacteria. This is the primary mechanism for aldose utilization in many bacteria. One of these mechanisms is the enzymatic conversion of glucose to gluconic acid and 2-keto gluconic acid by quinoprotein glucose dehydrogenase [6,7,8]. Carboxylic anion groups of the secreted acids chelate the metal ions of the mineral phosphate ($Ca^{2+}$ from tricalcium phospahate and hydroxyapatite) with ligand exchange reaction. The result of this reaction is the release of the soluble orthophosphate [9].

This fact was demonstrated in the case of many bacteria with phosphate solubilisation capacity. *Azospirillum* spp. produced different organic acids that take part in the mobilization of insoluble phosphates [10]. In *Rhizobium* species the phosphorus solubilisation is the result of the production of 2-glukonic acid [3]*. Burkholderia cepacia* DA23 released gluconic acid in medium during the solubilisation of approximately 800 mg/l orthophosphate. It was shown that the expression of this pathway in solubilising calcium phosphates may be induced by phosphate starvation conditions in the medium [11].

The other proposed mechanism of the solubilisation is through proton release from the cytoplasm of the bacteria to the outer surface. In this way the negative charge of the surface facilitate the sorption of negatively charged phosphorus ions [6].

For the genetics of this mechanism it was identified some genes and plasmids that play a role in the mineral phosphate solubilisation, such as *mps* in *Erwinia herbicola*, *gabY* in *Pseudomonas cepacia* [12].

The aim of this paper was to assay phosphorus mobilization from different inorganic phosphates (calcium and iron phosphate, hydroxyapatite) by bacteria, isolated from leguminous plants nodules and rhizospheric soil, proposed for biofertilizer production.

## RESULTS AND DISCUSSION

In this study, using the spectrophotometric method, we measured the solubilised orthophosphate content by eleven isolated bacteria in the presence of three insoluble phosphates. The isolated bacteria originated from the root nodule and rhizospheric soil of different leguminous plants. The orthophosphate concentration was measured during a period of ten days (72 h, 96h, 144 h, 172h, 240h).

From the assayed isolates the bacterial culture originated from the rhizospheric soil of *Cytisus hirsutu*s L. (T1310-2/1) had the maximum phosphate mobilization capacity (Fig.1). In the case of the calcium phosphate (CaP) the

measured orthophosphate concentration varied between 347.59 mg/l and 421.73 mg/l. The maximum value was detected on the eighth day. In the presence of hydroxyapatite (CaPOH), the obtained values were also similar. We measured also the maximum value in the case of iron phosphate (FeP). The maximum orthophosphate concentration was 89 mg/l after 240 h.

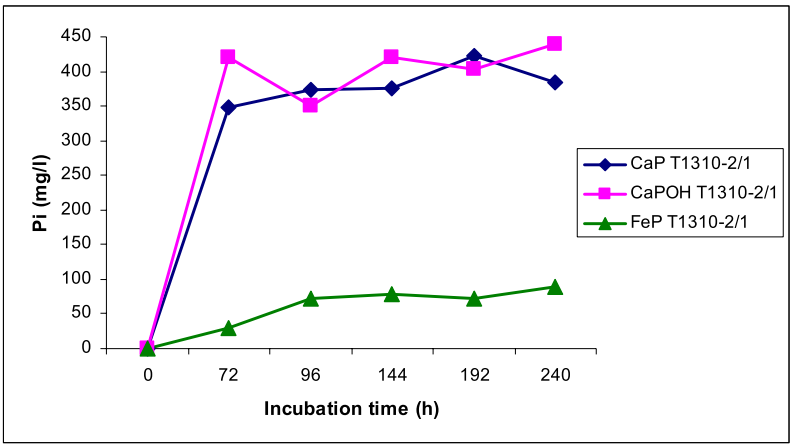


**Figure 1.** The measured phosphate concentration (in the liquid medium containing the three different phosphates) during the cultivation of the bacterial isolate originated from the rizosphere of *Cytisus hirsutus* L.

Bacterial isolate (T1110-2/3) originated from the rhizosphere of *Vicia sepium* L. had the lowest phosphate solubilisation capacity. The orthophosphate content (Fig.2) of the liquid culture medium, which contained calcium phosphate, varied between 1.75 mg/l and 114.82 mg/l.

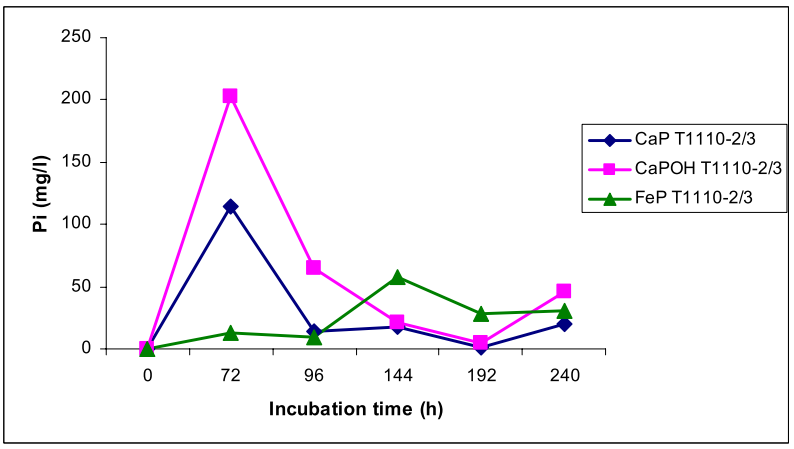


**Figure 2.** The measured phosphate concentration (in the liquid medium containing the three different phosphates) during the cultivation of the bacterial isolate originated from the rizosphere of *Vicia sepium L.*

In the presence of hydroxyapatite the measured values were between 4.3 mg/l and 202 mg/l. In both cases the highest concentration was measured on the third day of the incubation time. In the case of iron phosphate the measured values were between 9.4 mg/l and 57 mg/l.

The phosphate concentration mobilized by the bacterial isolate (1G/2) originated from the root nodule of the *Anthyllis vulneraria L.* changed between 148.76 mg/l (96 h) and 92.06 mg/l (Fig.3) (at 192 h).

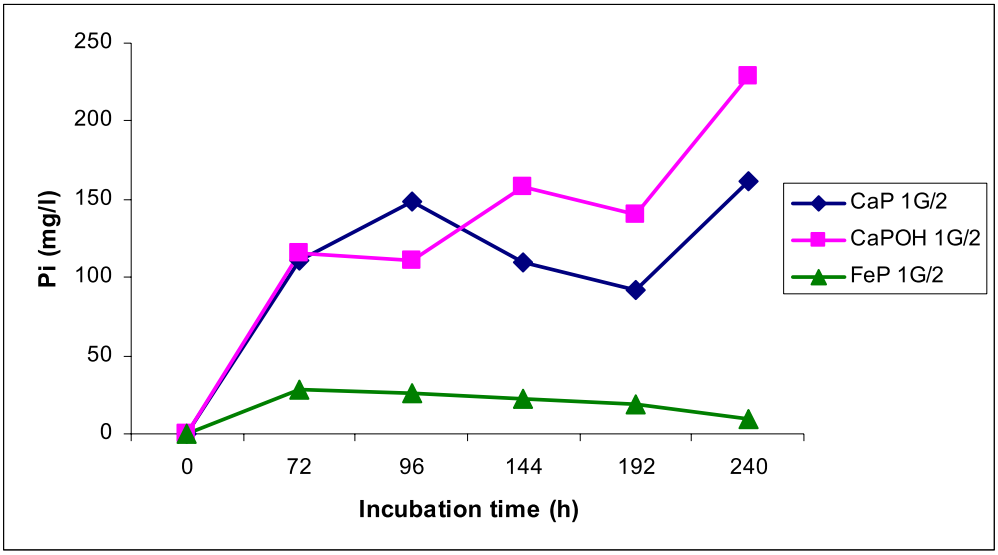


**Figure 3.** The measured phosphate concentration (in the liquid medium containing the three different phosphates) during the cultivation of the bacterial isolate originated from the root nodule of *Anthyllis vulneraria L.*

The free phosphate concentration varied between 110.68 mg/l and 228.97 mg/l in the presence of hydroxyapatite and 21 mg/l and 28 mg/l in the case of iron phosphate.

The free phosphate concentration (Fig.4.) solubilised by the bacteria isolated (T510-1/2) from the rhizosphere of *Trifolium montanum L.* changed between 80.68 mg/l and 181.43 mg/l in the presence of the calcium phosphate. In the case of hydroxyapatite we measured the highest concentration (231.64 mg/l) after 240 h. The highest solubilised phosphate content was 27.97 mg/l in the culture medium which contained the insoluble iron phosphate.

The maximum solubilised phosphate content (Fig.5) in the presence of calcium phosphate was 186.80 mg/l on the tenth day of the incubation. Again, the highest concentration was detected after 240 h in the presence of hydroxyapatite. The solubilised phosphate content was between 12.44 mg/l and 43 mg/l in the culture medium with iron phosphate content.

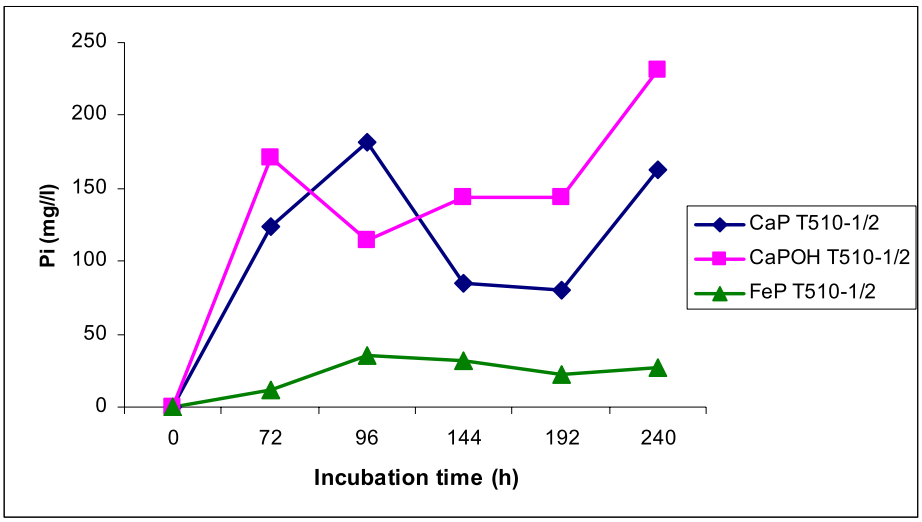


**Figure 4.** The measured phosphate concentration (in the liquid medium containing the three different phosphates) during the cultivation of the bacterial isolate originated from the rizosphere of *Trifolium montanum L.*

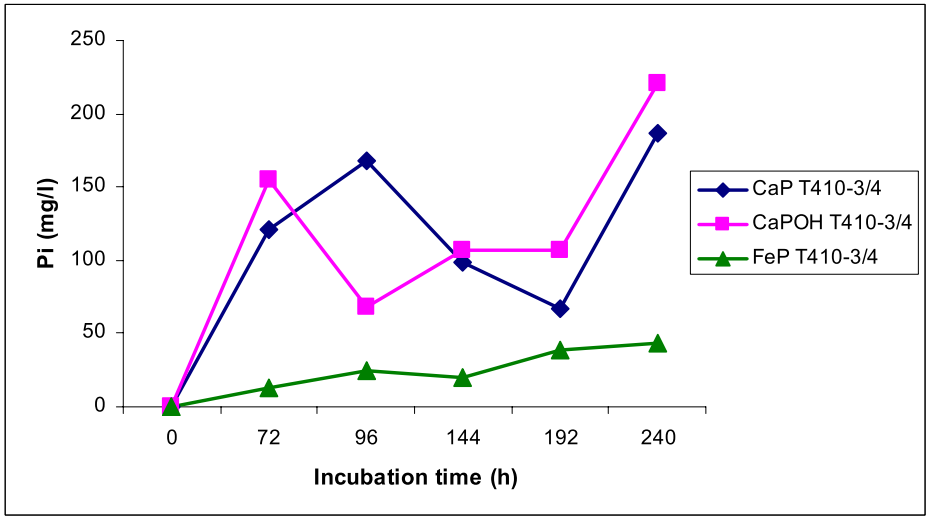


**Figure 5.** The measured phosphate concentration (in the liquid medium containing the three different phosphates) during the cultivation of the bacterial isolate (T410-3/4) originated from the rizosphere of *Trifolium repens L.*

The phosphate mobilization capacity differed in the case of two bacterial isolates (T810-2/1,T810-1/3) that originate from the rhizosphere of the same plant (Fig.6 and Fig.7).

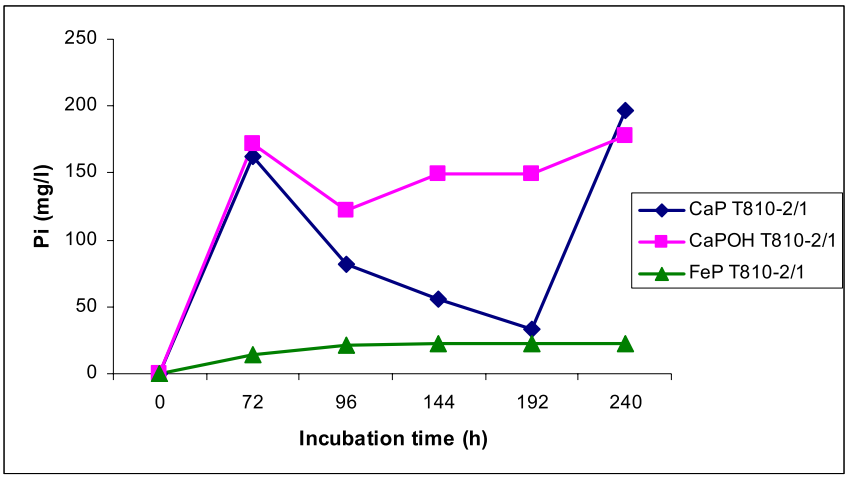


**Figure 6.** The measured phosphate concentration (in the liquid medium containing the three different phosphates) during the cultivation of the bacterial isolate originated from the rizosphere of *Trifolium alpestre L.*

The highest phosphate concentration was measured at both of the isolates on the tenth day of the incubation in the presence of the calcium phosphate.

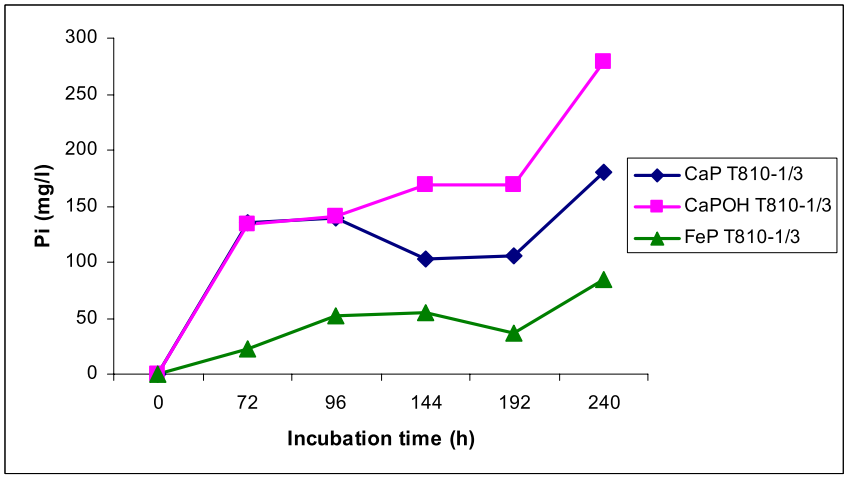


**Figure 7.** The measured phosphate concentration (in the liquid medium containing the three different phosphates) during the cultivation of the bacteria isolate originated from the rizosphere of *Trifolium alpestre L.*

The highest free phosphate concentration (Fig.8) (mobilized by the isolated bacteria originated from *Lupinus polyphyllus Lindl.*(KLG16) in the case of the three phosphates (calcium phosphate, hydroxyapatite and iron phosphate) were 203.14 mg/l, 209.14 mg/l and 59.83 mg/l.

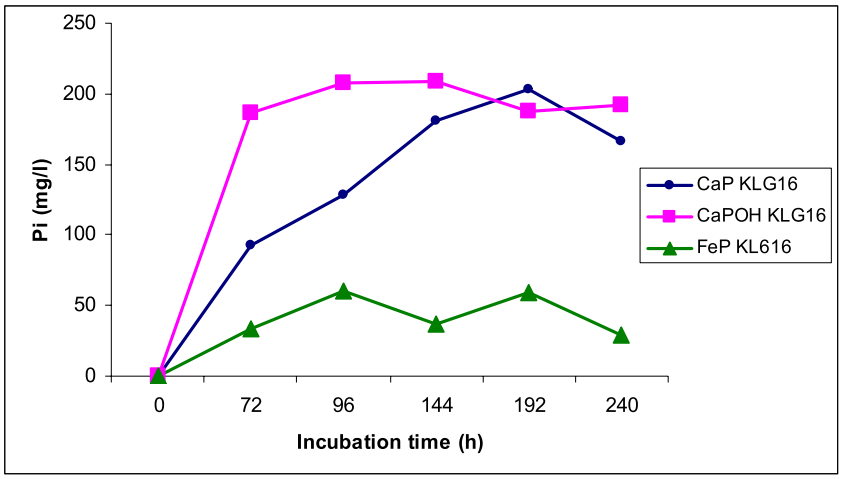


**Figure 8.** The measured phosphate concentration (in the liquid medium containing the three different phosphates) during the cultivation of the bacterial isolate originated from the root nodule of *Lupinus polyphyllus*

The detected phosphate concentration (Fig.9) solubilised by the isolate (KLT20) originated from *Lupinus polyphyllus* Lindl. in the presence of the calcium phosphate were between 65.9 mg/l and 170.33 mg/l. In the culture medium with hydroxyapatite content the measured free phosphate concentration was 86.23 mg/l and 220.04 mg/l. In the case of iron phosphate the highest orthophosphate concentration was measured on the tenth day.

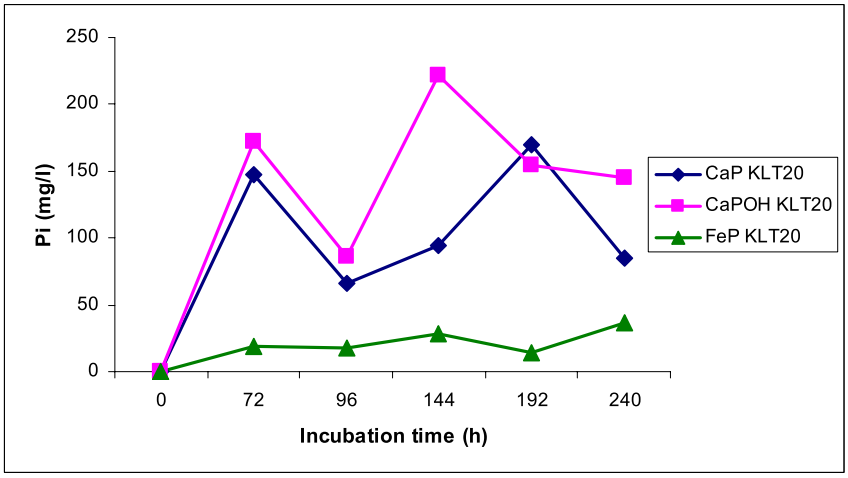


**Figure 9.** The measured phosphate concentration (in the liquid medium containing the three different phosphates) during the cultivation of the bacterial isolate originated from the the rizosphere of *Lupinus polyphyllus*

The detected phosphate concentration (Fig.10 and Fig.11) was between 92.7 mg/l and 203.4 mg/l, 81.05 mg/l and 148.58 mg/l in the presence of calcium phosphate in the case of the two bacteria cultures (H39, H31) isolated from the rhizosphere of *Trifolium hybridum* L. In the culture medium with iron phosphate the free phosphate concentration varied between 7.84 mg/l and 65.99 mg/l, 10.79 mg/l and 54.09 mg/l. The highest values were measured in these two isolates in the presence of hydroxyapatite 276.01 mg/l (Fig.11) and 335.55 mg/l (Fig.10).

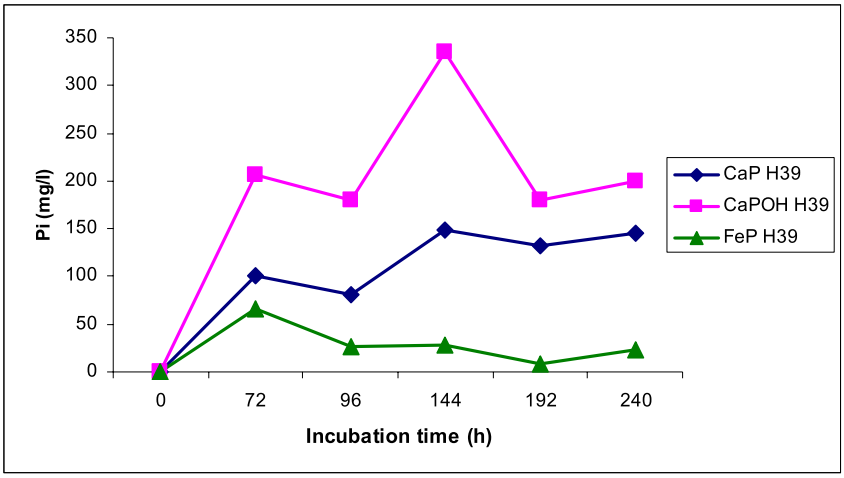


**Figure 10.** The measured phosphate concentration (in the liquid medium containing the three different phosphates) during the cultivation of the bacterial i solate originated from the rizosphere of *Trifolium hybridum L.*

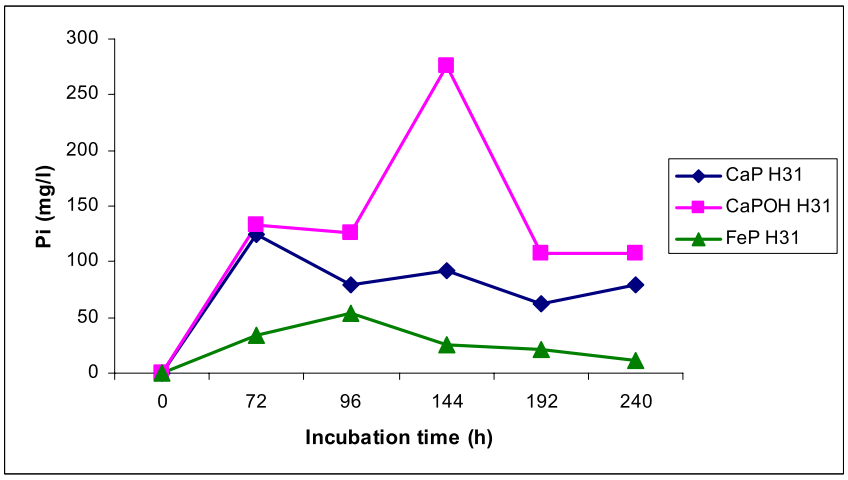


**Figure 11.** The measured phosphate concentration (in the liquid medium containing the three different phosphates) during the cultivation of the bacterial solate originated from the rizosphere of *Trifolium hybridum L.*

The measured solubilised phosphate concentration is very variable during the incubation period in all of the isolates. This variation is not linear, and it can be explained by the fact that many bacteria accumulate the inorganic phosphates in poly polyphosphate form if it is in excess in their environment. The phosphorus acquisition in bacteria takes place via inorganic transport system [13].

According to the principal component analysis, based on colony morphology properties, the bacteria isolates from the nodules and the soil samples are grouped in three main classes. The morphological properties, with the exception of a few strains, were the same or very similar (Fig 12).

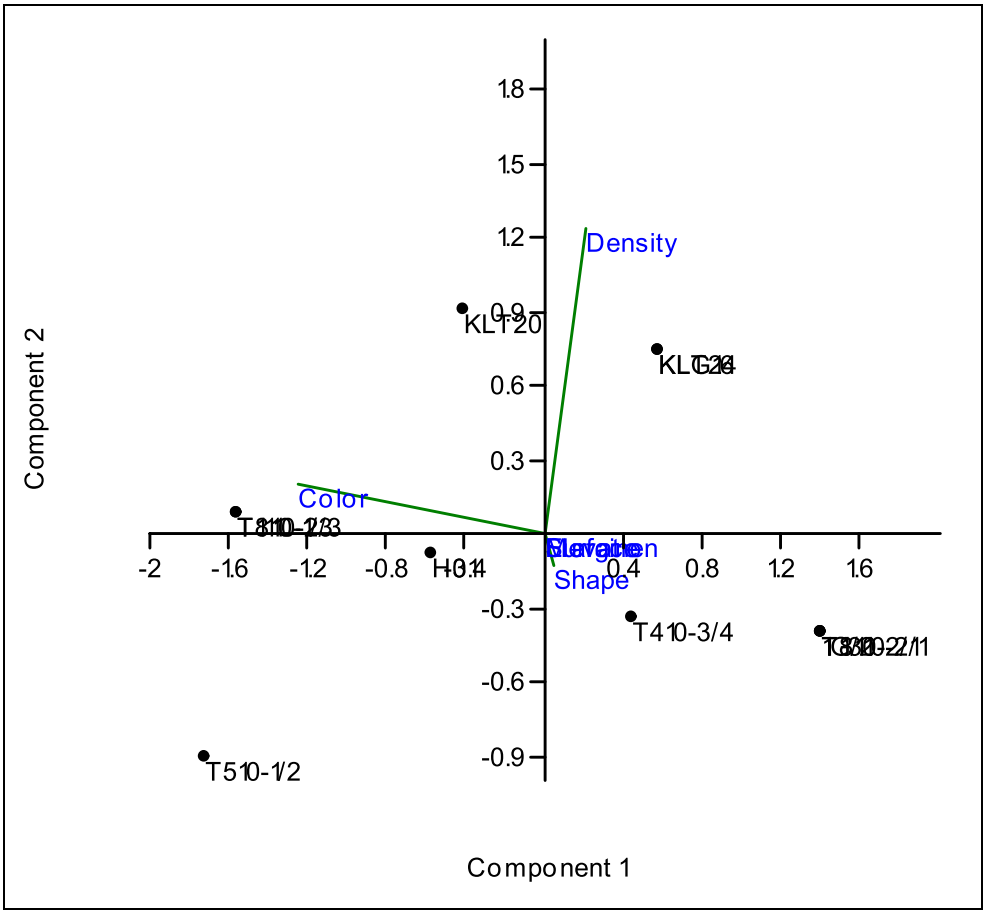


**Figure 12.** Principal component analysis of bacterial isolates based on morphological characteristics

In most of the cases, the shape of the colonies were round, only one of the colonies presented irregular shaped colony (T410-3/4). The elevation of the colonies was raised in all cases and the margins were entire. At three isolates (1G/2, T1310-2/1, T810-2/1) the middle of the colonies were yellow and the margins were creamy. In the case of six bacterial strains, the colonies were

yellow and one colony had a creamy color. The surfaces of the colonies of the isolates were glistening. The density of colonies in the middle were opaque with transparent margins at seven isolates, while in the case of three bacteria was transparent (KLT24, KLG16, KLT20). Only one bacterial colony was found to be opaque (T510-1/2).

## CONCLUSIONS

The eleven bacterial isolates are able to mobilize a relatively high amount of free phosphate, thus increasing the bioavailability of orthophosphates for plants.

The solubilised phosphate concentration from the different three highly soluble phosphate compounds in the case of some isolates is similar with the values described in the literature [15].

On the basis of the results these bacteria can be used for the development of phosphorus solubilisation biofertilizers.

## EXPERIMENTAL SECTION

### Bacterial Strains

The assayed bacterial cultures were isolated from the rhizosphere and root nodule of different leguminous plants: *Trifolium hybridum L, Lupinus polyphyllus, Trifolium alpestre L., Cytisus hirsutus L., Anthyllis vulneraria L., Trifolium montanum L., Trifolium repens L.*

The qualitative phosphate solubilisation capacity of these isolates was detected on Pikovskaya agar medium [14].

### Determination of solubilised phosphate content

The quantitative determination of phosphate solubilisation was carried out in modified Sperber medium (glucose 10 g/l, yeast extract 0.5 g/l, $CaCl_2$ 0.1 g/l, $MgSO_4 \cdot 7H_2O$ 0.25 g/l, $(NH_4)_2SO_4$ 0.5 g/l) with three different phosphates: calcium phosphate 5g/l, hydroxyapatite 5g/l, iron phosphate 3 g/l.

The 24 h cultures were inoculated in sterile physiology solution and cell density was adjusted to 55% transmittance on a Biolog turbidimeter for each. 90 ml of modified Sperber medium was inoculated with 250 μl bacterial suspension and incubated on rotary shaker at 28°C with 150 rpm for ten days. The mobilized free phosphate concentration was measured five times after 72 h, 96 h, 144 h, 192 h and 240 h.

Before the measurement of the phosphate content of the culture medium, the cultures were centrifuged at 6000 rpm for 15 min. 500 μl of the supernatant was mixed with 500 μl 10% trichloroacetic acid for the protein precipitation.

Then 4 ml of mixed reagent (ammonium paramolybdate, sulfuric acid, ascorbic acid, potassium-sodium tartarate) was added, and was incubated on room temperature for 15 min. The absorbance of the solution was measured at 880 nm. The amount of mobilized phosphate was detected from the standard curve of $KH_2PO_4$ [15, 16].

### Determination of the morphological characteristics

The colony morphology properties of the isolates with phosphate solubilisation capacity were determined on YEM medium (contained per liter of distilled water: 10 g mannitol, 0.5 g $K_2HPO_4$, 0.2 g $MgSO_4 \cdot 7H_2O$, 0.1 g NaCl, 1 g yeast extract, 0.2 $CaCl_2 \cdot 2H_2O$, 0.01 g $FeCl_3 \cdot 6H_2O$, 20 g agar, 25 μg/ ml bromthimol blue pH 6.7–7.0.).

The determined morphological characteristics included the colony size, elevation, density, color, shape and margin.

**ACKNOWLEDGMENTS**

The work has been funded by the Sectoral Operational Programme Human Resources Development 2007-2013 of the Romanian Ministry of Labour, Family and Social Protection through the Financial Agreement POSDRU/88/1.5/S/60203.

The laboratory experiments were prepared with the financial support from the “BIOPREP – Microbial biopreparates for increasing the productivity and crop protection” research funded by Sectoral Operational Programme, Increase of Economic Competitiveness Operation 2.1.1. of the Romanian Ministry of Labour, Family and Social Protection, through financial agreement POSCEE No. 469/11817.

## REFERENCES

1. A. Zaidi, M. Ahemad, M. Oves, E. Ahmad, M. S. Khan, "Microbes for Legume Improvement", Springer-Verlag, Wien, 2010, chapter 11.
2. A.H. Goldstein, P.U. Krishnaraj, *Dev Plant Soil Sci.*, **2007**, *102*, 203.
3. P. Gyaneshwar, G.N. Kumar, L.J. Parekh, P.S. Poole, *Plant Soil.*, **2002**, *245*, 83.
4. K.H. Park, Lee CY, Son HJ, *Let Appl Microbio.*, **2009**, *49*, 222.
5. P. Illmera, F. Schinnera, *Soil Bio Biochem.*, **1992**, *24*, 389.
6. B. Sashidhar, A.R. Podile, *J Appl Microbio.*, **2010**, *109*, 1.
7. A. Buch, G. Archana, G.N. Kumar, *Res Microbiol.*, **2008**, *159,* 635.
8. B. Sashidhar, A.R. Podile, *Microbial Biotech.*, **2009**, *2*, 521.

9. A.A. Khan, G. Jilani, M.S. Akhtar, S.M.S. Naqvi, M. Rasheed, *J Agr Biol Sci.*, **2009**, *1*, 48.
10. Y. Bashan, L.E. de Bashan, *Adv Agron.*, **2010**, *108*, 77.
11. O-R. Song, S-J Lee, Y-S Lee, S-C Lee, K-K Kim, Y-L Choi, *Braz J Microbio.*, **2008**, *39*, 151.
12. H. Rodrıguez, R. Fraga, T. Gonzalez, Y. Bashan*, Plant Soil.*, **2006**, *287*, 15.
13. R. Hirota, A. Kuroda, J. Kato, H. Ohtake, *J Biosci Bioeng.*, **2010**, *109*, 423.
14. É. Laslo, É. György, Gy. Mara, É. Tamás, I. Máthé, B. Ábrahám, Sz. Lányi, *Studia UBB Chemia*, **2009**, *LIV*, 53.
15. H.A. Alikhani, N. Saleh-Rastin, H. Antoun, *Plant Soil*, **2006**, *287*, 35.
16. M. Chaiharn, S. Lumyong, *World J Microb Biot.*, **2009**, *25*, 305.

STUDIA UBB CHEMIA, LV, Sp.Iss., 2010

# NEW COMPOSITE MATERIALS PLATES FROM VEGETAL FIBRES

**OVIDIU NEMES[a,*], AMALIA MIHAELA CHIPER[a], ANDREEA RAMONA RUS[a], VASILE FILIP SOPORAN[a], OVIDIU TATARU[a], PAUL BERE[a]**

**ABSTRACT.** The first step in obtained new composite materials plates from vegetal fibers is the chemical treatment of those fibers. Chemical treatments carried out on plant fibers lead to changes on their surface, changes that increase the adhesion between fiber and matrix. Treatment of vegetable fibers with alkaline solutions on different concentrations show that the changes on the fiber surface increased significantly with increasing concentration of alkaline solution. The best results were acquired in the case of a chemical treatment with a solution of KOH 10%.

***Keywords:*** *composite material plates, vegetal fibers, chemical treatments.*

## INTRODUCTION

Composite materials obtained using wood fibers or other plant fibers may be a potential candidate for partial replacement of the glass fiber or Kevlar fibers used in obtaining polymer matrix composites. Composite plates with wood fibers could provide an excellent eco-friendly solution to real problems regarding fast consumption of natural resources. Composite materials containing wood fiber or other plant fibers are more and more studied.

These new material configurations are attractive both in terms of lower costs but also because of their mechanical properties which recommend them as a new generation of materials [1-3]. Concerning the length and geometry of cellulosic fibers, they are cylindrical with approximately constant diameter and specific area. This is not the case for cellulosic fibers that present many defects caused by processing [4]. These defects are apparent as 'knees' at the fiber surface and constitute points where the fiber may fracture more easily. In addition, an important parameter is the aspect ratio (length/diameter), which has an influence on the mechanical properties of the composite. The aspect ratios of wood, including its physical structure, mechanical properties, and density, change

[a,*] *Universitatea Tehnica din Cluj-Napoca, Facultatea de Ingineria Materialelor si a Mediului, B-dul Muncii, Nr. 103 - 105, Cluj-Napoca, 400641, Cluj. România*

from species to species [5]. The fiber aspect ratio is a critical parameter in a composite material. An aspect ratio in the range of 100-200 after composite processing is recommended for high performance short fiber composites. The strength of the unidirectional aligned composites normal to the fiber alignment (transverse) is less than that of the randomly oriented fiber composite. When the fibers are aligned perpendicular to the force direction (transverse), fibers are not reinforcing the matrix to increase the strength of the composite in the direction of applied load [6].

A first step, in obtaining the composites plates, consists in the chemical treatment of fibers. Natural fibers can be chemically treated due to the presence of hydroxyl groups in lignin and cellulose. These OH groups can change the surface energy and polarity of the natural fibers during various treatments. The most common methods of surface treatment are mercerization (alkali treatment) [7], isocyanate treatment [8], acrylation [9], benzoylation [10], permanganate treatment, silane treatment [11] and peroxide treatment [12]. All these treatments can improve adhesion of the fibers with the polymer matrix and leads to higher impact resistance in comparison with samples containing fibers with no chemical treatment.

This paper presents a comparative study regarding the changes at the interfaces in wood and straw fibers treated with alkaline solutions (KOH) in different concentrations. The morphology of the fibers was investigated using scanning electron microscopy SEM.

## RESULTS AND DISCUSSION

Chemical treatments can increase the adhesion at the interface between the fiber and matrix and removed the non-cellulosic compounds, which constitute the main objective of the chemical treatments. Therefore, chemical treatments should be considered in modifying the properties of natural fibers.

During the chemical treatment, a part of hydroxyl groups of cellulose will be replaced with units Fiber-$O^-$-$K^+$.

$$\textbf{Fiber} - \textbf{OH} + \textbf{KOH} \rightarrow \textbf{Fiber} - \textbf{OK} + \textbf{H}_2\textbf{O}$$

This process was also observed in the case of wood fibers treated with NaOH solution [13].

Changes occurring at the fiber interface were analyzed using FTIR spectroscopy. FTIR spectra analysis shows no significant differences between the treatments of wood fibers realized with NaOH or KOH solution at similar concentrations. Specific signals in the case of fibers treated with KOH (5%) appear in the same area as in the case of samples treated with NaOH

reported in literature [14, 15] (3990 $cm^{-1}$, 1720 $cm^{-1}$ respectively). The intensity of signal situated at 3990 $cm^{-1}$ decrease with increasing concentration of KOH solution (8% and 10%), this is correlated with decreased number of -OH groups located on the fiber surface. A similar trend is observed for the signal situated at 1720 $cm^{-1}$ whose intensity decreases when Fiber-OK unit appear.

A usual method to study the morphology of plant fibers is the SEM method. SEM analysis was made on untreated and treated vegetal fibers. The treatment was realized with different concentrations of KOH solution.

## SEM microscopy study in the case of wood fibers

In this study we used a mixture of hardwood sawdust. One aspect to be taken into account in the characterization of wood fibers is the size (Figure 1).

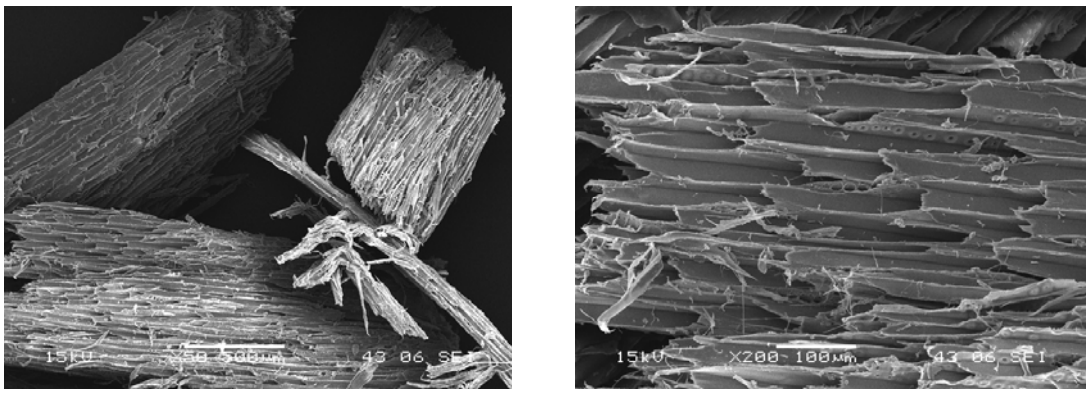


**Figure 1.** SEM images of wood fiber.

The morphology of the wood fiber, cell size and shape were investigated using scanning electron microscopy (JOEL JSM5510 LV). We observed the sawdust before and after alkaline treatments. In the case of untreated sawdust we can see the normal unchanged cellular structure of wood fiber. The fibers are arranged longitudinally with cellular communication channels (trachea) which transport water, minerals and elaborated sap from root to leaf area.

The SEM images (Figure 2) show the difference between treated and untreated wood fibers. Untreated fiber surface has many large impurities (Figure 2a). Treated wood fibers with KOH 5% solution (Figure 2b) are not affected, there is no fracture and provide a clean surface with few traces of impurities.

The treatment with KOH 10% cleans the fiber surface but affect it causing many fractures (Figure 2c).

The SEM images show the difference between treated and untreated wood fibers.

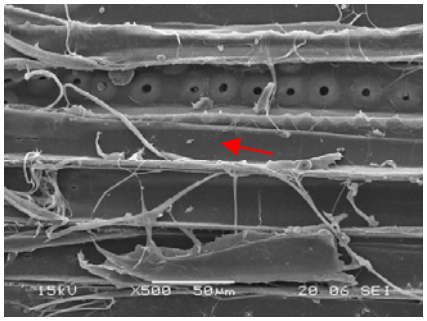


*(a)*

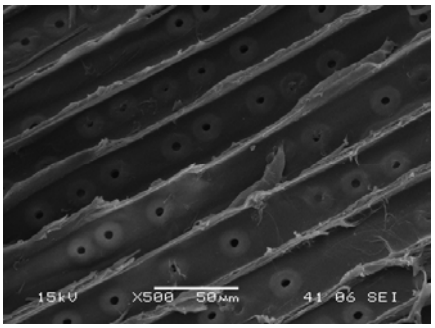


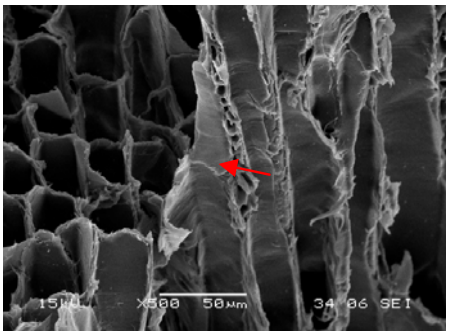


*(b)* *(c)*

**Figure 2.** SEM images of wood fiber: (a) untreated; (b) treated with KOH 5%; (c) treated with KOH 10%.

## SEM microscopy study in the case of vegetal fibers

SEM analysis examined the surface morphology of untreated and treated fibers. It is expected that the surface morphology of untreated fiber will be different to that of treated fiber particularly in terms of their level of smoothness and roughness. The removal of surface impurities on plant fibers is advantageous for fiber-matrix adhesion and increase fiber strength. Figure 3(a) and 3(b) shows the SEM images of untreated wheat straw and maize stalks, in both figures, there are still a lot of impurites.

SEM image show an improvement in surface morphology after applying a KOH treatment. The improvment can be seen in Figure 3 (c) and (d) which shows that using a KOH 5% solution for treatment, fibers are cleaner but still a large amount of impurities remain on the fiber surface. Figures 3 (e) and (f) shows the absence of impurities on the fiber surface treated with KOH 10%. As compared to the untreated fiber, the KOH 10% treated fiber has a cleaner surface but looks jagged and feels rougher when touched. The changes in morphology are important to predict fiber interaction with the polymer matrix in composites.

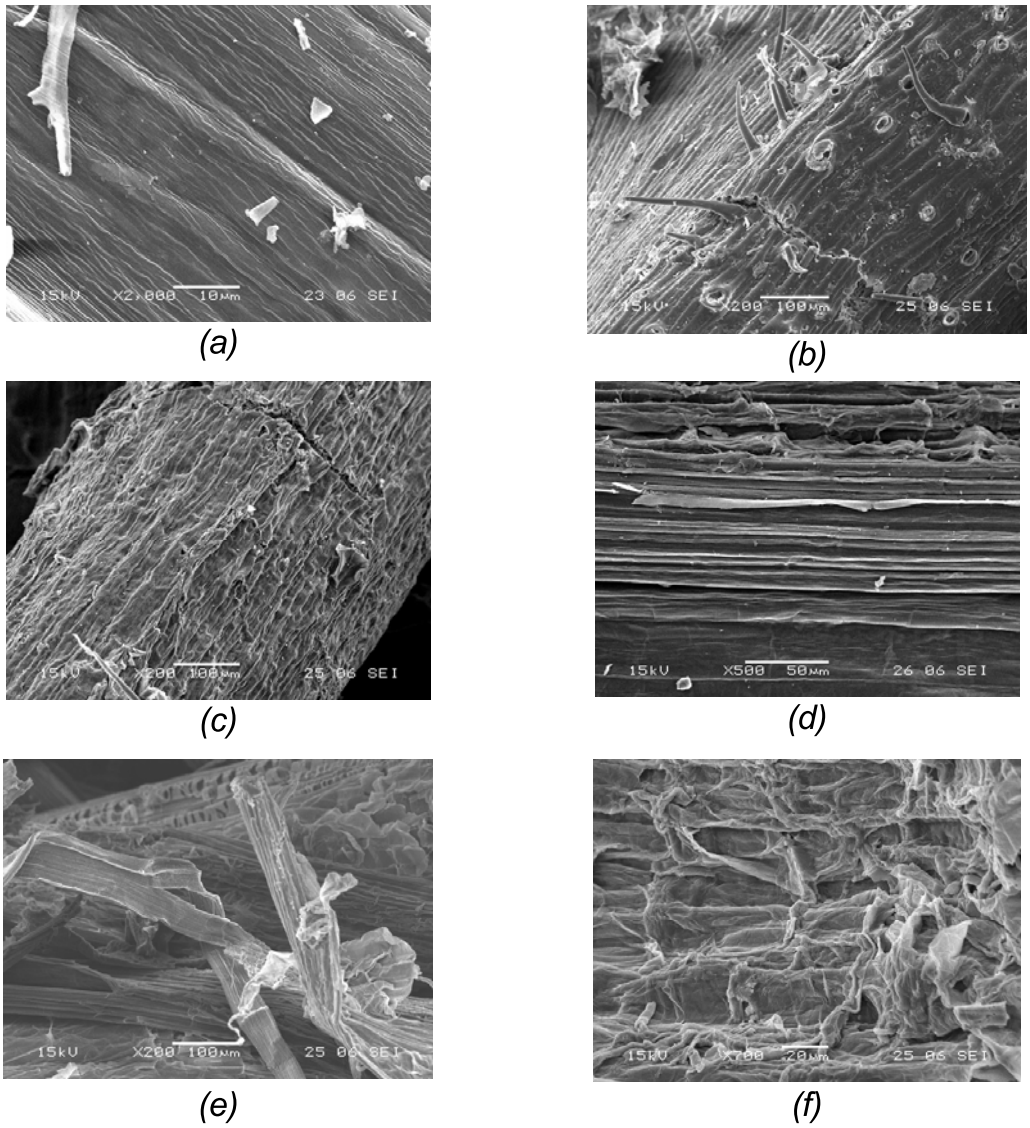


**Figure 3.** SEM micrograph of (a) untreated wheat straw, (b) maize stalks, (c and d) mixture wheat straw and maize stalks treated with KOH 5%, (e and f) mixture wheat straw and maize stalks treated with KOH 10%.

It has been shown that a KOH 5% solution treatment removes partial the impurities, while after a KOH 10% solution treatment the cleanest fibers surface was obtained. Therefore, chemical treatments can be considered as an important step in modifying the properties of natural fibers used for composite materials manufacturing.

## CONCLUSIONS

Development of bio-composites as an alternative to petroleum based materials addresses the dependence on imported oil, reduces carbon dioxide emission, and generates more economical opportunities for the agricultural sector.

The morphological changes were examined using scanning electron microscopy. It has been shown that KOH 5% remove partial the impurities and KOH 10% treatment showed the cleanest fiber surface. The main objective of the chemical treatments is to increase the interface adhesion between the fiber and matrix, and to remove non-cellulosic compounds from the fiber surface. Therefore, chemical treatments can be considered in modifying the properties of natural fibers. The treated fibers show smaller values of moisture content, which could indicate a change in their hydrophobic surface.

Thus, in order to develop composites with good properties, it is necessary to improve the interface between the matrix and the lignocellulosic material.

## EXPERIMENTAL SECTIONS

### Materials

In this study we used a mixture of hardwood sawdust (wood fiber). Fiber dimensions affect the quality of the interfaces that appear in the composite material, and its default properties. Grain size of the sawdust used was between 0,44 and 0,8 μm.

The non-wood fiber, wheat straw (*Triticum aestivum*) and maize stalks *(Zea mays L.)* were the sources of fibers used in this study. The major constituents of wheat straw are 71,24% cellulose and hemicellulose, 23,22% lignin and 5,54% ash and for maize stalks are 38 – 40% cellulose, 7 – 21% lignin, 28% hemicellulose and 3,6 – 7% ash [16]. Wheat straw and maize stalks were collected from local farmers and then chopped in a knife mill Grindomix GM 200. In the production of experimental panels, polyester ortophtalic resin Lerpol TIX 3603 was used as binder with a density 1110 – 1120 kg/m$^3$.

### Wood-fiber treatments

The fibers surficial treatment is an important step in the manufacturing process of obtaining composite materials with sawdust. These chemical treatments are designed to modify the fiber surface. This operation removes impurities, increase the roughness and ensure a high mechanical adhesion to the matrix. The most effective chemical treatments for natural fibers are the alkaline treatments. To achieve the fibers treatment operation, we used a solution of potassium hydroxide (KOH) of different concentration of 5%, 8% and 10% respectively.

Treatment was done by immersing the sawdust fibers in KOH solution with known concentrations for 3 hours at room temperature, being achieved the fiber surface degreasing. There followed a fiber washing with distilled water for 30 minutes. After this the fibers are immersed in a solution of acetic acid ($CH_3COOH$) for 30 minutes and washed again with distilled water for neutralization. Following this operations, sawdust was placed in the oven for 24 hours at a temperature of 105 °C.

### Non-wood fiber treatments

The fiber were first placed in solution of potassium hydroxide (KOH) with a concentration 5%, 8% or 10% for 3 h at room temperature. Afterward, the alkalized fibers were washed with distilled water, followed by neutralization with 20 mL of acetic acid solution. Wheat straw and maize stalks were then washed with distilled water again and dried at 105 °C for 24 h.

**ACKNOWLEDGEMENTS**

This work was supported by CNCSIS-UEFISCSU, project number PNII-IDEI ID_1100/2007. O.N. thank the project "Progress and development through post-doctoral research and innovation in engineering and applied sciences – PRiDE – Contract no. POSDRU/89/1.5/S/57083", both co-funded from European Social Fund through Sectorial Operational Program Human Resources 2007-2013

## REFERENCES

1. S. Yasar, E. Guntekin, M. Cengiz, H. Tanriverdi, *Scientific Research and Essays*, **2010**, *5(8),* 737. 2. S.C. Mishra, *Journal of Reinforced Plastics and Composites*, **2009**, *28*, No18.3. M. Botros, Intertech Conference “The Global Outlook for Natural and Wood Fiber Composites” New Orleans, December 3 – 5, **2003**.
4. S.P. Rowland, E.J. Roberts, *Journal of Polymer Science, Polymer Chemistry Edition*, **1972**, *10*, 2447.
5. A.K. Bledzki, S. Reimane, J. Gassan*, Polymer Plastic Technology and Engineering*, **1998**, *37*: 451.
6. P.V. Joseph, J. Kuruvilla, S. Thomas, *Composites Science and Technology*, **1999**, 59(11), 1625.
7. S.C. Mishra, M. Misra, S.S. Tripathy, S.K. Nayak, A.K. Mohanty, *Journal of Reinforced Plastic Composites*, **2001**, *20*, 321.
8. S.N. Maiti, R. Subbaro, M.N. Ibrahim, *Journal of Applied Polymer Science*, **2004**, *91*, 644.

9. R. Ghautier, C. Joly, A.C. Coupas, H. Ghautier, *Polymeric Composites,* **1998***, 19,* 287.
10. A.K. Mohanty, M. Misra, L.T. Drzal, *Composite Interfaces,* **2001***, 8*, 313.
11. Y. Seki, *Mat Sci Eng A*, **2009**, *508*, 247.
12. S. Sapieha, P. Allard, Y.H. Zang, *Journal of Applied Polymer Science*, **1990**, *41*, 2039.
13. M.S. Huda, L.T. Drzal, A.K. Mohanty, M. Misra, *Composite Science and Technology*, **2008**, *68*, 424.
14. I. Ghasemi, M. Farsi, *Iranian Polymers Journal*, **2010**, *19(10),* 811.
15. J.G. Gwon, S.Y. Lee, G.H. Doh, J.H. Kim, *Journal of Applied Polymer Science***, 2010**, *116*, 3212.
16. Z. Yi, H. Shah, Y. Yiqi, *Bioresource Technology*, **2010**, *101*, 2026.

STUDIA UBB CHEMIA, LV, Sp.Iss., 2010

# ALKALINE RECYCLING WITH BOUNDARY LAYER SEPARATION METHOD (BLSM)

**RIPPEL-PETHŐ DÓRA[a], HORVÁTH GÉZA[b], SZENTES ADRIENN[c]**

**ABSTRACT.** A new method for the treatment of industrial waste water, called Boundary Layer Separation Method (BLSM) has been developed. The phenomena of ion enrichment in the boundary layer of the electrically charged electrode surface compared to the bulk liquid phase have been applied. The essence of the method is that the boundary layer, at a correctly chosen movement velocity, can be taken out of the waste water without damage, and the ion enriched boundary layer can be recycled. For the experiments a batch and a continuous device were built. Graphite was used as working electrode. The extent of ion transport has been compared in the two devices.

***Keywords:*** *boundary layer, electrosorption, cyclic mass transport, graphite electrode*

## INTRODUCTION

The hazards of industrial waste materials are widely known. This is reflected by the increasingly strict environmental laws which regulate the amount of contaminants released by chemical plants (e.g. metals, salts, other organic and inorganic components). In order to comply with regulations, environmental-friendly production methods are needed which either do not emit contaminants into the environment at all, or are capable of handling the incidental waste materials in an up-to-date manner.

One of the problems during the olefin production is the high level of $Na^+$ in the wastewater. The pyrolysis gases that evolve during the pyrolysis process are absorbed in alkaline washing towers. Sodium hydroxide is fed constantly into the system and the sludge is constantly removed. The “traditional”

[a] *University of Pannonia, Institute of Chemical and Process Engineering, Str. Egyetem Nr. 10., H-8200 Veszprém, Hungary, pethod@almos.uni-pannon.hu*
[b] *University of Pannonia, Institute of Chemical and Process Engineering, Str. Egyetem Nr. 10., H-8200 Veszprém, Hungary, ghorvath@almos.uni-pannon.hu*
[c] *University of Pannonia, Institute of Chemical and Process Engineering, Str. Egyetem Nr. 10., H-8200 Veszprém, Hungary, szentesa@almos.uni-pannon.hu*

wastewater treatment is capable of removing the organic, but not the alkaline contents. The alkaline contents can be neutralized, but then salt is formed, the release of which is very strictly regulated by environmental laws. Knowing the composition of the wastewater, the aim was to devise a technology which is capable of reducing the $Na^+$-ion concentration and enriching it in another system, thus enabling its recirculation in the technology. The release of harmful materials can thus be significantly reduced.

A new method for the treatment of industrial wastewaters, called Boundary Layer Separation Method (BLSM) has been develeped. The method is based on the electrosorption phenomenon. Electrosorption is the absorption process that takes place on the surface of charged electrodes [1]. The electric polarization can be carried out galvanostatically or potentiostatically [2]. Generally, the galvanostatic method is favored in practice [3,4]. The electrosorption of cations takes place on a cathodically polarized (negative) electrode. This electrosorption is superposed onto the physical adsorption which takes place without charge. If the polarity is reversed, the cations undergo desorption [5-8]. This phenomenon can be used to produce ion transport with a cyclic method.

During electrosorption, an electrical double-layer forms on the electrode-solution interface. The electrical double-layer has two main parts: the Helmholtz-layer and the diffuse layer. If the electrode is moved, the diffuse layer might be torn apart, producing a zeta-potential between the stationary and the moving parts. The essence of BLSM is that – with an appropriately chosen velocity – the boundary layer which is rich in ions can be removed from the wastewater, and can be recycled.

The advantage of the procedure is that it does not use dangerous chemicals, only inert electrodes, which do not produce pollutants. The electrochemical parameters can easily be measured and adjusted. The drawback is that it is not ion selective to ions and the hydrogen that emerges during the electrolysis might be dangerous.

Electrosorption is a surface phenomenon. It can only be utilized with good efficiency if the surface area of the electrode is high. Mostly, porous carbon electrodes with high specific surface areas are used [9-11]. Electrodes of high surface area can also be made of metals. With the reduction of NiO, $Co_3O_4$ and $Fe_2O_3$ with hydrogen, macroporous Ni, Co and Fe can be produced [12]. Porous Ni, Cu, Ag, Pt and Au can be produced by precipitating the metal onto colloidal silicic acid [13]. Silicon-dioxide is removed with HF after calcination. Among electrochemical methods, the production of platinized platinum is well-known. High specific surface area “black” or “gray” nickel electrodes can be made by the same method [14,15]. The high surface area is not always an advantage because if the pore size distribution is not adequate, parts of the surface might become electrochemically inaccessible.

Nickel electrodes were manufactured for the boundary layer separation method [16]. The electrochemically effective surface area of the electrodes was estimated in our earlier works. The presence of the diffuse part of the double layer has been experimentally proven. The capacitance of the electrolytic double layer has been determined [17].

With the use of electrosorption, inorganic [18] and organic ions, such as thiocyanate [1], pyridine [2], aniline and bipyridines [3] can be removed from aqueous solutions. Among the practical applications is wastewater cleaning [19].

In this manuscript ion transport by boundary layer separation is presented, which was realized as a cyclic procedure. For the experiments a batch automatic electrosorption device and a continuous cascade appliance were built. A graphite electrode was used as working electrode instead of nickel electrodes. The extent of the ion transport in the two systems have been compared.

## RESULTS AND DISCUSSION

The aim of the experiments was to determine the extent of ion transport. The amount of ions transferred from one cell into another can be given relative to area (mg $Na^+$ $m^{-2}$ $cycle^{-1}$) or mass unit (mg $Na^+$ $kg^{-2}$ $cycle^{-1}$) per one cycle.

The optimal operational parameters were determined in our earlier works for nickel electrodes manufactured by our research group. The best mass transport can be achieved with the use of 1200 mV polarization potentials in the examined system. The necessary operation intervals were determined with the examination of the velocity of the electrochemical processes. When using 1200 mV polarization potential, the necessary adsorption interval is at least 25 seconds and the desorption interval at least 300 s with the use of the nickel electrode [22]. The measurements were conducted with ~2 m/m% NaOH solution.

The batch and the continuous devices were compared by these experiments. Since graphite electrodes were used in the continuous device, results under similar conditions (i.e. with graphite electrodes) had to be collected with the batch device as well. The experiments were also conducted with graphite electrodes in the batch device. The experiments proved, that the optimal parameters determined with the nickel electrodes gave equally the best mass transfer with graphite electrodes. The extent of mass transfer is given in mg $Na^+/m^2$ per cycle (Figure 1). The mass transfer is lower compared to the nickel electrodes but in the continuous device these graphite electrodes were used.

The experiments were also conducted with the continuous device at optimal operation parameters (adsorption interval: 25 s, desorption interval: 300 s, polarization potential: 1200 mV) with graphite working electrodes. The amount of transferred ions from the anode to the cathode compartment was calculated for the mass unit of the electrode per cycle (mg $Na^+$ ion/ kg cycle) in order to have comparable results.

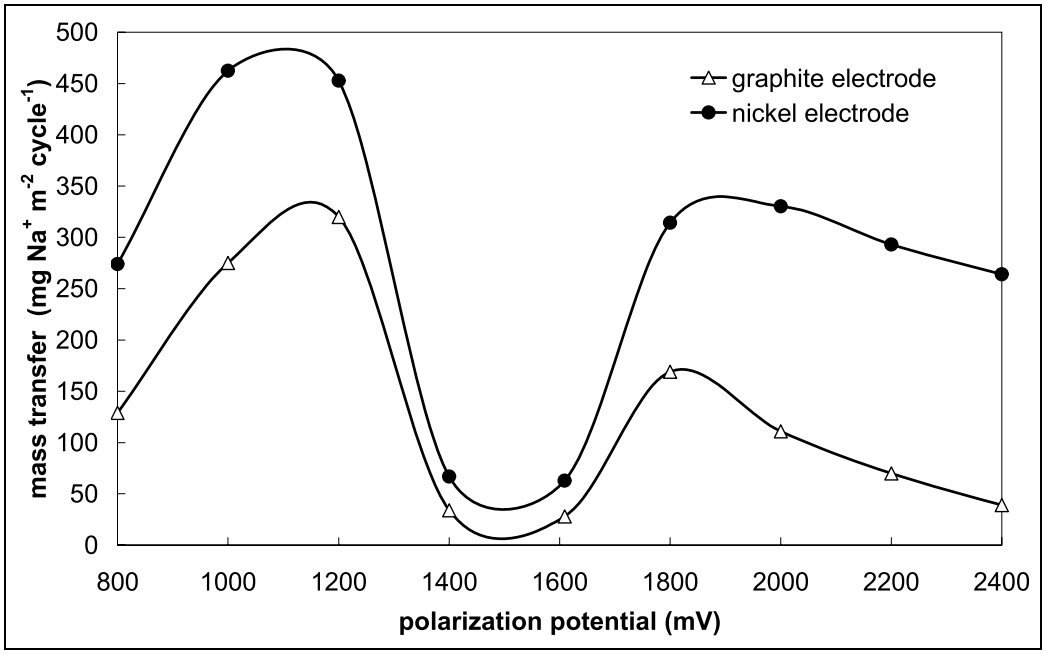


**Figure 1.** Mass transfer measurements with graphite and nickel electrodes on the batch device (adsorption interval: 25 s, desorption interval: 300 s)

Figure 2 illustrates that mass transfer is greater in the continuous device at the same parameter.

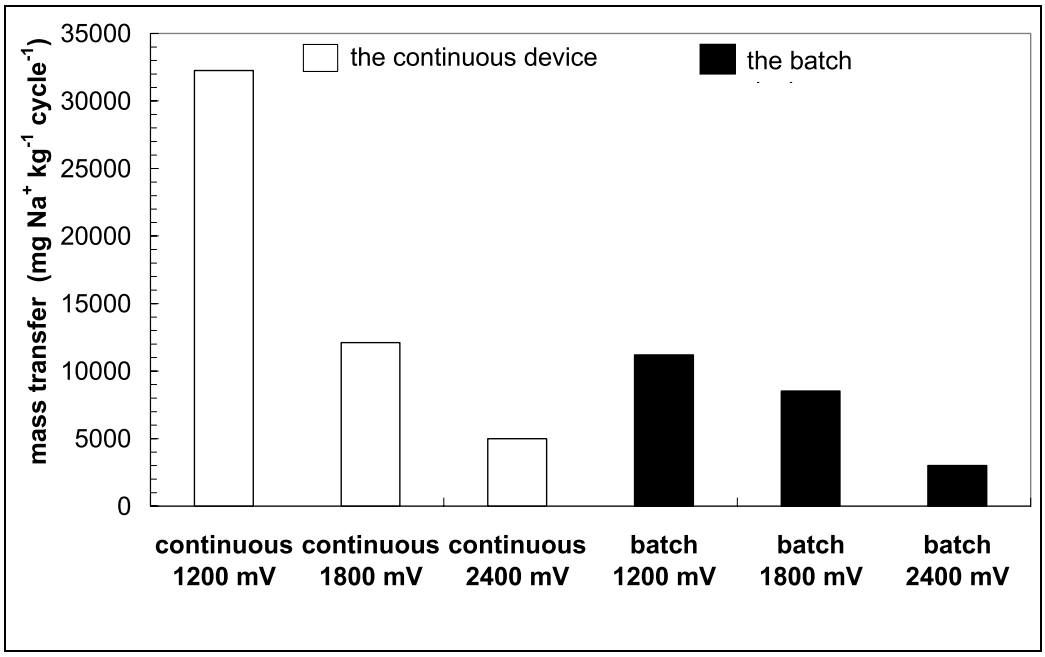


**Figure 2.** Mass transfer measurements relative to mass unit on the batch and the continuous devices (adsorption interval: 25 s, desorption interval: 300 s)

The extent to which the mass transfer is increasing is not proportionate to the extent of which the area was increased. The reason for this is that the effect of physical adsorption is superposed onto the electrosorption and that the hydrodynamic adhesive layer also takes part in the ion transport. Let factor f stand for the proportion of the mass of the hydrodynamic adhesive layer that is formed on the surface of the electrodes compared to the mass of the original solution. The hydrodynamic layer formed on the surface of the planar electrodes of the batch device is significantly smaller ($f_{batch}$=0.025) than that formed on the granular packing in the continuous device ($f_{continuous}$=0.14). Because of this, the efficiency of the separation is deteriorated by the greater back-mixing in the two cells.

This is also proved by giving the experimental results of the continuous and the batch device with graphite electrodes relative to unit of surface (Figure 3). Because of back-mixing the ion transport is lower in the continuous device. However, almost the same ion transport can be reached with the continuous device as well if the pore size is chosen appropriately and the value of the f factor is minimized.

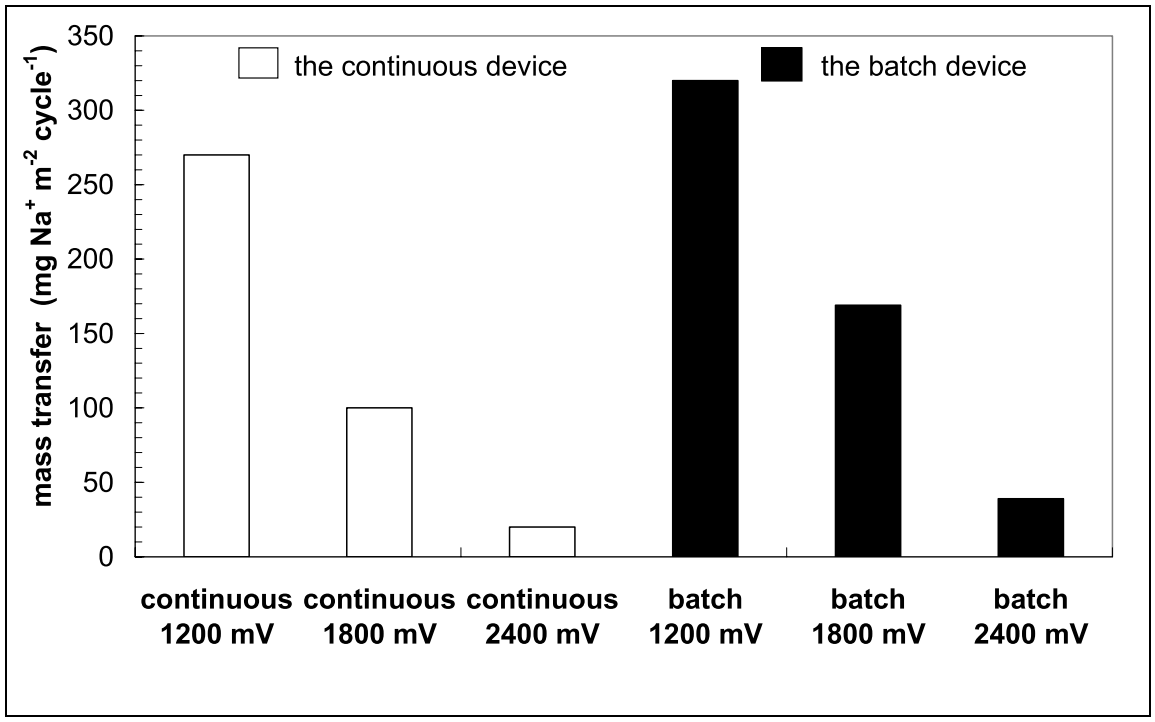


**Figure 3.** Mass transfer measurements relative to surface unit on the batch and the continuous devices (adsorption interval: 25 s, desorption interval: 300 s)

## EXPERIMENTAL SECTION

### Experimental setup – Batch device

The laboratory scale experimental equipment and peripheral instruments are presented in Figure 4 [20, 22].

The basic control is done by the process control computer, with which the polarization potentials can be set. This also controls sample-taking. A power supply unit, which provides the necessary voltage, is attached to the computer. Adsorption and desorption intervals can be set by the control unit's interval-switch. The desired number of cycles can be set on the programmable cycle-counter.

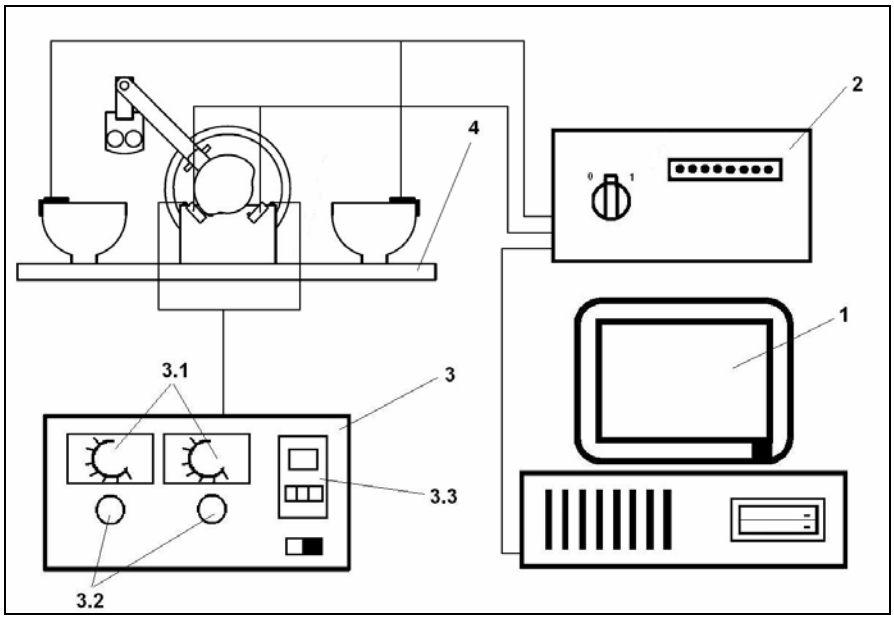


**Figure 4.** Experimental equipment and peripheral instruments, where
1. Process control computer, 2. Power supply, 3. Regulator unit, 3.1. Adjustable interval-switches, 3.2. Control lamps, 3.3. Programmable cycle-counter, 4. Automatic electrosorption device

The main part of the system is the automatic electrosorption equipment. Structure and units of equipment are presented by Figure 5.

The mobile counter-electrodes are fixed to a driven axle, which is leveled by a lever from the anode compartment into the cathode compartment. The lever is moved by the driven axle, at one end of which there is a program dial and four joint micro-switches. These micro-switches are responsible for stopping the lever in a given position, turning the polarization potential on and off, and changing polarity. To the other end of the driven axle is attached a

transmission electric motor by transmission, which drives the axle. Graphite counter-electrodes are fixed inside the compartments. The mobile working electrodes were placed between these. The experimental device is stable, reliable, and easy-to-handle. The electrochemical parameters can be set quickly and on a broad spectrum. A 0.05 M aqueous solution of NaOH (Fluka) was used as a model solution.

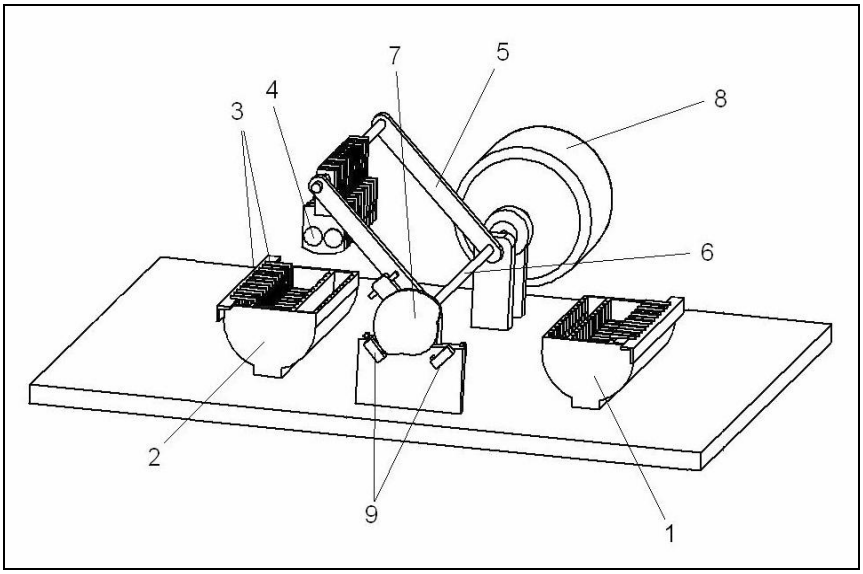


**Figure 5.** The automatic batch electrosorption device, where
1. Anode compartment 2. Cathode compartment 3. Graphite counter-electrodes
4. Mobile working electrodes 5. Lever 6. Driven axle
7. Program dial 8. Electric motor 9. Microswitches

In the Boundary Layer Separation Method (BLSM) the electrosorption process that undergoes on the surface of the charged electrode is used in a cyclic procedure. Two separate fluid compartments (anode and cathode compartments) were formed.

50-50 $cm^3$ of fluid are poured into the anode and cathode compartments. 6 graphite counter-electrodes are fixed inside the compartments. The high surface area nickel working electrodes are dipped into the solution inside the anode compartment, between the graphite counter-electrodes. The appropriate polarization potential is switched onto the cell so that the working electrode becomes the negative (cathode) and the counter-electrode becomes the positive (anode). Then the positively charged ions move to the working electrodes and bond to their surfaces. This is the electroadsorption phase. The saturation of the working electrode can be monitored by measuring the current that passes trough the cell. After electrosorption took place, the working electrode, with the boundary layer that is saturated with ions, is pulled out of the solution (from the

anode compartment) and the polarization potential is switched off. The working electrode is then put into the other solution (cathode compartment) where the polarity is reversed. Now the working electrode is the positive, and the counter-electrodes in the other cell are the negative. The ions desorbe from the surface of the working electrode due to the electrostatic repulsion, and enter the solution. This process can also be monitored by measuring the current passing through the cell. The working electrode is once again taken out of solution and the potential is switched off. The procedure described above is one cycle. By using appropriate cycles, the ion concentration is reduced in the anode compartment while it is risen in the cathode compartment.

**Experimental setup – Continuous device**

The advantage of this device is that instead of moving the electrode, the liquid is flowing. The device is different from those that can be found in the literature [21] in the followings: the electrodes are not separated by a separator (ion-exchange membrane), and the work done in the cell and the surface area of the counter-electrode are orders of magnitude different. The absence of membrane was solved with the different surfaces of the electrodes and the selection of operation intervals. The structure of the columnar device is illustrated in Figure 6.

The counter electrode in the chemical cell is the acid-proof steel cylinder that functions as the column's lateral surface. Appropriate electric connections are mounted to the packing and the lateral surface. The inlet and outlet of the electrolyte solution from the anode and cathode compartments is carried out through the connections at the bottom of the column. The working electrode in the column is build from graphite particles of 1-1.5 mm diameter filled in a packing net. The counter electrode in the chemical cell is the acid-proof steel cylinder that functions as the column's lateral surface. Appropriate electrical connections are mounted to the packing and the lateral surface. The inlet and outlet of the electrolyte solution from the anode and cathode compartments is carried out through the connections at the bottom of the column.

During the measurement, a cycle consists of the following steps takes place: filling of the column from the anode compartment; switching the appropriate polarity onto the column (packing: negative, lateral surface: positive); electrosorption for a given interval while the liquid is stationary; draining down the liquid into the anode compartment; ceasing the column's polarity (possibly by discharge); filling the column with liquid from the cathode compartment; switching the appropriate polarity onto the column (packing: positive, lateral surface: negative); desorption for a given interval while the liquid is stationary; draining down the liquid into the cathode compartment.

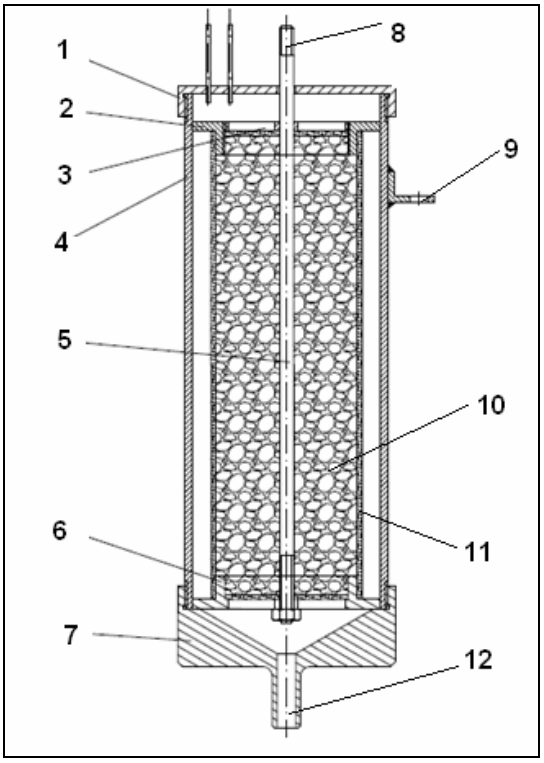


**Figure 6.** Continuous electrosorption device

1. Cover, 2. Top packing closure 3. Fluid splitter, 4. Lateral surface, 5. Metallic rod, 6. Bottom packing closure, 7. Bottom closure, 8-9. Electrical connection, 10. Graphite packing, 11. Packing holder, 12. Fluid inlet and outlet

## CONCLUSIONS

We have developed a new method for the treatment of industrial wastewaters and given it the name Boundary Layer Separation Method (BLSM). The phenomenon, that ions can be enriched in the boundary layer, as compared to the liquid phase on the surface of an electrically charged electrode has been utilized. If this boundary layer is then immersed into another liquid phase, separation is realized. A batch and a continuous device were built for the experiments. Graphite was used as the working electrode. It has been concluded, that the optimal parameters determined with the nickel electrodes gave equally the best mass transfer with graphite working electrodes. The extents of the ion transport in the two devices were compared. Under similar conditions, the extent of the mass transfer is greater in the continuous device. The increase of the mass transfer is not proportionate to the increase of surface area because the formation of the hydrodynamic adhesive layer causes back-mixing between the two cells.

The procedure might be successfully improved with the use of electrodes produced with nanotechnology, or with placing the device into a cascade system.

**ACKNOWLEDGMENTS**

The authors express their gratitude to the Chemical Engineering Cooperative Research Center of the University of Pannonia for financial support of this research study.

## REFERENCES

1. C. Rong, H. Xien, *Journal of Colloid and Interface Science*, **2005**, *290*, 190.
2. J. Niu, B.E. Conway, *Journal of Electroanalytical Chemistry*, **2002**, *521*, 16.
3. J. Niu, B.E. Conway, *Journal of Electroanalytical Chemistry*, **2002**, *536*, 83.
4. A. Vaškelis, E. Norkus, J. Stalnioniene, G. Stalnionis, *Electrochimica Acta*, **2004**, *49*, 1613.
5. A. Afkhauni, B.E. Conway, *Journal of Colloid and Interface Science*, **2002**, *251*, 248.
6. Y. Xu, J. W. Zondlo, H.O. Finklea, A. Brennsteiner, *Fuel Processing Technology*, **2000**, *68*, 189.
7. J.C. Farmer, D.V. Fix, G.V. Mack, R.W. Pekala, J.F. Poco, *Journal of the Electrochemical Society*, **1996**, *143*, 159.
8. E. Ayranci, B.E. Conway, *Analytical Chemistry*, **2001**, *73*, 1181.
9. E. Bayram, N. Hoda, E. Ayaranci, *Journal of Hazardous Materials*, **2009**, *168*, 1459.
10. L. Pan, X. Wang, Y. Gao, Y. Zhang, Y. Chen, S. Zhuo, *Desalination*, **2009**, *244*, 139.
11. A. Bán, A. Schäfer, H. Wendt, *Journal of Applied Electrochemistry*, **1998**, *28*, 227.
12. H. Yan, C.F. Blanford, B.T. Holland, M. Parent, W.H. Smyrl, A. Stein, *Advanced Materials*, **1999**, *11*, 1003.
13. P. Jiang, J. Cizeron, J.F. Bertone, V.L. Colvin, *Journal of the American Chemical Society*, **1999**, *121*, 7957.
14. S.J. Berezina, G.S. Vozdvizsenszkij, G.P. Deziderev, *Doklady Akademii Nauk SSSR*, **1951**, *77*, 53.
15. G. Horányi, E.M. Rizmayer, *Journal of Electroanalytical Chemistry*, **1984**, *180*, 97.
16. D. Pethő, GY. Gáspár, G. Horváth, J. Liszi, R. Szakály, I. Tóth, *Hungarian Journal of Industrial Chemistry*, **2008**, *36*, 101.
17. D. Pethő, G. Horváth, J. Liszi, I. Tóth, D. Paor, *Acta Chimica Slovenica*, **2010**, *57*, 758.
18. Y. Oren, A. Soffer, *Journal of the Electrochemical Society*, **1978**, *125*, 869.
19. V. Ganesh, V. Lakshminarayanon, *Electrochimica Acta,* **2004**, *49*, 3561.
20. Hungarian Patent Office, **2009**, Reg. No: P0900569
21. Y. Oren, A. Soffer, *Journal of Applied Electrochemistry*, **1983**, *13*, 473.
22. D. Pethő, G. Horváth, J. Liszi, I. Tóth, D. Paor, *Water Environment Research*, **2010**, *82*, 2379.

STUDIA UBB CHEMIA, LV, Sp.Iss., 2010

# LAB SCALE SEQUENCING BATCH REACTOR CONSTRUCTION AND CHARACTERIZATION FOR DYNAMIC MODELLING WITH ACTIVATED SLUDGE MODEL

**SZILVESZTER SZABOLCS[a,*], RÁDULY BOTOND[b], MIKLÓSSY ILDIKÓ[b], ÁBRAHÁM BEÁTA[b], LÁNYI SZABOLCS[b], DAN ROBESCU NICULAE[a]**

**ABSTRACT.** Activated sludge wastewater treatment is one of the most commonly used domestic wastewater treatment methods. Modelling and simulation of the treatment process allow for a deeper insight into, and a better understanding of the system, enabling a better control of the treatment facility and high quality effluent production. The characterization of the system is crucial for getting accurate simulation results that correctly represent the studied system. In this paper we present the construction details of a laboratory-scale activated sludge sequencing batch reactor (SBR), and we provide a step-by-step description of the methodology used for wastewater and system characterization with the aim of process modelling and simulation. As the Activated Sludge Model No. 3 (ASM3) has been chosen for later modelling and simulation work, the fractionation of the wastewater was done such way to finally obtain the ASM3 state variables.

***Keywords:*** *SBR, wastewater treatment, ASM3 modelling, wastewater fractionation*

## INTRODUCTION

The modern activated sludge processes are reliable, produce high quality effluent and are considered to be the most cost-effective way for the removal of organic materials from wastewater [1]. Today's activated sludge wastewater treatment plants (WWTPs), besides the oxidation of organic matter, provide biological nutrient removal, meet the newest emission limits and are able to deal with the increasing magnitude and complexity of wastewater loads. Among other activated sludge systems, the SBR activated-sludge systems represent a re-emerging, highly efficient wastewater treatment technology, with several advantages over the continuous activated-sludge plants: they combine all of the

[a] *"Politehnica" University of Bucharest, Faculty of Energetics, Bucharest, Romania, [*]email: szilveszterszabolcs@sapientia.siculorum.ro*

[b] *Sapientia University, Cluj-Napoca, Faculty of Technical and Natural Sciences, Miercurea Ciuc, Romania*

treatment steps and processes into a single basin, or tank, whereas conventional facilities rely on multiple basins [2]; they can easily be controlled on a time-schedule; they are much less affected by the variation of hydraulic loads than the continuous plants, meaning that they can provide a constantly high pollutant removal efficiency.

Simulation models of activated sludge WWTPs have been successfully used for a number of tasks, such as WWTP design and retrofitting, process control and optimization. Simulation can also help the understanding of the underlying phenomena [3, 4]. While it is now widely accepted, that a mathematical model of a WWTP, able to predict how the plant will react under various operating conditions, is an excellent tool for the design, analysis, control, forecasting and optimization of WWTPs [5], modelling studies mainly focused on the more widespread, continuous activated sludge processes, SBR modelling being a bit neglected.

A number of activated sludge models (ASMs) exist, describing the biochemical processes involved in the technical purification of wastewater. Through these biochemical processes the organic matter and nutrient content of the wastewater is eventually converted into carbon-dioxide, nitrogen and a particulate fraction (cell material) [5].

The modelling of the biochemical processes is based on several basic kinetic equations, describing bacterial growth, substrate utilization and the endogenous metabolism (decay) of bacteria, as well as the hydrolysis of entrapped organics. In the last 40 years several activated sludge models have been developed, describing the biochemical processes in a various manner ([6]; [7]; [8]). The “state-of-the-art models” for activated sludge processes are considered to be the ASM1 – ASM3 models developed by the IWA Task Group [9]. These models incorporate carbon oxidation, nitrification, denitrification, and ASM2d also describes the biological and chemical phosphorus removal. The ASM models have been “updated” several times since the first coming out of the ASM1 and most of the problems identified in the earlier versions have been corrected. The models are based on COD units (use chemical oxygen demand to define carbonaceous material); ASM3 has a total organic carbon (*TOC*) based version as well.

The main difference between ASM1 and ASM3 is the recognition of the importance of storage polymers in the heterotrophic conversions in the activated sludge processes in ASM3 [4]. The aerobic storage process in ASM3 describes the storage of the readily biodegradable substrate ($S_S$) into a cell internal component ($X_{STO}$). This approach requires that the biomass is modelled with cell internal structure, similar to ASM2 which will be described later in this work. The energy required for this process is obtained via aerobic respiration. This internal component is then subsequently used for growth. In ASM3 it is assumed that all $S_S$ is first taken up and stored prior to growth. A division of the

storage and growth process, allowing growth to take place on external substrate directly, is not considered. The death regeneration concept is replaced by endogenous respiration, which is closer to the phenomena observed in reality. Also, ASM3 allows differentiating between aerobic and anoxic decay. Figure 1 illustrates the difference in COD flows between ASM1 and ASM3. The first thing to notice is that the conversion processes of both groups of organisms (autotrophs and heterotrophs) are clearly separated in ASM3, whereas the decay - regeneration cycles of the autotrophs and heterotrophs are strongly interrelated in ASM1. This change of decay concept (and introduction of the storage step) means that there exist more “entry” points for oxygen utilization resulting in, at some points, easier separation and characterization of the processes. Second, there is a shift of emphasis from hydrolysis to storage of organic matters. This gives a change in how wastewater characterization should be defined since the separation between $S_S$ and $X_S$ now should be based on the storage process rather than on the growth process. Still, the separation remains somewhat based on biodegradation rates. In ASM3 hydrolysis represents a less dominating importance on the rates of oxygen consumption since only hydrolysis of $X_S$ in the influent is considered.

The compounds present in the wastewater are divided in 13 categories; these constitute the state variables of ASM3:

***$S_{ALK}$*** - alkalinity of the wastewater [mole $HCO_3/m^3$] Alkalinity is used to approximate the conservation of ionic charge in biological reactions. Alkalinity is introduced in order to obtain an early indication of possible low pH conditions, which might inhibit some biological processes. For all stoichiometric computations, $S_{ALK}$ is assumed to be bicarbonate, HCO3, only.

***$S_I$*** - inert soluble organic material [g COD/$m^3$] The prime characteristic of $S_I$ is that these organics cannot be further degraded in the treatment this material is assumed to be part of the influent and may be produced in the context of hydrolysis of particulate substrates $X_S$.

***$S_S$*** - readily biodegradable organic substrates [g COD/$m^3$] This fraction of the soluble COD is directly available for consumption by heterotrophic organisms. In ASM3, for simplification, it is assumed that all these substrates are first taken up by heterotrophic organisms and stored in the form of $X_{STO}$.

***$S_{N2}$*** - nitrogen [g N/ $m^3$] is assumed to be the only product of denitrification. $S_{N2}$ may be subject to gas exchange, parallel with oxygen, $S_{O2}$.

***$S_{NH4}$*** - ammonium plus ammonia nitrogen [g N/ $m^3$] For the balance of the ionic charges, $S_{NH4}$ is assumed to be all $NH_4^+$.

***$S_{NOX}$*** - nitrate plus nitrite nitrogen [g N/ $m^3$] $S_{NOX}$ is assumed to include nitrate as well as nitrite nitrogen.

***$S_{O2}$*** - dissolved oxygen [g COD/$m^3$] Dissolved oxygen can directly be measured and is subject to gas exchange.

***$X_A$*** - nitrifying organisms [g COD/m$^3$] Nitrifying organisms are responsible for nitrification; they are obligate aerobic, chemo-litho-autotrophic. It is assumed that nitrifiers oxidize ammonium, $S_{NH4}$, directly to nitrate, $S_{NOX}$.

***$X_H$*** - heterotrophic organisms [g COD/m$^3$] These organisms are assumed to be the all type heterotrophic organisms, they can grow aerobically and many of them also anoxically (denitrification). These organisms are responsible for hydrolysis of particulate substrates XS and can metabolize all degradable organic substrates. They can form organic storage products in the form of poly-hydroxyalkanoates or glycogen. $X_H$ are assumed to have no anaerobic activity except cell external hydrolysis, which is the only anaerobic process in ASM3.

***$X_I$*** - inert particulate organic material [g COD/m$^3$] This material is not degraded in the activated sludge systems it is flocculated onto the activated sludge. $X_I$ may be a fraction of the influent and is produced in the context of biomass decay.

***$X_S$*** - slowly biodegradable substrates [g COD/m$^3$] Slowly biodegradable substrates are high molecular weight, soluble, colloidal and particulate organic substrates which must undergo cell external hydrolysis before they are available for degradation. It is assumed that the products of hydrolysis of $X_S$ are either readily biodegradable ($S_S$) or inert ($S_I$) soluble organics.

***$X_{SS}$*** - suspended solids [g/m$^3$] Suspended solids are introduced into the biokinetic models in order to compute their concentration via stoichiometry.

***$X_{STO}$*** - organics stored by heterotrophic organisms [g COD/m$^3$] It includes poly-hydroxy-alkanoates (PHA), glycogen, etc. It occurs only associated with $X_H$; it is, however, not included in the mass of $X_H$.

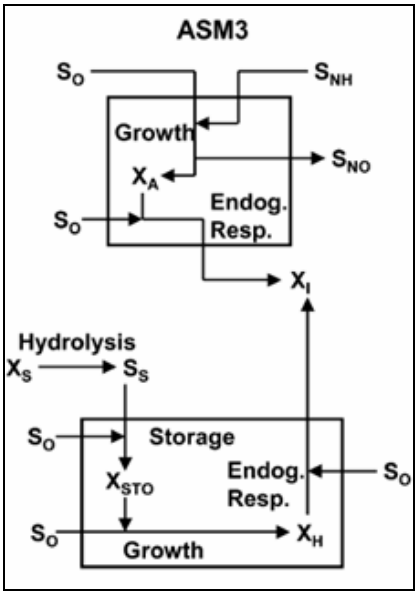


**Figure 1.** Substrate flows for autotrophic and heterotrophic biomass in the ASM1 and ASM3 models (modified from Gujer et al., 1999) [4]

There are a total of 12 biochemical processes modelled in ASM3. Figure 1 presents in a schematic way how the different compounds participate in the conversion processes. The kinetic expressions of the conversion processes are presented in detail elsewhere [9]; due to space limitations here only a list of them is provided:

- hydrolysis of organic matter in readily available soluble substrate
- anoxic and aerobic storage of soluble substrate
- growth of heterotrophic organisms under aerobic and anoxic conditions
- endogenous respiration of the heterotrophic organisms under aerobic and anoxic conditions
- aerobic growth of autotrophic organisms
- aerobic and anaerobic endogenous respiration of the autotrophic organisms
- aerobic and anaerobic respiration of the storage products

The ASM models however are all conceptual models, their state variables being conceptual wastewater fractions that are not commonly used in “real-world” wastewater characterisation and WWTP operation. Unlike the common wastewater indicators (such as pH, chemical oxygen demand (COD) or biochemical oxygen demand (BOD5)), the ASM fractions include readily and slowly biodegradable organic matter ($S_S$ and $X_S$), heterotrophic and autotrophic organisms ($X_H$, $X_A$), biochemically inert soluble and particulate matter ($S_I$, $X_I$), etc. Fractionation in such conceptual groups of the wastewater components is called characterisation of wastewater for modelling purposes, and it is as important for successful modelling of the treatment process as the model itself. An adequate wastewater characterization is one of the dominating factors for the quality of model description.

It might be generally stated that the development of activated sludge models [9,10] led to a much better understanding of different treatment processes but it also required a more intensive wastewater characterization. In accordance with practical experiments, it was proposed that the biodegradable COD in the influent wastewater consisted of two fractions: readily and slowly biodegradable COD ($S_s$ and $X_s$). The readily biodegradable COD was assumed to consist of simple molecules able to pass through the cell membrane and immediately used in biosynthetic processes by the organisms. Moreover, the active biomass was divided into two types of organisms: heterotrophic biomass ($X_H$) and autotrophic biomass ($X_A$) in accordance that which kind of substrate types they need for metabolism and process, autotrophic biomass produce nitrate ($S_{NO}$) from ammonium ions ($S_{NH}$) by nitrification process and heterotrophic biomass use oxygen ($S_O$) for the hydrolysis of substrate ($S_S$, $X_S$). The slowly biodegradable COD ($X_S$), which consists of larger complex molecules, was found to be enmeshed by the sludge mass, adsorbed and then required extracellular enzymatic breakdown before being transferred through the cell wall and used for metabolism.

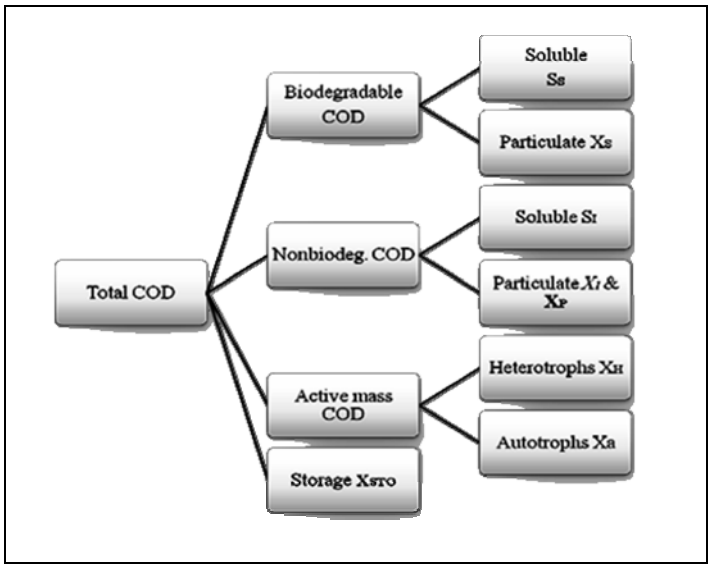


**Figure 2.** COD components in ASM3 (redrawn after Jeppson, 1996 [11])

Fractionation of the wastewater components is measurement-intensive and should be done with great care (possibly according to standardized protocols) when reliable simulation results are desired. In this work the standardized guidelines for wastewater characterization advised by the Dutch Foundation for Applied Water Research (STOWA) have been used. STOWA made an inventory of different methods and evaluated them on reproducibility and ease of use in practice [12]. Their standardized guidelines for wastewater characterization are based on a physical-chemical method to characterize the sum of the soluble COD fractions $S_I$ and $S_S$. This is combined with a BOD-analysis for determining the biodegradable fraction of the influent COD ($S_S$+$X_S$). The fraction $X_I$ is found as the difference between the total COD and other COD fractions. One important assumption in the fractionation of the influent COD is the negligence of biomass fractions in the influent. These fractions are usually very small in the influent and can be neglected in comparison with total COD [10]. Neglecting biomass assumption is sustained by the theory that the bacterial diversity in activated sludge is a product of selection by the environment rather than inoculation by wastewater [12].

## RESULTS AND DISCUSSION

A laboratory-scale activated sludge SBR system has successfully been constructed and put in operation using artificial wastewater. The operating parameters of the SBR have been determined in order to get high COD removal efficiency. A treatment cycle of 4 h has been found to be adequate for providing a treatment efficiency of at least 90%. According to our settings a treatment cycle consists of:

- 15 minutes of fill phase
- 3 hours of aeration and mixing
- 30 minutes of settling
- 15 minutes of drawn phase

With such settings and a reactor load of 0.3 kg $BOD_5/m^3$/day, the resulting average COD removal efficiency of the reactor turned out to be around 92% (Table 1), which is in good concordance with literature values [14]. The duration of the different operation phases found by us are also are close to real-scale activated-sludge SBR operation phases. These reactor settings led to a sludge concentration in the reactor of MLSS = 1300 mg/l and to a SVI of the settled sludge of 98 ml/g. The goodness of the established process parameters is reflected also by the good settling properties of the activated sludge, meaning that "healthy" activated sludge flocs are formed during the treatment process. When trying to use longer aeration in order to further improve organic matter removal, an increase of the final DO values and a simultaneous decrease of the MLSS has been observed. Such behaviour can be explained by the lack of biodegradable substrate, leading to the intensification of the endogenous respiration of the microorganism.

**Table 1.** Effluent COD variation and COD removal efficiency of the SBR for 6 consecutive treatment cycles

| Influent COD [mg/L] | Effluent COD [mg/L] | COD removal Efficiency % |
|---|---|---|
| 575 | 40.81 | 92.9 |
| 575 | 37.77 | 93.43 |
| 575 | 26.21 | 95.44 |
| 575 | 55.71 | 90.31 |
| 575 | 49.45 | 91.4 |
| 575 | 53.62 | 90.67 |
| **Average: 575** | **43.92** | **92.36** |

The artificial wastewater used proved to be adequate for the activated sludge experimentation. The wastewater has been characterized according to the STOWA guidelines for wastewater characterization, in order to get input variables for later modelling work. The wastewater characterisation procedure proved to be very labour-intensive, but the results of the fractionation (presented in Table 2) give valuable information about the possibilities of the treatment process and the expectable removal rates. For example, the total biodegradable COD shows the potential of the treatment plant, and the particulate COD provides information about the expected sludge production.

**Table 2.** Results of the wastewater fractionation

| Analysed parameters [mg/L] | Calculated components [mg/L] |
|---|---|
| $BCOD = 483 \pm 10.3$ | $S_I = 17.35 \pm 0.35$ |
| $COD_{\text{inf},tot} = 575 \pm 12.5$ | $S_S = 191.14 \pm 4.18$ |
| $COD_{\text{inf},sol} = 208.5 \pm 3.68$ | $X_S = 292.38 \pm 10.11$ |
| $COD_{eff} = 44.5 \pm 9.11$ | $X_I = 74.61 \pm 5.52$ |

As can be seen in Table 2, the COD of the wastewater is around 575 mg/L, with a biodegradable part of 483 mg/L, which corresponds to 84%. Apparently this is contradictory to the measured COD removal of 92%. The explanation is, that not only the BCOD is removed during the treatment process, but also part of the biologically inert particulate COD ($X_I$) enmeshed into (and thus settled and removed together with) the activated sludge.

The ASM3 state variables obtained are summarized in Table 3. These variables can readily be used as inputs for ASM3-based WWTP models, enabling thus the simulation of the constructed reactor.

**Table 3.** The ASM3 fractions obtained from the wastewater characterization

| No. | Variable name | Symbol | Value [mg/L] |
|---|---|---|---|
| **1** | Dissolved Oxygen | $S_{O2}$ | 0 |
| **2** | Soluble inert organics | $S_I$ | 17.35988 |
| **3** | Readly biodegradable substrate | $S_S$ | 191.1401 |
| **4** | Ammonium | $S_{NH4}$ | 6.4 |
| **5** | Dinitrogen | $S_{N2}$ | 0 |
| **6** | Nitrite plus nitrate | $S_{NOx}$ | 0 |
| **7** | Alkalinity, bicarbonate | $S_{Alk}$ | 5 |
| **8** | Inert particulate organics | $X_I$ | 74.6103 |
| **9** | Slowly biodeg. Substrate | $X_S$ | 292.3899 |
| **10** | Heterotrophic biomass | $X_H$ | 0 |
| **11** | Organics stored by heterotrophs | $X_{STO}$ | 0 |
| **12** | Autotrophic biomass | $X_A$ | 0 |
| **13** | Total suspended solids | $X_{SS}$ | 483.53 |

## CONCLUSIONS

The constructed lab-scale activated-sludge SBR and the established process parameters provide satisfactory wastewater treatment, achieving very good pollutant removal efficiency. The characterization of the artificial wastewater following the STOWA guidelines proved to be labour-intensive, but it is pretty straightforward, and it can be performed using basic experimental equipment.

The wastewater fractionation done in this work opens the possibility of modelling and simulation of the treatment process, as the parameters calculated can directly be used as input variables for the ASM3. Future modelling will allow for the optimisation of the process, bettering also the nitrogen removal. Moreover, since this paper provides the detailed composition of the artificial wastewater, other modellers also can use the results of the fractionation as input for their models, saving precious time and work. The obtained wastewater fractions present high similarity with literature values for urban wastewater. The stringency of the analysis and the truthfulness of the calculated parameters can be further tested in the calibration process of the mathematical model of the treatment process.

## EXPERIMENTAL SECTION

### Reactor details and set-up

The laboratory scale reactor used in this study is of cylindrical shape, with a diameter of 190 mm and a height of 320 mm. The reactor was made of 5 mm thick Plexiglas (10 mm thick at the bottom) and has a total volume of 9 litre, of which 6 litres are effectively used (Figure 3). In each treatment cycle 1 l of raw wastewater was added to 5 l of mixed liquor present in the reactor (left from the previous cycle).

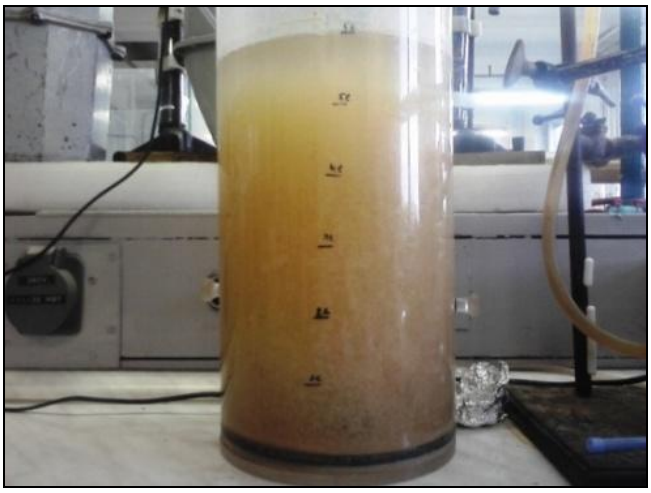

**Figure 3.** The constructed lab-scale SBR reactor

The aeration equipment consists of an air pump with a nominal 5 L/min air flow rate and two pieces of coarse aquarium aeration elements positioned at the bottom of the reactor (fine ceramic aeration elements were also tried but they proved to be unsuitable because of clogging with activated sludge). The

concentration of the dissolved oxygen was kept during aeration at DO = 2.2±0.2 mg/l. DO levels were measured using a luminescent DO sensor. In addition to the pneumatic mixing induced by aeration, additional mixing was provided with a magnetic laboratory stirrer at 500-600 rpm. The reactor has been operated at room temperature; however, at the beginning of each treatment cycle a small temperature drop was observed, due to the low temperature influent (synthetic wastewater kept at 4ºC to avoid deterioration).

The seed sludge was taken from the activated sludge tank of the municipal wastewater treatment plant of Veszprém (Hungary). Excess sludge has been removed at the end of each complete cycle such way to keep the sludge retention times at 6 days. After the settling phase, a sludge volume index of SVI = 98 ml/g was obtained. Mixed liquor suspended solids concentration (MLSS) was approx. 1300 mg/l for each new treatment cycle.

In order to minimize odour problems in the laboratory, synthetic wastewater has been used for this work (for its exact composition see Table 4). The use of synthetic wastewater has also the advantage of having a known composition that makes fractionation easier. The COD/N/P ratio of the synthetic wastewater was around 100:17:5, its theoretical $BOD_5$ was 300 mg/l, assuming a COD to BOD conversion factor of 0.65. [15]

**Table 4.**Composition of the synthetic wastewater used in the experiments, modified from Nopens*et al*. 2001 [15]

| | **mg/l** | | **mg/l** |
|---|---|---|---|
| ***Chemical Compounds*** | | ***Trace Metals*** | |
| **Urea** | 91.74 | **$Cr(NO_3)_3.9\ H_2O$** | 0.770 |
| **$NH_4Cl$** | 12.75 | **$CuCl_2.2\ H_2O$** | 0.536 |
| **o Na-acetate . $3H_2O$** | 131.64 | **$MnSO_4.\ H_2O$** | 0.108 |
| **Peptone** | 17.41 | **$NiSO_4.6\ H_2O$** | 0.336 |
| **$MgHPO_4.3H_2O$** | 29.02 | **$PbCl_2$** | 0.100 |
| **$KH_2PO_4$** | 23.4 | **$ZnCl_2$** | 0.208 |
| **$FeSO_4.7H_2O$** | 5.80 | | |
| ***Food ingredients*** | | | |
| **Starch** | 122.00 | | |
| **Milk powder** | 116.19 | | |
| **Yeast** | 52.24 | | |
| **Soy oil** | 29.02 | | |
| Total | **631.21** | | |

The efficiency (E) of COD removal of the reactor was calculated as follows: $E\ (\%) = [(COD_{influent} - COD_{effluent}) / COD_{influent}] \times 100$. For the determination of the nominal efficiency, six sets of measurements have been performed for six complete treatment cycles, and the average efficiency was calculated (Table 1).

MLSS, COD and SVI measurements were performed according to *Standard Methods* [16].

## Wastewater characterization

*Determination of the organic and inorganic fractions*

For the future modelling of our activated sludge SBR we have chosen the ASM3, the most recent activated sludge model developed by the International Water Association [3]. Thus wastewater characterization was done with the aim of obtaining the ASM3 state variables. Wastewater fractionation has been done according to the STOWA wastewater characterization guidelines [12]. This protocol seemed to be somewhat simpler than other methods and the artificial wastewater used for this work has no microorganisms at all, meaning that the simplifying assumptions of STOWA are completely correct in this case. More detailed (and also more measurement-intensive) wastewater characterisation methods can be found in the literature [11, 12 and 13].

The working sequence was composed of the following steps:

1. Determination of $S_I$ based on the inert soluble COD in the effluent of the WWTP.
2. Determination of $S_S$ by subtracting the fraction $S_I$ from the soluble COD in the influent.
3. Determination of $X_S$ by subtracting the fraction $S_S$ from the biodegradable COD (BCOD, Figure 5.)
4. Determination of $X_I$ with the equation presented in table 5.

For the determination of $S_S$ and $S_I$ filtration and chemical precipitation was used to differentiate the soluble components in the wastewater. After filtration on 1.2 µm pore size filter the particulate fractions of the wastewater are mainly held up by the filter but colloidal part of COD ($S_{COL}$) still making part of the particulate fraction can pass and chemical precipitation is needed prior to a 0.45 µ membrane filtration (Figure 4) to separate this fraction. Chemical precipitation/flocculation was made using $ZnSO_4$ and NaOH. Since both biodegradable and inert COD pass through the 0.45 µm pore size filter, the inert fraction $S_I$ has to be determined independently and subtracted from the soluble COD to give the fraction $S_S$.

The biodegradable COD (BCOD) in the influent is the sum of the readily biodegradable soluble COD ($S_S$) and the slowly biodegradable particulate COD ($X_S$). According to the STOWA the BCOD fraction is determined from BOD analysis where BOD is measured as a function of time. $BOD_5$ is determined in general but does not represent the total biodegradable fraction of the COD. Depending on the wastewater, 50 - 95 % of the COD is oxidized after 5 days, and after 20 days 95 - 99 % of the COD is oxidized. The total biodegradable fraction of the COD can be calculated by following the BOD-course as a function of time, and calculating $BOD_{tot}$ of the wastewater. Figure 5 shows the BOD curve of the synthetic wastewater, together with the equations used for $BOD_{tot}$ and BCOD calculations. On days 1-10 two parallel BOD measurements were performed for increased accuracy.

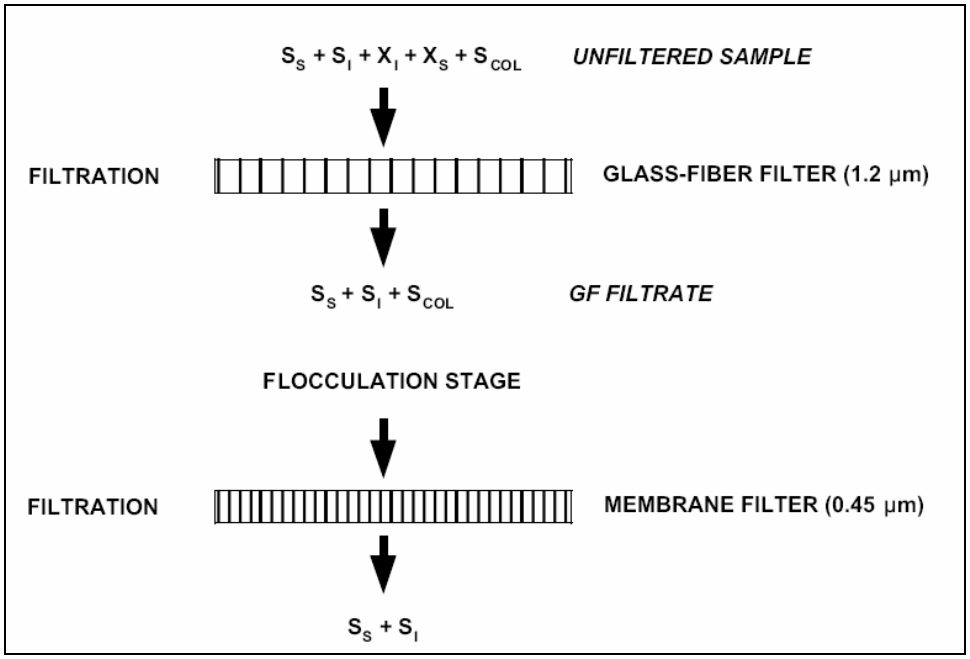


**Figure 4.** Retention/Passage of Influent Wastewater COD Components through Sequential1.2 µm Glass-Fiber Filtration, Flocculation and 0.45µm Membrane Filtration [13]

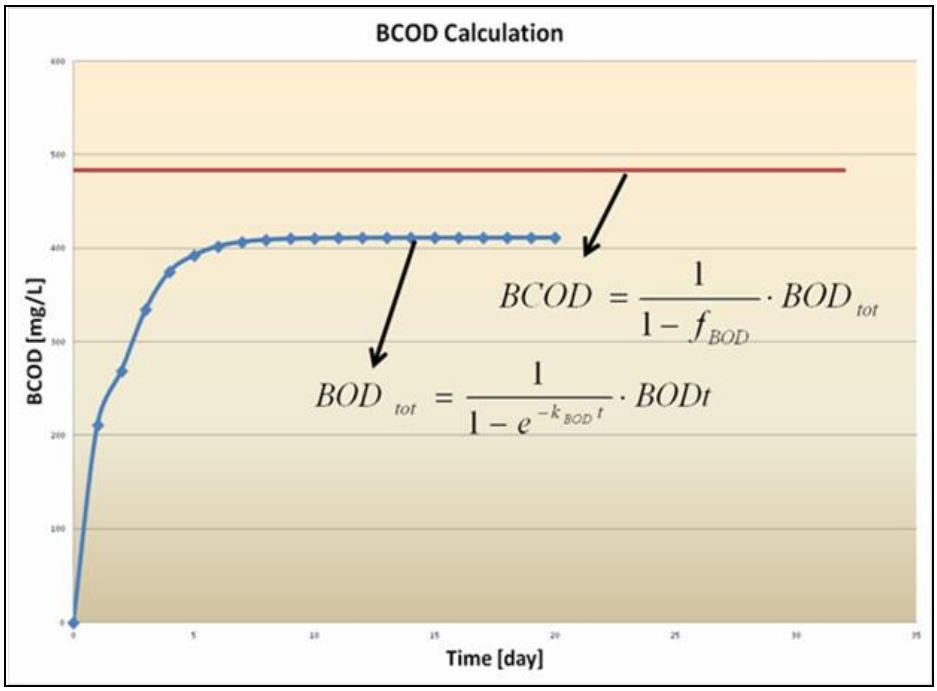


**Figure 5.** Fitted BOD curve for determination of $k_{BOD}$, $BOD_{tot}$ and BCOD.$k_{BOD}$ constant is the first order constant of the BOD vs. time measurements and can be determined by fitting the BOD-curve on the measured data with $BOD_{tot}$ equation [12].

During the BOD-measurements there is an interaction of growth and decay of biomass, and for long-term BOD measurements this results in the partial conversion of the biodegradable COD into an inert fraction. Therefore, the initial concentration of BCOD will be higher than the determined $BOD_{tot}$ and a correction factor ($f_{BOD}$) has to be used. For $f_{BOD}$ a value of 0.15 (0.1-0.2) can be taken, which is in close accordance with the ASM literature value for inert COD [12].

*Determination of the nitrogen fraction of the wastewater*

The major part of the nitrogen in a wastewater treatment system is present as ammonium, which has no coupling to organic components and can be measured analytically. For this synthetic wastewater the ammonium concentration is 6.3 mg/L. For the calculus of the organic part of the nitrogen fixed nitrogen conversion factors can be used ($i_N$) for the various COD components [11, 12, 13]. These conversion factors represent the nitrogen part of different COD components playing role in the total nitrogen load of the system (Table 5.)

**Table 5.**Conversion factors for nitrogen

| Conversion factors for nitrogen | | Typical Ranges |
|---|---|---|
| $i_{NSI}$ | 0.01 g N/g COD | 0.01-0.02 g N/g COD |
| $i_{NSA}$ | 0 g N/g COD | 0 g N/g COD |
| $i_{NSF}$ | 0.03 g N/g COD | 0.02-0.04 g N/g COD |
| $i_{NXI}$ | 0.03 g N/g COD | 0.01-.06 g N/g COD |
| $i_{NXS}$ | 0.04 g N/g COD | 0.02-0.06 g N/g COD |

The equations required for the calculus of the different wastewater components are summarized in Table 6.

**Table 6.**Equations of calculating the different wastewater fractions as applied in activated sludge models

| Equations for wastewater characterization | Calculation of wastewater characteristics |
|---|---|
| $COD_{\inf,tot} = S_I + S_S + X_I + X_S$ assumption $X_A, X_H = 0$ | $S_I = 0.9 * COD_{eff}$ for low loaded WWTP [12] |
| $COD_{\inf,tot} = COD_{\inf,sol} + COD_{\inf,part}$ | $S_S = COD_{\inf,sol} - S_I$ |
| $COD_{\inf,sol} = S_I + S_S$ | $X_S = BCOD - S_S$ |
| $COD_{\inf,part} = X_I + X_S$ | $X_I = COD_{\inf,tot} - S_I - S_S - X_S$ |
| $BCOD = S_S + X_S$ | $X_A, X_H = 0$ |
| $N_{tot} = S_{NH} + S_{NO} + S_{N_2} + i_{NSI} \cdot S_I + i_{NSS} \cdot S_s + i_{NXS} \cdot X_S + i_{NBM} \cdot (X_H + X_A) + i_{NXI}$ | |
| $COD_{tot} = S_I + S_S + X_I + X_S + X_H + X_A$ | |

**ACKNOWLEDGMENTS**

I would like to thank for the tireless help and valuable advice of the colleagues of the Institute of Environmental Engineering, Pannon University Veszprém, Hungary, who helped me enormously in the laboratory work on the lab-scale SBR. The work has been funded by the Sectoral Operational Programme Human Resources Development 2007-2013 of the Romanian Ministry of Labour, Family and Social Protection through the Financial Agreement POSDRU/6/1.5/S/19.

## REFERENCES

1. Hulsbeek J.J.W., Kruit J., Roeleveld P.J., van Loosdrecht M.C.M., (2002), A practical protocol for dynamic modelling of activated sludge systems, *Water Science and Technology*, **2002**, *45*, 127–136.
2. Curtis T.P., Craine N.G. and Milner M.G., The Comparison of Biological Diversity in Wastewater and Mixed Liquor in Activated Sludge, Proceedings of the Fourth Kollekolle Seminar on Activated Sludge modeling, Copenhagen, Denmark, **1998**.
3. Banihashemi A., Moghadam M.R.A., Maknoon R., Nikazar M., Development of a coagulation/flocculation predictive model for turbidity removal from Tehran water treatment plants, *Environmental Engineering and Management Journal*, **2008**, *7*, 13-16.
4. Gujer W., Henze M., Mino T., van Loosdrecht M.C.M., Activated sludge model No. 3, *Water Science and Technology*, **1999**, *39*, 183-193.
5. Raduly B., Gernaey K.V., Capodaglio A.G., Mikkelsen P.S. and Henze M. Artificial neural networks for rapid WWTP performance evaluation: Methodology and case study. *Environ. Modell. Softw.,* **2007**, *22*(8), 1208-1216.
6. Eckenfelder W.W., Industrial Water Pollution Control, McGraw-Hill Book Company, New York, **1966**.
7. Marais G.v.R., Ekama G.A., “The activated sludge process: Part 1 - Steady state behavior” Water S.A., **1976**, *2*, 163-200.
8. Van Haandel A.C., Ekama G.A., Marais G.v.R. “The Activated Sludge Process: Part 3 - Single Sludge Denitrification” Water Research, **1981**, *15*, 1135-1152.
9. Henze M., Gujer W., Mino T., van Loosdrecht M.C.M., Activated Sludge Models ASM1, ASM2, ASM2d, and ASM3, International Water Association Scientific and Technical Report No. 9,IWA Publishing, London, UK, **2000**.
10. Szabolcs Szilveszter, Botond Ráduly, Beáta Ábrahám, Szabolcs Lányi, Dan Robescu Niculae, Mathematical models for domestic biological wastewater treatment process, *Environmental Engineering and Management Journal*, **2010**, 9(5), 629-635.

11. Jeppsson U., Modelling aspects of wastewater treatment processes, Ph.D. Diss, Department of Industrial Electrical Engineering and Automation (IEA), Lund Institute of Technology, Sweden, **1996**.
12. P.J. Roeleveld and M.C.M. van Loosdrecht, Experience with guidelines for wastewater characterization in The Netherlands, *Water Science Technology,* **2002**, *45*(6), 77-87.
13. H. Melcer*et. al*, Methods for Watewater Characterization in Activated Sludge Modeling, *Water Environment Federation*, **2003**.
14. Al-Rekabi WS., Qiang H, Qiang WW., Review on Sequencing Batch Reactors, *Pakistan Journal of nutrition*, **2007**, *6*(1), 11-19.
15. Nopens I., Capalozza C., Vanrolleghem PA., Stability analysis of a synthetic municipal wastewater, GentUniversity, **2001**, weblink: http://biomath.ugent.be/~peter/ftp/pvr334.pdf
16. APHA, Standard methods for the examination of water and wastewater, American Public Health Association, Washington, DC, USA, **1998**.

STUDIA UBB CHEMIA, LV, Sp.Iss., 2010

# SOCIOMICROBIOLOGICAL PROPERTIES OF ANTAGONISTIC BACTERIA ISOLATED FORM BORSÁROS RAISED BOG

**SZENTES SAROLTA[a], MARA GYÖNGYVÉR[b], MÁTHÉ ISTVÁN [b], LASLO ÉVA[a], LÁNYI SZABOLCS[b], GABRIEL-LUCIAN RADU[a]**

**ABSTRACT.** The main aim of our study is the development of new antagonistic bacterial based biopreparates. The sociomicrobiological analyses gives information about the bacterial communication forms. These communication forms are important in bacterial antagonism. In this study we analyzed the biofilm formation ability of the isolated bacterial strains in single and co-cultures.

***Keywords:*** *antagonism, soil bacteria, biofilm formation, bacterial communication, bryophyte associated bacteria*

## INTRODUCTION

A novel formulation of broad spectrum bacterial biopreparates is the objective of sustainable agriculture. Our main aim is to develop biopreparates, carrying living antagonistic soil bacteria. In order to select bacterial strains for such biopreparates it is important to analyze their ability to colonize plant surfaces [1 and 2].

Antagonistic bacteria are microorganisms which can control the proliferation of plant pathogens [3]. These bacterial strains exert their action by synthesising antimicrobial compounds, such as antibiotics, siderophores, biosurfactants, and antifungal metabolites [1, 4 and 5]. All these metabolites are important in displacement of competing microbial populations. Recent studies show that colonization of the plant surfaces by biocontrol bacteria is more effective when bacteria form microcolonies, called biofilms [1].

Biofilms are multicellular aggregates; bacterial cells being adhered to a surface and each other through an exopolysaccharide matrix [6]. Biofilms are advantageous to bacteria; microorganisms within biofilm are more resistant to environmental stress conditions (e.g. nutrient lack, antibiotics, pH etc). The biofilm forming bacteria also show a higher survival rate, than the planktonic (free-living) organisms [6 and 7]. In biofilm communities can be involved a large number of different bacterial species. This explains the importance of studying biofilm profiles of bacterial co-cultures [8].

[a] *Universitatea POLITEHNICA, Facultatea de Chimie Aplicată şi Ştiința Materialelor, Splaiul Independenței 313, RO-060042 Bucureşti, Romania, szentessarolta@sapientia.sciulorum.ro*

[b] *Universitatea Sapientia, Facultatea de Ştiințe, Piața Libertății nr. 1, RO-530104 Miercurea Ciuc, Romania, maragyongyver@sapientia.siculorum.ro*

The studied bacterial strains were isolated from Borsáros natural reserve, near Miercurea Ciuc, Harghita County (Romania). In this nutrient poor oligotrophic raised bog the main biomass is given by the *Sphagnum sp.* mosses (*Bryophyta)*. According to Opelt and Berg [9], the *Sphagnum sp.* mosses can be associated with antagonistic bacteria, appropriate to be used as biopreparates [9].

The aim of the current study is to determine the biofilm production ability of the isolated bacterial strains. The best biofilm forming bacterial strains were selected for compatibility study. Those bacteria that showed a good coexistence property were analyzed for their biofilm production in co-cultures.

## RESULTS AND DISCUSSION

A total number of sixty six bacterial strains were isolated from Borsáros raised bog. The isolated bacterial strains were sorted in three groups: 22 *Enterobacteriaceae*, 23 *Pseudomonas sp*. and 21 *Bacillus sp*. The selected bacterial strains were studied for their antagonistic properties against plant pathogen microorganisms (*Phytium sp*. and *Erwinia carotovora*) [13].

The biofilm forming capacity of 66 bacterial strains were analyzed. The determination of biofilm production was realized using crystal violet staining, by spectrofluorometric method. Bacterial strains were grown in microtiter plates for 24 h. The optical density of the cell suspension was determined at 620 nm. Biofilms were stained with crystal violet, followed by a dissolving of the bounded dye in absolute ethanol. The optical density of the stained ethanol was measured at 492 nm.

The biofilm forming ability of *Bacillus sp.* strains is presented in Figure 1. The ratio of OD492/OD620 represents the real value of the biofilm production.

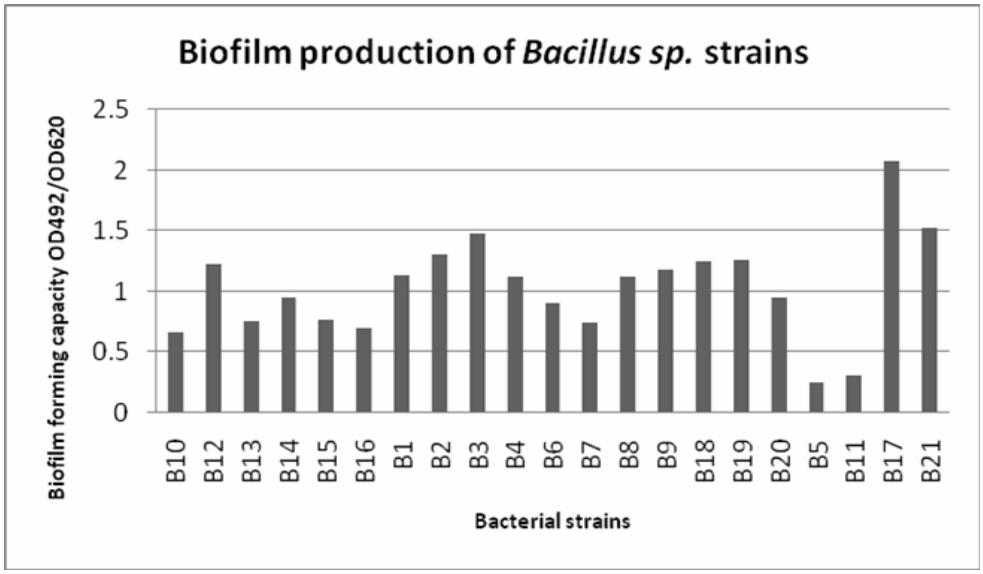


**Figure 1.** Biofilm production ability of *Bacillus sp.* Strains

From the analyzed bacterial strains a number of 3 (B3, B17 and B21) were selected for further study. These bacterial strains proved to be good biofilm producers.

From the analyzed *Pseudomonas sp.* a number of 6 strains (P6, P8, P10, P11, P18 and P19) were selected for compatibility study (Figure 2.)

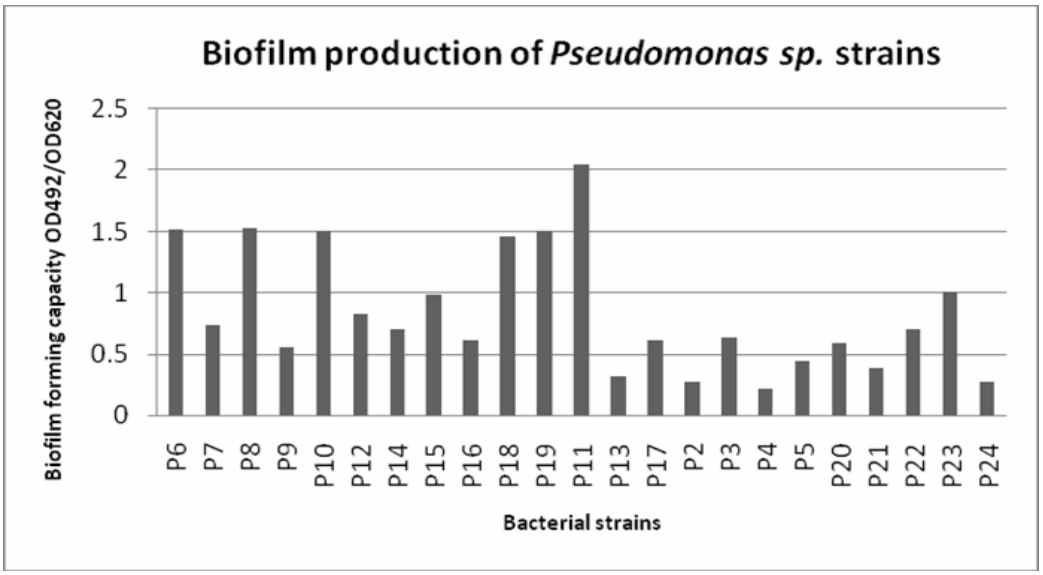


**Figure 2.** Biofilm production ability of *Pseudomonas sp.* bacterial strains

We also selected 2 strains of *Enterobacteriaceae* for further analysis. In Figure 3. the real values of the biofilm quantity (OD492/OD620) are presented. The good biofilm forming bacteria, selected for further analysis are: E2 and E20.

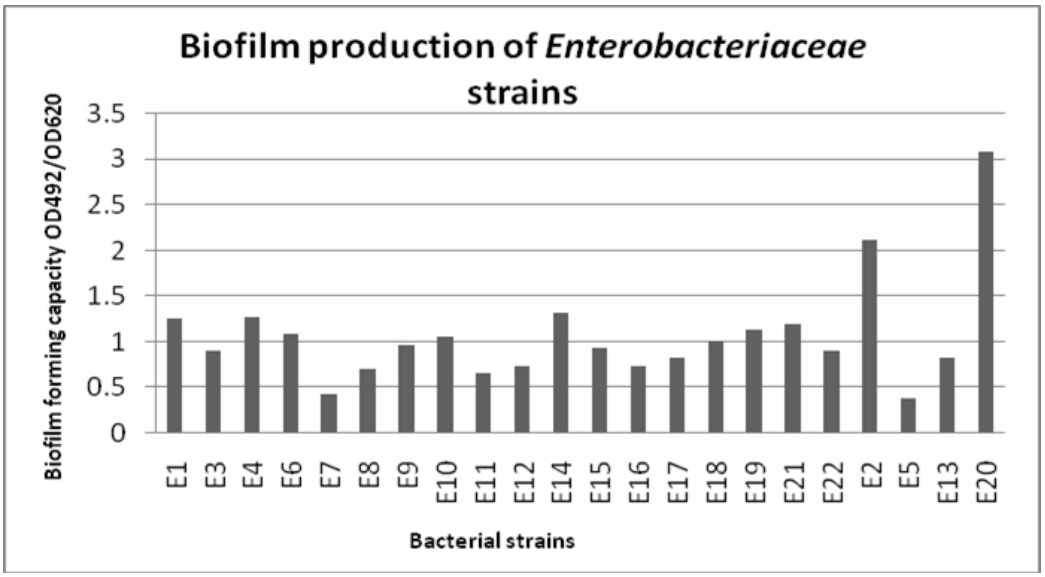


**Figure 4.** Biofilm production ability of *Enterobacteriaceae* bacterial strains

Compatibility test was realized with agar diffusion assay for the selected biofilm producing bacterial strains. Figure 5. shows the compatibility of E2 bacterial strain with P6, P11, P18, P19 and B3 bacterial strains. Inhibition zone formed in case of P6 bacteria refers that this strain inhibits the proliferation of E2 bacterial strains. In case of P11, P18, P19 and B3 bacterial strains the inhibition zone is not visualized.

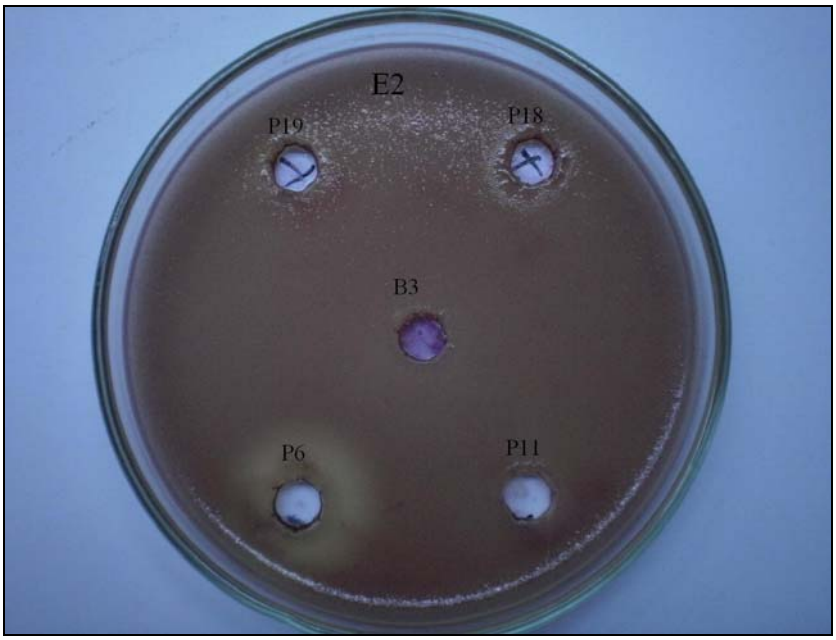


**Figure 5.** Compatibility test with agar diffusion assay, P6 bacterial strain inhibits the proliferation of E2 bacterial strain

We found 8 similar cases, when bacterial strains inhibited the proliferation of each other. Inhibition zones were formed between bacterial strains as follows: P6-P8, P6-P11, P6-E20, P10-P6, P18-P11, P19-P6, P19-P11 and B17-P8. P6 bacterial strain, isolated as *Pseudomonas sp.* showed the highest number of antagonistic activity.

In order to develop a bacterial based biopreparate it is essential, to analyze the biofilm formation ability of bacterial co-cultures. We selected the following bacterial strains: P10, P18, P19, B3, B17, B21, E2 and E20. In Figure 5. are shown the biofilm production ability of the co-cultures compared with the single cultures. The grey columns represent the biofilm forming ability of the single bacterial strains; the black column represents the biofilm production of the co-cultures. In case of 5 samples the biofilm forming ability of the co-cultures showed a higher value, than in the case of single bacterial strains. B3, P10, E2 are the bacterial strains that reinforce the biofilm production in co-cultures.

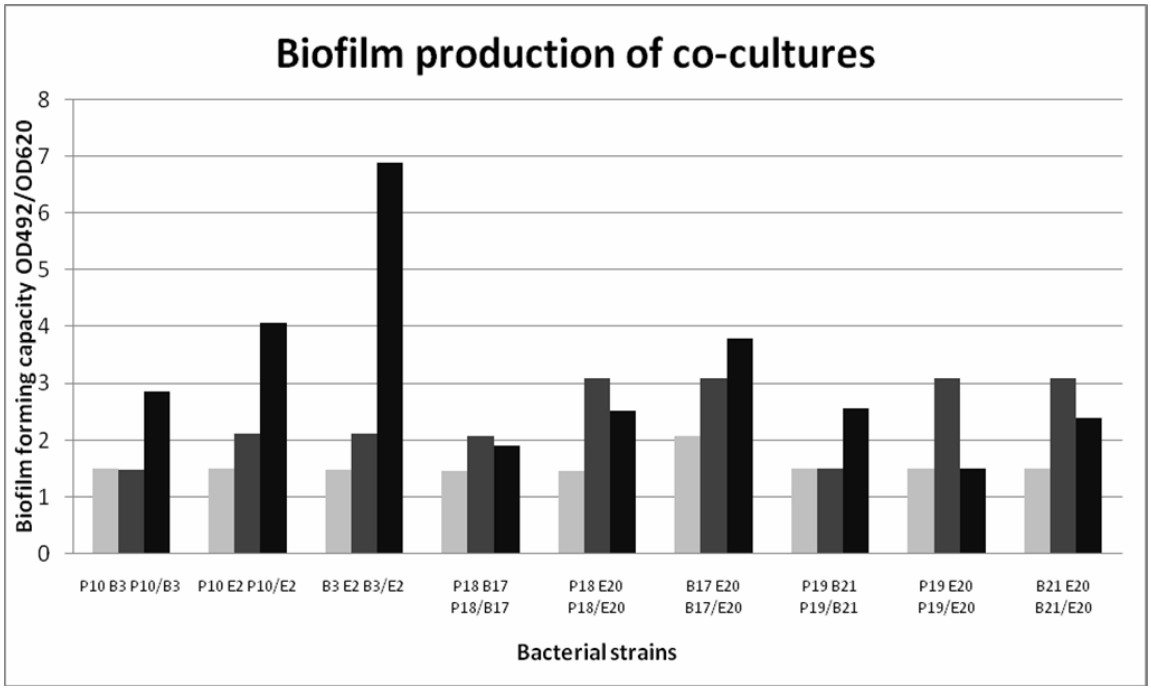


**Figure 5.** Biofilm production of co-cultures

## CONCLUSIONS

Preliminary study was made in order to develop antagonistic bacterial based biopesticides. Compatibility test and biofilm formation ability of single strains and co-cultures of isolated antagonistic bacterial strains were studied.

The importance of biofilm production was demonstrated by Simoes et al. [10]. Biofilms are protecting area for bacteria, allowing bacterial strains to survive in hostile environments. In case of soil bacteria – such as plant growth promoting and biocontrol bacteria- biofilms play key role in the colonization of root surfaces and survival in the harsh environment [1]. According to Maheswari [11] the biofilm formation on the plant surfaces protects the plant against phytopathogen microorganisms, trough resistance mechanisms such as Quorum sensing or antibiotic production. Although microtiter plate assay is a very easy method to measure the quantity of the bacterial biofilm, in case of soil bacteria is not commonly used.

Rinaudi et al. [12] studied biofilm formation ability of soil bacterial strain *Sinorhizobium meliloti* on different nutritional conditions. According to their results the biofilm formation in nutritionally limited conditions increases. This indicates a survival strategy of bacteria, colonizing the root surface by bacteria has the advantage to increased capture of nutrients that may be absorbed to the surface. In our study the analyzed sixty six bacterial strains were isolated from

a nutrient poor environment. From bacterial strains isolated as *Pseudomonas sp.*, *Bacillus sp.* and *Enterobacteriaceae,* 11 strains proved to be good biofilm producers. These bacterial strains can be categorized as good surface colonisers. These bacterial strains were further analyzed for their compatibility.

One of the analyzed bacterial strains (P6 strain) proved to be the less compatible with the other strains. Five bacterial strains (B3, B21, P8, P11 and E2) showed a good coexistence property.

Liu et al. [8] compared biofilm formation of two bacterial strains under single culture and co-culture. During the study was proved that under co-culture conditions bacterial biofilm form more densely then in single culture conditions. We analysed the biofilm forming capacity of 9 bacterial pairs. In case of 5 pairs the biofilm forming capacity proved to be better then in single cultures. These strains could be good root surface colonizing bacteria.

Further analyses - such as the ability of signal molecules production, studying the antimicrobial products secreted by bacterial strains, optimization of culturing conditions, testing the isolated bacterial strains on plants - are necessary for these bacterial strains to be used as potential biopreparates.

## EXPERIMENTAL SECTION

### Bacterial strains

Bacterial strains were isolated from Borsáros raised bog, form the surface, the tissues and the rhizosphere of *Sphagnum sp.* The moss samples were collected in summer of 2010. For bacterial isolation, three different selective growth medium was used: King B agar (proteose peptone 20 g/L, glycerol 10 ml/L, di-potassium hydrogen phosphate 1,5 g/L, magnesium sulphate* $7H_2O$ 1,5 g/L, agar 20 g/L) for *Pseudomonas sp.*, Nutrient agar (peptone 5 g/L, sodium chloride 5 g/L, yeast extract 2 g/L, meat extract 1 g/L, agar-agar 15 g/L) for *Bacillus sp.* and MacConkey agar (peptone form casein 17 g/L, peptone from meat 3 g/L, sodium chloride 5 g/L, lactose 10 g/L, Bile salt mixture 1,5 g/L, neutral red 0,03 g/L, crystal violet 0,001 g/L, agar-agar 13,5 g/L) for selection of *Enterobacteriaceae* bacterial strains. The isolates were tested of their antifungal (Phytium sp.) and antibacterial (Erwinia carotovora) activity [13].

### Biofilm formation assay

Biofilm formation assay were conducted according to the methods of Tamás et al. [14]. Bacterial strains were grown in Nutrient broth, for 24 h cultures. For each culture dilution series were made (1 ml of bacterial strain was loaded in 9 ml of Nutrient broth). 200 μl of bacterial suspension was

loaded in a 96 well microtiter plate (SPL). 200 μl of sterile Nutrient broth was used as a control. The optical density of the cell suspension was measured before and after the incubation at 620 nm (Fluorostar Optima, BMG Labtech, microtiter plate reader). After 24 h incubation at 28 °C, cells were washed twice with 300 μl distilled water (StatFax 2600). Biofilms were stained 40 minutes with 300 μl crystal-violet solution (0.1%). Wells were washed two times with 300 μl of demineralised water. The bounded crystal-violet dye was dissolved in 300 μl ethanol (96%). 200 μl of solubilised ethanol solution was transferred into a new microtiter plate. The optical density of the wells was measured at 492 nm. The biofilm formation assay was repeated eight times.

The biofilm formation study of the co-cultures was performed as described above. The selected bacterial strains were as follows: P10, P18, P19, B3, B17, B21, E2 and E20. Bacterial cells were grown in pairs in Nutrient broth. The bacterial pairs were as follows: P10-B3, P10-E2, B3-E2, P18-B17, P18-E20, B17-E20, P19-B21 and B21-E20.

## Agar diffusion assay

The compatibility test was performed for the best biofilm forming 11 bacterial strains. Bacterial strains were cultured for 24 h, at 28 °C. After the incubation bacterial cultures were diluted in sterile distilled water, until the optical density at 660 nm ($OD_{660}$) was 0.3. Nutrient agar, containing 1 % TTC (triphenyl tetrazolium chloride) was tempered at 40-50 °C, and inoculated with the test organisms. The inoculated medium was poured in sterile Petri dishes. After solidification, wells of 5 mm diameter were cut, with the use of sterile glass tubes (5 wells in each Petri dish, 2 Petri dishes for every bacterial strain).Test bacterial cells, were grown in Nutrient broth for 1 week, at 28 °C. After incubation the cells were centrifuged at 5000 RPM for 30 minutes, and separated with membrane filters to obtain the bacteria free supernatant. 100 μl of supernatant was added in each well. Red coloration of the nutrient medium refers to the growth of bacterial cells. Appearance of inhibition zones around the wells refers to antagonistic property of the tested bacterial strain. We tested the compatibility of each bacterial strain with the other 10 strains.

## ACKNOWLEDGMENTS

This work was prepared with the financial support from the “BIOPREP – Microbial biopreparates for increasing the productivity and crop protection” research funded by Sectoral Operational Programme, Increase of Economic Competitiveness Operation 2.1.1. of the Romanian Ministry of Labour, Family and Social Protection, through financial agreement POSCEE No. 469/11817.

The work has been funded by the Sectoral Operational Programme Human Resources Development 2007-2013 of the Romanian Ministry of Labour, Family and Social Protection through the Financial Agreement POSRDU/88/1.5/S/61178.

## REFERENCES

1. M.A. Molina, J.L. Ramos, M. Espinosa-Urgel, *Reviews in Environmental Science and Biotechnology*, **2003**, *2,* 101.
2. Al-Taweil H.I., Osman M.B., Hamid A.A., Yusoff W.M.W., *American Journal of Agricultura land Biological Sciences*, **2009**, *4*(1), 79.
3. D. Chandler, G. Davidson, W.P. Grant, J. Greaves, G.M. Tatchell, *Trend sin Food Science & Technology*, **2008**, *19*, 276.
4. B.R. Glick, Y. Bashan, *Biotechnology Advances*, **1997**, *15* (2), 356-360.
5. M. Shoda, *Journal of Bioscience and Bioengeneering*, **2000**, *89*(6), 516.
6. B.E. Ramey, M. Koutsoudis, S.B. Bodman, C. Fuqua, *Current Opininon in Microbiology*, **2004**, *7*, 604.
7. E.D. Elder, A.S. Fenech, A.D. Zink, T.P. Bradley, A.L. Fuller, *Proceedings of the 1995 Georgia Water Resources Conference*, **1995**, 386.
8. L. Liu, L. Chu, Q. Liu, C. Wang, Y. Xia, X. Peng, *African Juornal of Microbiology Research*, **2010**, *4*(3), 180.
9. K. Opelt, G. Berg, *Applied and Environmental Microbiology*, **2004**, *70* (11), 6569.
10. M. Simoes, L.C. Simoes, M.J. Vieira, *Food Science and Technology*, **2010**, *43*, 575.
11. D.K. Maheshwari, "Plant Growth and Health Promoting Bacteria", Springer, Münster, **2010**.
12. L. Rinaudi, N.A. Fujishige, A.M. Hirsch, E. Banchio, A. Zorreguieta, W. Giordani, *Research in Microbiology*, **2006**, *157*, 869.
13. S. Szentes, Gy. Mara, Sz. Lányi, G.L. Radu, *Scientific Bulletin of Mineral Resources and Environment Faculty, North University of Baia Mare,* **2010**, *16*(2), 54.
14. É. Tamás, Gy. Mara, É. Laslo, É. György, B. Ábrahám, Sz. Lányi, *Studia UBB Chemia*, **2009**, Special Issue No. 2, 51.

STUDIA UBB CHEMIA, LV, Sp.Iss., 2010

# DETECTION OF GENES FROM SOIL BACTERIA WITH ROLE IN THE ORGANIC NITROGEN AND PHOSPHORUS MOBILIZATION

**TAMÁS ÉVA[a,*], MARA GYÖNGYVÉR[b], SIPOS RITA[c], MÉSZÁROS ÉVA[c], MÁRIALIGETI KÁROLY[c], LÁNYI SZABOLCS[b]**

**ABSTRACT.** The main aim of our study is the development of bacterial biopreparates based on organic nitrogen and phosphorus mobilizing microorganisms. As an important step of bacterial strain selection, in this study, we performed the detection of functional genes (*apr, npr*) that play role in the organic nitrogen mobilization. The amplified *apr* genes were controlled using DNA sequence analysis.

***Keywords:*** *soil bacteria, nitrogen mobilization, apr, npr gene detection*

## INTRODUCTION

In the living systems most of the organic nitrogen is built-in proteins and nucleic acids. A large proportion (40%) of the soil nitrogen content is bounded in proteinaceus compounds like enzymes, structural proteins, glycoproteins, peptides and amino acids [1]. These protein residues with organic nitrogen content are prone to mineralization processes.

When an organism dies, its proteins are attacked by the proteases of soil bacteria to produce polypeptides and amino acids. Proteases mediate the first steps of mineralization that often are rate-limiting for the nitrogen cycle. Soil proteases are derived mainly from heterotrophic soil bacteria. Władyka and coworkers divided the proteases depending on the location of reaction they catalyse, into endopeptidases (peptidases that hydrolyse peptide bonds in the inner regions of peptide chains) and exopeptidases (with activity directed to the amino- or carboxyl-termini of proteins) [5].

[a] *Politehnica University, Faculty of Applied Chemistry and Material Science, Spl. Independenței, 313, Sector 6, Cod 77206, Bucharest, Romania, Tel: 40 21 402 91 00, Fax: 40 21 318 10 05.*
**Author to whom correspondence should be addressed E-Mail: tamaseva@sapientia.siculorum.ro*
[b] *Sapientia University, Cluj-Napoca, Faculty of Sciences, Miercurea-Ciuc, Bioengineering Department, Piața Libertății, 1, Cod 530104, Miercurea-Ciuc, Romania, Tel.: +40 266 317 121, Fax: +40 266 372 099*
[c] *Eötvös Loránd University, Faculty of Science, Department of Microbiology, H-1117 Budapest, Pázmány Péter sétány 1/c, Hungary, Tel.: (36-1) 381-2177*

The following step in the mineralization process of the organic nitrogen iscalled ammonification, through which the organic compounds are transformed to ammonia. In addition to the ammonification of amino acids, other compounds such as nucleic acids, urea, and uric acid go through the ammonification process, due to the microbial extracellular enzyme activity [2]. There are numerous bacterial species that were previously described as having a decisive role in the nitrogen mineralization: *Bacillus cereus, B. megaterium, B. subtilis, Serratia marcescens, Achromobacter* spp., *Flavobacterium* spp., *Mycobacterium* spp., *Nocardia* spp., *Bactoderma* spp. [2, 3, 4].

Proteases, based on their catalytic mechanism were divided into seven groups. Depending on the amino acids that serve as nucleophilic amino acid for the active site of the enzyme the following protease groups were distinguished: aspartic acid proteases, cysteine proteases, glutamic-acid proteases, metalloproteinases, serine proteases, threonine proteases, and assigned group without any particular catalytic type. It is presently known that extracellular peptidases of fungal origin are mostly cysteine and aspartic peptidases, while those of bacterial origin are alkaline metallopeptidases (Apr), neutral metallopeptidases (Npr) and serine peptidases (Sub) [6, 7, 8]. Singh and coworkers [12] described the presence of the alkaline protease enzymes in salt-tolerant alkaliphilic actinomycetes.

Bacterial proteases were studied by Bach and coworkers [6] in several bacterial strains. The *sub* and *npr* genes, coding serine peptidases and neutral metallopeptidases were mainly found in *Bacillus* species, whereas *apr* genes coding alkaline metallopeptidases in *Pseudomonas fluorescens* biotypes and also in *Flavobacterium – Cytophaga* strains [6, 7, 9].

The main aim of the present study was to detect bacterial peptidase (*apr* and *npr*) genes from the genome of 37 bacterial strains isolated from Harghita County mountainous regions [10] in order to select bacterial strains with important role in nitrogen mineralization.

## RESULTS AND DISCUSSION

In this study, the detection of alkaline metalloproteinase (*apr*) and neutral metalloproteinase (*npr*) genes of the 37 bacterial strains (Table 1.) was performed using degenerated primer pairs. The annealing temperatures of the primer pairs were optimised using as controls the *Pseudomonas fluorescens* ATCC 13525 strain for *apr* and the *Bacillus cereus* ATCC 14579 strain for *npr* gene detection.

A gradient polymerase chain reaction (PCR) was performed in order to determine the optimal annealing temperature of primers setting a 9ºC gradient from 49ºC to 58ºC. As it is shown on Figure 1, the amplicons resulted from the *apr* gene amplification are varying with temperature. At lower temperatures the

products are slightly visible, whereas the amount of amplification product is increasing between the temperature ranges from 49 to 55.7ºC, and is decreasing with the further increase in temperature. Between the temperatures set from 52.9ºC to 58ºC by-products were generated (not only a single band detected). The optimal annealing temperature chosen for *apr* gene amplification was 57.3ºC because on this temperature the ratio between the expected PCR product and the by-product was considered most adequate. The amplification of the *npr* gene was observed only on 52.9ºC (Figure 1.) for the *Bacillus cereus* ATCC 14579 strain. The *npr* primer pair gave a 233 bp amplicon and some additional unspecific bands with the lowered temperature was observed for *Bacillus cereus DSMZ 3101*, *Bacillus cereus NCBI M38910* strains at 53ºC in case of Bach and coworkers study[6, 9].

**Table 1**. The bacterial strains used in this work and the results of the proteinase gene amplifications (+ – positive results, - – negative results)

| Bacterial strain No | Isolated from | Species affiliation | *apr* gene | *npr* gene |
|---|---|---|---|---|
| 1BS | soil – Borsáros | *Pseudomonas* sp. | + | - |
| 2BR | rhizosphere of *Carex* sp. – Borsáros | | - | - |
| 11BS | soil – Borsáros | | + | - |
| 12BS | soil – Borsáros | | + | - |
| 13BS | soil – Borsáros | | + | - |
| 19BS | soil – Borsáros | | + | - |
| 20BS | soil – Borsáros | | + | - |
| 2BS | soil – Borsáros | *Delftia lacustris* | + | - |
| 3BS | soil – Borsáros | | + | - |
| 4BS | soil – Borsáros | | + | - |
| 6BS | soil – Borsáros | | + | - |
| 8BS | soil – Borsáros | | + | - |
| 17BS | soil – Borsáros | | + | - |
| 1BR | rhizosphere of *Carex* sp. – Borsáros | | + | - |
| 3BR | rhizosphere of *Carex* sp. – Borsáros | *Bacillus cereus* | + | - |
| 14BS | soil – Borsáros | | + | - |
| 16BS | soil – Borsáros | | - | - |
| 21BS | soil – Borsáros | | - | - |
| 4BR | rhizosphere of *Carex* sp. – Borsáros | *Serratia plymuthica* | + | - |
| 5BS | soil – Borsáros | | - | - |
| 9BS | soil – Borsáros | | + | - |
| 10BS | soil – Borsáros | | + | - |
| 15BS | soil – Borsáros | | + | - |
| 18BS | soil – Borsáros | | + | - |

| Bacterial strain No | Isolated from | Species affiliation | *apr* gene | *npr* gene |
|---|---|---|---|---|
| 1CNS | not fertilized soil – Cristuru Secuiesc | *Acinetobacter lwoffii* | - | - |
| 2CNS | not fertilized soil – Cristuru Secuiesc | | - | - |
| 1CZR | rhizosphere of *Zea mays* – Cristuru Secuiesc | | - | - |
| 2CZR | rhizosphere of *Zea mays* – Cristuru Secuiesc | | - | - |
| 3CZR | rhizosphere of *Zea mays* – Cristuru Secuiesc | | - | - |
| 4CZR | rhizosphere of *Zea mays* – Cristuru Secuiesc | | - | - |
| 7BS | soil – Borsáros | *Bacillus fordii* | + | - |
| 3CCR | rhizosphere of *Carex* sp. – Cristuru Secuiesc | *Erwinia cypripedii* | + | - |
| 5CZR | rhizosphere of *Zea mays* – Cristuru Secuiesc | *Pseudomonas fluorescens* | + | - |
| 6CZR | rhizosphere of *Zea mays* – Cristuru Secuiesc | *Pseudomonas fluorescens* | + | - |
| 1CCR | rhizosphere of *Carex* sp. – Cristuru Secuiesc | *Pseudomonas jessenii* | + | - |
| 2CCR | rhizosphere of *Carex* sp. – Cristuru Secuiesc | | - | - |
| 4CCR | rhizosphere of *Carex* sp. – Cristuru Secuiesc | | + | - |

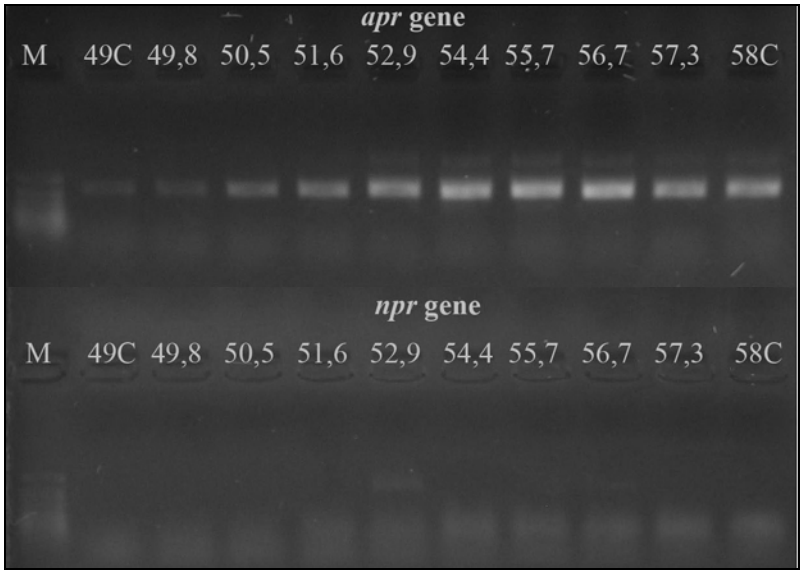


**Figure 1.** The products of *apr* and *npr* gene amplification of control strains by gradient PCR.

The presence of *apr* gene was detected in the genome of the studied strains, giving a 194 base pair (bp) product, compared to the positive control *Pseudomonas fluorescens* ATCC 13525 (Figure 2.).

In several isolates (1BR, 3BS, 4BS, 6BS and 8BS) additional multiple unspecific bands were observed (Figure 2.), due to the degenerated nature of the used primers. The sequence analysis of these isolates showed the closest homology with the *Delftia lacustris* DMS 21246$^{(T)}$ strain (unpublished data). According to the *Gene Bank* data the genome of *Delftia sp.* strains also encodes protease enzymes. Using the *NCBI Protein Blast* program the similarities between the amino acid sequences of *Pseudomonas fluorescens* and *Delftia* metalloproteinase were analyzed *in silico.* A difference in size of *Pseudomonas fluorescens* and *Delftia* metalloproteinases were observed, the amino acid sequences for *Delftia* metalloproteinase were found to be longer.

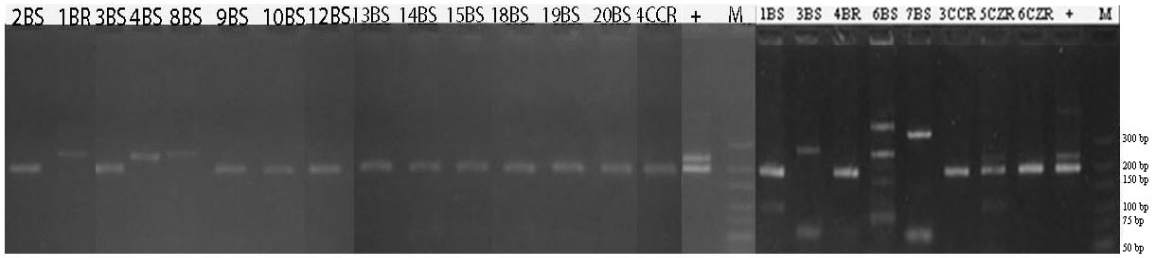


**Figure 2.** The amplified *apr* gene products separated by agarose gel electrophoresis (M - GeneON LowRange DNA Ladder, + positive control, 2BS, etc. - bacterial strain Nos). The 194 bp bands represent the target *apr* gene. In some cases additional unspecific bands appeared.

The *npr* gene failed to amplify from the samples, which implies that the genome of the isolates not likely contains genes homologous to the *npr* amplified by the primers.

**Table 2.** Sequences showing significant homology with our isolated *apr* gene sequences retrieved from the *NCBI Nucleotide Collection* database.

| **Strain** | **Description** | **Similarity** |
|---|---|---|
| *Erwinia cypripedii* strain 3CCR | *Pseudomonas fluorescens aprA* gene, *aprI* gene, *aprD* gene and *aprE* gene (partial), strain M114 | 95% |
| | *Pseudomonas fluorescens* Pf0-1, metalloprotease | 91% |
| | *Pseudomonas fluorescens* No.114 gene for metalloproteinase | 91% |
| | *Pseudomonas fluorescens* CIP7325 *AprX* gene | 91% |
| | *Pseudomonas fluorescens* strain CHA0 metalloproteinase (*aprA*) | 90% |
| *Pseudomonas fluorescens* | *Pseudomonas fluorescens* genes for ABC exporter operon, complete cds (coding region) | 92% |

| Strain | Description | Similarity |
|---|---|---|
| strain 6CZR | *Pseudomonas fluorescens* SBW25, metalloproteinase | 90% |
| | *Pseudomonas fluorescens* CIP7325 *AprX* gene | 89% |
| | *Pseudomonas tolaasii eprA, eprI, eprD, eprE, eprF* genes | 88% |
| | *Pseudomonas fluorescens* strain TSS extracellular metalloproteinase (*aprX*) gene | 88% |

The amplified genes for two strains (3CCR and 6CZR) were further analyzed using DNA sequence determinations. The sequences of the PCR products showed similarities to metalloproteinase enzyme sequences isolated from different *Pseudomonas* strains (Table 2.). Thus it can be concluded that the amplified sequences encode alkaline metalloproteinase enzyme genes.

## CONCLUSIONS

During the work the *apr* gene was positively amplified for 26 bacterial strains (Table 1.) using degenerate primers designed for amplification of metalloproteinase enzymes by Bach and coworkers [6,9]. The isolated bacterial strains that produce alkaline metalloproteinase enzymes possibly participate in the mobilization of nitrogen from organic sources. The *npr* gene failed to amplify from the samples, which implies that the genome of the isolates not likely contains genes homologous to the tested ones. The amplified *apr* genes were sequenced in case of two strains, and showed acceptable similarity to *Pseudomonas fluorescens* metalloproteinase genes (Table 2.).

The bacterial strains that gave positive results for the analysed functional gene (*apr,* alkaline metalloproteinase) have an important role in nitrogen mineralization and can be selected as potential plant growth promoting bacteria.

## EXPERIMENTAL SECTION

### Bacterial strains and growth medium

The bacterial strains were isolated from soil and rhizosphere of *Carex* sp. and *Zea mays* from Cristuru Secuiesc region; from soil and rhizosphere of *Carex* sp. fromBorsáros raised bog natural reserve. The used isolatory medium was King's B agar, containing 20 g/L proteose peptone, 10 ml/L glycerol, 1.5 g/L $K_2HPO_4$, 1.5 g/L $MgSO_4.7H_2O$, 18 g/L agar, pH = 7.2.

### Cell lysis and DNA purification

Genomic DNA was obtained using the NaOH-based DNA extraction method. In 1.5 ml Eppendorf-tubes 25 µl 0.5 M NaOH solution was distributed and a loopful of bacteria suspended in it thorough vortexing and incubated at

room temperature for 15 minutes. After that 25 µl 1 M Tris solution (pH 8) and 300 µl ultra-pure $H_20$ was added, and centrifuged for 30 seconds at maximum speed to remove the cell debris. The supernatants were used as DNA samples, which were stored at -20ºC.

## Polymerase Chain Reaction

For the detection of the *apr* and *npr* genes using PCR the following primer pairs were selected: FP *aprI* (5'-TAYGGBTTCAAYTCCAAYAC-3'), RP *aprII* (5'-VGCGATSGAMACRTTRCC-3'), FP *nprI* (5'-GTDGAY GCHCAYTAYTAYGC-3') and RP *nprII* (5'-ACMGCATGBGTYADYTCATG-3'). The gradient PCR was performed setting a gradient from 49ºC to 58ºC. The reaction mixture in a 25 µl final volume contained the following for each reaction: 2.5 µl 5x PCR buffer, 5 µl dNTP, 2 µl 25mM $MgCl_2$, 1 µl of each primer (FP *aprI* and RP *aprII* or FP *nprI* and RP *nprII*) and 1 µl *Taq polymerase* (2U/µl). The used temperature profile for the PCR was the following: preheating at 98°C for 5 minute for denaturation of DNA and activation of polymerase, 40 cycles with denaturation at 95ºC for 30 seconds, annealing at 49…58ºC for 30 seconds, extension at 72ºC for 30 seconds and a final extension at 72ºC for 10 minutes. The results of amplification were analysed using agarose gel electrophoresis (2% agarose gel, 80 V, 20 minutes, GeneOn 10bp LowRange DNA-Ladder). Further PCR reactions for selected bacterial strains were performed on the optimum annealing temperatures. Amplicons were analysed using agarose gel electrophoresis (1,8% agarose [Cambrex MetaPhor] in TBE buffer, 70 V, 60 minutes, GeneOn 10bp LowRange DNA-Ladder).

## Amplicon sequencing

The purification of the DNA was made using *PCR-MTM CleanUp System* (*Viogene,* Sijhih, Taiwan) according to the manufacturer's description. After purification the products were visualized using agarose gel electrophoresis (2% agarose gel, 80 V, 20 minutes, GeneOn 10bp LowRange DNA-Ladder). The sequencing reaction was realised using *AmpliTaq® FS Big Dye ™ Terminator* sequencing kit (Applied Biosystems). The reaction was performed for two bacterial strains (3CCR, 6CZR). The reaction mixture contained 2.25 µl 5x Big Dye buffer, 1.5 µl Big Dye, 1 µl forward primer, 4.5 µl DNA, 5.75 µl $dH_2O$ in a 15 µl final volume. The amplification program was the following: 28 cycle with denaturation at 96ºC for 10 seconds, annealing at 50ºC for 5 seconds and extension at 60ºC for 4 minutes. The products were precipitated using a premix of: 62.5 µl absolute ethanol, 19.5 µl $dH_2O$ and 3 µl 3M sodium acetate, for 15 µl PCR products, followed by a 15 minutes incubation at room temperature and a centrifugation on 14000 rpm, 4ºC for 20 minutes and supernatant removal. This step was repeated for each sample adding an amount of 250 µl 70% ethanol. After precipitation, the DNA fragments were dried using vacuum centrifugation

for 20 minutes. Sequence data were obtained using an ABI 310 Automated Genetic Analyser. The sequences were manually checked using the *CHROMAS 2.33* (Technelysium Pty Ltd) software. The sequences were compared with those of the *NCBI* (National Center for Biotechnology Information) Gene Bank public database. Alignments were carried out by the *NCBI Blast* program and the sequences showing highest similarity were aligned by *MEGA4* (Molecular Evolutionary Genetics Analysis) program.

**ACKNOWLEDGMENTS**

The work has been funded by the Sectoral Operational Programme Human Resources Development 2007-2013 of the Romanian Ministry of Labour, Family and Social Protection through the Financial Agreement POSDRU/6/1.5/S/16.

This work was prepared with the financial support from the "BIOPREP – Microbial biopreparates for increasing the productivity and crop protection" research funded by Sectoral Operational Programme, Increase of Economic Competitiveness Operation 2.1.1. of the Romanian Ministry of Labour, Family and Social Protection, through financial agreement POSCEE No. 469/11817.

## REFERENCES

1. Geisseler, D., Horwath, W. R., *Soil Biology & Biochemistry*, **2008**, *40*, 3040.
2. Rodríguez, H., Fraga, R., *Biotechnology Advances*, **1999**, *17*, 319.
3. Bach, H.-J., Munch, J. C., *Biol. Fertil. Soils*, **2000**, *31*, 219.
4. Hayano, K., Takeuchi, M., Ichishima, E., *Biol. Fertil. Soils*, **1987**, *4*, 179.
5. Władyka, B., Pustelny, K., *Cellular & Molecular Biology Letters*, **2008**, *13*, 212.
6. Bach, H.-J., Hartmann, A., Schloter, M., Munch, J.C., *Journal of Microbiological Methods*, **2001**, *44*, 173.
7. Sakurai, M., Suzuki, K., Onodera, M., Shinano, T., Osaki, M., *Soil Biology & Biochemistry*, **2007**, *39*, 2777.
8. Mrkonjic Fuka, M., Engel, M., Gattinger, A., Bausenwein, U., Sommer, M., Munch, J.C., Schloter, M., *Soil Biology & Biochemistry*, **2008**, *40*, 1646.
9. Bach, H.-J., Tomanova, J., Schloter, M., Munch, J.C., *Journal of Microbiological Methods*, **2002**, *49*, 235.
10. Tamás, É., Mara, Gy., Laslo, É., György, É., Ábrahám, B., Lányi, Sz., *Studia UBB Chemia*, **2009**, *LIV, Sp.Iss. 2*, 45.
11. Cotar, A.-I., Chifiriuc, M.-C., Dinu, S., Bucur, M., Iordache, C., Banu, O., Dracea, O., Larion, C., Lazar, V., *International Journal of Molecular Sciences,* **2010**, *11*, 5273.
12. Singh, S.P., Thumar, J.T., Gohel, S.D., Purohit, M. K., *Current Research, Technology and Education Topics in Applied Microbiology and Microbial Biotechnology*, **2010**, *1*, 280.

STUDIA UBB CHEMIA, LV, Sp.Iss., 2010

# COMPARATIVE STUDY ON QUANTITATIVE CHARACTERIZATION OF SPIN TRAPPING BY NITRONES

**TŐKÉS BÉLA[a,*], DONÁTH-NAGY GABRIELLA[a], ALINA BALINT[a], DANCS ISTVÁN-PÁL[a]**

**ABSTRACT.** The aim of this paper is the quantitative, comparative study of chemical structure dependence of free radical trapping capacity in the case of some different, but structurally related nitrones. This dependence hasn't been described yet in the literarure. The free radical trapping was studied mostly by ESR and polarographic methods. The obtained simulated spectra were in good agreement with the experimentally obtained ones. The structure of the ESR spectra showed a high dependence on the nature of applied solvent. The quantitative, structural evaluation of the free radical production was performed by polarographically induced Fenton reactions' parameters.

***Key-words:*** *free radicals, nitrones, ESR spectra, polarography*

## INTRODUCTION

It is well known [1,2] that the ESR spectra represent the first derivative of the absorbance vs. the intensity of the magnetic field. The interpretation of ESR spectra presumes the correlation of the experimental data with the structural parameters of the researched paramagnetic unit. The calculation of the g giromagnetic factor is one of the best ways to obtain a good result. The number of the observed bands in the hyperfine spectrum is higher than the number of equivalent protons with one unit, and their relative intensity corresponds to the coefficients of binomial expansions.

If a free radical contains more than one magnetic nuclei, each of them contribute to the splitting of spectrum according to Pascal triangle.

Since in this paper are prezented some results regarding the spectra of nitrones [3-5] of which structures contain an unpaired electron in the neighborhood of a nitrogen atom, so the spectrum splat into three (or more) lines with equal (or different) intensity, it is reasonable to start with some nitroxides are, as model molecules.

The tetramethylpypimidyl-N-oxyde (TEMPO) free radical (figure 1.) is often used as standard molecule [6]. In this case the number of spectral lines is (the nuclear spin of nitrogen is I = 1):

[a] *University of Medicine and Pharmacy of Targu Mures, Faculty of Pharmacy, str. Gh. Marinescu nr. 38, 540139, Targu Mures, Romania, belatokes@yahoo.com*

$$N = 2x1x1 + 1 = 3$$

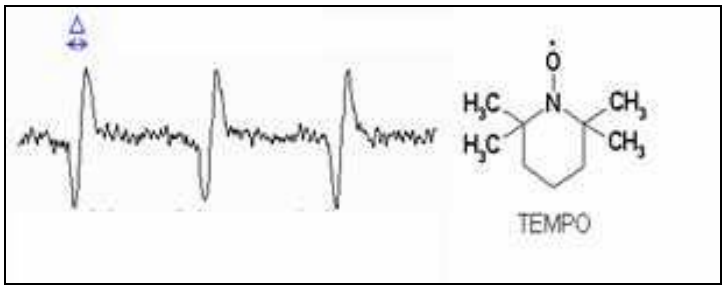


**Figure 1.** The ESR spectrum of tetrametylpyrimidyl-N-oxyde

The interaction with the 12 protons of the four methyl groups can be neglected. The stable diphenyl picrilhydrazyl (DPPH) free radical is also used as standard molecule [7]. In this case the two nitrogen atoms can be considered being equivalent, so the number of spectral lines (figure 2):

$$N = 2x2x1 + 1 = 5$$

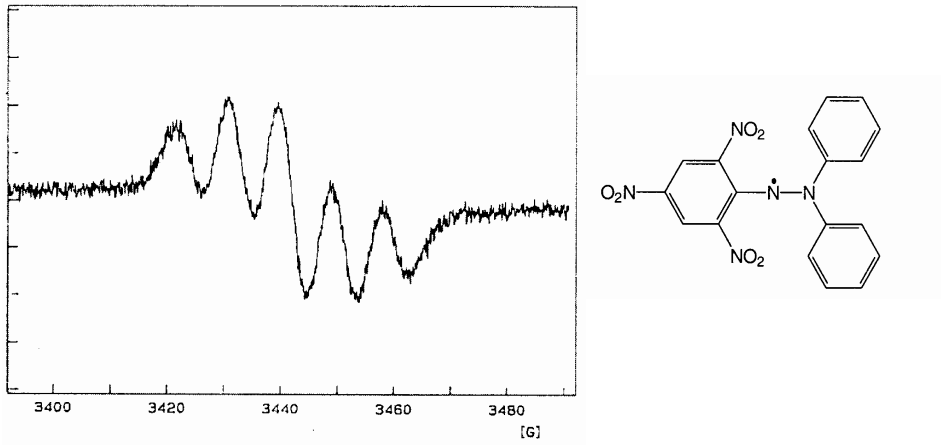


**Figure 2.** The ESR spectrum diphenyl picrilhydrazyl (DPPH) free radical

This specrum were verified experimentally by us, too.

## RESULTS AND DISCUSSION

The spectrum of hydroxyl-diphenyl nitrone adduct can be explained in the same terms. The effect of the solvent must also be taken into account. The organic solvents usually give rise to broader, blurrier spectral lines. In ethanol/water or methanol/water mixtures besides the OH free radical in some of the cases appeared the hydroxyethyl and hydroxymethyl free radicals, as well. In case of diphenyl nitrones due to their bigger size comparing to the t-butyl-

phenyl-nitrone, the rotation is slower, the spectral lines are broadened, so the resolution is poorer. As the nitrones are only slightly soluble in water, but easily soluble in organic solvents (methanol, ethanol, chloroform, dimethylsulfoxide), the ESR spectra were taken in different pure solvents, or mixture of them. Some example: the adduct of diphenyl nitrone in methanol (figure 3):

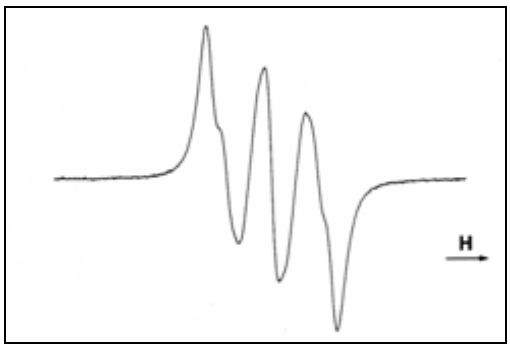


**Figure 3.** The ESR spectrum of the diphenyl nitrone adduct in methanol

in ethanol (figure 4):

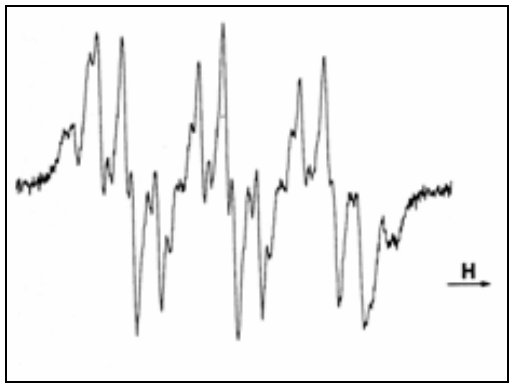


**Figure 4.** The ESR spectrum of the diphenyl nitrone adduct in ethanol

in dimethylsulfoxide (figure 5):

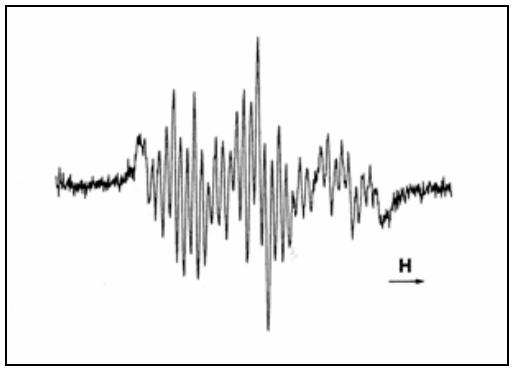


**Figure 5.** The ESR spectrum of the diphenyl nitrone adduct in dimethylsulfoxide

in ethanol/water mixture (figure 6):

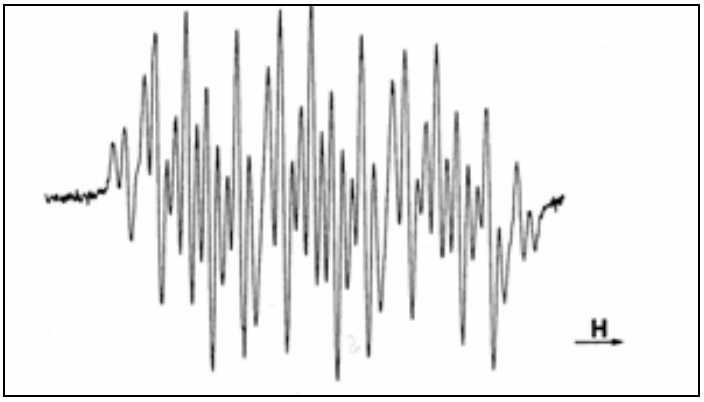


**Figure 6.** The ESR spectrum of the diphenyl nitrone adduct in methanol-water mixture

It can be seen that the spectrum taken in methanol is the most simple, but its disadvantage is that it does not reflect the hyperfine structure. Regarding this observation, the formation of other adducts must be taken into account besides the expected one – depending on the structure of the solvent – which makes the spectrum being much complicated [8]. Table 1. shows some examples of splitting constant is case of several free radicals captured by phenyl-butyl-nitrone.

**Table 1.** Splitting constants of several free radicals captured by phenyl-butyl-nitrone

| **The captured R• free radical** | **The source of free radical** | **The splitting constants** | |
|---|---|---|---|
| | | $a_N$ (G) | $a_H$ (G) |
| OH | $H_2O_2$ + UV | 15.62 | 2.71 |
| •$CH_2OH$ | $CH_3OH$ + $H_2O_2$ + UV | 16.06 | 3.87 |
| •$CH(CH_3)OH$ | $C_2H_5OH$ + $H_2O_2$ + UV | 16.16 | 3.37 |
| •$C(CH_3)_2OH$ | $(CH_3)_2CHOH$ + $H_2O_2$ + UV | 16.12 | 3.61 |
| •$CH_3$ | DMSO + $H_2O_2$ + UV | 16.47 | 3.57 |
| •$OCH_3$ | DMSO + $H_2O_2$ + air + UV | 15.13 | 3.37 |

The ESR spectra of some other, NO-centered free radicals derived from nitrones are relatively similar to the above presented ones, but – naturally – dependent on the structure of R• free radical (Scheme 1).

The same free radicals are formed in the Fenton reactions' condition.

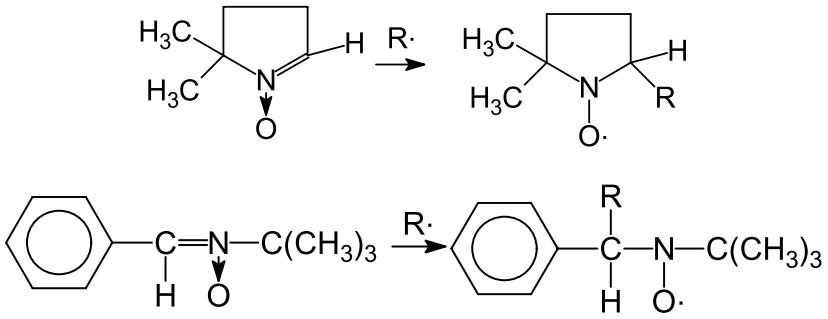

**Scheme 1**. Structures of the studied nitrones

Diphenyl nitrone captures mostly the HO• free radicals (Scheme 2):

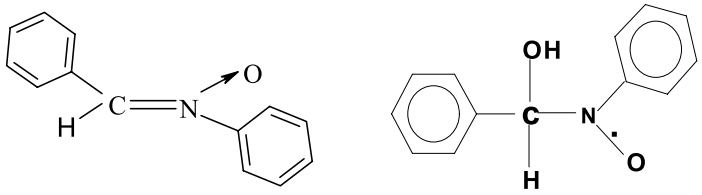

**Scheme 2**. The capture of free radicals by diphenyl nitrone.

The g-factor of diphenyl nitrone's hydroxyl adduct can be calculated using the g factor value of dipicrylhydrazyl etalon, by the following proportionality:

$$g = g_{etalon}B_{etalon}/B_{sample}$$

The obtained value is specific to the nitoxyde-type free radical. Compared to the theoretically obtained parameter, the match is not perfect, which can be explained by unique feature of concrete compunds. Figure 7. shows the ESR spectra of some diphenyl nitrone derivatives synthesized by us.

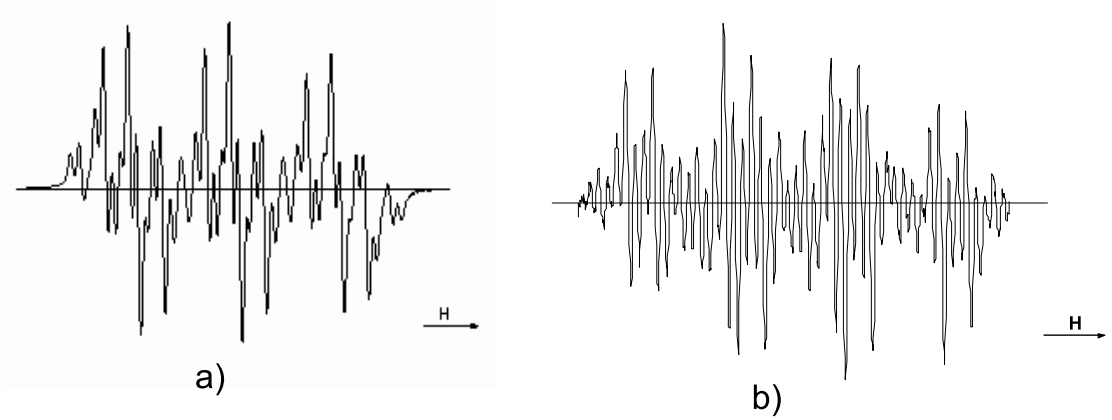


**Figure 7.** The ESR spectrum of the studied nitrones in methanol-water a) and ethanol-water b) mixture

The hydroxyl spin adduct's life time is about 16 hours, the concentration of the free radicals can be traced approximatively after 3 hours.

Our aim was the  to describe the comparative and quantitative study of free radical trapping capacity of different, but structurally related nitrones [4]. Due to the organic solvents the spectral lines are broadened, so only the coupling provenient of N-atom and β-hydrogen was detectable. The fundamental spectrum in methanol is triplet, and in ethanol is quartet.

The spectra could be reproduced with good agreement by simulation. During the interpretation of these spectra several questions arose. One of the questions is, how can be interpreted the interaction of three equivalent protons with the unpaired electron, which influences the primary coupling (3.45 G) of the α-proton with a splitting of $a_H$ = 2.8 G. The interaction suppose a dynamic structure, the static structure does not show which are the protons that – because of the quick molecular movement – are „seen" being magnetically the same by the 2p electrons localized on the N atom. This rotation could cause the unexpected interaction with three protons.

It was revealed, that the spectra of C-3,4-dimetoxy-derivative and the unsubstituted diphenyl nitrone are practically the same, but the those of the C-2,3,4-trymetoxy-nitrone is somewhat different. In the first two cases the orto position is free. Regarding the electronic effects, the metoxy-group causes shifts: from meta- position it has an electron attractive, from para- position it has a repulsive effect. So the simultaneous presence of the two groups diminishes the overall effect. In case of spin trapping, the free radical attacks the azomethinic carbon, the C=N double bond is cleaved, and the conjugation is ceased. In case of single bonds the electronic effects decay in approximately two bond-lengths, so the effect does not reach to the nitrogen. The effect of a substituent in orto- position is about the same intensity as of the para- position, but because of the steric impediment the ring is contortioned, and the conjugation is ceased before the attack of free radical, moreover, the coupling of free radical to the carbon atom is also more difficult. Finally, the conjugation is ceased in both of the cases, so the nitrogen atom is affected always by the same coupled group (captured free radical) [5].

The ESR spectra can be interpreted clearly only in the simplest cases. The physico-chemical information is often masked by different factors, especially when more paramagnetic nuclei are present. That is the reason why is important to generate the simulated spectra, to compare the spectral parameters. For this purpose the EasySpin (Matlab) software package is appropriate. The experimental spectrum taken in metanol-water mixture was compared with the simulated one (figure 8). The match is striking. The effect of the meta-positon protons of the N-coupled aromatic ring is negligible. All of this describe the structure of the adduct in the way above indicated.

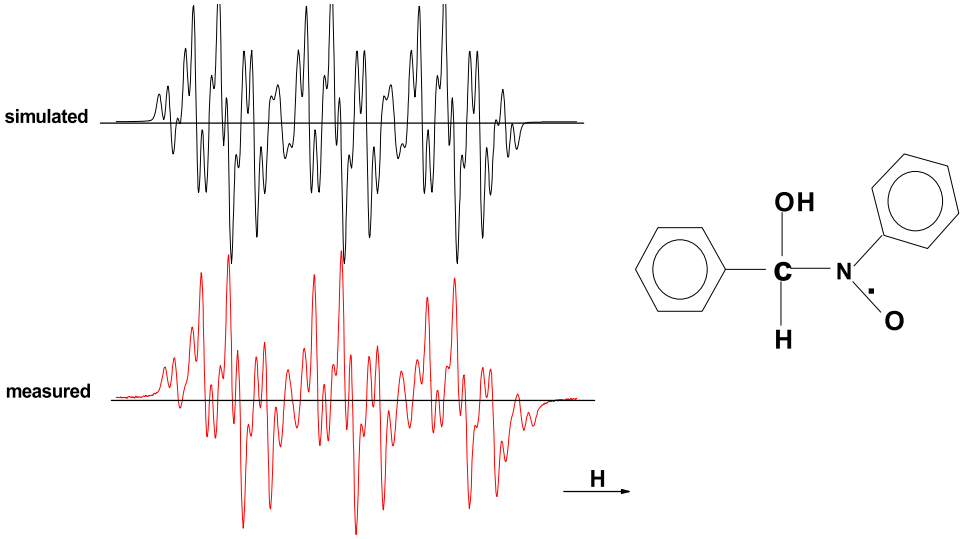


**Figure 8.** Comparison of the experimental and simulated spectra

In ethanolic medium also the hydroxyethyl adduct is formed (figure 9).

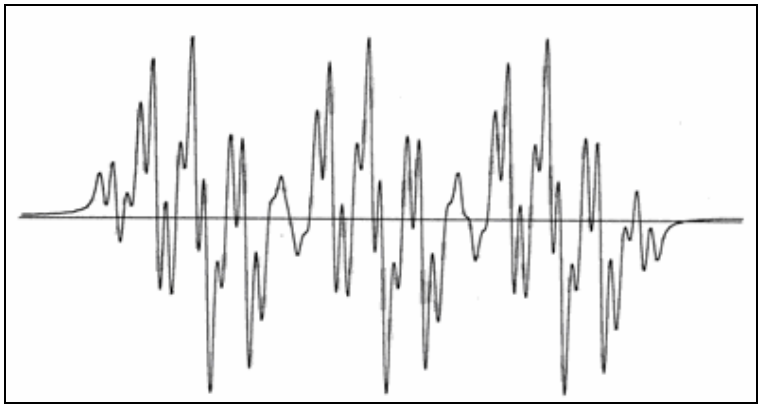

**Figure 9.** The ESR spectrum of hydroxyethyl spin adduct by diphenyl nitrone spin trap

In figure 10 the ESR spectrum of 2,3,4-trimetoxy-C-phenyl-nitrone can be seen. Because of substitution of orto-H, the spectrum is somewhat different from the unsubstituted basic nitrone.

In the following session for describing the free radical source and trapping will use the electrochemical analogy. As in the redox processes the electrons always passes from one reactant to other one by one, this process can be considered being analogue with the attack of free radicals. In the complex mechanism of the electrode processes one or more chemical steps could be inserted, so most of these transformations are of chemical/ electrochemical nature (CE, EC, ECE, etc.). The analogy between the chemical and electrochemical reactions can be generalized as follows (scheme 3.) [9,10]:

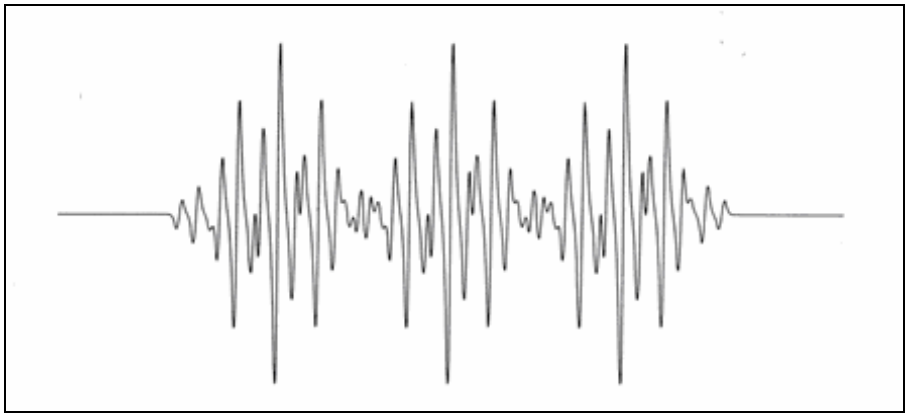

**Figure 10.** The ESR spectrum of 2,3,4-trimetoxy-C-phenyl-nitrone

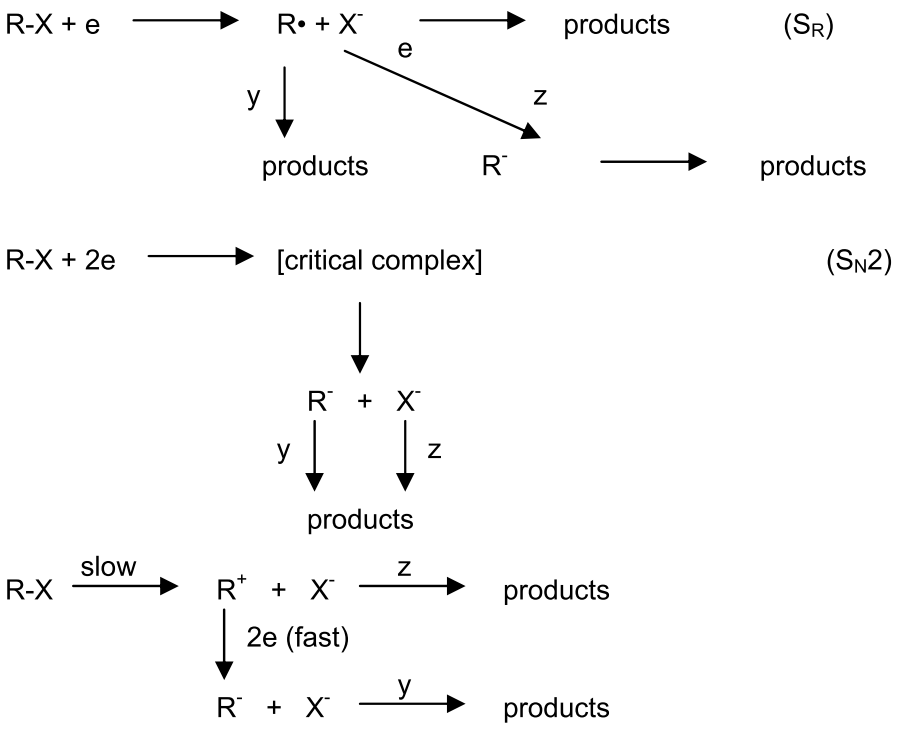


**Scheme 3.** The analogy of chemical and electrochemical reactions

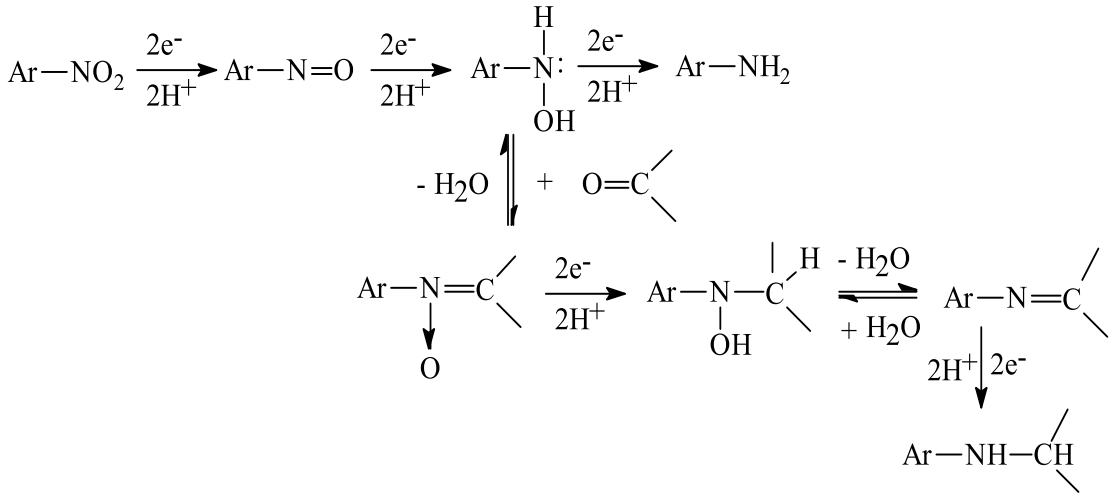

**Scheme 4.** The synthesis of the studied nitrones

This system also contains the free radicalic transformation. Based on the analogy of unpaired electron-containing free radical and cathodic attack, the electrochemical (polarographic, cathodic) reduction of several hundreds of substituted diphenyl nitrones was done by us. The half-wave potentials differ significantly in case of meta- and para-substituted derivatives. In this experiment the whole nitrone-molecule constituted a single conjugate system, therefore was nearly coplanar (scheme 4.) [11-13].

The general formula of the two ring-substituted diphenyl nitrone depolarizers was (scheme 5):

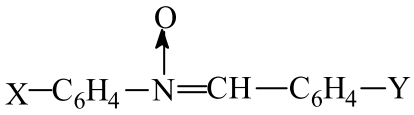

**Scheme 5.** The general formula of the two ring-substituted diphenyl nitrone

The X and Y orto-, meta- or para-substituted diphenyl nitrones allowed the tracing of the structure effect during the polarographic reduction of oxyazomethine group. The effect of substituents was taken into account via σ constants. The trap in the free radical capture determinations was also the nitrone group. These measurements were done on C-phenyl-substituted derivatives. Firstly the X = H and Y was H (unsubstituted basic compound), then $NH_2$, OH, Cl, $N(CH_3)_3$, $NHCOCH_3$, in orto-, meta- and para- positions. Their effect could be described with the following linear equation:

$$E_{1/2} = (0.098 \pm 0.031)\,\sigma - (0.925 \pm 0.007)$$
$$N = 10,\ r = 0.990$$

The half-wave potentials characterize the electron transfer (electron capture) energy. The ESR data and the polarographic parameters are completing each other reciprocally.

Our team proposed a method based on the kinetic polarographic currents for quantitative characterization of free radical activity and the trapping capacity. The method has the following idea. The literature propose principally the Fenton reaction (Fe(II) + $H_2O_2$) for obtaining free radicals, but better is the tert.-butyl-hydroperoxide (TBH), which has already been used for characterization and comparison of many free radicals. In this case the question is, what is the trapping capacity of a given compound (ex. the basic diphenyl nitrone) against free radicals with different structure. And, besides the structure, the solvent has a major effect. After the first works of Wiesner the possibility of polarographic tracing of very fast reactions ($k \approx 10^3 – 10^{10}$ $s^{-1}$) was contoured. This goal can be reached by the kinetic polarographic currents [14]. The corresponding theoretic problems were solved by the Prague school.

In complex electrode processes the mass transport is ensured by diffusion. But, under certain conditions, this transport is influenced by chemical reactions which, together with the diffusion, contribute to balance the concentration-changes due to the electrolysis in the neighborhood of the electrode. In consequence, the polarographic currents may depend on the speed of the mentioned reactions. These currents are called kinetic currents.

The reactions between organic hydroperoxides and transition metals (especially $Fe^{2+}$) were thoroughly studied lately. These redox systems (Fenton reactions) are free radical sources widely used both in basic research and applicative one. From this point of view, the speed of reaction between peroxide and metallic ion is decisive. In present, only the reactions of cumene-hydroperoxide and the TBH with transition metals are studied.

Our team studied the kinetics and mechanism of the reaction between TBH (the typical representative of hydroperoxides) and $Fe^{2+}$ ions. Considering TBH the benchmark of the free radical sources, it becomes possible the numerical determination of the free radical trapping capacity of different compounds (ex. nitrones). In the polarographic cell, under certain conditions, when the $Fe^{3+}$ ions are reduced at less negative potential than the hydroperoxide ($E_{1/2,Fe3+}$ = – 0.265 V, against $E_{1/2,ROOH}$ = - 0.660 V, vs. NSE, in 1.0 M $H_2SO_4$), the $Fe^{2+}$ ions formed are partially regenerated by the hydroperoxide, so the limiting current of the $Fe^{3+}$ ions increases. The increase in current depends on the rate of reaction between hydroperoxide and $Fe^{2+}$ ions, which means that its value allow the calculation of the rate of free radical trapping reaction. The principal steps of the depolarisation process can be described by the following scheme (scheme 5):

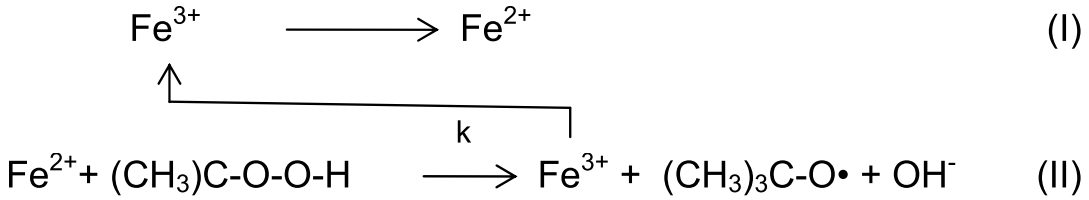


**Scheme 5**. The principal steps of the depolarisation process

The $(CH_3)_3C$-O• can be coupled to a free radical trap, or can initiate a chain reaction depending on the composition of the system.

Koutecký demonstrated that the ratio of the average total current density and the average diffusion current density can be described by the following asymptotic equation:

$$\frac{\bar{i}_l}{i_d} = 0.812(kCt_1)^{\frac{1}{2}} + 1.92(kCt_1)^{-\frac{7}{6}}$$

where C is the concentration of hydroperoxide.

For a correct interpretation of the results the ratio of the oxidized $Fe^{2+}$ and consumed $(CH_3)_3C$-OOH moles (R) must be known. The experimentally obtained value in our case was R ≈ 1.0, which indicates that one hydroperoxide molecule oxidize only one $Fe^{2+}$ ion, according to the proposed reaction scheme.

It is resulting that the reaction between $Fe^{2+}$ and TBH is of first order referring to both partners. This stoechiometric relation differs in case of reaction between $Fe^{2+}$ and HOOH, which was found to be R = 2. Our experimental results are presented in the table 2. ([$Fe^{2+}$] = 1.0x10$^{-3}$ M]:

**Table 2**. The experimental results

| [HTB] (M) | $\bar{i}_l / \bar{i}_d$ | $t_1$(s) | k ($M^{-1}s^{-1}$) | $\bar{i}_l / \bar{i}_d$ | $t_1$(s) | k ($M^{-1}s^{-1}$) |
|---|---|---|---|---|---|---|
| | T = 303 K, | | | T = 298 K, | | |
| 0.045 | 1.818 | 2.86 | 30.13 | 1.657 | 3.17 | 20.93 |
| 0.040 | 1.700 | 2.70 | 29.83 | 1.539 | 3.04 | 19.06 |
| 0.030 | 1.645 | 3.10 | 31.45 | 1.441 | 3.15 | 19.70 |
| 0.020 | 1.391 | 2.70 | 30.07 | 1.244 | 2.72 | 17.91 |
| $\bar{k} \pm S_M$ | | 30.37 ± 0.36 | | | 19.53 ± 0.62 | |
| | T = 293 K, | | | T = 288 K, | | |
| 0.045 | 1.460 | 3.22 | 13.47 | 1.281 | 3.26 | 7.72 |
| 0.040 | 1.443 | 3.24 | 14.50 | 1.263 | 3.30 | 8.05 |
| 0.030 | 1.303 | 3.20 | 12.78 | 1.196 | 3.25 | 7.88 |
| 0.020 | 1.183 | 2.80 | 12.79 | 1.112 | 2.83 | 7.63 |
| $\bar{k} \pm S_M$ | | 13.38 ± 0.40 | | | 7.77 ± 0.10 | |

$$\lg k = (3395 \pm 140)1/T + (12.68 \pm 0.45)$$

$$r = - 0.998 \qquad s_0 = \pm 0.018$$

or

$$k = 4.8 \times 10^{12} \exp\left(-\frac{15500}{RT}\right) \ M^{-1}s^{-1}$$

The activation parameters are: $\Delta H^{\neq}_{298}$ = 14.9 ± 0.6 kcal/mol; $\Delta S^{\neq}_{298}$ = - 2.5 ± 2.1 cal/molK; $\Delta G^{\neq}_{298}$ = 15.6 ± 0.6 kcal/mol.

This rate is 3-4 times smaller as those of the reaction between $Fe^{2+}$ and $H_2O_2$. The kinetic data regarding the reaction of TBH with $Fe^{2+}$ are missing from the literature. It is foreseen that the value of catalytic current decreases when a free radical trap is added to the system. For this purpose we used nitrones in our experiments. The decrease of catalytic wave height can be explained by interaction between the HO• free radicals and the trap. In case of a sufficiently high concentration of spin trap the catalytic current density approaches to a limit value:

$$\frac{\bar{i}_l}{i_d} = 0.812(k[H_2O_2]t_1)^{\frac{1}{2}}$$

which, compared to the value observed is absence of the spin trap:

$$\frac{\bar{i}_l}{i_d} = 0.812(2k[H_2O_2]t_1)^{\frac{1}{2}}$$

is about 30% less, according to the:

$$Fe^{2+} + HOOH \rightarrow Fe^{3+} + HO^- + \bullet OH$$

reaction.

## CONCLUSIONS

Taking into account the presented results it becomes obvious that the ESR spectra can provide basic information regarding the spin trapping capacity of nitrones, the kinetics and mechanism of spin trapping.

Using polarographic kinetic data the free radical producing capacity of some free radical sources can be obtained.

The results obtained from magnetic spectra and those obtained from the electrochemical methods are mutually complementary in study of free radical interactions.

## EXPERIMENTAL SECTION

The ESR and the polarographic studies were made by a method described earlier by us [9-11], using a Polarograph LP-55, system Heyrovsky, connected to a recorder EZ-2 and an ultrathermostat type Höppler. Respectively, the components were mixed and filled into a flat cell (Wilmad, USA, type WG-808 Q), and the ESR spectrum recorded.

The data used for simulations were: number of components: 1; resolution of the magnetic field: 0.05; number of coupling constants: 4; particular line width: 0.60 G; the Lorenz/Gauss factor: 0.75/0.25; microwave frequency: 9.756 GHz; magnetic induction: $H_0$: 3482.0 G; Sweep: 50.0 G; g-factor: 2.0027; the hfs. coupling of N atom: $a_N$ = 12.26 G; the a hfs. coupling of Hα proton: $a_H$ = 3.45 G; the a hfs. coupling of the three a equivalent H(3) protons: $a_H$ (3) = 2.80 G; the hfs. coupling of the two equivalent H(2) protons: $a_H$ (2) = 0.90 G.

### ACKNOWLEDGMENTS

This paper was realized within the CEEPUS HU-00-10 Network range.

## REFERENCES

1. S.A. Goudsmit, “Foundations of modern EPR”, World Scientific Publishing Co, **1997**, 3-12.
2. W.G. Richards, P.R. Scott, “Energy levels in atoms and molecules”, Oxford University Press, **1994.**
3. R.A. Floyd, K. Hensley, M.J. Forster et al, *Ann.N.Y.Acad.Sci*, **2002**, 959, 321-329.
4. E.G. Janzen, “Foundations of modern EPR”, World Scientific Publishing Co, **1997**, 241-264.
5. G.M. Rosen, B.E. Britigan, H.J. Halpern et al, “Free radicals, biology and detection by spin trapping”, Oxford University Press, **1999.**
6. R.L. Fey, M. Workman, H. Marcellos, M.J. Burke, *Olant Physiol*., **1971**, 63, 1220-1222.
7. J. Rodrigez, C. Olea-Azar, C. Cavieres, E. Norambuena, T. Delgado-Castro, J. Soto-Delagado, B. Araya-Maturana, *Bioorg. Med. Chem*, **2007**, 15, 7059-7065.
8. D.I. Metelitsa, *Russ. Chem. Rev*., **1971**, 40, 573-580.
9. B. Tőkés, G. Suciu, G. Nagy, *Pharmazie*, **2002**, 5, 122-126.
10. G. Suciu, B. Tőkés, *Revista de Medicină şi Farmacie – Orvosi és Gyógyszerészeti Szemle*, **2001**, 47, 249-253.

11. G. Suciu, B. Tőkés, *Revista de Medicină şi Farmacie – Orvosi és Gyógyszerészeti Szemle*, **2002**, 48, 232-236.
12. G. Suciu, B. Tőkés, *Revista de Medicină şi Farmacie – Orvosi és Gyógyszerészeti Szemle*, **2002**, 48, 236-240.
13. G. Suciu, B. Tőkés, *Revista de Medicină şi Farmacie – Orvosi és Gyógyszerészeti Szemle*, **2003**, 49, 57-61.
14. B. Tőkés, *The 9$^{th}$ International Conference of Chemistry. Hungarian Technical Scientific Society of Transilvania*, Cluj, nov. **2003,** Vol. p. 166-170.

STUDIA UBB CHEMIA, LV, Sp.Iss., 2010

# CHARACTERIZATION OF ITO NANOSCALED LAYERS APPLIED TO THE ENVIRONMENT PROTECTION

**DORIN MANCIULA[a], ADRIENNE NAUMESCU KOZAN[b], EMIL HOLCZER[c], FIAMETTA KORMOS[c]**

**ABSTRACT.** The ITO (indium doped $SnO_2$) is an n-type semiconductor material, which belongs to the transparent conductive oxides category (TCO). ITO presents also excellent features, such as good electrical conductivity, high mechanical resistance, antistatic effect, outstanding chemical resistance, optical transparency in the range of visible, protective properties against electromagnetic waves and the capability of reflecting the IR-rays and absorbing solar energy. Another advantage comes from its possibility of covering different materials such as glass, metal or flexible plastics at low temperatures. This paper reports a study regarding the ITO structure and several ITO film properties (electrical conductance, VIS transmittance and anticorrosive stability) when deposited on glass substrates by pyrosol method, next to its application in environmental protection after used as a long life resistant anode for destroying different organic pollutants by electrochemical oxidation.

***Keywords:*** *ITO films, characteristics, environmental protection applications.*

## INTRODUCTION

The ITO (indium doped $SnO_2$) is an n-type semiconductor material, which belongs to the category of transparent conductive oxides (TCO). ITO shows excellent properties such as good electrical conductivity [1], outstanding mechanical and chemical resistance, optical transparency in the range of visible [2], protective properties against electromagnetic waves [3], antistatic effect and also the capability of reflecting IR-rays and absorbing solar energy [4]. More benefits comes from the possibility of covering different surfaces (glass, metal or flexible plastics) with ITO films at low-temperatures [5, 6]. For this reason ITO coatings are widely used in a large number of technical applications, e.g. for constructing window electrodes in solar cells [7, 8], transparent electrodes

[a] *Babeş-Bolyai University, Faculty of Environmental Science, Fântânele Str. No. 30, 400294, Cluj-Napoca, Romania, Tel. +40.0264.307.030, Fax: +40.0264.307.032, email: dimro21@gmail.com*

[b] *Babeş-Bolyai University, Faculty of Psychology and Educational Sciences, Kogălniceanu Str., No.1, 400084, Cluj-Napoca, Romania, Tel.+40.0264.405.300, email: kozanadrienne@yahoo.com*

[c] *Dekra Certification SRL RO, Brâncuşi Str., No. 131, 400.458, Cluj-Napoca, Romania, Tel. 0264-443.598, Fax: 0264-443598; email: metti@email.ro*

in display devices (liquid crystal display [9], electro-luminescent display, and electro-chromic and LED displays [10]), conductive windscreens for aircraft, or EMI shielding [3, 11], also in architectural applications (e.g. IR reflective coatings and heat mirrors) and recently employed in environmental protection as a sensor for detecting the hydrogen gas above $50^{o}$ C [12], or as biosensor substrate for detection of the virus bovine diarrhea [13]).

This paper reports a study upon the structure and several ITO film properties (electrical conductance, VIS transmittance and anticorrosive stability) when deposited on glass substrate by using the pyrosol method, along with its application in environmental protection as a long life resistant anode used for destroying organic pollutants by electrochemical oxidation.

## RESULTS AND DISSCUSIONS

Table 1 presents the characteristics of the ITO film depending on the doping level with indium.

**Table 1.** Characteristics of the ITO film depending of the doping level.

| $In^{3+}$ mol % | CHARACTERISTICS | | | |
|---|---|---|---|---|
| | Grain size (nm) | Resistivity (Ω*cm) | Charge carrier number/$cm^3$ | VIS transmittance (%) |
| 3,5 | 120 | 45 | $4,0x10^{20}$ | 76 |
| 4,5 | 80 | 35 | $4,8x10^{20}$ | 82 |
| 6,5 | 174 | 52 | $3,2x10^{20}$ | 70 |

This values show that the best transmittance and the best electrical conductance are obtained for a doping level of 4,5 mol % $In^{3+}$.

Figure.1 shows the presence of a uniform deposited nanoscaled film, with a globular shape of the grain particles.

The corrosion resistance of ITO films is very important for numerous applications in environmental protection. For that reason in figure 2 are presented the results of best ITO film stability in three different chemical media: $H_2SO_4$ (1M), NaOH (1M) and HOCl (1M).

The graphics illustrated in figure 2 confirms a good stability after 30 days in all three media. In $H_2SO_4$ media the variation of both resistance (R) and corrosion potential (E) were smaller comparing to NaOH. After 60 days the largest variation of studied properties for the exposed films was detected in HOCl media. On the other hand, these films have shown a very good stability in $H_2SO_4$, thus demonstrating an excellent long life of over two months.

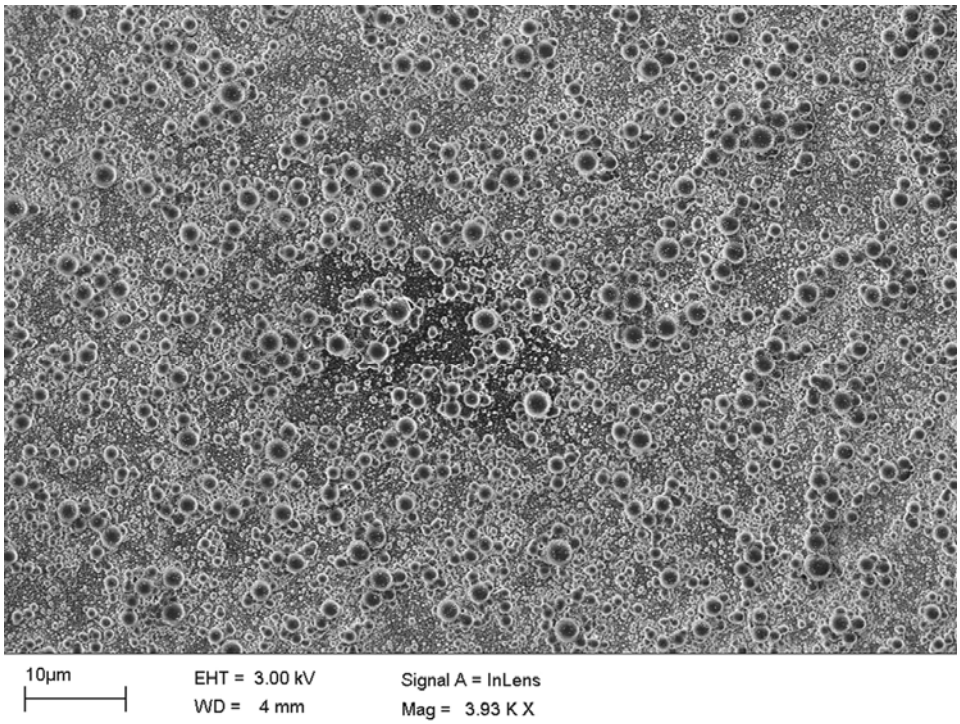


**Figure 1.** SEM images of ITO films structure.

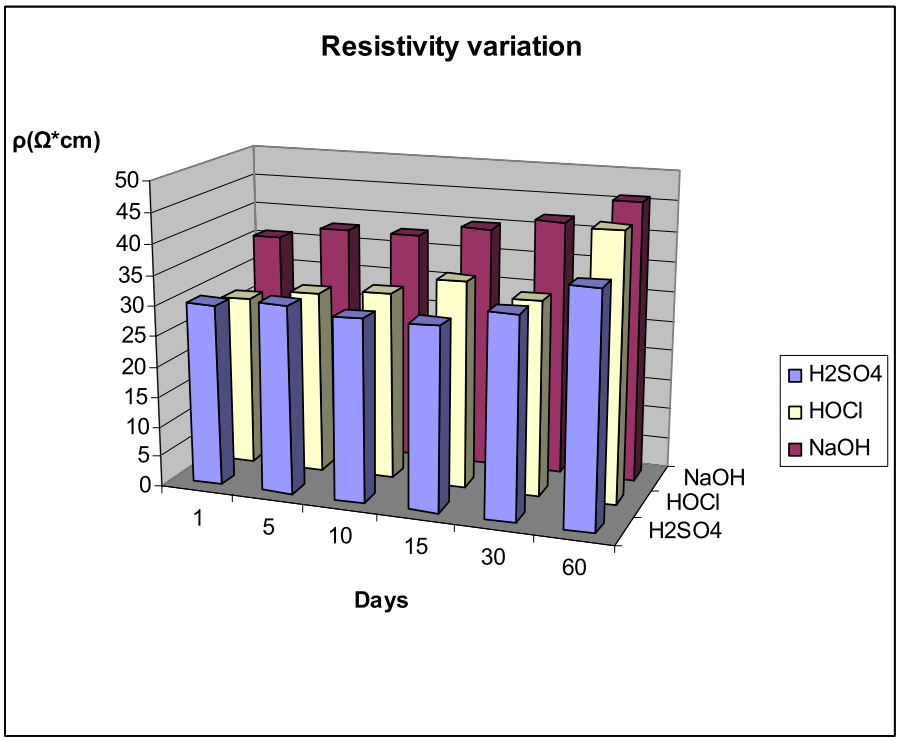

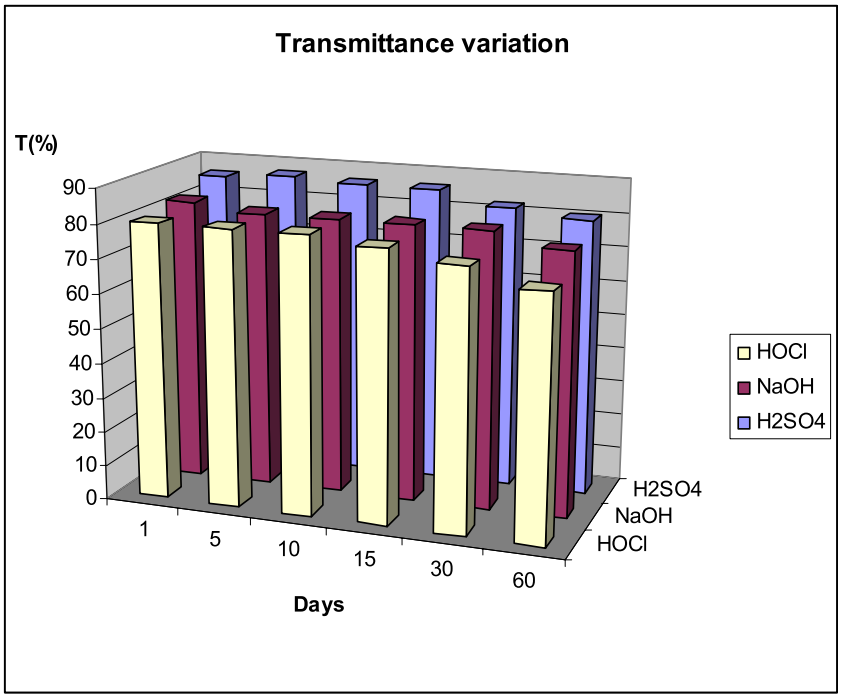


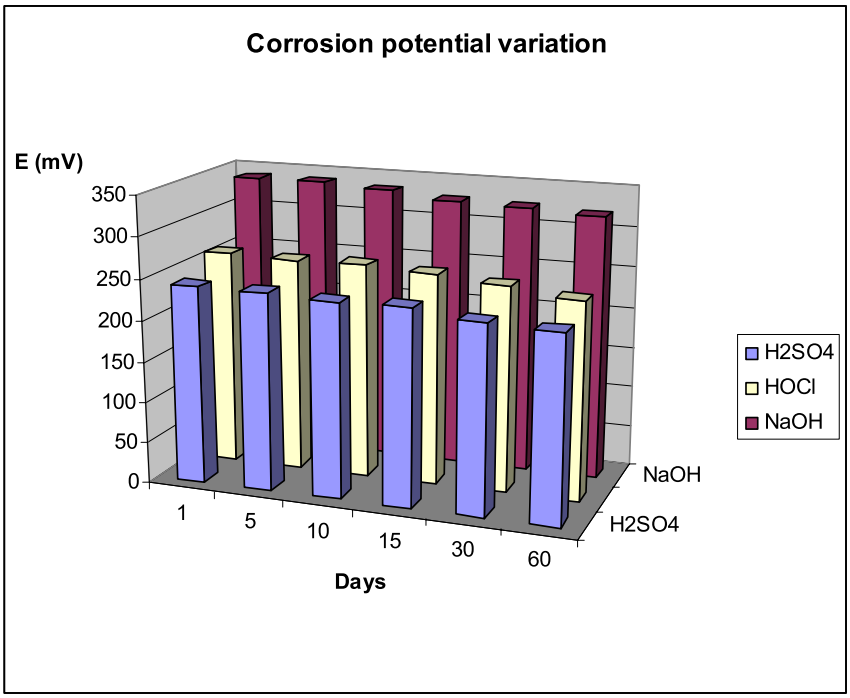


**Figure 2.** ITO corrosion.

Another TCO films we previously prepared and analyzed [14] was an ATO type (antimony doped tin dioxide) film. The data presented in table 2 compares the characteristics of the ATO and ITO films which we prepared.

**Table 2.** Comparison of the ITO and ATO films characteristics, with best doping level.

| Characteristics | ITO 4,5% | ATO 2% |
|---|---|---|
| **Grain size (nm)** | 80 | 85 |
| **Resistivity (Ω*cm)** | 35 | 42 |
| **Charge carrier numbers/cm$^3$** | $4{,}8\times10^{20}$ | $4{,}0\times10^{20}$ |
| **VIS transmittance (%)** | 82 | 76 |
| **Stability (days)** | 60 | 54 |
| **Preparation temperature ($^o$C)** | 200 | 425 |
| **Preservation temperature ($^o$C)** | 25 | 25 |
| **Electrocatalytical activity (%)** | 30 | 65 |

The experimental data presented in table 2 confirms that both TCO films show excellent properties. The ITO film demonstrates a better transmittance and high electric conductivity, while for the chemical stability a small difference can be noticed. Another advantage of the ITO film it is given by the possibility of depositing the film at low temperature (200$^o$C) comparing to ATO film (425$^o$C) [10]. For the ATO film, a more electro oxidation activity has been noticed.

The ITO film we obtain presents a good anticorrosive stability and it was further used for constructing a dimensionally stable anode (DSA) [15] with good electro catalytically properties and then applied in the process of degradation of organic pollutants from waste waters. The general scheme of the DSA it is presented in figure 3.

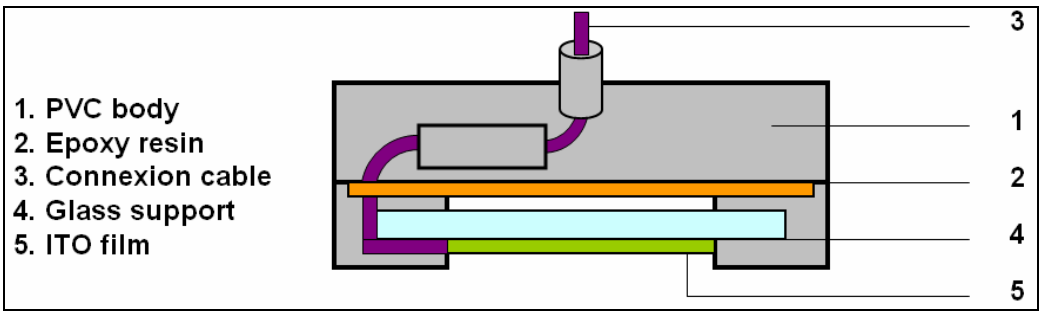


**Figure 3.** Schematic representation of the DSA anode.

Since formaldehyde is a hazardous waste in the textile industry, it must be eliminated especially for environmental protection. DSA-ITO anode was tested in the electrochemical oxidation of formaldehyde and the cyclic voltammetry results can be seen in figure 4.

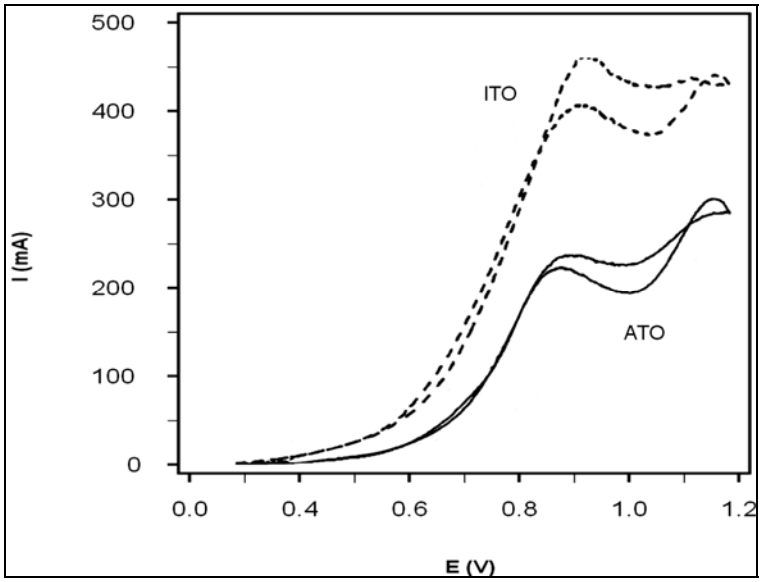


**Figure 4.** Cyclic voltammetry of formaldehyde oxidation.

The oxidation currents are higher for the ITO electrode versus ATO electrode, which demonstrates that ATO is more electrocatalitycaly active.

## CONCLUSIONS

The properties of the TCO films received in the last decade much attention due to their large number of important applications. The nano-crystal films, ITO and ATO deposited on glass substrate give approximately identical stability results. However the ITO film has a low depositing temperature and also the best transmittance in VIS, at the same time as the ATO film demonstrate better electro catalytically properties. Both TCO were employed for constructing the DSA, which further was used to degrade the organic pollutants from waste waters

## EXPERIMENTAL SECTION

The preparation of ITO is possible by using the following chemical reactions:

$$SnCl_4 + 4\ ROH \longrightarrow Sn(OR)_4 + 4\ HCl$$

$$Sn(OR)_4 + H_2O \longrightarrow Sn(OR)_3OH + ROH$$

$$Sn(OR)_3OH + Sn(OR)_4 \longrightarrow (RO)_3\ Sn\text{-}O\text{-}Sn\ (RO)_3 + ROH$$

The sol-gel preparation method of ITO by pyrosol technique [16, 17] uses as precursors the following solutions: $SnCl_4$ x $4H_2O$ and $InCl_3$ dissolved in isopropanol. The optimum doping level with $InCl_3$ was obtained by using three indium chloride concentration levels: 3 mol%; 4,5 mol% and 6,5 mol %. The preparation process has followed several steps, which are next presented. The glass substrate (soda lime silica glass plate 5x10 mm) is first pretreated with sulfuric acid for 15 minutes, then with acetone for another 15 minutes and next dried in air, also for 15 minutes. Then, the substrate is calcined for 15 minutes at 200$^o$C. The precursor solution was prepared from 100ml $SnCl_4$, 0.2M dissolved in isopropanol and 15ml $InCl_3$, 0.5M dissolved as well in isopropanol. Both solutions were mixed under constant stirring for 2 hours. The chemical composition has been checked by AAS (atomic spectra absorption). The mixture is further agitated for 1,5 hours with gradual addition of 200 ml of boric acid, 0.2M and then by ultrasonic for 2 hours to get the soil, which is further sprayed with compressed air over the glass substrate for 3 minutes. The spraying process was repeated five times. The coated glass with ITO film is finally heated at 200°C for 30 minutes.

The methods used for characterize of ITO nanofilms were: XRD (X-ray diffraction, Philips PW 3710, Cu Kα radiation) for measuring the grain size n (nm); SEM (scanning electron microscope, Hitachi 20kV accelerate voltage, 1000-10000 magnification) for verifying the film structure; UV-VIS spectroscopy (Pye-Unicam UV-VIS spectrophotometer 200-900 nm spectra transmittance) for confirming the transmittance T (%). and EIS (electrochemical impedance spectroscopy, Solartron 1286) for determining the number of charge carriers ($N/cm^3$). The carrier charge numbers were determined by the Mott-Schottky equation, measuring impedance at 1000 Hz. For estimation of corrosion potential E (mV) electrochemical potential measurements were made in three-electrode cells equipped with Ag/AgCl, (Radiometer) as reference electrode and platinum sheet as counter electrode (Potentiostat model PG STAT 10 - Autolab). The working electrode was glass covered by ATO films. Cyclic voltammetry was used for determining the electro catalytic activity (CV:BAS 100B, Autolab type) and Van der Pauw method for validating the electrical resistivity: [$\rho = R / A * d$], where R is resistance, A surface area and d the film thickness (ohm*cm). The sheet resistance of the films (ohm/□) was measured by four point method (by using a self made device).

**ACKNOWLEDGEMENTS**

The authors would like to thank the staff from Chemical Research Center of Hungarian Academy of Sciences - Budapest, especially to dr. I.Felhosi and dr. I.Sajo for all their help and support.

## REFERENCES


1. X. Wang, L. Zhi, K. Mullen, Transparent, *Nano Lett*ers, **2008**, *8*, 323.
2. C.K. Choi, C.H. Margraves, S.I. Jun, A.E. English, P.D. Rack, K.D. Kihm, *Sensors,* **2008**, *8*, 3257.
3. J. Eite, A.G. Spencer, "Indium Tin Oxide for transparent EMC shielding and Anti-static applications", Presented at EMCUK 2004, Newbury, UK, **2004**.
4. Y. Galagan, J. Rubingh, R. Andriessen, C. Fan, P. Blom, S. Veenstra, J. Kroon, *Solar Energy Materials & Solar Cells*, **2011**, *95*, 1339.
5. N. Al-Dahoudi, M.A. Aegerter, *Journal of Sol-Gel Science and Technology*, **2003**, *26*, 693.
6. R. Saidur, M.M. Hasan, A.S.M.A. Haseb, H.H. Masjuki, *Journal of Applied Sciences*, **2008**, *8*, 1883.
7. J. Kois, S. Bereznev, J. Raudoja, E. Mellikov, A., *Solar Energy Materials and Solar Cells*, **2005**, *87*, 657.
8. L. Kerkache, A. Layadi, F.Hadjersi, E. Dogheche, A. Gokarna, A. Stolz, M. Halbwax, J.P. Vilcot, D.Decoster, B. El Zein, S.S. Habib, "Sputtered Indium Tin Oxide thin films deposited on glass substrate for photovoltaic application", Proceedings of the ICREPQ **2010**, Granada (Spain).
9. H. Kawamoto, "The History of Liquid-Crystal Displays", Proceedings of the IEEE, **2002**, Vol. 90.
10. K. Kim, H. Kim, S.N. Lee, S. Cho, *Electronic Materials Letters*, **2011**, Vpl. 7, 2, 145.
11. Y. Choa, H. Kima, J. Hongb, Gi-Ra Yi, S. Jangb, S. Yang, *Colloids and Surfaces A: Physicochem. Eng. Aspects*, **2009**, 336, 88.
12. S. Shukla, S. Seal, L. Ludwig, C. Parish, *Sensors and Actuators B*, **2004**, *97*, 256.
13. Z.M. Tahir, E.C. Alocilja, D.L. Grooms, *Sensors*, **2007**, *7*, 1123.
14. G. Tolnai, I. Sajo, P. Nagy, M. Pavai, E. Holczer, A. Kozan Naumescu, F. Kormos, E. Kalman, *Rev. Chim. (Bucuresti)*, **2010**, *61*, 238.
15. I. Sajo, K. Papp, P. Nagy, D. Manciula, I. Tarsiche, F. Kormos, E. Kalman, *Rev. Chim.*, **2011**, Vol. 62, 2, 250.
16. R. Rugescu, Solar energy, **2010**, Ed. INTECH, ISBN 978-953-307-052-0, p. 432.
17. A. Chebotareva, G. Untila, T. Kost, S. Jorgensen, A. Ulyashinc, *Thin Solid Films*, **2007**, Vol. 515, 24, 8505.